School of Civil and Mechanical Engineering
Department of Civil Engineering

Durability Related Properties of Low Calcium Fly Ash Based Geopolymer Concrete

Monita Olivia

This thesis is presented for the Degree of
Doctor of Philosophy
of
Curtin University of Technology

May 2011

Curtin University

DECLARATION

To the best of my knowledge and belief this thesis contains no material previously published by any other person except where due acknowledgement has been made.

This thesis contains no material which has been accepted for the award of any other degree or diploma in any university.

Signature:

Monita Olivia

Date: May 2011

ABSTRACT

Geopolymer material using by-products can lead to a significant reduction of the carbon footprint and have positive impact on the environment. Geopolymer is recognized as an alternative construction material for the Ordinary Portland Cement (OPC) concrete. The mechanical properties of geopolymer concrete are superior for normal exposure environments. In terms of durability in the seawater, a limited number of publications were available. The seawater environment contains chloride ions and microorganisms that are harmful for reinforced concrete structures. Hence, a study of the durability of fly ash geopolymer concrete is essential when this material is to be used in a real application. The present study aims to investigate the durability of fly ash geopolymer concrete mixture in a seawater environment such as seawater resistance and corrosion of steel reinforcement bars. The development of mixtures and their mechanical properties were also presented.

The concrete mixtures were developed using the Taguchi optimization method. Three mixtures, labelled T4, T7, T10 and a control mix were investigated further. Mechanical properties such as compressive strength, tensile strength, flexural strength, Young's Modulus of Elasticity were determined for each mix. In addition the water absorption/AVPV and drying shrinkage were also measured. The seawater resistance study comprises chloride ion penetration, change in strength, change in mass, change in Young's Modulus of Elasticity, change in effective porosity and change in length. The corrosion performance of steel reinforcement bars in fly ash geopolymer concrete was determined by measuring the corrosion potential by half-cell potential, accelerated corrosion test by impressed voltage method and microbiologically influenced corrosion incorporating algae. The microstructure of the samples was also investigated using SEM and microscope.

It can be summarized that the fly ash geopolymer concrete has an equivalent or higher strength than the OPC concrete. The seawater resistance revealed a high chloride ion penetration into the fly ash geopolymer concrete due to lack of a chloride binding ability and continuous hydration under aqueous medium. The geopolymer concrete had a higher strength and small expansion following exposure to wetting-drying cycles. There was a rapid depassivation of steel reinforcement bars in fly ash geopolymer concrete, although it has a smaller corrosion rate than the OPC concrete. This could delay the pressure in generating cracks in the concrete cover which is not favourable in the long term, due to a sudden loss of load carrying capacity. A novel study on the corrosion performance in algae medium demonstrated a risk of steel bar corrosion in fly ash geopolymer concrete due to the low alkalinity of this concrete. It can be concluded that the low calcium fly ash geopolymer offers some advantages in durability for reinforced concrete in seawater environments.

ACKNOWLEDGEMENTS

Alhamdulillah, ya Allah, finally I could accomplish my PhD study. Thank you very much for Your great hidayah and rahmah during this heroic journey.

I would like to acknowledge a number of people who supported me to produce this thesis.

Firstly, I would like to express my gratitude to Professor Hamid Reza Nikraz, the best supervisor that I have ever had, for his invaluable support, encouragement, assistance and guidance throughout this PhD study. I have learned a lot during this learning process mainly from the opportunities that were introduced by him.

I would like to acknowledge University of Riau my current employer in Indonesia. I also would like to thank the Australian Development Scholarship for the financial support and assistance. Thank you to Mr David Spiller, Mr Reza Reinanto, Ms Julie Craig, Ms Sarah Treagold, Ms Chris Kerin and Ms Kristen Soon for their support for me and my family during my study in Perth.

I received help and support from many wonderful technical staff in the department and laboratory of the Faculty of Science, Engineering and Computing, Curtin University of Technology. Thank you very much to Mr Ashley Hughes, Mr Robert Cutter, Mr John Murray, Mr Carl Lewis, Mr Bradley Frank, Mr Mike Appleton, Mr Michael Ellis, Ms Karen Haynes, Ms Ann Carol, Mr Mark Whittaker, Mr Russel Wilkinson, Mr Jo Justin, Mr Jim Sherlock, Mr Mark Fowler, Prof Vijay Rangan, Dr Ian Chandler, Dr Prabir Sarker, Ms Liz Field, Ms Dianne Garth, and Ms Sucy Leong.

I am grateful to Dr Reza Javaherdashti, Dr Navid Mohamaeni and Prof Michael Borowitzka from Algae R&D, Murdoch University, Western Australia, for their help in some parts of my thesis; Dr John Fielder (Teaching & Learning Development) and Prof Jeanne Dawson (The Learning Support). I acknowledge Dr Navid Nikraz and Julia Lightfoot for helping me in proofread the final manuscript.

It is also important to acknowledge friends who always help and give me spark of ideas throughout my experimental work and analysis. Thank you very much to Dr Hanisom Abdullah, Dr Djwantoro Hardjito, Dr Iwan Hwan Harsono, Dr Noor Hakim bin Rafai, Dr Ee Hui Chang, Dr Miftahul Fauziah, Ms Mareese McCloughin, Pei Wen Lau and all the wonderful friends that I could not mention one by one here. Thank you for helping me in different aspects of my research.

On my journey, I met some scientists and engineers from Concrete Institute of Australia who gave valuable input for my research. Thank you very much to Dr Shindunata and Andrew Peek (GHD Pty), Dr David Law (RMIT), Dr Kwesi Sagoe Krentsil (CSIRO), Dr Tony Song (Boral), Ms Elaine Miller (Centre for Material Research, Curtin University) and Nhu Nguyen (SGS Laboratory).

I'd like to give the biggest appreciation to my husband, Gunawan Wibisono, who's very patient and helpful, always there for me in the good and bad times or up and down situation during my study. Thank you so much for your constant love, dear. I'd like to thank my dear parents & parents-in law, Papa Hailubis & Mama Lisma Erni, Bapak Wadijono & Ibu Supiyani for their constant support, prayers and love for us. Finally, I am grateful to my sister Ms Paulina Atry, my brother Mr Wahyudi, sister Cut Wulan and my little niece, Alila.

LIST OF PUBLICATIONS

The following publications were produced during my PhD research:

1) **Olivia, M**. and Nikraz, H., 2011 "Durability of Fly Ash Geopolymer Concrete in Seawater Environments", In: Proceedings of Concrete11, Concrete Institute of Australia Biennial Conference, October 2011, Perth, paper number 27.3.

2) **Olivia, M**. and Nikraz, H. 2011, "Strength and Water Penetrability of Low Calcium Fly Ash Geopolymer Concrete", ARPN Journal, Volume 6 no 7, July 2011.

3) **Olivia, M**. and Nikraz, H. 2010. "Corrosion Performance of Embedded Steel in Fly Ash Geopolymer Concrete by Impressed Voltage Method", In: 21st Australian Conference On Mechanics of Structures and Materials, Melbourne, December 2010, p.781-786.

4) **Olivia, M**. and Nikraz, H., 2009, "Corrosion of Low Calcium Fly Ash Geopolymer Concrete: a Preliminary Analysis", In: Proceedings of the 6th Asian Symposium on Polymers in Concrete, Shanghai, October 2009, p. 142-152.

5) **Olivia, M**. and Nikraz, H., 2009, "Durability of Low Calcium Fly Ash Geopolymer Concrete in Chloride Solution", In: Proceedings of the 6th Asian Symposium on Polymers in Concrete, Shanghai, October 2009, p. 153-161.

6) **Olivia, M**. and Nikraz, H., 2009, "Optimization of Fly Ash Geopolymer Concrete Mixtures in a Seawater Environment", In: Proceedings of the 24th Biennial Conference of the Concrete Institute of Australia, September 2009, Sydney, p. 188-189.

7) **Olivia, M**., Nikraz, H. and Sarker, P., 2008, "Improvements in the Strength and Water Penetrability of Low Calcium Fly Ash Based Geopolymer Concrete", In: Proceedings of 3rd ACF International Conference- ACF/VCA: Sustainable Concrete Technology and Structures in Local Climate and Environments Conditions, Ho Chi Minh City, October 2008, p. 384-391.

8) **Olivia, M**., Sarker, P. and Nikraz, H., 2008, "Water Penetrability of Low Calcium Fly Ash Geopolymer Concrete", In: Proceedings of the International Conference on Construction and Building Technology: Emerging Technology in Construction Materials, Kuala Lumpur, June 2008, p. 517-530.

9) **Olivia, M**. and Nikraz, H. 2011, "Properties of Fly Ash Geopolymer Concrete Designed by Using Taguchi Method", Materials and Design, in press, accepted manuscript

10) Javaherdashti, R., Nikraz, H., Borowitzka, M., Moheimani, N. and **Olivia, M**., 2009, "On the Impact of Algae on Accelerating the Biodeterioration/Biocorrosion of Reinforced Concrete: A Mechanistic Review" European Journal of Scientific Research, Volume 3, Issue 3, pp 394-40

TABLE OF CONTENTS

LIST OF FIGURES

LIST OF TABLES

Chapter 1

INTRODUCTION

1.1 Background

The production of Ordinary Portland Cement (OPC) contributes approximately 7-10% of the total carbon dioxide (CO_2) emissions globally. It was found that one tonne of the OPC produced by calcinations releases one tonne of CO_2 into the atmosphere. With an increase of the OPC production to supply a huge concrete demand for infrastructure projects in some highly populated countries such as India and China, a significant impact on the environment is inevitable. A high level of carbon emission contributes to global warming and climate change. There is a need to reduce the OPC usage by partial or total replacement of cement in the concrete mixture in order to deal with the environmental issue. Waste, or by-product, such as fly ash from coal combustion and slag from iron ore becomes a popular choice due to their positive contribution on strength and durability of the concrete. Also, those materials become increasingly available as by-products of industries such as power stations. In Australia alone, the production of fly ash was approximately 1.46 million tonnes per year in 2008, with only 35% being used in various applications.[1]

Geopolymer concrete has emerged as an alternative construction material that completely replaces the cement in the mixture. Starting with metakaolin and slag, fly ash has now transformed as a primary component of the geopolymer. The synthesis of fly ash geopolymer involves an activation of reactive amorphous silica and alumina in the fly ash by alkaline solutions. Considering the abundant amount of fly ash in landfill, the fly ash geopolymer could add more value to the by-product and simultaneously reduce the carbon footprint from a non-green cement production. To meet such a demand, the fly ash geopolymer has been studied extensively over the past several decades from an empirical standpoint to a science-based approach in order to explore its technical viability. The material apparently has a different composition, final product and characteristics than the OPC concrete. This is certainly can influence its mechanical properties and durability performance in various environments.

Nevertheless, the fly ash geopolymer concrete now faces a new challenge in implementing its application. The fly ash geopolymer concrete was reported to have good engineering properties that were comparable, or even higher, than the OPC concrete. However, durability or the ability of material to withstand deterioration caused by the environment in the long term has not been proven. It was reported the fly ash geopolymer is durable in some aggressive

environments, such as acid, sulphate and fire.[2-4] The low calcium content in the geopolymer is one reason for this behaviour, given that concrete with high calcium content is more susceptible to acid, sulphate and CO_2 ions attack. Calcium can be transformed into $CaSO_4$, $CaCO_3$, and $Ca(OH)_2$ once those aggressive ions attack the concrete. Nevertheless, studies on the fly ash geopolymer concrete durability in a seawater environment have been limited until now. Reinforced concrete structures in seawater environments are more prone to chloride-induced corrosion of steel reinforcement bars. Steel mass loss and cracking of concrete cover due to corrosion could reduce the serviceability of the structures in the long term. Surface degradation in the presence of salts and a temperature difference in continuous immersion and wetting-drying exposure of seawater environments increases the concrete porosity and affect the durability. Seawater is also a medium that contains microorganisms which causes microbial corrosion on steel reinforcement bars in concrete. Hence, with a combination of the harmful ions, environmental conditions and microorganism presence, it is important to design a durable fly ash geopolymer concrete for application in the seawater environment.

1.2 Research Significance

Geopolymer has been the subject of significant research and commercial interest over the past decade. The geopolymerisation process provides an opportunity for by product materials to be used as a valuable product, although the variability in the source materials results in different performance levels of the geopolymer products. In the meantime work is being carried out on the factors affecting geopolymerisation, mechanical properties, mechanisms of the process, and some brief aspects of durability. The research carried out concluded that the concrete has superior engineering properties as a construction material. However, in the longer term, the exposure of this concrete in severe environments, such as seawater, is inevitable and greater knowledge about its durability is important. Some reports stated that geopolymer has good durability; however these are very limited because of the use of different sources materials and activators, types of specimens and types of tests that were employed. The results of this research will provide scientific data and information about mixture optimization, strength development and durability of low calcium fly ash based geopolymer concrete that has been developed at Curtin University. Some important properties of concrete were used to determine its durability, namely water penetrability, seawater resistance and corrosion of steel reinforcement bar. More information regarding the durability of geopolymer concrete will lead to a wider acceptance of this material in engineering practices.

1.3 Research Objectives

The aim of the research is to study strength and durability of fly ash geopolymer concrete in seawater environment.

The objectives are:

a) To develop fly ash geopolymer concrete mixtures for reinforced concrete structures in seawater environments.
b) To assess the strength development, namely compressive strength, tensile strength, flexural strength, modulus of elasticity; water penetrability and drying shrinkage of the optimized mixtures.
c) To study the seawater resistance under continuous immersion and wetting-drying cycles by measuring change in mass, change in compressive strength, change in modulus of elasticity, change in effective porosity, and change in length of the optimum mixtures specimens. In addition, a chloride ion penetration is investigated.
d) To investigate the corrosion performance by half-cell potential measurement, an accelerated corrosion test under impressed voltage, and in a medium incorporating microorganisms.

1.4 Scope of Work

Class F fly ash from Collie, Western Australia was used as a single source material in this research. A combination of sodium hydroxide (NaOH) and sodium silicate was used to activate the fly ash. The basic mixture proportion calculation was developed by Geopolymer Research Group Curtin University. Some tests have been used in this research for strength and durability in compliance with certain guidelines.

1.5 Thesis Structure

The thesis is divided into five chapters as can be seen in Figure 1-1.
Chapter 1 introduces the background, research significance, and objectives of the thesis.

Chapter 2 gives an overview of fly ash geopolymer concrete in general, a recent development, performance criteria of concrete in the seawater environment, a mixture development, and durability of concrete in a seawater and microbiologically induced corrosion environment. The aim is to review the potential of fly ash geopolymer concrete to be used in the seawater environment.

Chapter 3 provides material properties data, preliminary study results on optimization of fly ash geopolymer concrete, testing methods for strength and durability and some developed in

house methods for a study of corrosion. The aim of this chapter is to present the research design that has been carried out to investigate the suitability of fly ash geopolymer concrete in a seawater environment.

Chapter 4 describes results and discussions of the experimental work. The aim is to provide information of the preliminary study, results from experimental work, display data and analysis of the findings.

Chapter 5 presents the final conclusions and recommendations for future work.

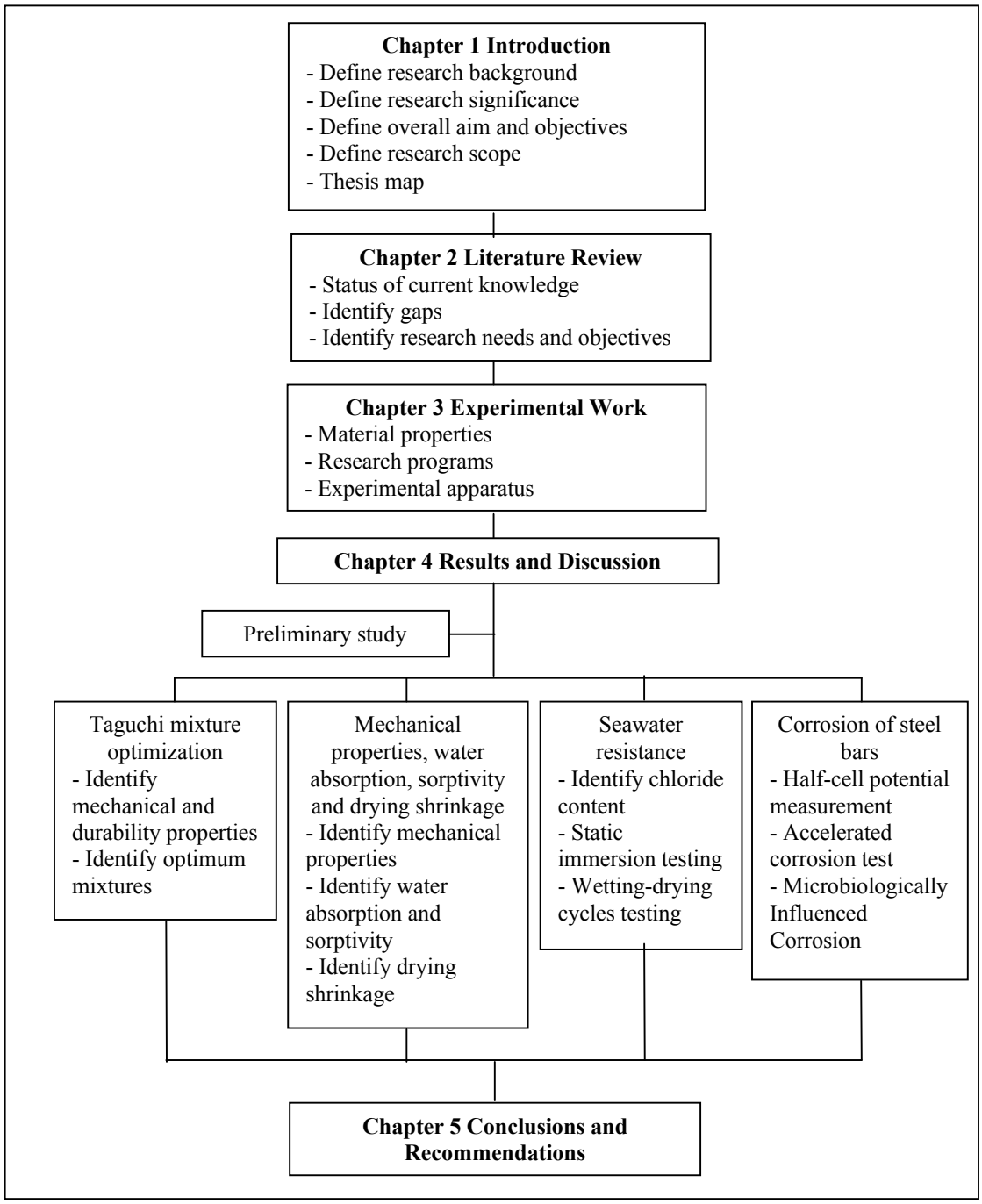

Figure 1-1 Thesis map.

Chapter 2

LITERATURE REVIEW

2.1 Introduction

Geopolymer is a material that can be used as a binder, coating, adhesive and cement. Davidovits initially invented the geopolymer in the 1970s in his search for a fire resistant material. An extensive research and development in a science and engineering background eventually recognized the geopolymer potential as an alternative construction material to Ordinary Portland Cement (OPC).

This chapter presents a background of geopolymer and a general overview of fly ash geopolymer concrete. A brief introduction of the fly ash geopolymer concrete and its components is presented. A mixture design of fly ash geopolymer concrete is also discussed in this chapter. Concrete in a seawater environment, the deterioration mechanism and its performance criteria are then reviewed. Key hardened properties of the fly ash geopolymer concrete in terms of strength and durability are discussed in detail. The final section presents a summary of the research needs and research objectives of the thesis. Figure 2-1 shows the layout of this chapter.

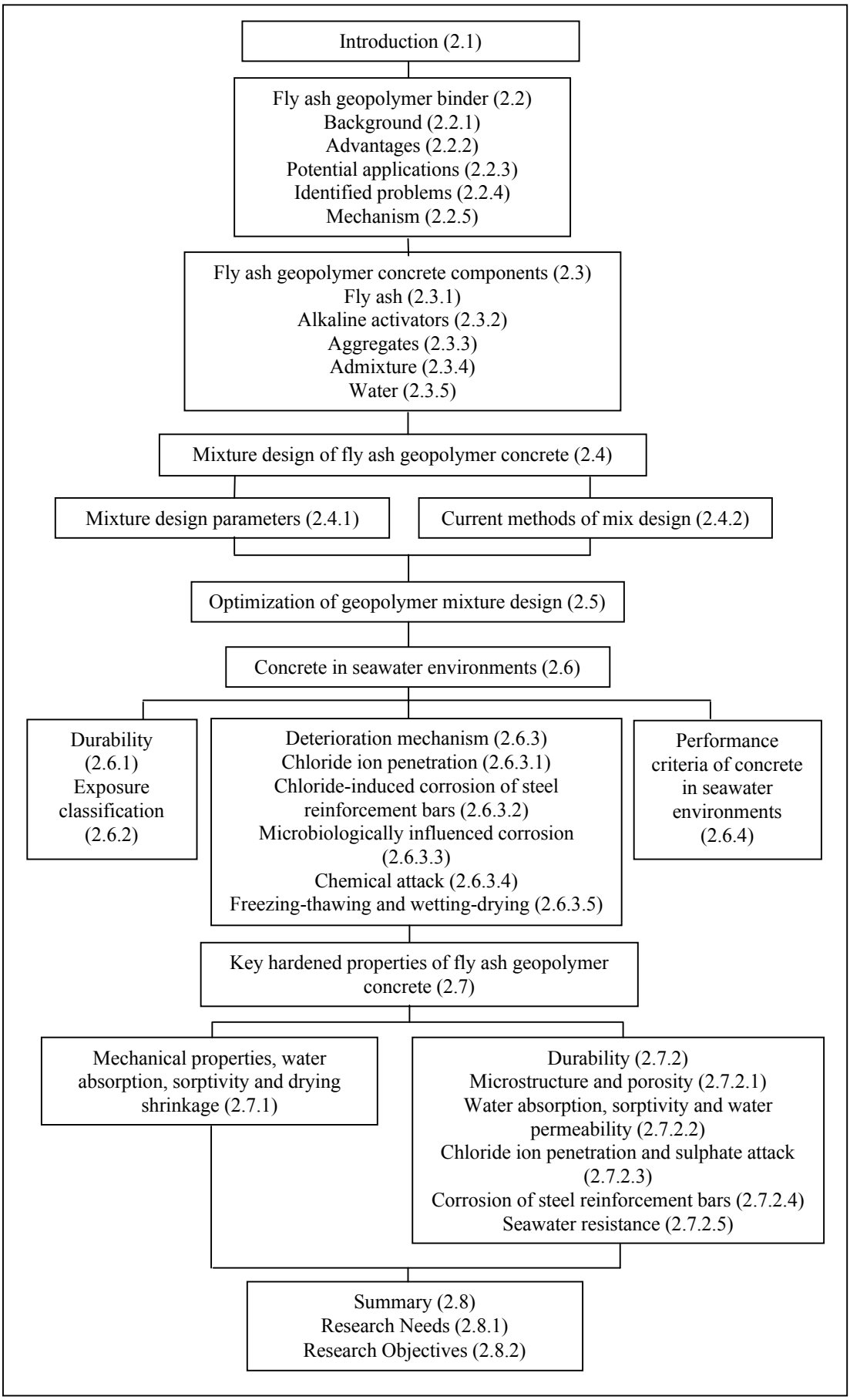

Figure 2-1 Layout of literature review.

2.2 Fly Ash Geopolymer Binder

2.2.1 Background

Geopolymer or polysialate was introduced by Davidovits as the amorphous to semi-crystalline three dimensional aluminosilicates.[5, 6] The chemical structure of geopolymer is formed by a tetrahedral SiO_4 and AlO_4 that connect and share all the oxygen atoms. To balance the negative charge of Al^{3+} in IV-fold coordination of the network, positive ions such as Na^+, K^+, Li^+, Ca^{2+} are required in the system. Early geopolymer that was made from metakaolin activated by NaOH and KOH became the model of this framework. The network configuration is shown in Figure 2-2.

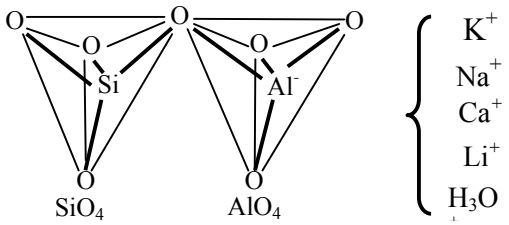

Figure 2-2 Tetrahedral configuration of sialate, ionic concept.[7]

There are three types of polysialate, i.e. polysialate (PS), polysialate-siloxo (PSS) and polysialate-disiloxo (PSDS). The empirical formula of polysialate was determined as follows:

$$Mn(-(SiO_2)_z\text{-}Al\text{-}O)_n, wH_2O \quad (2.1)$$

with Mn = alkaline element, - = bond, z = 1, 2, 3, and n = degree of polymerization.

The development of geopolymer material is basically driven by the availability of source material. Metakaolin was mostly used in the early development of geopolymer by various researchers.[8-10] The metakaolin geopolymer performed good mechanical properties, fire resistance and durability in seawater environment.[4, 11, 12] This material is limited for research purposes since it is not only expensive, but also requires a large amount of liquid to make it workable. Another source that is rich in SiO_2 and Al_2O_3 and which can be activated with the alkaline activators such as slag and fly ash is more potential to be developed.[13, 14] Both materials are by-products that are available abundantly in landfill, so the initial cost of producing geopolymer could be reduced. Slag and fly ash geopolymer produce different final products, namely Calcium Silicate Hydrate (CSH) and aluminosilicate, respectively. Until now, research and development for both materials are still progressing to make the slag and fly ash geopolymer more viable in applications.

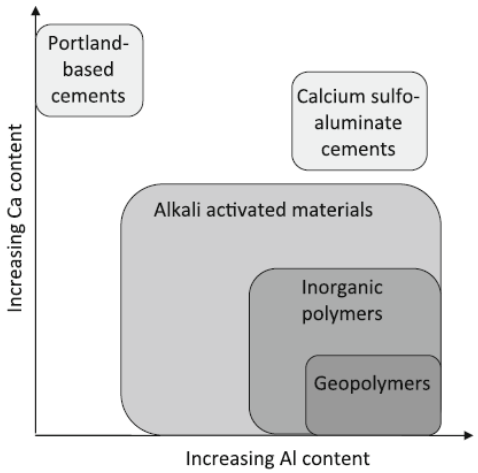

Figure 2-3 Classification of different subsets of AAMs, with comparisons to OPC and calcium sulfoaluminate binder chemistry.[15]

It is interesting to observe that in its development, the terminology used by many researchers for geopolymer may cause confusion. A schematic distinction of the terminology is given in Figure 2-3. Various material ranging from metakaolin, slag, fly ash, waste mud[16], and rice husk[17] that activated with many types of activators slightly changed the original terminology. Currently, van Deventer et al.[15] distinguished a definition of alkali activated materials, inorganic polymers and geopolymers based on the source material, alkaline activator and final product. Geopolymers are defined as a division of inorganic polymers and alkali activated materials that produce aluminosilicates as their final product. The source material is usually low calcium fly ash and calcined clays, with alkaline activators from alkali metal hydroxide or silicate. The inorganic polymers are part of the alkali-activated materials that has disordered silicate network as the final product. Alkali activated slag with a final product called Calcium Silicate Hydrate (CSH), is included in the inorganic polymers. The broader type is any binder system from a reaction of alkaline salt with a solid silicate powder, known as the alkali activated materials.

2.2.2 Advantages

Some advantages offered by the utilization of fly ash geopolymer concrete as construction material are as follows[3, 4, 18-22]:

a. Contributes to a reduction of carbon footprint by releasing only 78 kg/m^3 CO_2 through its production, compared to 248 kg/m^3 from OPC+slag concrete production.
b. Adds value to industrial by-products without using a conventional cement binder in the mixture.
c. Produces a high early strength concrete in a relatively short time due to a high temperature curing method.

d. Performs a low shrinkage concrete when it is cured at high temperature curing.
e. Performs a greater resistance to fire.
f. Improves concrete durability due to low calcium content in the mixture that can resist acid and sulphate attacks.

2.2.3 Potential Applications

The application of fly ash geopolymer concrete depends on its superior characteristics on mechanical strength and durability. Until recently, little information was available about the geopolymer concrete in application. Some trial projects on the fly ash geopolymer concrete has been successfully applied, such as sewer pipeline components and railway sleepers by Rocla[23] and an in-situ cast geopolymer pedestrian footpath at Curtin University[24]. Meanwhile, various studies have done identified further potential applications, which are mentioned in Table 2-1.

Table 2-1 Potential applications of fly ash geopolymer concrete

Structural/Elements Application	Geopolymer used purpose	Reference
Manhole structures and sewer pipes	Grout for rehabilitation in underground facilities	25
Sewage sewer pipes	Durable underground facilities	2, 26
Structural/non-structural laminates	Fire resistance elements and coatings	27, 28
Precast box culvert	Durable structural element in highly corrosive sulphate environment	29, 30
Reinforced concrete structures	Durable structural elements in seawater	31-33
Toxic waste containment	Toxic waste encapsulation	7, 22, 34
Brick lining at steel pickling tanks	Acid resistance material	35

2.2.4 Identified Problems

Despite the superiority of geopolymer in some areas, particularly where the OPC concrete does not perform well, the actual in-situ casting for application of the fly ash geopolymer remains an issue. Some problems regarding in-situ casting were identified as follows[7, 20, 36-38]:

a. The mixture needs to have very low water content, thereby reducing workability.
b. The mixture needs to be cured at a high temperature, which means finding an efficient technology to perform it.
c. Safety procedure of handling the mixture due to caustic chemicals involved
d. Efflorescence on the concrete surface that reduces the aesthetic appearance
e. Durability in application is still unproven, especially for corrosion of steel reinforcement bars in concrete structures.

2.2.5 Mechanism

Some theories were proposed by various researchers to explain the geopolymerisation mechanism.[39-41] The mechanism of geopolymerisation was described as being similar to

zeolite, which requires high pH, concentrated alkali, high pressure and high temperature in the system.[6] Initially, a reaction mechanism for the alkali-activated cement that contains silica and alumina was proposed by Glukhovsky in 1967.[40] The model has three stages comprising destruction-coagulation; coagulation-condensation; and condensation-crystallization. The theory was elaborated by many researchers studying the alkali activated cement mechanism based on their current knowledge of the zeolite formation.

Fernandez-Jimenez et al.[39] proposed dissolution and polymerization steps as a main part of the geopolymer reaction mechanism. In a descriptive diagram of geopolymerisation (Figure 2-4) the dissolution process starts with a chemical attack by hydroxyl ions on the surface of fly ash particles (Figure 2-4 a, b). The attack starts at one point of the particle surface, and then disperses to a wider area until the fly ash particle shell is totally covered by the reaction product (Figure 2-4c). The reaction product mentioned here is the aluminosilicate. The penetration of alkaline solution is progressing into the smaller particles located inside the fly ash spheres. An interior space is filled with the reaction product and a dense paste is produced at the same time. The process is not uniform due to the fly ash particle size distribution and local particle chemistry such as pH. Pore development and microstructure of the fly ash geopolymer are generated in this stage**.** It could be seen now the system consists of the complete reacted particles, reaction product and unreacted fly ash particles (Figure 2-4 d). The unreacted fly ash results from inhibition of the alkaline solution reacting with small spheres by the reaction products (Figure 2-4 e).

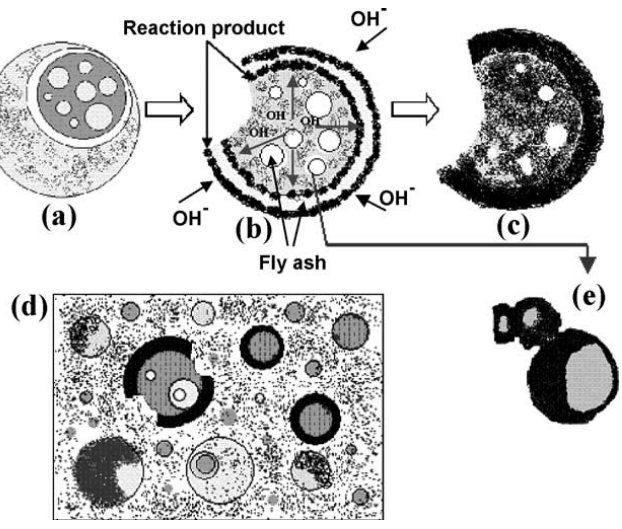

Figure 2-4 Descriptive model of the alkali-activation fly ash.[39]

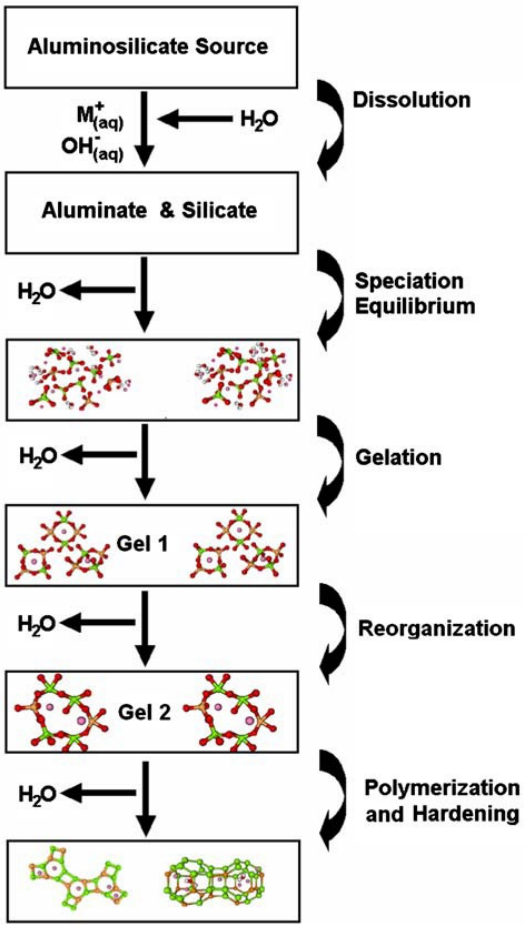

Figure 2-5 Conceptual model for geopolymerisation.[40]

Duxson et al.[40] proposed another mechanism of the geopolymer reaction that consisting of five major steps in Figure 2-5. First, dissolution of the source material by high alkaline ions produces aluminate and silicate species. Second, silicate and aluminate species are mixed together at speciation equilibrium stage to form aluminosilicate solution. It can be seen that water is released from the system after the dissolution process. Third, when a high concentration solution is formed at high pH, the gelation process takes place producing geopolymer gel. Fourth, the next process is a reorganization of the gel network, where pore and microstructure of geopolymer are developed. In the final step, a three dimensional geopolymer is produced.

The reaction steps of geopolymerisation is affected by several factors.[37] The first factor is aluminosilicate composition and mineralogy, comprising the amount of amorphous SiO_2 and Al_2O_3 in the material, the rate of dissolution of SiO_2 and Al_2O_3, the physical properties of raw material and impurities. The second factor is the activating solutions relating to silicate concentration (SiO_2/M_2O ratio), type of alkali metal cations, concentration of alkali solution (H_2O/M_2O ratio, where M is equal to Na and K), and water content (water/binder ratio). The

final influential factor is curing conditions, noting the effect of temperature, curing duration and temperature scheme, and humidity. Those factors were identified as parameters of the geopolymer mixture design in Section 2.4.1.

2.3 Fly Ash Geopolymer Concrete Components

2.3.1 Fly Ash

Fly ash can be defined as a fine-grained product from bituminous hard coal combustion in power station furnaces.[42] The product consists of oxides of silica, aluminium, iron and some calcium. Since it is created at high temperature, the fly ash is glassy and chemically stable. It can be used in fly ash geopolymer synthesis because it is rich in silica and alumina, two major sources of the geopolymerisation process. The activator is needed in this process to initiate reaction and hardening, given that fly ash cannot naturally harden in water.[41] Fly ash from various sources is claimed to have different mineralogy and solubility that influence the reaction rate and finally the physical characteristics of the geopolymer.[43] Clearly, the analytical calcium (CaO) content, glassy phase and particle size distribution were the main factors that distinguished the final geopolymer product. The high CaO content (more than 15%) could increase a setting time. Fly ash with the high content of glass phase and finer particles could increase a degree of reaction and reactivity, resulting in higher degree of geopolymerisation and consequently higher compressive strength.[44]

The fly ash particles vary in physical and chemical properties due to the coal source and type, the minerals and metals in the coal, the furnace type and the combustion temperature.[45] The physical and chemical properties determine the fly ash utilisation in practice. The physical properties of fly ash exhibit a different range of values, appearance and particle size. Some particles have low density (hollow), which is less than 1000kg/m^3, while others may have a density of more than 2600kg/m^3. The fly ash is usually light to mid-grey colour and looks like cement powder. The size ranges from 1μm to larger than 300 μm. In general, Australian fly ash has more than 75% of particles passing through a 45 μm sieve which indicates a fine grade, according to AS3582.1.[46] The percentage of ash passing the 45 μm is one of the criteria to classify fly ash as an inclusion in Portland or blended cement concrete mixture. Finer ash particles has a positive effect on the final strength of geopolymer concrete.[44, 46] Optimal binding of geopolymer requires 80-90% of particles with sizes less than 45 μm.[47] Figure 2-6 shows the typical raw fly ash particles from Collie, Western Australia under SEM having spherical particles with different sizes.

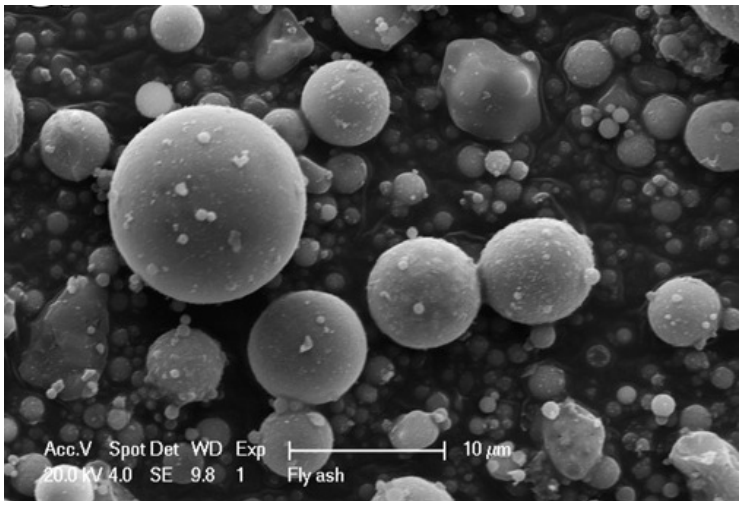

Figure 2-6 Raw Collie fly ash particles.[48]

The fly ash can also be classified by its chemical composition. According to ASTM C618, there are two classes of fly ash, class F (low calcium) and C (high calcium). Class F fly ash has a total sum of silicon dioxide, aluminium dioxide and iron oxide (SiO_2+Al_2O_3+Fe_2O_3) of minimum of 70%, loss on ignition (carbon content) maximum of 6% and calcium oxide less than 10%. Class C fly ash has a minimum of 50% total of the major elements (SiO_2+Al_2O_3+Fe_2O_3) and calcium content of 20-40%. The fly ash in Australia is normally classified as class F, based on the chemical properties of various ashes produced by some power stations in New South Wales, Queensland and Western Australia.[46] The low calcium fly ash is frequently used in the geopolymer manufacturing by many researchers since the high calcium fly ash is unstable in the geopolymerisation. This high calcium content in the geopolymer system can increase the reaction rate that leads to a fast setting and production of Calcium Silicate Hydrate (CSH) in the microstructure. The CSH was susceptible to change the ordinary geopolymer network that leads to mechanical strength reduction.[49-53] Only a few authors have reported their work on the high calcium fly ash geopolymer.[50, 54]

2.3.2 Alkaline Activators

Alkaline activators have a function in generating the geopolymerisation and increasing the kinetic of the reaction. The activator can be a single material such as $Ca(OH)_2$, NaOH, or Na_2SiO_3 (sodium silicate).[55, 56] It can be also a combination of materials such as NaOH and sodium silicate, a combination of KOH and NaOH, KOH, potassium silicate and its combination.[20, 57-59] The sodium silicate is included instead of NaOH, to enhance polymerisation of ionic material in the geopolymer system.

NaOH is used because it is cheap, has low viscosity and is the most widely available geopolymer production. Also, the hydroxyl ion ⁻ in NaOH is an important element in starting

the geopolymerisation process. In an aqueous system, this ion is essential in increasing the reaction rate of the dissolution of alumina and silica bond.[60] When a high concentration of the ion OH^- is available in the system, the silica-alumina classy chains will rapidly disintegrate and develop a large number of Si-OH and Al-OH groups or a geopolymer network.[61] The dosage of NaOH used in the geopolymer production can determine the final strength of material, since the compressive strength increase with increase in the molar concentration of NaOH.[62]

Sodium silicate (Na_2SiO_3) is available on the market in both a liquid and a powder form. It has a high viscosity that influences the geopolymer mixture workability when a highly concentrated one is used. Sodium silicate in the geopolymer system, is not only useful to increase the final strength of the paste,[41] but is also used to bind the material together to produce a dense paste. When the sodium silicate (Na_2SiO_3) reacts with water (H_2O), it results on NaOH and hydrolysed sodium silicate. This combination produces a very high pH environment that disintegrates the silica alumina chain in fly ash.[41] Both chemicals, NaOH and sodium silicate, when combined in a correct ratio, produces a solid material almost without pores and has a strong bond between aggregate and geopolymer paste.[63] However, an excessive content of sodium silicate not only increases the mixture's flow ability but also the porosity.[49]

2.3.3 Aggregates

The quantity of aggregate comprises of 70-80% of normal concrete mixture in general practice. In the OPC mixture, the aggregate/cement ratio controls the strength properties. A high aggregate content in the mixture leads to low shrinkage, low bleeding, and small voids of concrete.[64] In contrast, there is no correlation between the aggregate and the final strength of geopolymer concrete. An increase in the aggregate content in the geopolymer mixture normally results in a smaller amount of alkaline solution left to react with the fly ash. However, no decline of mechanical strength is reported afterwards.[65] It was also found that a strong chemical bonding between the aggregate and the geopolymer paste changes the interfacial transition zone (ITZ) in the geopolymer microstructure. A partial dissolution of aggregate surface with geopolymer gel could be a reason for the non existence of ITZ, particularly when the geopolymer is activated with the soluble silicates.[66] The only drawback of mixture with a low amount of alkali and a high quantity of aggregates was a very low workability and flow ability.

2.3.4 Admixture

High range water reducer admixture has a role to maintain workability of a low water content mixture. A study on naphthalene admixture used in alkali activated cement, such as slag,

indicates an increase in mechanical strength and workability.[67] In contrast, the naphthalene formaldehyde in the geopolymer mixture caused a quick set although there was an improvement on the workability.[68] The inclusion of naphthalene sulphonate superplasticizer in the fly ash geopolymer mixture showed a workability improvement without a significant increase in compressive strength.[69] A recent finding suggested an elimination of the superplasticizer in the geopolymer mix. The superplasticizer was insignificant in improving the workability due to the spherical nature of fly ash particles that make it flow more easily with an appropriate composition of alkaline activators.[70]

2.3.5 Water

As one of the components in fly ash geopolymer mixture, water is used in a very small amount compared to the OPC mixture. Water content in the geopolymer mixture is a total of extra water, and water from NaOH and sodium silicate. Water quantity is critical due to its role in the geopolymerisation. It was observed that a high water content delays the disintegration of silica and alumina in fly ash particles and also the formation of geopolymer gel.[37] This could lead to a reduction of the mechanical properties of concrete. The quantity of water content needs to be kept as low as possible in the mixture in order to produce higher mechanical strength. On the other hand, a further decrease of water content in the geopolymer could reduce the workability making it difficult to compact and mould.[71]

2.4 Mixture Design of Fly Ash Geopolymer Concrete

2.4.1 Mixture Design Parameters

Fly ash geopolymer components such as source material, alkaline activator and curing method are some major parameters that influence the final properties of the geopolymer product. Table 2-2 summarises some parameters affecting the final product of the geopolymer concrete from selected literature. Compressive strength and porosity are two main properties described in the summary.

Table 2-2 Summary of mixture design parameters obtained from selected literatures

No	Fly ash type	Fly ash quantity	Alkaline activator						Curing method	Water content	Aggregate	Property measured/ values	Significant findings	Ref
			NaOH concen-tration	Sodium silicate	SiO_2/Al_2O_3 ratio	Na_2O/Al_2O_3 ratio	Sodium silicate/ NaOH	Alkaline solutions/ fly ash ratio						
1	class F	36.96-73.91%	14M	SiO_2/Na_2O = 2.0			2.5	0.35	24 hours at 70^{O}C		Binder/sand ratio: 1.0-9.0	UCS: 50-60 MPa Density: 2-2.9 g/cm^3 Open porosity: 6.1-9.8% Young's Modulus: 227-2.44 GPa	The open porosity decreased as the level of aggregate increased. An increase in aggregate proportion reduced the amount of geopolymerisation, but strength reduction was marginal.	65
2	class F + Rice husk ash	0-100%	14M, 18M	SiO_2/Na_2O = 1.57	4.03-1035	1.07-138	(1): 2.5 (2): 0.5-3.5		Room temp. (27^{O}C) + 24 hours at 60^{O}C			UCS (28d) series 1: 34.0-56.0 UCS (28d) series 2: 21.8-39.4	SiO_2/Al_2O_3 = 15.9 was used to achieve optimum compressive strength. An increase in SiO_2/Al_2O_3 ratio lead to elastic materials. Compressive strength increased with a decrease of Na_2O/Al_2O_3 ratio.	72
3	class C	Sand:FA ratio 2.75	10, 15, 20M	SiO_2/Na_2O = 2.14			0.67-3.0		(a) 1, 2, 3, 4 days at 60^{O}C; (b) 0, 1, 3, 6 hours delay + 24 hours at 60^{O}C; (c) 24 hours at 30, 45, 60, 75, 90^{O}C	2.3-7.9% of FA		Flowability: 110±5, 125±5, 135±5% UCS: 10-65 MPa	The mortar flow was decreased with an increase of NaOH and sodium silicate concentration. The optimum sodium silicate/NaOH ratio: 0.67-1.0. Prolong curing of 1 hour, curing at 75^{O}C and less than 2 days gave a high strength concrete.	70
4	class F		5, 8, 12M						Pre cured for 24 hours at room temp. + 6-48 hours at 40-80^{O}C	Liquid/soli d ratio = 0.3-0.4		UCS: 15-70MPa	High compressive strength produced from mixes that was cured for 48 hours at 80^{O}C and used 12M NaOH.	73
5	class F		6M					0.50	(a) 28 days at 27^{O}C (b) 24 hours at 27^{O}C + 4 hours at 60^{O}C	Liquid /solid ratio = 0.35		UCS of mechanically activated fly ash	Compressive strength increased with median particle size due to reactivity of fly ash.	74
6	class F		2-10% Na	SiO_2/Na_2O = 2.02					(a) 24 h at room temp. + 24 h at 75^{O}C/95^{O}C; (c) 24 hat room temp. + 6 h at 75^{O}C/95^{O}C	Water/ binder ratio = 0.3		UCS: 5-45MPa	Precuring at room temperature followed by high temperature was advantageous for strength development.	20
7	class C		5, 10, 15M	SiO_2/Na_2O = 3.2	3.3-4.5	0.8-1.2	0.5-2.0	FA/NaOH ratio = 3	48 hours at 65^{O}C	FA/liquid ratio = 1.5	Sand/FA ratio: 2.75	UCS: 15-70 MPa	The high compressive strength of 60-70MPa was achieved using 10M and 15M NaOH, SS/NaOH: 1.0 (separate mixing: fly ash+NaOH for 10 minutes).	75
8	class F		98%	SiO_2/Na_2O = 0.5-2.0	1.99-3.44				24 hours at room temp. + 6 days at 55±2^{O}C	Water/FA ratio = 0.50-0.87	Sand/binder ratio: 3	UCS: 0.26-43.21 MPa	Fly ash fineness, particle size distribution, sodium silicate SiO_2/Na_2O = 1.5, contributed to a high compressive strength.	76
9	class F		4, 6, 8M		1.75			Alkaline sol./binder = 0.4, 0.5, 0.6	24 hours at room temp. + 24/48 hours at 60^{O}C/75^{O}C			UCS: ±5 - ±30 MPa Porosity: 7-16%	Compressive strength increased with high curing temperature, activator concentration and decreased in activator/binder ratio. Porosity decreased with an increase in alkaline solution/binder ratio.	62
10	class F		8-16M	SiO_2/Na_2O = 2.0	2.0-3.5		0.4, 2.5		6-96 hours at 30-90^{O}C	H_2O/Na_2O = 10		UCS: 25-80MPa	Compressive strength increased with high NaOH concentration, high sodium silicate/NaOH ratio, and high curing temperature.	69
11	class F		12M					0.25, 0.30	2, 5, 24 hours at 65^{O}C and 85^{O}C			UCS 24 hours: 3.9-68.7 MPa	Type of activator and curing temperature were significant parameter for mechanical strengths. Alkaline solutions/fly ash ratio was a marginal parameter.	59
12	class F + kaolin								6, 12, 24, 48 hours at 30, 50, 70^{O}C	Water/fly ash = 0.33-0.43		UCS 12 hours at 70^{O}C: 34 MPa; UCS 24 hours at 70 ^{O}C: 33 MPa	Water content and curing influenced the mechanical strength. Curing for 12 hours at 70 ^{O}C gave the highest strength.	9
13	class F								24 hours at 30, 50, 75^{O}C	Water/fly ash = 0.3			High temperature curing and silicate content increased the strength and reduced the pores.	49

FA: fly ash; GP: geopolymer; UCS: Unconfined Compressive Strength

It can be seen from Table 2.2 that the fly ash, aggregate, alkaline activator and curing are some parameters that determine the geopolymer final compressive strength and porosity. Fly ash with a high degree of particle fineness and glassy phase is more reactive and can increase the geopolymerisation rate that eventually produces a high strength concrete.[44, 74, 76] The alkaline activator type and dosage are significant to achieve high compressive strength and decrease the porosity. Generally, various researchers used SiO_2/Al_2O_3 and Na_2O/Al_2O_3 ratios as a composition range in producing geopolymer material. Mixtures with good strength properties and durability is usually produced using composition range from $1<SiO_2/Al_2O_3<5$ and Na_2O/Al_2O_3 ratios ~1.[77] The concrete produced with SiO_2/Al_2O_3 <1 or SiO_2/Al_2O_3 >5 tend to have poor strength, low chemical resistance, excessive amount of Na/Al which increase the tendency to dissolve in water and greater efflorescence on the concrete surface. Therefore, good strength properties were obtained by using low Na_2O/Al_2O_3 ratio, high NaOH concentration, high sodium silicate/NaOH ratio, and low alkaline/fly ash ratio in the mixture.[62, 69, 72] Curing at high temperatures and for a longer period of time, for example at least 24 hours at 60^0C, 12 hours at 70^OC and 24 hours at 75^OC normally produces high strength properties.[9, 49, 69] A very high temperature and curing period longer than two days could damage the microstructure. Concrete becomes more porous even though it has a high strength. It was found that a high amount of aggregate in geopolymer concrete mixture is not significant enough to increase the compressive strength.[65] However, mixes with a high aggregate content could decrease the porosity due to less porous geopolymer paste in the system.

2.4.2 Current Methods of Mix Design

A development of fly ash geopolymer mix design is a critical issue because standard method is not available. There is no systematic development in this area until now, which is probably due to a variability of local source materials and alkaline activators. The composition range of SiO_2/Al_2O_3 and Na_2O/Al_2O_3 ratios, alkaline/fly ash ratio, H_2O/Na_2O ratio obtained from previous research is normally used in designing the geopolymer mixture composition. Previous investigators reported successful mix designs.[49, 69, 78] High mechanical strength properties became a main indicator of this success.

To make the geopolymer more viable in application, the next stage of mix design was aimed to fulfil a durability requirement. A method that combines several factors using optimization by Taguchi method was used by Song[79] to design the geopolymer mixtures composition. Parameters such as Kaolite fly ash content, dosage of alkaline activator solution, composition of alkaline activators and curing conditions were employed in the study. The optimum mixtures were used to produce geopolymer concrete that can sustain a sulphuric acid environment.

Another issue that needs to be addressed is the porosity of fly ash geopolymer paste. Although the previous mix design produced fly ash geopolymer mixtures with acceptable strength properties and durability, high porosity concrete is still apparent.[65, 80] Another method was proposed to minimize the porosity by taking a particle packing density approach.[81] By applying this method, one could tailor all requirements to produce high strength and low porosity geopolymer concrete to ensure its durability in the long term. Since currently there is no standard for designing the fly ash geopolymer concrete, a systematic approach to produce a design mix guideline is needed.

2.5 Optimization of Geopolymer Mixture Design

In a conventional experimental design, one factor at a time is a common approach. This means that one factor is kept varied and the other factors are kept constant. This approach is costly and time consuming, particularly in testing all parameters. For a material like the geopolymer concrete with its many related variables, it is important to find the most efficient way to obtain an optimum mix design for a certain application. The Taguchi experimental design is a popular statistical method for quality engineering and has been used by some researchers in concrete technology areas for optimizing blended cements, self-compacting concrete and durable mixtures.[82-84] Concrete mixtures can be designed efficiently by minimizing the variability of the investigated parameters and focusing on the target values with this method.

The basic principle is to combine all potentially good parameters and test them to achieve optimum results. It can save on the cost and time of doing many trials to try all possible combinations. This approach can reduce time and cost on testing all possible combinations by using one factor at a time to fulfil Full Factorial Experiment (FFE). The procedure and steps of the Taguchi Parameter Design are to select factors, to select number and levels for the factors, to select appropriate Orthogonal Array (OA), to assign factors and interactions, to conduct tests, to analyze results and to carry out a confirmation experiments.[85] In this method, every combination of levels appears in the same repetitions. This approach creates the opportunity for all variables to be tested to obtain the optimum mixture. An example of orthogonal array of OA_9 (3^4) is given in Table 2-3.

Table 2-3 A combination of OA_9 (3^4) orthogonal array that can produce nine trials mixes.[85]

Trial	Factor A	Factor B	Factor C	Factor D
1	1	1	1	1
2	1	2	2	2
3	1	3	3	3
4	2	1	2	3
5	2	2	3	1
6	2	3	1	2
7	3	1	3	2
8	3	2	1	3
9	3	3	2	1

To study a response of the experiment that combine repetitions and the effect of noise levels into one data point, we can use Signal/Noise (S/N) ratio analysis.[85] The ratios were created in the Taguchi method to combine some repetitions into one value, which reflects the amount of variation present. Some S/N ratios such as Lower is Better (LB), Nominal is Best (NB) or Higher is Better (HB) were provided and the equations for calculating these characteristics were as follows:

Lower is Better (LB)

$$S/N_{LB} = -10\log(\frac{1}{r}\sum_{i=1}^{r} y_i^2) \tag{2.2}$$

where r = number of tests in a trial (number of repetition regardless of noise levels)

Nominal is Best (NB)

$$S/N_{NB_1} = -10\log Ve \text{ (variance only)} \tag{2.3}$$

$$S/N_{NB_2} = +10\log(\frac{Vm - Ve}{rVe}) \text{ (mean and variance)} \tag{2.4}$$

Where Vm = degree of freedom associated with the mean (always 1), Ve = degrees of freedom associated with error

Higher is Better (HB)

$$S/N_{HB} = -10\log(\frac{1}{r}\sum_{i=1}^{r}\frac{1}{y_i^2} \tag{2.5}$$

2.6 Concrete in Seawater Environments

2.6.1 Durability

Durability issues become a main concern of the designer and the engineer, where formerly their focus had been mostly on the strength characteristics of concrete. Durability of concrete can be defined as the ability of concrete to withstand the environment during service life

without any significant deterioration such as weathering action, chemical attack and abrasion. When concrete is able to provide the desired service life in its environment without a high maintenance cost to repair it due to deterioration, the concrete is considered durable.[86] In fact, the quality of concrete governs its durability in the aggressive environments.

Durability is related with the reinforced concrete structures performance in the long term. Figure 2-7 shows the relation between durability and performance, based on Comite Euro International du Beton (CEB) design guide.[87] In the initial stage of producing durable concrete, a design, material selection, execution and curing was determined. The resulting concrete usually has various pore distribution characteristics that can influence the transport properties, such as absorption, diffusion, sorptivity that determine the concrete quality.

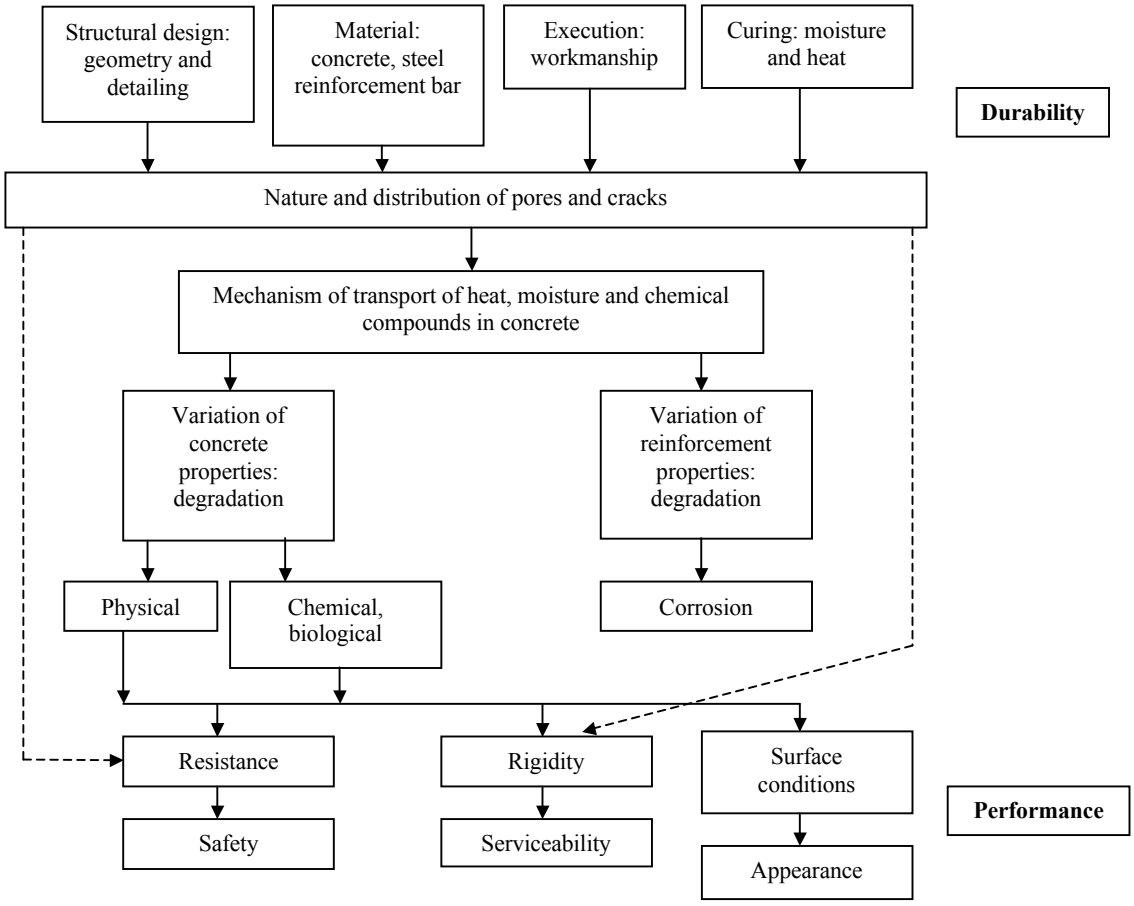

Figure 2-7 Relationship between durability and performance.[87]

In the next stage, degradation due to physical, chemical and biological factors occurring over time is identified. Physical degradation such as abrasion of heavy particle suspended in water and freezing thawing in the frost environment might change the physical appearance of the reinforced concrete. Chemical deterioration is generally caused by factors such as carbonation,

an acid attack, a sulphate attack to aluminates in the cement, and alkali-aggregate reaction with reactive aggregates in the concrete. Cracks, decomposed concrete, and expansion due to an accumulation of reactive substances can increase the rate of concrete deterioration. Biological degradation on concrete is usually due to microorganisms such as microalgae, bacteria and fungi. This biological attack leads to mechanical deterioration such as cracking and decomposition of concrete. It may also cause a chemical attack, since microorganism such as Sulphate Reducing Bacteria (SRB) produces strong acid that can dissolve cement paste. Corrosion of steel reinforcement bars in concrete is not only due to variation of material, but also due to loss of alkalinity in the concrete, which induced this mechanism. This is the most detrimental type of degradation and can lead to a total loss of the load-carrying capacity of structures in the long term. As can be seen in the figure, the durability of hardened concrete certainly affects the resistance, rigidity and surface conditions or the performance of concrete during its service life.

2.6.2 Exposure Classification

Structures in the seawater environment exposed to chlorides in four different exposure conditions, namely coastal, splash, tidal, and submerged zones (Figure 2-8). The coastal zone is the marine atmospheric zone where concrete is not in direct contact with seawater and not receiving any salt from blown spray. Concrete in the tidal and splash zone is submerged for certain periods each day and normally is subjected to a cyclic exposure to seawater. The submerged zone is located below tide where the concrete is continuously submerged.

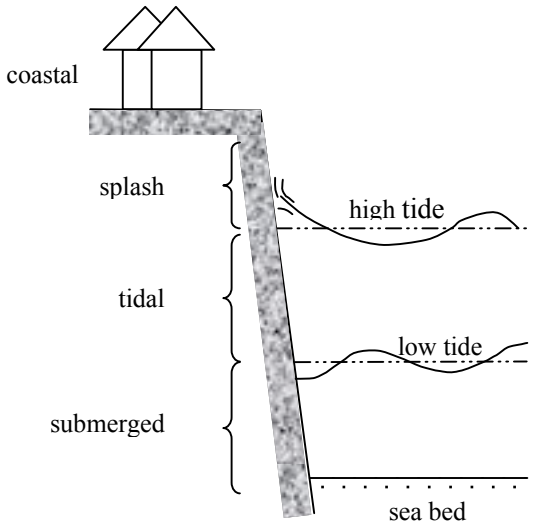

Figure 2-8 Types of marine exposure.[87]

Deterioration of concrete structures in the seawater environment occurs in various zones. Figure 2-9 displays specifically the types of deterioration of concrete structures in the seawater. The most prevalent deterioration in the coastal zone is the corrosion of steel reinforcement bars induced by chloride and frost damage. While in the splash zone, the corrosion of reinforcement, abrasion due to the wave action and frost damage could deteriorate the concrete. The harshest environment is the tidal zone, causing abrasion due to wave action, floating ice and ship collisions; chloride induced corrosion; frost damage; biological fouling and chemical attacks on concrete. In the submerged zone, the common deterioration is the chemical attack on concrete and biological fouling and attack by organisms.

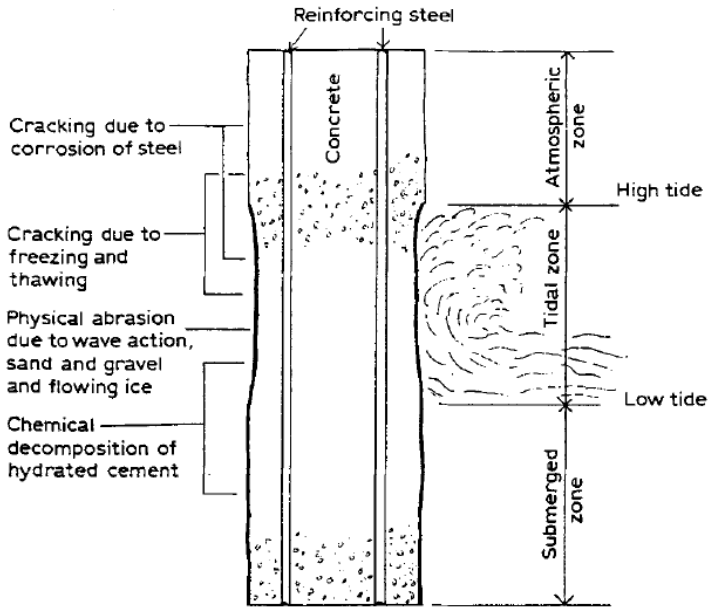

Figure 2-9 Deterioration of reinforced concrete structures in seawater.[88]

2.6.3 Deterioration Mechanism

2.6.3.1 Chloride Ion Penetration

Chloride ion in seawater is the most common cause of corrosion of steel bars in the concrete structures. Chlorides destroy the passive film that surrounds steel reinforcement bars in an aqueous medium, generating corrosion. The chlorides also reduce the solubility of $Ca(OH)_2$ and pH of pore water solution. The chlorides increase the moisture content of concrete pores due to its hygroscopic properties. Finally chlorides can increase the electrical conductivity of concrete.[89] The transport mechanism of the chlorides into the concrete depends on exposure conditions. Diffusion, permeation, and capillary absorption are some of the mechanisms that can occur in reinforced structures in the seawater environment. Table 2-4 summarises the primary chloride transport mechanism for various exposures.

Table 2-4 Chloride transport mechanism for various exposures.[90]

Exposure	Example of structures	Primary chloride transport mechanism
Submerged	Substructures below low tide	Diffusion
	Basement exterior walls or transport tunnel liners below low tide. Liquid containing structures.	Permeation, diffusion and possibly Wick's action
Tidal	Substructures and superstructures in the tidal zone	Capillary absorption and diffusion
Splash	Superstructures about high tide in the open sea	Capillary absorption and diffusion (also carbonation)
Coastal	Land based structures in coastal area or superstructures above high tide in river estuary or body of water in coastal area	Capillary absorption (also carbonation)

The most important transport mechanism on the chloride movement is the chloride diffusion that can be modelled on a Fick's second law of diffusion. This law can quantify chloride in marine environments despite multiple transport phenomena. The law can be expressed as follows[91]:

$$C(x,t) = Cs\left[1 - erf\left(\frac{x}{2\sqrt{Dt}}\right)\right] \tag{2.6}$$

where C(x,t) = chloride concentration at depth x at time t, D = diffusion coefficient, Cs = surface chloride concentration, erf = error function.

The chloride penetration in concrete is governed by physical factors such as the type of binder, water/binder ratio, mixture proportions, compaction, curing, exposure period that mostly influence the porosity or permeability of the concrete.[92] Low water to binder ratio, good compaction and good curing are normally suggested to produce low porous concrete that can resist chloride ion penetration. An inclusion of mineral admixtures such as slag, fly ash and silica fume, could significantly increase the concrete's resistance to chloride penetration by improving the pores and resistivity.[93]

The chloride concentration or chloride threshold level in concrete plays a major role initiating the corrosion of reinforcement steel bars. A chloride threshold can be defined as a chloride content at the depth of the steel that will result in the breakdown of passive film.[94] Concrete composition and quality, exposure conditions and rebar surface characteristics are some factors that change the chloride threshold concentration. The chloride concentration in a water-soluble chloride form (free chlorides) influences the corrosion process more than acid soluble chloride (total chloride content in concrete). The water-soluble chloride threshold values for different types of reinforcement are given in Table 2-5.

Table 2-5 Maximum water soluble chloride values from ACI and EN Standards.[95]

Maximum % chloride by mass of cementing material	ACI C318-05	EN 206.1:2000
Prestressed	0.06	0.10 (0.20 if dry*)
Reinforced and exposed to chlorides	0.15	0.20
Reinforced in dry conditions	1.0	0.40*
Reinforced in damp conditions	-	0.20*
Other reinforced concrete construction	0.30	-
Non-reinforced	-	1.0

*Assumed, since it was not clear from Table 10 of EN 206.1

The chloride binding capacity of concrete is another issue related to chloride ion penetration. Chlorides can be chemically bound by a reaction of chlorides with C_3A to form calcium chloroaluminate $3CaO.Al_2O_3.CaCl_2.10H_2O$ or Friedel's salt.[93] It means a high C_3A content in concrete is desirable to minimize chloride-induced corrosion, despite some disadvantages such as sulphate attack and a high early of heat evolution during hydration process. Another way to increase the chloride binding capacity is to use blended cements. Blended cements incorporating fly ash and slag contain Al_2O_3 which can enhance the chloride binding capacity. An increase in the fly ash content can increase the alumina in the concrete, hence the chloride binding capacity of concrete.[96, 97]

2.6.3.2 Chloride-induced Corrosion of Steel Reinforcement Bars

Chloride-induced corrosion is one of the main factors that cause corrosion in seawater environments.[98-101] The corrosion process is an electrochemical process involving chemical reactions and electrical current flow. The two-electrochemical reactions are known as anodic and cathodic reactions that occur at the anode and cathode of the steel bar. The anodic reaction represents dissolution of metal, while the cathodic reaction represents a combination of water, oxygen and electron to form hydroxyl ions. Figure 2-10 illustrates the electrochemical process occurs in the corrosion of reinforcement steel bar in concrete.

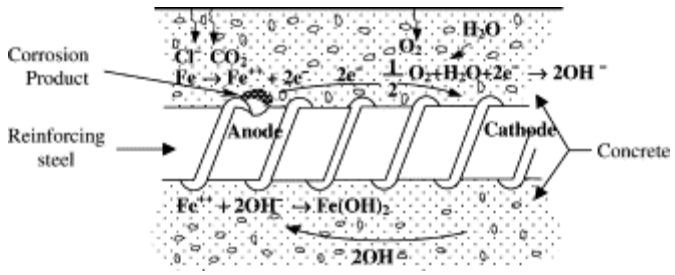

Figure 2-10 Schematic illustration of the corrosion of reinforcement steel in concrete—as an electrochemical process.[102]

The anodic reaction depending upon the pH of electrolyte, the presence of harmful ions and the existence of an appropriate electrochemical potential at the steel surface[102]:

$$Fe \rightarrow Fe^{2+} + 2e^{-} \quad (2.7)$$

The cathodic reaction is influenced by the availability of O_2 and pH of the steel surface. The reactions at cathode are as follows:

$$2H_2O + O_2 + 4e^{-} \rightarrow 4OH^{-} \quad (2.8)$$

Corrosion of reinforcement steel bars in concrete is critical for three reasons.[103] First, corrosion of the embedded steel causing volumetric expansions, rust stains, continuous cracking, and spalling of the concrete. Second, as a corrosion process is progressing, a loss in cross sectional area of the steel is inevitable. A reduction of the steel cross-sectional area reduces a load-bearing capacity of the reinforcement. Third, loss of bond because of corrosion reduces a transfer of high tensile strength of steel to concrete. The most damaging effect of the corrosion is cracking and spalling of concrete cover due to continuous expansion of corrosion product.[104] Cracking occurs when the concrete cannot prevent the pressure from corrosion product further. Cracks causing a high rate of oxygen and water penetrate into the concrete thus increasing the corrosion rate. Spalling of concrete cover indicates a serious damage on the concrete structures since it cannot be repaired or replaced.

Corrosion measurements can be used to obtain the corrosion rate or corrosion mechanisms. Electrochemical techniques, such as half-cell potential measurements are the simplest technique, which can be used to determine corrosion potential. In this test, a voltage difference between a reference electrode and steel reinforcement bar is measured. When the corrosion starts in the concrete in the presence of moisture and oxygen, there is a short-circuit galvanic cell formed from passive and corroding areas in the steel reinforcement bar. The corroding area serves as anode and the passive area as cathode. The current flow, which is proportional to steel mass loss in the anodic reaction, results in equipotential lines where most corroded areas have negative values.[104, 105] The corrosion potential then was compared with threshold values to allow interpretation of corrosion risk. The values are presented in Table 2-6.

Table 2-6 Interpretation of half-cell potential values (mV) relative to reference electrode

$Cu/CuSO_4$ reference electrode[105]		SCE reference electrode[106]	
Values	Risk of corrosion	Values	Risk of corrosion
>-200	Low	>-200	90% probability of no corrosion
-200 to -350	Moderate	-200 to -350	Moderate risk of corrosion
>-350	High	>-350	90% probability of corrosion

Some conceptual service life models were proposed to understand the corrosion stages of reinforcement steel bars in concrete.[107, 108] The first model, developed by Tuutti[107] consists of two stages called initiation and propagation. Figure 2-11 shows a schematic illustration of the corrosion process of steel in concrete. The initiation stage or depassivation is the stage when the harmful ions penetrate into the steel surface, destroy the passive film of rebar, and start the corrosion. This stage occurs as a result of CO_2 and Cl^- penetration into the concrete. Hence the concrete quality, cover thickness, exposure conditions and chloride ion content influence this initial stage. The second stage is a propagation or corrosion process. This is where the corrosion takes place. Oxygen availability, concrete electrical resistance or resistivity and relative humidity control the corrosion rate. Although it is widely used to model serviceability, it was found that this model underestimates the time to corrosion cracking of specimens in a real application.

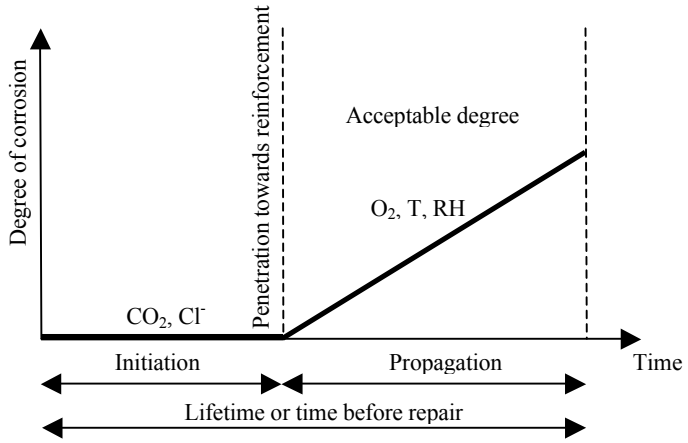

Figure 2-11 Schematic drawing of the corrosion process of steel in concrete.[107]

Corrosion products are not only generating stress around the concrete, but also filling the voids and pores around the steel reinforcement bars. Sometimes the corrosion products migrate away from steel bar surface through concrete pores into the outer surface. Figure 2-12 illustrates the corrosion cracking process that consists of three stages, namely free expansion, stress initiation and concrete cracking. In the free expansion stage, as long as the total amount of corrosion products (W_T) is less than the amount of corrosion products required to fill the porous zone (W_P) there will be no stress generated in the concrete. In the second stage, stress is initiated when W_T exceeds W_P and creates pressure around the steel reinforcement bar. However, since the limiting amount of the corrosion products needed to induce cracking of the cover concrete (W_{crit}) is not achieved yet, there is no cracking. In the final stage, when W_T is higher than W_{crit}, the internal pressure exceeds the tensile strength of concrete, and cracking of concrete cover occurs.

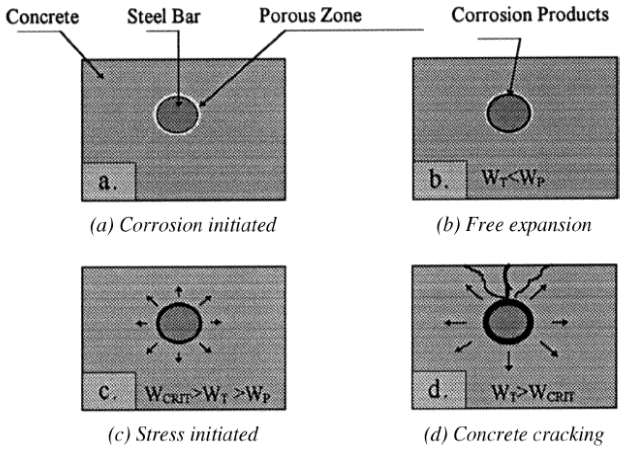

Figure 2-12 Schematic diagram of corrosion cracking processes.[109]

Figure 2-13 shows a modified service life model by Liu and Weyers.[109, 110] This model divides the propagation stage into free expansion and stress initiated periods. The time needed for corrosion products to fill the porous zone around the steel reinforcement bar (T_{free}) was defined in the expansion stage. In the second stage, T_{stress} is defined as the time when the stress builds up and expansive pressure on the surrounding concrete begins. Cracking of concrete cover occurs when the internal tensile stress exceeds the tensile strength.

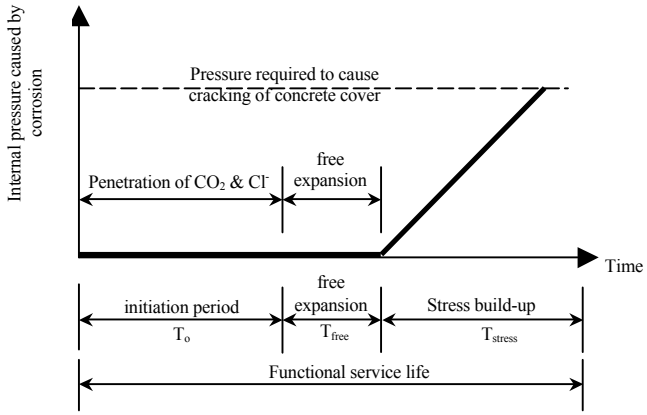

Figure 2-13 A modified service life model from Liu and Weyers.[110]

2.6.3.3 Microbiologically Influenced Corrosion

Microbiologically Influenced Corrosion (MIC) is known as one type of corrosion involving microorganisms. In general, the microorganisms associated with the MIC can be classified into three groups, namely fungi, algae, and aerobic/anaerobic bacteria. Anaerobic bacteria could initiate and enhance the corrosion through a production of acidic metabolites such as sulphuric acid. Aerobic bacteria and algae form biofilm that could alter the oxygen content to allow differential aeration in the steel surface, thus starting the corrosion.

Various authors have reported the effect of MIC on reinforced concrete structures with different microorganisms involved. Sulphate Reducing Bacteria (SRB) has a major role in sewer pipes by producing hydrogen sulphide that deteriorates concrete with an extremely low pH.[111-114] The impact of microalgae on water distribution canals through a reduction of water quality and its flow rate in the channels has also been reported.[115] The MIC was also found in many historical buildings caused by algae, cyanobacteria and fungal. The attack causes water retention, biodeterioration and discoloration of the exterior surfaces of the buildings.[116]

There is no a new form of corrosion process in MIC, since a presence of the microorganisms only changes the environment around the metal surface to facilitate the corrosion process. Some processes involved in the MIC were identified, such as production of differential aeration and concentration cells due to the absorption of nutrients; and production of corrosive metabolites.[117] In determining the corrosion mechanism of MIC, two terms are used: anaerobic and aerobic. Corrosion under the anaerobic condition is usually from microorganisms such as algae, protozoa and iron oxidizing bacteria incorporating oxygen. Sulphate Reducing Bacteria, which grows without oxygen can be classified as aerobic.

Another type of concrete deterioration in submerged or tidal zones is a biological fouling or Microbiologically Influenced Corrosion (MIC). However, there is little literature associated with MIC inducing corrosion in concrete in a marine environment.[118, 119] Marine structures such as offshore oil drilling steel platforms are often used as a study of MIC corrosion. It was found that microalgae can induce corrosion on welds joints of massive marine structures such as North Sea oil drilling platforms.[120, 121] Micro algae are a type of microorganism that can cause MIC by producing oxygen through the photosynthetic process and building up the oxygen in the biofilm. The accumulated oxygen increases the cathodic reaction and the subsequent corrosion rate.[122] Judging by the severe impact of MIC, research and development involving MIC corrosion of steel embedded for concrete in a seawater environment is urgently needed.

MIC due to biological fouling or biodeterioration could be incorporated in the design or modelling of the durability of reinforced concrete structures in the seawater environment. Figure 2-14 illustrates the biodeterioration effect on the concrete integrity.[123] The biodeterioration becomes active in the second stage after concrete pH decreases and the biofilm formation begins. The diagram shows that a chemical barrier such as pH or alkalinity is always essential in extending the service life of structures due to chloride induced corrosion and MIC.

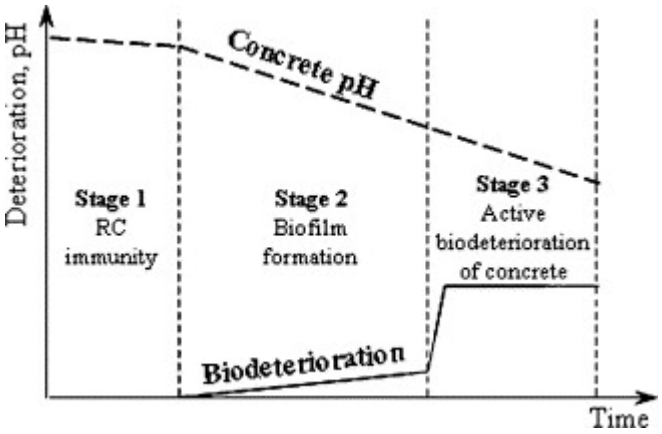

Figure 2-14 Conceptual model of biodeterioration.[123]

2.6.3.4 Chemical Attack

Seawater normally has 3.5% dissolved salts comprising magnesium sulphate and sodium chloride. Sulphate ions cause a common attack on cement paste by promoting chemical reactions that result in expansion, cracking and spalling. Although the exact mechanism remains unclear, a reaction between the sodium sulphate (Na_2SO_4) with portlandite (CH), monosulphate and unreacted C_3A, forms gypsum (CSH) and ettringite ($C_6AS_3H_{32}$).[124] It was found that softening, erosion and loss of concrete constituents is more prevalent than expansion due to the ettringite formation. Concrete which is in seawater for an extended time may endure many different types of attacks, as shown in Figure 2-15.

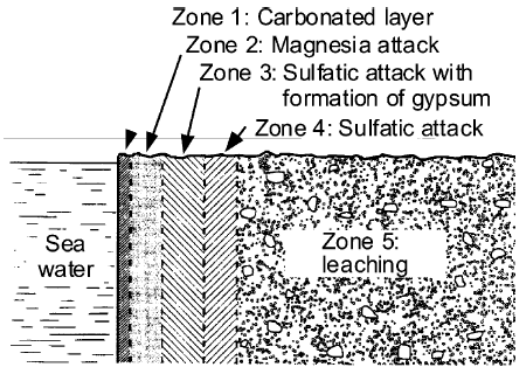

Figure 2-15 Schematic representation of the different altered layers found in concrete marine structure.[125]

It is generally known that the sodium chloride alone is not as destructive as the dissolved sulphate ions on concrete in seawater environments.[64, 126] A severe chemical attack of chloride ions normally occurs in collaboration with dissolved CO_2 or high temperatures and humidity. It was reported that a subsequent effect due to chloride reactions and the seawater environment

favour the reactions. The chloride and CO_2 combination could lower the concrete pH and increase the chance of $Ca(OH)_2$ solubility by leaching. This is due to a change in pore composition and ionic force of the pore solution. When chlorides diffuses into the cement paste, there is a counter-diffusion of hydroxide ions to maintain the solution electro neutrality that results in an increase of portlandite solubility.[127, 128]

2.6.3.5 Freezing-Thawing and Wetting-Drying

The marine environment has tidal and splash zones, where extreme conditions of freezing-thawing and wetting-drying occurs. These mechanisms are influenced by seawater temperature and type of seasons. In subtropical waters the freezing thawing is a common mechanism with a consequence of concrete spalling or cracking due to an extreme temperature difference.

Cyclic wetting-drying is more dominant in tropical waters, which could lead to erosion, salt crystallization in the concrete pores and expansion of the concrete cover. The wetting-drying process in the seawater environment was described by Neville as follows.[93] The cyclic wetting by seawater and drying by air causes continuous moisture movement through the concrete pores. When the dry concrete is exposed to seawater, the salts are absorbed by the concrete until it is saturated under some conditions. If the external surface is dry again, the water evaporates from capillary pores, leaving the salts behind. For particular time, there is a concentration gradient inside the concrete; the salts travel further into the internal side of the concrete by diffusion. The excess salts inside the concrete precipitates out as crystals in the concrete pores. Finally, after the concentration gradient decreases from a peak value, some salts diffuse toward the surface of the concrete. Salt crystals will appear on the surface of the concrete. The accumulative salt crystals in the concrete pores may generate pressure and expansion, which could lead to the concrete cover cracking.

2.6.4 Performance Criteria of Concrete in Seawater Environments

Concrete structures in the seawater environment need to be designed to follow a strict regulation with strength and durability requirements. The Australian Standard 3600[129] (AS3600) is used as a key standard in designing concrete structures for durability in Australia. Several other codes such as AS 5100 for bridges, AS 4200 for marine structures, AS 4048 for concrete pipes, AS 3735 for liquid retaining structures are used for structures with specific requirements and environments. According to AS 3600, the exposure classifications determine the designed concrete characteristics. A revision has been made for exposure classification C, which has been divided into two classes, C1 and C2. Table 2-7 shows the exposure classification by AS 3600.

Table 2-7 Exposure classification by AS 3600[129]

Surface and exposure environment	Exposure classification
In contact with ground	A1, A2, U
In interior environment	A1, A2, B1
Above ground	A1, A2, B1, B2
In water	B1, U
In sea water	
(a) Permanently submerged	B2
(b) In spray zone	C1
(c) In tidal/splash zone	C2
Other environments	U*

*Refer to AS 3735

The minimum strength, curing requirement and strength at the time of formwork removal for concrete in various exposure classifications is given in Table 2-8. AS 3600 also limits the required cover thickness for corrosion of steel reinforcement bar protection (Table 2-9).

Table 2-8 Minimum strength and curing requirement for concrete[129]

Exposure	Minimum characteristic strength, f'c (MPa)	Minimum initial curing requirement	Minimum average compressive strength at the time of stripping of forms or removal from moulds (MPa)
A1	20	Cure continuously for at least 3 days	15
A2	25		
B1	32	Cure continuously for at least 7 days	20
B2	40		25
C1	50		32
C2	50		

Table 2-9 Corrosion protection of cover to reinforcement where standard formwork and compaction are used[129]

Exposure classification	Required cover (mm) Characteristic strength, f'c				
	20 MPa	25 MPa	32 MPa	40 MPa	≥ 50 MPa
A1	20	20	20	20	20
A2	(50)	30	25	20	20
B1		(60)	40	30	25
B2			(65)	45	35
C1				(70)	50
C2					65

The performance specification is not only used as a design tool, but can also be used in the pre-qualification and as a quality control on postproduction. Durability of concrete in seawater environment cannot be specified from compressive strength only, since other measures such as chloride penetration and sorptivity are important properties that reflects the durability in the long term.[130] It is interesting to note that in a real application, many specifications for high risk and structures in severe exposures are used to compliment AS 3600. For example, the Road

Transport Authority (RTA) and Main Roads use methods developed in house for application with no precise guideline in the code of standard. As there is no other detail performance criteria requirement except the compressive strength and concrete cover, a standard with a detail guideline for durability is greatly needed. It also has to accommodate new binder types other than the OPC, such as blended cement and geopolymer. The performance criteria for concrete in marine environments are given in Table 2-10.[95, 130]

Table 2-10 Performance criteria for concrete in seawater environment in Australia[95, 130]

Type of test	Standard Method	Property measured	Performance criteria	Ref.
Mass increase under unit of time	ASTM C1585, GHD, CSIRO, RTA B80, Ho [131]	Sorptivity/ Rate of water absorption	B2: 0.442-0.52 mm/min$^{0.5}$ C: 0.208 mm/min$^{0.5}$ (maximum) Poor: >0.2 mm/min$^{0.5}$ Acceptable: 0.1 – 0.2 mm/min$^{0.5}$ Very good: <0.1 mm/min$^{0.5}$	90 132
	BS 1881	Initial Surface Absorption Test (ISAT)	Durability ranking : #1, <50 (ml/m^2/sec x10^{-2}) # 2, 51-70 (ml/m^2/sec x10^{-2}) #4, 91-110 (ml/m^2/sec x10^{-2}) #3, 71-90 (ml/m^2/sec x10^{-2}) #5, >110 (ml/m^2/sec x10^{-2})	105
Absorption by water saturation/ boil method	ASTM C642 AS 1012.21	Absorption and permeable voids (AVPV) (rodded cylinders)	Excellent: VPV <12%, immersed & boiled absorption <5% Good: VPV 12-14%, immersed & boiled absorption 5-6% Normal: VPV 14-15%, immersed & boiled absorption 6-6.5% Marginal: VPV 15-17%, immersed & boiled absorption 6.5-7.5% Bad: VPV >17%, immersed & boiled absorption >7.5%	133
Torrent permeability	RILEM	Porosity	Good: <10%, Average: 10-15%, Poor: >15%	105
	RILEM TC 116-PCD	Gas permeability	Good: <2x10^{-18} m/s, Average: 2x10^{-18} – 2x10^{-17} m/s, Poor: >2x10^{-17} m/s	
Electric/conductivity charge passed	ASTM C1202/ AASHTO T277	RCPT	Charge passed: > 4,000 High 2,000-4,000 Moderate 100-1,000 Very Low 1,000-2,000 Low <100 Negligible	134
Immersion, profile grinding and titration	Nord Test Build 443	Chloride ion diffusion	Good: <1x10^{-12} m^2/s, Average: 1x10^{-12} – 5x10^{-12} m^2/s, Poor: >5x10^{-12} m^2/s	105
Long term corrosion data	ASTM C876	Corrosion potential	Half-cell potential vs CSE: >-200 90% probability of no corrosion -200 – -350 Moderate risk of corrosion >-350 90% probability of corrosion	106
Water permeation by pressure method	DIN 1048	Water permeability coefficient	Good: <10^{-12} m/s, Average: 10-^{12}-10^{-10} m/s, Poor: > 10^{-10} m/s	105, 132
Wetting-drying cycle in 3.5% chloride solution	CIA	Cyclic chloride penetration test	Chloride penetration depth sprayed by $AgNO_3$ solution and chloride content	130, 135

2.7 Key Hardened Properties of Fly Ash Geopolymer Concrete

During the last decade much of the research reported the fly ash geopolymer hardened properties. Most of the studies carried out explored the strength properties and durability as a

key performance in application. This section briefly overviews the strength properties and durability of the fly ash geopolymer concrete.

2.7.1 Mechanical Properties, Water Absorption, Sorptivity and Drying Shrinkage

Numerous studies have been reported to measure of the compressive strength, tensile strength, flexural strength and modulus of elasticity of fly ash geopolymer mortar and concrete.[78, 136, 137] The fly ash geopolymer concrete has a high early compressive strength gain that is equivalent to the OPC concrete. High temperature curing, high silicate concentrations in concrete and very low water content contribute to this positive behaviour. The application of this material for structures that require a high early strength is promising. The compressive strength within a range of 20 to 95 MPa has been reported.[138] There was no significant reduction of compressive strength with the concrete age due to the available alkalinity, reaction to refill the aluminosilicate gel and crystallization.[71, 139] A decline of strength of geopolymer made from a combination of the fly ash with rice husk ash has highlighted this issue.[140] The lack of geopolymer binder, the occurrence of micro cracks, high drying shrinkage were some reasons for such behaviour.

Tensile strength is another favourable property for the seawater structures. High tensile strength could reduce the early crack propagation due to stress accumulation by corrosion product of steel reinforcement bars. The tensile strength of fly ash geopolymer concrete is equivalent or higher than the OPC concrete.[136] The high tension properties of concrete was assumed from a good bonding between geopolymer paste and the interface of aggregates.[137] However, there is no report on the tensile strength development with age of the fly ash geopolymer concrete, which is important for the application purposes.

The flexural strength becomes one of the criteria for concrete in the seawater environment. Flexural strength represents the tension properties of concrete and could be related to cracking of concrete cover. The high flexural strength is favourable due to lack of tension stress produced by internal or external loading factors in the concrete. Fly ash geopolymer concrete usually exhibits a higher flexural strength than the OPC concrete. When it was compared with the Australian Standard design equation, the flexural strength of geopolymer concrete was very high.[136] It seems that a similar process in the compressive strength development discussed previously also occurs in the tension properties of the fly ash geopolymer concrete. The flexural strength demonstrated by the fly ash geopolymer concrete is advantageous in decreasing the rate and extent of cracking due to the corrosion of reinforcement.[141]

Modulus elasticity is also an important measurement in application although it is not included in the performance criteria for concrete in the seawater environment. In application, a high modulus elasticity material is essential to ensure the available stiffness to minimize a deflection of reinforced beams due to continuous loading. The geopolymer concrete has a considerably smaller value than the OPC concrete.[78, 136] It is known that the modulus elasticity of concrete depends on the modulus of elasticity of the aggregate and modulus of elasticity of geopolymer paste.[64] The concrete paste is typically influenced by its microstructure. Concrete microstructures which are porous with a high amount of ITZ could reduce the modulus of elasticity significantly. However, the geopolymer concrete has a good bonding or adherence between paste and aggregates without ITZ. Initially, the aggregate type was suspected in contributing to the low modulus of elasticity of geopolymer concrete.[142] However, a recent investigation by Sofi et al.[136] shows that the inclusion of coarse aggregate in the geopolymer mixture actually increases the modulus of elasticity. Another finding stated that the modulus elasticity is largely determined by the geopolymer microstructure.[143] Therefore, this area needs further investigation to obtain a clear explanation for this property.

Certainly, from the above review there is still considerable scope to develop further research. Studies on the effect of the various parameters on the mechanical strength, the mechanisms, which lie behind the mechanical properties behaviour, and model development to predict the behaviour in compliance with some standard application are necessary.

2.7.2 Durability

2.7.2.1 Microstructure and Porosity

A number of studies have been conducted on the microstructure of fly ash geopolymer using SEM, XRD, and EDX.[20, 39, 41, 49, 51, 76, 144] The morphological analysis was taken by scanning electron microscopy (SEM) and energy dispersive X-ray analysis (EDX). EDX was employed to study elemental composition analysis. The X-ray Diffraction (XRD) was used to determine the phase composition of the reaction products. The geopolymer has a heterogeneous microstructure with fully or partially unreacted fly ash particles. The product is an amorphous material with nanosize pore characteristics that contains crystalline phases (zeolite).[41, 49, 62, 76]

The microstructure of geopolymer is governed by the particle size distribution and chemical composition of fly ash, the type of alkaline activator and dosage, and the curing temperature. Fernandez-Jimenez et al.[39] investigated the morphological of fly ash mix with three different alkali activators, namely NaOH, NaOH+sodium silicate and NaOH+Na_2CO_3. The study found the main reaction product of all types of mixtures is aluminosilicate gel. The first mix has a considerable amount of unreacted fly ash, indicating that a moderate degree of reaction in the

system uses NaOH as a single activator. The final product of the second system activated with NaOH+sodium silicate showed a compact material with a small amount of pores. The bond between paste and aggregates was very good. The final mix that activated with NaOH+Na_2CO_3 has the most porous paste. The phase composition observed by XRD then revealed the zeolite such as herschelite formed in all types of mixtures; hydroxysodalite was also formed in the mixture activated with sole NaOH solution.

The alkaline solution type and dosage produced a different type of microstructure. The microstructure of fly ash activated with three different NaOH concentrations as observed by Ravikumar et al.[62] NaOH concentration increases a degree of reaction to form more aluminosilicate gel, which has a positive effect on the geopolymer strength. Another research[41] highlighted that the microstructure of fly ash geopolymer activated using a combination of NaOH and sodium silicate. It has a stronger bond, more adhesion between pastes, has an excellent connectivity between gels and produces high strength material. SEM analysis shows the high silicate concentration in the system leads to a high compressive strength due to lack of zeolite (crystalline phases) is produced.[76] In contrast, a low silicate concentration in the system could produce large particles which may be a reason for lower compressive strength.[49]

The effect of curing temperature and duration can be observed through microstructure. Jo et al.[41] confirmed a system cured at low temperature (20^OC) has more unreacted fly ash as the result of low adherence between particles. The same conclusion was also found when the geopolymer cured at 30^OC.[49] The resulting geopolymer shows more porous structures compared to the one that was cured at 75^OC. High temperature curing results in a greater degree of aluminosilicates gel formation than low temperature, hence affecting the final strength of the geopolymer. Hence, the high temperature curing was recommended due to the resulting strong bond in the geopolymer paste.[41]

Microstructure could give an indication of pore structures, however but the accurate porosity measurement can be investigated using other techniques. Fly ash activated with NaOH+sodium silicate has porosity of 20-40%.[144] By using the vacuum saturation technique[62], the porosity of fly ash geopolymer was around 8.5-14%. Pores larger than 200nm resulting from the geopolymer mixture cured at 30^OC indicated the influence of curing temperature in the pore formation.[49] High temperature and high silicate concentration can decrease the pore size. High concentrated NaOH was also recommended to decrease geopolymer porosity. It was found the porosity increases when the system has a high activator/binder ratio.[62] The curing temperature and the activator concentration also influences porosity, hence those critical parameters need to be investigated to modify the geopolymer porosity.

2.7.2.2 Water Absorption, Sorptivity and Water Permeability

The water absorption, sorptivity and permeability are some key parameters of concrete cover quality. In the seawater application, it is important to have watertight concrete, which can prevent the ingress of harmful ions such as chloride and sulphate into the concrete, especially in the seawater and sulphate environments. These properties are actually linked to the concrete porosity. There have not been many publications in this area until very recently. Some publications indicated that the water absorption always exhibits lower values than the corresponding OPC control mixture which is a good characteristic for durable concrete.[79, 145] Adam et al.[31] observed the effect of changing alkali modulus on the sorptivity of fly ash geopolymer. When the alkali modulus was increased from 0.75 to 1.25, the sorptivity or rate of water absorption decreased. The effect of increasing SiO_2 content in the system was also significant in changing the capillary porosity of the geopolymer.[49] Interestingly, an increase in the Na_2O content in the fly ash geopolymer system also reduces the sorptivity.[146, 147] Thus variation in the mixture compositions and the role of alkaline activators are quite significant in changing these property values. It was reported that the water permeability coefficient of some fly ash geopolymer concrete mixtures was classified 'low'.[29] Since the water absorption, sorptivity and water permeability become a key performance of the concrete in seawater environment, more data with various mixes regarding these properties is strongly desirable.

2.7.2.3 Chloride Ion Penetration and Sulphate Attack

Chloride ion in seawater plays a role in destroying the passive film of steel reinforcement bars and starting corrosion. Certain methods quantifying chloride ion penetration of geopolymer concrete have been used by various researchers.[148, 149] An investigation using RCPT (Rapid Chloride Penetration Test) indicated the presence of various anions in the fly ash geopolymer system has distorted the test by performing a high temperature over a 6 hours testing period.[148] A very high charge values that is an anomaly in testing of the normal concrete was observed. The applied voltage of 60V also induced heating and the test had to be stopped after 30 minutes. It might be a result of high conductivity due to various ions in the concrete microstructure. This shows that the RCPT is not suitable to measure chloride ion penetration in the geopolymer concrete. Similar findings were also confirmed for blended cement concrete.[150] Another finding shows a very low chloride ion penetration in fly ash geopolymer using Rapid Chloride Migration apparatus.[149] Recently Llyod et al.[151] argued that there was an anomaly in that result since the low chloride ion diffusion coefficient in a range of 10^{-15}-10^{-18} m^2/s was too low compared to the OPC concrete mixed with any mineral admixture. There are no indicative chloride ion diffusion values for fly ash geopolymer concrete; hence, it is important to obtain the data. The test should be carried out using a method without any electrical circuit to eliminate the magnetic effect on the various anions in the fly ash geopolymer system.

Sulphate attack on fly ash geopolymer concrete is also another threat in the seawater environment instead of the chloride penetration. The geopolymer shows no change in mass and compressive strength up to one year in the artificial sulphate environment.[3,152] It seems that the alkaline activator influences the stability of the polymer structure in sulphate solution. The paste that was activated by sodium silicate could form ettringite and results in a strength loss, while the paste that was activated with sodium hydroxide was more stable in the seawater environment due to porosity reduction and the increased strength of the concrete. The high alkali content (Na_2O) in the mixture that can improve the fly ash geopolymer concrete performance in sulphate environment was also confirmed.[153] Further observation showed the sulphate ions migrated inward into the concrete pores in a form of sodium sulphate. Traces of ettringite in the fly ash geopolymer concrete pores were discovered through EDX due to the presence of low calcium content.

2.7.2.4 Corrosion of Steel Reinforcement Bars

Corrosion of steel reinforcement bars embedded in geopolymer material has been an object of study by a limited number of researchers. It was started by Morris and Hodges[154], various metals such as carbon steel, stainless steel and aluminium were embedded in fly ash geopolymer mortar. A risk of corrosion by half-cell potential measurement, and corrosion rate by Electrochemical Impedance Spectroscopy (EIS) and Linear Polarization Resistance (LPR) were investigated. There was a small risk of corrosion and corrosion rate was considerably low for normal carbon steel. It was concluded that the corrosion resistance of steel reinforcement embedded in the fly ash geopolymer is high as long as the paste could maintain its alkalinity. Another study was carried out on the corrosion resistance of steel reinforcement bar in the fly ash geopolymer mortar in a chloride free environment.[155] It was concluded that the geopolymer paste could perform the same role as the OPC paste, which could maintain the passive film of the steel bar. The highlighted key problem is the alkalinity of fly ash geopolymer paste that determines the corrosion risk in the long term. Once the fly ash geopolymer mortar reinforced with steel bars was immersed in 2% chloride, it was found that the chloride destroyed the passive film of the rebar as fast as the OPC concrete.[33] This fact shows that the alkalinity might be decreased by another mechanism such as leaching that was influenced by the concrete permeability.

The alkalinity in the cement system is an essential property, which prevents the passive film of steel bar from corroding. Initially, the alkalinity of geopolymer material was suspected to be harmful for alkali-silica reaction, however it was beneficial in maintaining the passivity of the steel bars in the concrete.[156] The high alkalinity from alkaline activators is actually being used for geopolymerisation to produce the aluminosilicate gel. However, a significant alkalinity

reduction was observed when the geopolymer was hardened. A residual alkalinity in the range of pH 8-10 is considered quite low and can increase a corrosion risk in the long term.[102] Another finding also revealed that after 6 years, there was a reduction of alkalinity by 1.22-3.43 fold from the initial alkalinity values at one hour.[157] It becomes a serious issue, because the alkalinity of the cement is the first type of protection from harmful chloride ions in the seawater environment.

Corrosion study is a slow process that occurs over a long period until the specimens crack by the corrosion products. Some studies were dedicated to justify the accelerated corrosion test by impressed current or voltage for studying the corrosion performance of rebars in particular materials.[158,159] Fly ash geopolymer was exposed to the accelerated corrosion test by impressed voltage method initially by Yodmunee and Yodsujai.[160] They concluded a good corrosion resistance was performed by the fly ash geopolymer concrete than the control OPC concrete mixture. However, a limited time of charging by up to 72 hours, low voltage used and low compressive strength of specimens in the study are not significant to represent the corrosion performance of concrete in the long term and application. Hence, it is desirable to continue this study using a higher impressed voltage into the system, a longer exposure charging time and a higher strength concrete that meet requirements for marine structures. Further study on the corrosion rate due to weight loss compared with theoretical Faraday's Law is also important and needs to be investigated.

The corrosion study of fly ash geopolymer concrete is still a new area where the previous studies are limited to the corrosion risk. There is still a lack of study on corrosion rate, microstructure and characterisation of corrosion product of the fly ash geopolymer concrete. It is also important to develop a service life model for this type of concrete in the seawater environment, to predict the durability of structures in the long term. Then, there is a considerable scope to explore this area to obtain more data in corrosion of steel reinforcement bar in fly ash geopolymer. Inclusion of various factors such as fly ash material, alkaline solutions and curing contribute to a better understanding of corrosion performance in the geopolymer system. Another interesting area that needs to be explored is microbial corrosion by micro algae and bacteria to study the corrosion in aqueous medium. A previous study reported the use fly ash geopolymer as biocide to reduce algae fouling in water canal systems.[115] There was also an effort to analyse the role of micro algae in bio corrosion of structures in seawater environment.[161] Hence, it is relevant to investigate the corrosion resistance of steel bar in fly ash geopolymer exposed to Microbiologically Induced Corrosion (MIC), another type of corrosion that can be found in seawater environments.

2.7.2.5 Seawater Resistance

Changes in weight, compressive and flexural strength of fly ash geopolymer concrete have been investigated by Fernandez-Jimenez et al.[162]. There was no sign of surface deterioration, significant weight loss and only a minor change in compressive strength after the samples were immersed in the ASTM seawater for one year. This result confirmed the chloride ion precipitations in the concrete pores is not damaging or causing further reaction with the binder causing the concrete degradation. Microstructure of the fly ash geopolymer shows the unreacted fly ashes and some fissures. In the ASTM seawater there was a sporadic ions exchange between Na and Mg from seawater that shows no significant effect on mechanical strength. Low calcium content in the fly ash geopolymer used in this investigation perhaps could minimize a reaction with chloride salt. Another investigation immersing the specimens for two years showed that no Friedel salt formed in the fly ash geopolymer concrete pores, which is normally found in the mixture containing C_3A.[163]

The above investigation illustrates the specimens in the continuous immersion and its effect on the concrete degradation. The most severe condition is in the tidal and splash zones where the cyclic wetting-drying occurs on a daily basis. Instead of the accumulated salt crystallization on the concrete pores due to the cycles, an increase of corrosion rate in reinforced concrete structures is possible due to the cyclic action.[164] The oxygen and chloride ion in the concrete pores at drying process increases the chance for corrosion to occur at faster rate than the concrete in a fully submerged zone. Hence, further research is needed to investigate the fly ash geopolymer concrete resistance under wetting-drying condition to simulate concrete tidal and splash zone.

2.8 Summary

2.8.1 Research Needs

The fly ash geopolymer concrete is a potential construction material to be used in seawater structures application. The key challenge is to prove the durability and the resultant strength of this material so it can fulfil the design requirements in the seawater environment. At present, the durability of fly ash geopolymer concrete is still measured from its resistance on acid, sulphate and fire environments. Further research and development is needed to study the durability of fly ash geopolymer concrete in the seawater environment, including:

a) Systematic development of mixture proportions based on local material properties and techniques that could optimize the concrete mixtures for various structures application. A development of high strength and low permeability concrete is imperative.
b) Collection of data to investigate the effect of the various parameters on the mechanical strength, study of the lying mechanism behind the mechanical properties behaviour

and the development of a model to predict the mechanical properties in compliance with some application standards.

c) Systematic durability study for seawater structures application under chloride ion penetration, corrosion due to chloride and microorganism, pH reduction, leaching, freezing-thawing, wetting-drying, chloride attack, sulphate attack, and carbonation.
d) Systematic study on the corrosion rate, microstructure and characterisation of corrosion product. An inclusion of microbial corrosion by micro algae and bacteria in the system is also more relevant to the actual seawater condition.
e) Development and improvement of suitable test methods and accelerated test methods that can accommodate the fly ash geopolymer concrete performance in the chloride ion and corrosion study.
f) Development of service life models and life cycle analysis for fly ash geopolymer concrete in seawater application to predict the durability performance.

2.8.2 Research Objectives

The above literature review has identified various research gaps in the field. It is unachievable to carry out complete research to address all the issues. Therefore this thesis focuses on an investigation of the strength and durability of fly ash geopolymer concrete in seawater applications. The objectives are:

a) To develop fly ash geopolymer concrete mixtures for reinforced concrete structures in seawater environments.
b) To assess the strength development, namely compressive strength, tensile strength, flexural strength, modulus of elasticity, water penetrability and drying shrinkage of the optimized mixtures.
c) To study the seawater resistance under continuous immersion and wetting-drying cycles by measuring change in mass, change in compressive strength, change in modulus of elasticity, change in effective porosity, and change in length of the optimum mixtures specimens. In addition, a chloride ion penetration is investigated.
d) To investigate the corrosion performance by half-cell potential measurement, an accelerated corrosion test under impressed voltage, and in a medium incorporating microorganisms.

Chapter 3

RESEARCH METHODOLOGY

3.1 Introduction

This chapter presents an experimental work procedure to study strength and durability of the fly ash geopolymer concrete in seawater environment based on the objectives determined in Chapter 2. The aim of the experimental investigation was to examine the design mixtures and to observe the strength and durability performance of optimum mixtures. The OPC concrete with an equivalent strength was used as a control mix in this research. The layout of the research plan is shown in Figure 3-1.

There were three stages conducted in this thesis. In the first stage, the study began with material properties investigation, concrete mix design, and a preliminary study. The materials for concrete were collected and tested for some main properties. The mix design methods were determined for both of concrete mixes. In the preliminary study, some mixtures were designed using different variables and tested to obtain their strength and water penetrability, such as water absorption, sorptivity and water permeability. The water penetrability has a significant role in determining the durability of concrete in eroding environments, such as seawater.

In the second stage the concrete was designed based on some parameters in the preliminary stage. An optimization of fly ash geopolymer mixtures using the Taguchi method was carried out using various parameters. Some tests such as compressive strength, water penetrability, and accelerated wetting-drying cycles were used to select the resultant mixtures that meet performance criteria of concrete in seawater environment.

The third stage consisted of strength properties and durability investigation for the optimum geopolymer optimum mixtures and a control mix. The strength properties including compressive strength, tensile strength, flexural and Young's Modulus were carried out for all concrete mixtures. A durability study in seawater environment was carried out for chloride ion penetration, seawater resistance, corrosion and microbiological influenced corrosion.

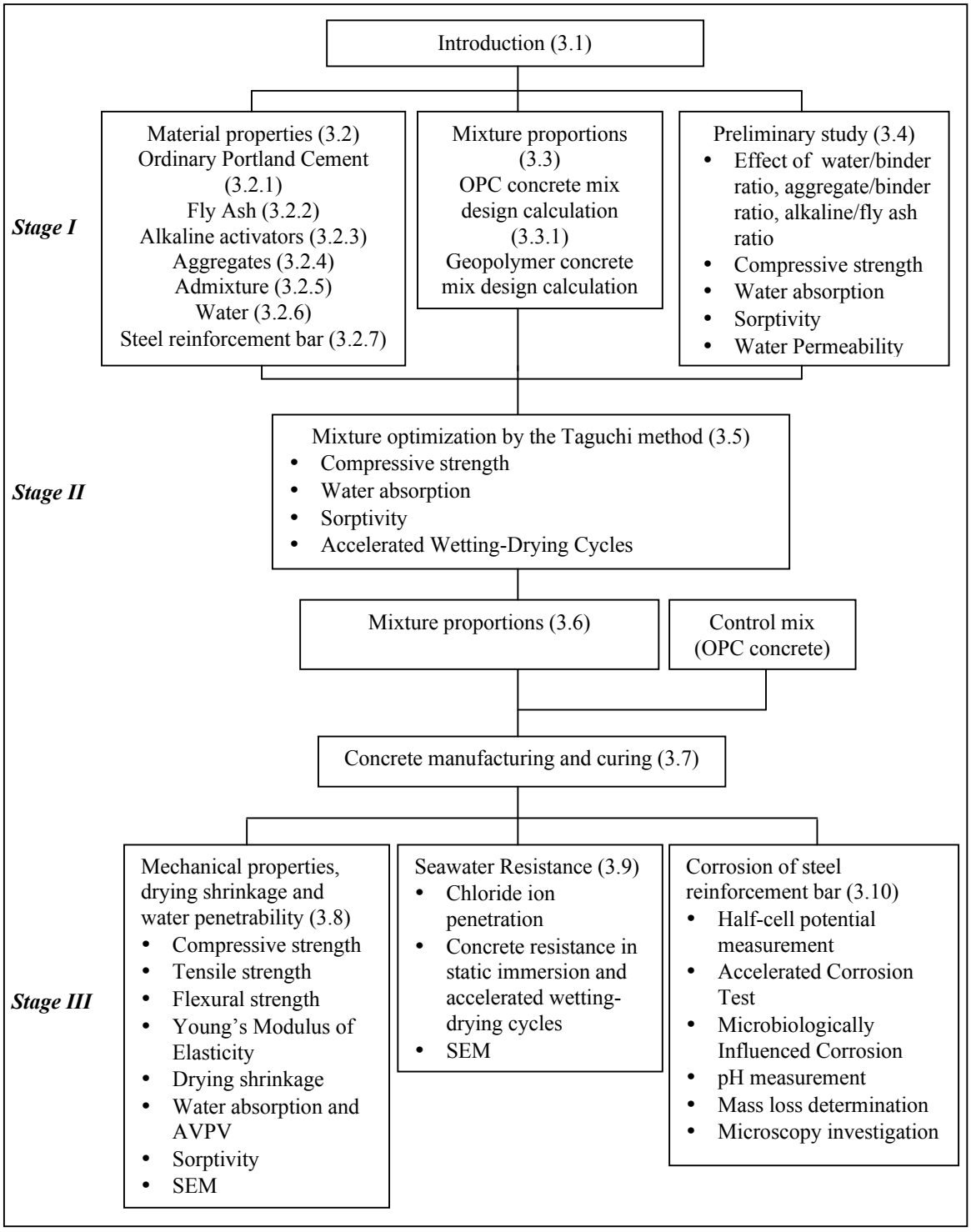

Figure 3-1 Layout of the research plan.

3.2 Material Properties

3.2.1 Ordinary Portland Cement

Ordinary Portland Cement was used to produce a control mix concrete in this research. The physical characteristics of Cockburn General Purpose Portland Cement are shown in Table 3-1. The initial and final setting times, soundness and compressive strength of this cement were in

the range of AS 3972[165] and ASTM C150[166] permissible limits. The fineness index of cement was above the minimum specified limit by ASTM C150. The fineness index related with a rate of hydration of cement when it is mixed with water and strength class produced. The compressive strength of cement is a major characteristic which is determined by its chemical composition and fineness[167]. High cement strength at 7 and 28 days of OPC concrete was above the limit set by AS 3972. The compressive strength of cement is typically above 7 MPa according to ASTM C150.

Table 3-1 Physical characteristics of Cockburn GP Portland Cement*

Parameter	Typical	Range	Permissible limits
Fineness index, m^2/kg	400	375-425	≥ 260 (ASTM C150)
Normal consistency, %	29.5	28.5-30.5	-
Setting Times, Initial, min	135	105-150	45 min, min (AS 3972)
Setting Times, Final, min	195	165-225	6h, max (AS 3972)
Soundness, mm	1.0	0-2.0	5mm, max (AS 3972)
Compressive strength, 3 days (MPa)	38	35-41	-
Compressive strength, 7 days (MPa)	48	44-52	35 MPa (AS 3972)
Compressive strength, 28 days (MPa)	60	56-64	45 MPa (AS3972)

*Provided by manufacturer

The chemical compositions of the OPC cement are presented in Table 3-2. The cement has magnesium oxide (MgO), sulphuric anhydride (SO_3), free lime and alkaline oxide (Na_2O equivalent) below the permissible limit specified by AS 3972 and ASTM C150. Excessive content of those chemicals could change the cement soundness.[168] Magnesium oxide and sulphuric anhydride in excessive levels contribute to a long-term expansion of cement. High alkaline oxide content in the cement is prone to cause alkali-silica reaction with reactive aggregates in the mixture. Chloride found in the cement is normally added to accelerate early strength and reduce setting time. Calcium chloride is added into the cement in a quantity of less than 2%.[169] Based on the physical and chemical characteristics, the Cockburn cement is suitable to produce a control mix in this research.

Table 3-2 Chemical characteristics of Cockburn GP Portland Cement*

Chemical composition	Typical	Range	Permissible limits
Silica (SiO_2), %	20.2	19.8-20.6	-
Alumina (Al_2O_3), %	4.9	4.6-5.2	6%, max (ASTM C150)
Ferric oxide (Fe_2O_3), %	2.8	2.6-3.0	6%, max (ASTM C150)
Calcium oxide (CaO), %	63.9	64.7	-
Magnesium oxide (MgO), %	2.0	1.5-2.5	4.5% max (AS 3972)
Sulphuric anhydride (SO_3), %	2.4	2.1-2.7	3.5% max (AS 3972)
Loss on ignition (LOI), %	2.5	2.1-2.9	3%, max (ASTM C150)
Chloride, %	0.015	0.005-0.025	-
Na_2O equiv ($Na_2O + 0.658K_2O$), %	0.5	0.4-0.6	0.52% (ASTM C150)

*Provided by manufacturer

3.2.2 Fly Ash

Fly ash from the coal combustion process is one of the primary materials used in manufacturing geopolymer concrete. The geopolymer concrete developed at Curtin University of Technology has been using fly ash supplied by Fly Ash Australia Pty Ltd. The fly ash was obtained from the Collie power plant, Western Australia. Two batches of fly ash were used for all mixtures in this research. Batch 1 was used for a preliminary study (Section 3.4) and the second batch was used to cast the specimens developed by the Taguchi method (Section 3.5).

Table 3-3 Chemical composition of Collie fly ash

Chemical composition	Batch 1*	Batch 2**
Silica (SiO_2),%	50.20	50.50
Alumina (Al_2O_3),%	26.30	26.57
Calcium oxide (CaO), %	2.27	2.13
Ferric oxide (Fe_2O_3), %	14.40	13.77
Potassium oxide (K_2O), %	0.58	0.77
Magnesium oxide (MgO), %	1.48	1.54
Sodium oxide (Na_2O), %	0.36	0.45
Phosphorus pentoxide (P_2O_5), %	1.57	1.00
Sulphuric anhydride (SO_3), %	0.32	0.41
Loss on ignition (LOI), %	0.58	0.60

*XRF analysis by Cockburn Cement, **XRF analysis by CSIRO

Table 3-3 presents the chemical composition of the fly ash that was analysed by XRF by Cockburn Cement and CSIRO, Western Australia. Both batches had similar chemical characteristics which could reduce margin variability of specimens produced. Silica (SiO_2), alumina (Al_2O_3) and ferric oxide (Fe_2O_3) are the major components of the fly ash utilized in the geopolymer process. The Collie fly ash could be classified into class F or low calcium fly ash based on its chemical composition as specified in ASTM C618-05.[170] The total sum of the silica, alumina and iron oxide of class F fly ash is greater than 70% with sulphuric anhydride (SO_3) and LOI quantities less than 5% and 6%, respectively. The calcium content of the fly ash is below 5%, which is preferable in manufacturing geopolymer concrete. High calcium fly ash is unstable since the calcium content can induce flash setting of the fresh geopolymer.

Particle size distribution of the fly ash is shown in Figure 3-2 and 3-3. The test was carried out by the laser diffraction method (Malvern) to estimate the distribution of fly ash particle sizes from 0.01 to 1000 µm. The percentage of particles passing 45µm sieve for fly ash batch 1 and 2 were 75.49% and 85.88%, respectively. The fly ash with 75% fineness, loss on ignition of less than 4% and SO_3 content less than 3.0%, could be classified as fine ashes according to the threshold given in AS3582.1.[171] The finer particle size of fly ash determines its reactivity, increases the surface area, and improves the particle packing in the binder paste. Thus, the fly

ash from the Collie Power Plant was physically suitable to produce geopolymer concrete in this research.

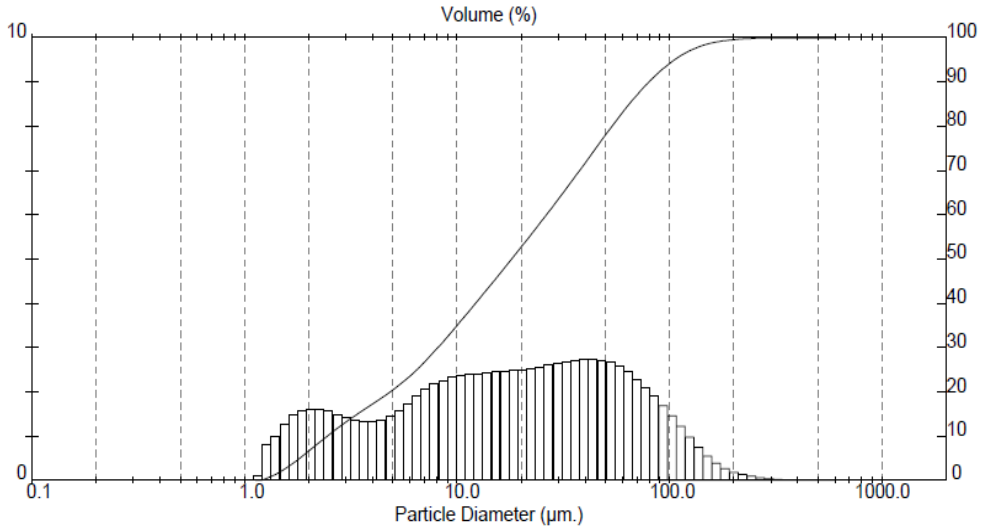

Figure 3-2 Particle size distribution of fly ash batch 1.

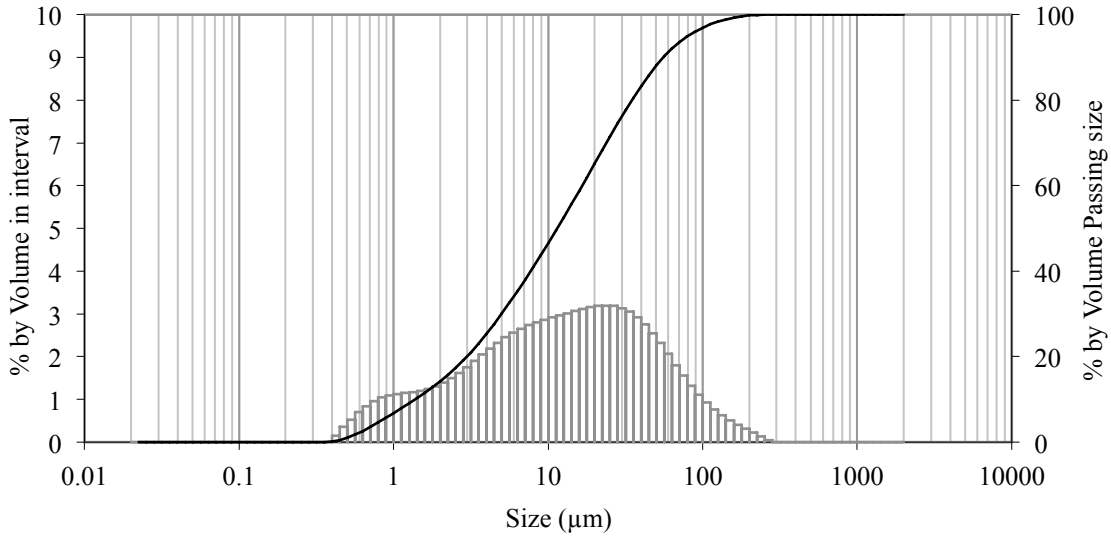

Figure 3-3 Particle size distribution of fly ash batch 2.

3.2.3 Alkaline Activators

A combination of sodium hydroxide and sodium silicate was used in this study. Both of these chemicals are commercially available in the market.

3.2.3.1 Characteristics of Sodium Hydroxide (NaOH)

Sodium hydroxide is one of the alkalis commonly used in producing geopolymer concrete. It is usually prepared in concentration of 8 to 16M.[172] In this investigation, sodium hydroxide 14M was used for all mixtures. Sodium hydroxide in pearl solid form with a quantity of 404.3g

NaOH pearl solid was dissolved in 1 litre of distilled water to make 14M solutions. The solution was kept in a fume cupboard overnight to release exothermic heat resulting from mixing. Then the sodium hydroxide solution was stored in airtight containers in a chemical storage for dangerous goods until concrete pour time. The solution had to be stirred before combining it with other liquids, such as sodium silicate, water and superplasticizer. The composition of caustic soda pearl from specification sheet is presented in Table 3-4.

Table 3-4 Sodium hydroxide pearl composition*

Chemical compound	Composition
Sodium hydroxide, NaOH (% wt)	min 99.0
Sodium Carbonate, Na_2CO_3 (% wt)	max 0.4
Chlorides, Cl (ppm)	max 80
Iron, Fe (ppm)	max 7

*Provided by manufacturer

3.2.3.2 Characteristics of Sodium Silicate (Na_2SiO_3)

Sodium silicate in liquid form with modulus silicate (*Ms*) of 2.00 was prepared in two batches. The first batch was Sodium silicate A53, was supplied by Swift Chemical and only used in a preliminary study. The second batch was provided by PQ Australia and used for the optimum mixes in this investigation. The chemical composition, specific gravity, density and viscosity of both sodium silicates from specification sheet are presented in Table 3-5.

Table 3-5 Chemical and physical characteristics of sodium silicate*

Chemical and Physical Characteristics	Sodium silicate A53	Sodium silicate D
Na_2O, %wt	14.70	14.50 - 14.90
SiO_2, %wt	29.40	29.10 - 29.70
Solids, %wt	-	43.60 - 44.60
Ratio (SiO_2%/Na_2O%)	2.00	1.95 - 2.05
Density, g/cc at 20^0C	1.53	1.50 - 1.53
Viscosity, cps at 20^0C	300	250 - 450

*Provided by manufacturer

3.2.4 Aggregates

A combination of coarse aggregates with maximum size of 20mm and fine aggregates was included in the fly ash geopolymer mixtures. Coarse aggregates with diameter of 7, 10, 14 and 20mm were crushed granite, and the fine aggregate was sand. BGC Concrete and Asphalt supplied the coarse aggregates. Fine aggregate was uncrushed yellow sand, supplied by Rocla. Grading and physical properties of both types of aggregates were investigated to determine their suitability for producing concrete mixtures. Four grading combinations, i.e. 20:10:7mm: sand, 14:10:7mm: sand, 20:10mm: sand, 10:7mm: sand were plotted to obtain optimum proportion percentage for each aggregate size. The combinations should comply with grading

requirement as outlined in BS 882:1992. The physical properties of coarse and fine aggregates investigated are shown in Table 3-6.

Table 3-6 Physical properties of coarse aggregates

Property	Standard/Method Coarse aggregate	Standard/Method Fine aggregate
Particle density (kg/m^3)	AS 1141.6.1 [173]	AS 1141.5 [174]
Oven dry basis specific gravity	ASTM C127 [175]	ASTM C128 [176]
SSD basis specific gravity	ASTM C127	ASTM C128
Apparent specific gravity	ASTM C127	ASTM C128
Absorption (%)	ASTM C127	ASTM C128
Moisture content (%)	ASTM C566 [177]	ASTM C566

*Recommended values in practice

3.2.5 Admixture

Admixture is used in the production of geopolymer concrete to improve workability of concrete mixtures. A naphthalene sulphonate based superplasticizer with a commercial name Rheobuild 1000 was by BASF. The superplasticizer has a dark brown appearance and is soluble in water. The chemical and physical properties of the superplasticizer from the supplier's specification sheet are presented in Table 3-7.

Table 3-7 Chemical and physical characteristics of superplasticizer*

Chemical and physical characteristics	Values
Naphthalene Sulphonic Acid derivative	30 - 60%
Non-hazardous ingredients	to 100%
Boiling point (^{0}C)	>100
Vapour pressure at 25^{0}C (kPa)	<3.2
Specific gravity (g/cm^3)	ca. 1.2
pH	7.0

*Provided by manufacturer

3.2.6 Water

There were two types of water included in the testing and concrete production, deionised and tap water. Deionised water was used for dissolving sodium hydroxide and sodium chloride. In geopolymer and concrete manufacture, tap water was added in the alkaline solution as extra water. Deionised water was obtained from Chemical Engineering Laboratory and tap water was taken from Concrete Laboratory. Deionised water has a uniform quality, suitable for dissolving chemicals. It is important to ensure chloride ions content was minimal so as to reduce chloride-induced corrosion on steel bars of the concrete specimens. The tap water at Concrete Laboratory was considered suitable for mixing fly ash geopolymer and OPC concrete and its quality is presented in Table 3-8.

Table 3-8 Quality of normal tap water*

Parameter	Value contained	Permissible limits
TDS (mg/L)	463	50mg/L (AS 1379-07), 50000ppm (ASTM C1602)
Chloride as Cl^- (ppm)	n/a	500ppm (ASTM C1602)
Turbidity (NTU)	0.3	-
pH	7.84	> 5 (AS 1379-07)
Sulphate as SO_4	n/a	3000 (ASTM C1602)

*Provided by Water Corporation

3.2.7 Steel Reinforcement Bar

Hot-rolled deformed bar has been used for corrosion performance of steel reinforcement in geopolymer concrete. Steel reinforcement bar with diameter of 10 and 16mm or N10 and N16, respectively, has yield strength of 500 MPa. The Onesteel reinforcing company supplied fresh steel reinforcement bars with a diameter of 16mm and a length of 350mm. The bars were tightly wrapped in plastic to avoid prolonged exposure in order to prevent corrosion.

3.3 Mixture Proportions

3.3.1 OPC Concrete Mix Design Calculation

Ordinary Portland Cement (OPC) concrete was included in this research as a control mix for some tests. The mixture was designed according to Theycenne et al.[178] The target strength of the OPC concrete control mixes was 55 MPa with a water/cement ratio of 0.45. The superplasticizer was not included in the mixtures to improve workability. A detail of mix design calculation is presented in Appendix A. The mixture proportion of the control mix is given as follows:

Cement = 422.3 kg/m^3

Coarse aggregates = 1252 kg/m^3

Fine aggregates = 536.3 kg/m^3

Water = 190 kg/m^3.

3.3.2 Geopolymer Concrete Mix Design Calculation

The geopolymer concrete mixtures were originally designed using a calculation developed by Rangan[57] by assuming some parameters such as aggregate content, alkaline/fly ash ratio and sodium/sodium hydroxide ratio. The calculation was used to obtain fly ash, aggregate, solid sodium hydroxide, sodium silicate, and water quantities. An example of mix design calculation is presented in Table 3-9. A detailed calculation to determine molar ratios such as Na_2/SiO_2, SiO_2/Al_2O_3 and H_2O/Na_2O is given in Appendix B. The resulting mixture proportion produces concrete with compressive strength of 35 MPa and was used in the preliminary stage as mix GP2 (Section 3.4).

Table 3-9 Geopolymer concrete mix design

Stage	Item	Values	Unit	Reference
I	Assumed values for calculation			
1.1	Total unit weight of the concrete	2400	kg/m^3	[64]
1.2	Mass of combined aggregates (of the mass of the concrete)	77	%	75-77%
1.3	Composition of aggregates	30% 10 mm 35% 7mm 35% sand	kg/m^3	Grading curve (Figure 4.4)
1.4	Alkaline liquid to fly ash ratio	0.35	by mass	[59]
1.5	Ratio of sodium silicate to sodium hydroxide solution	2.5	by mass	[69]
1.6	Sodium hydroxide molar	14	M	[172]
1.7	Sodium silicate modulus	2.0		[172]
II	Calculation of fly ash, alkaline solution and combined aggregates mass			
2.1	Mass of combined aggregates	77% x 2400 = 1848	kg/m^3	
2.2	Mass of fly ash and alkaline solution	2400-1848 = 552	kg/m^3	
2.3	Mass of fly ash	552/(1+0.35) = 408	kg/m^3	
2.4	Mass of alkaline solution	552-408 = 144	kg/m^3	
2.5	Mass of sodium hydroxide solution	144/(1+2.5) = 41	kg/m^3	
2.6	Mass of sodium silicate	144-41 = 103	kg/m^3	
2.7	Mass of 10mm aggregates	1848 x 30% = 554	kg/m^3	
2.8	Mass of 7mm aggregates	1848 x 35% = 647	kg/m^3	
2.9	Mass of sand	1848 x 35% = 647	kg/m^3	
III	Calculation of water to solids ratio and aggregate to solids ratio			
3.1	Water to solids ratio = total water used in the mixture	408	kg/m^3	
3.2	Water in sodium silicate solution	0.559x103 = 58	kg	
3.3	Solids in sodium silicate solution	103x58 = 45	kg	
3.4	Water in sodium hydroxide solution	41x59.57% = 24.4	kg	
3.5	Solids in sodium hydroxide solution	41-24.4 = 16.6	kg	
3.6	Extra water	20.7	kg	
3.7	Total mass of water	58+24.4+20.7 = 103	kg	
3.8	Total mass of solids	45+16.6+408 = 469.9	kg	
3.9	Water to solids ratio	103.1/469.6 = 0.22		
3.10	Aggregate to solids ratio	1848/469.6 = 3.94		
IV	Final mass of each component			
4.1	Fly ash	408	kg/m^3	
4.2	Aggregate 10mm	554	kg/m^3	
4.3	Aggregate 7mm	647	kg/m^3	
4.4	Sand	647	kg/m^3	
4.5	Sodium hydroxide	41	kg/m^3	
4.6	Sodium silicate	103	kg/m^3	
4.7	Extra water	20.7	kg/m^3	

3.4 Preliminary Study

In the preliminary stage, trial mixes were investigated to study various parameters on strength and water penetrability of fly ash geopolymer concrete. Some parameters have been chosen to

obtain concrete with good strength and durability properties in a seawater environment. The concrete needs to be workable, have a high strength, low porosity and permeability. In order to achieve the purpose, parameters that have been used to achieve good strength and low permeability were selected. The water to solids ratio, alkaline to fly ash ratio, aggregate to solids ratio and aggregate grading were derived from Hardjito et al.[69] in the previous investigation of fly ash geopolymer concrete at Curtin University. A new set of parameters was designed from the initial values and presented in Table 3-10.

Table 3-10 Parameters and values of trial mix

Parameters	1	2	3
Water to solids ratio	0.20	0.22	0.23
Aggregate to solids ratio	3.50	3.90	4.70
Alkaline/fly ash ratio	0.30	0.35	0.45
Aggregate grading	7:10	7:10:20	10:20

A control mix or mix GP1 was intended to produce geopolymer concrete that has properties and performance equivalent to OPC concrete with strength of 35 MPa. This particular mix has a water/solids ratio of 0.23, an aggregate/solids ratio of 3.90, an alkaline/fly ash ratio of 0.35, and uses 7:10mm grading of coarse aggregates. Other mixtures, i.e. GP2-GP9 were developed by varying the water/solids ratio (0.20, 0.22), aggregate/solids ratio (3.5, 4.7), alkaline to fly ash ratio (0.30, 0.45) and grading of coarse aggregates (7:10:20mm, 10:20mm). The preliminary mixture proportions are shown in Table 3-11.

Table 3-11 Mixture proportions of preliminary study

Mix no	w/s	a/s	alk/FA	Quantity (kg/m^3)								
				water	Coarse aggregate (mm)			sand	fly ash	NaOH (14M)	SS	SP
					7	10	20					
GP1	0.23	3.90	0.35	25.8	647	554		647	408	41	103	6.1
GP2	0.22	3.90	0.35	20.7	647	554	-	647	408	41	103	6.1
GP3	0.20	3.90	0.35	16.5	647	554	-	647	408	41	103	6.1
GP4	0.22	3.50	0.35	25.8	630	540	-	630	444	44	111	6.1
GP5	0.24	4.70	0.35	25.8	672	576	-	672	356	36	89	6.1
GP6	0.23	3.90	0.30	25.8	647	554	-	647	424	36	91	6.1
GP7	0.23	3.90	0.45	25.8	647	554	-	647	381	49	122	6.1
GP8	0.23	3.90	0.35	25.8	645	370	277	554	408	41	103	6.1
GP9	0.23	3.90	0.35	25.8	-	924	370	554	408	41	103	6.1

GP = Geopolymer mixture, w/b = water/solids ratio, a/b = aggregate/solids ratio, alk/FA = alkaline/Fly Ash ratio, SS = sodium silicate, SP = superplasticizer.

The cylinders then were tested for compressive strength, water absorption and AVPV and sorptivity. The preliminary testing results were intended to indicate the effect of changing some basic parameters on the strength and durability performance of fly ash geopolymer concrete.

3.5 Mixture Optimization by the Taguchi Method

The Taguchi experimental method is a popular statistical method for quality engineering. This method is used in the production area to achieve optimum results from a variety of good combinations. In concrete technology, the Taguchi orthogonal array was found suitable for designing different mixtures with different effects and constituents. The basic principle of orthogonal array is to use an economical combination but having the same effect as using a full factorial design. A combination of OA_9 (3^4) orthogonal array that can produce nine trial mixes presented in Section 2.5 was used in this research.

Four key parameters that can have a significant influence on achieving a durable geopolymer concrete were selected from the literature. The choice for each factor and level was based on intensive literature reviews of factors affecting the durability of geopolymer concrete. Aggregate content was a new parameter introduced to study the effect of aggregate content on geopolymer concrete durability. Since the aggregate comprises 75-80% of the concrete, then the amounts of 75%, 77% and 79% by concrete unit weight were adopted. The alkaline solution/fly ash ratio was a significant factor in improving the properties of the geopolymer concrete. The ratio of 0.3-0.4 was used based on the previous finding.[59] The ratio of sodium silicate to sodium hydroxide was taken in the range of 1.5-2.5 to optimize the alkaline solution used in this research.[69, 70] Three curing methods, 24 hours-60^{O}C, 12 hours-70^{O}C and 24 hours-75^{O}C were adopted from various authors.[9, 49, 69] Table 3-12 shows the experimental factors and levels (maximum and minimum) used in this research.

Table 3-12 Factors and levels

Factor	Level 1	Level 2	Level 3
A: aggregate content (kg/m^3)	1800	1848	1896
B: alkaline solution/fly ash ratio	0.30	0.35	0.40
C: sodium silicate/sodium hydroxide ratio	1.5	2	2.5
D: curing method	24 hours 60^{O}C	12 hours 70^{O}C	24 hours 75^{O}C

3.6 Mixture Proportions

Three mixes were produced by mix design optimization using the Taguchi method. A detailed process will be explained in Section 4.4. Mixes T7 and T4 were selected among the other mixes, while mix T10 was yielded from parameters evaluation. The water content was adjusted by changing H_2O/Na_2O ratio to obtain concrete with a minimum strength of 55 MPa as specified for class B2 according to AS 3600.[129] The superplasticizer used in the mixes was also adjusted to 1.5% of fly ash by weight. The adjusted mixture proportions of the concrete mixes are shown in Table 3-13. Table 3-14 displays the OPC and geopolymer mixture

proportions for corrosion of steel bars in an algae medium study. There was a change in maximum aggregate size to accommodate the specimen's size for the MIC test.

Table 3-13 Optimum mixture proportions of geopolymer concrete

Mixes	T4	T7	T10
Fly ash (kg/m^3)	461.54	424.62	498.46
Total aggregates (kg/m^3)	1800	1848	1752
20mm (kg/ m^3)	270.00	277.20	262.80
10mm (kg/ m^3)	360.00	369.60	350.40
7mm (kg/m^3)	630.00	646.80	613.20
sand (kg/m^3)	540.00	554.40	525.60
NaOH 14M (kg/m^3)	46.15	36.40	42.73
Sodium silicate (kg/m^3)	92.31	90.99	106.81
Superplasticizer (kg/m^3)	6.90	6.40	7.50
Added water (kg/m^3)	18.83	17.93	18.87
SiO_2/Na_2O	0.99	1.11	1.11
SiO_2/Al_2O_3	3.60	3.63	3.63
Na_2O/Al_2O_3	0.40	0.39	0.39
H_2O/Na_2O (design)	11.68	12.10	11.86
Curing	24h-75^{0}C	12h-70^{0}C	24h-75^{0}C

Table 3-14 Mixture proportions of OPC and geopolymer concrete for MIC test

Mixes	OPC	T10
Fly ash (kg/m^3)	-	498.46
Cement (kg/ m^3)	422.5	-
Aggregates (kg/m^3)	1788.3	1752
14mm (kg/m^3)	313.00	262.80
7mm (kg/m^3)	375.60	350.40
10mm (kg/m^3	563.40	613.20
sand (kg/m^3)	536.30	525.60
NaOH 14M (kg/m^3)	-	42.73
Sodium silicate (kg/m^3)	-	106.81
Superplasticizer (kg/m^3)	-	7.50
Added water (kg/m^3)	190	18.87
SiO_2/Na_2O	-	1.11
SiO_2/Al_2O_3	-	3.63
Na_2O/Al_2O_3	-	0.39
H_2O/Na_2O (design)	-	11.86
Curing	28 days in water	24h-75^{0}C

3.7 Concrete Manufacturing and Curing

3.7.1 Preparation of Material

3.7.1.1 Aggregates

In manufacturing the geopolymer concrete, both coarse and fine aggregates were treated to achieve a Saturated Surface Dry (SSD) condition. First the aggregates were washed out for two or three times and immersed in water for 24 hours. The next day, all aggregates were removed from the water bath to pan trays for air-drying. Depending on the season, it may take one or two days to achieve SSD condition of the aggregates. Saturated Surface Dry condition for

coarse aggregates could be observed from a visual inspection when there was no visible film around the grains but when the aggregates were still damp. Then the moisture content was determined from a change in mass before and after drying. The SSD of fine aggregate looks damp and appears to be free flowing. Figure 3-4 shows the aggregate preparation for SSD condition and typical SSD appearance of 10mm aggregate.

Figure 3-4 Coarse aggregate: (a) SSD preparation, (b) typical SSD appearance of 10mm aggregate.

3.7.1.2 Fly Ash

The first batch of 3 tonnes contained in metal drums arrived in May 2008. The second batch was delivered in three aggregate bags with a total quantity of 3 tonnes. The fly ash containers were placed on wooden pallets to prevent direct contact with the damp floor. The fly ash needed to be crushed by hands because it was slightly limp due to moisture absorption. Since the moisture content influence was negligible in the mixing process, there was no need to dry it before using them in the mixtures. Figure 3-5 presents the typical Collie fly ash for making the geopolymer concrete.

Figure 3-5 Fly ash, chemical solution, admixture and water used in this research.

3.7.1.3 Alkaline Solution

Chemicals such as sodium hydroxide, sodium silicate and superplasticizer in Figure 3-5, were carefully weighed then placed in clean and dry containers. In this research, it was found that mixing the alkaline 24 hours before concrete pouring resulted in a hard gel material. The alkaline solution then was mixed for at least two hours before pouring time. The mixing procedure was as follows: firstly, the sodium silicate, followed by sodium hydroxide solution was poured in a clean container. Both solutions were stirred continuously until uniformly mixed and appearing as clear as water. The extra water was poured into the solution, followed by stirring the mix for a few seconds. Finally, the superplasticizer was included while still stirring the solution slowly and evenly to avoid heterogeneity in the mix. The alkaline solution is a brown colour and needs to be handled cautiously. The sequence of the alkaline solution mixing process is shown in Figure 3-6.

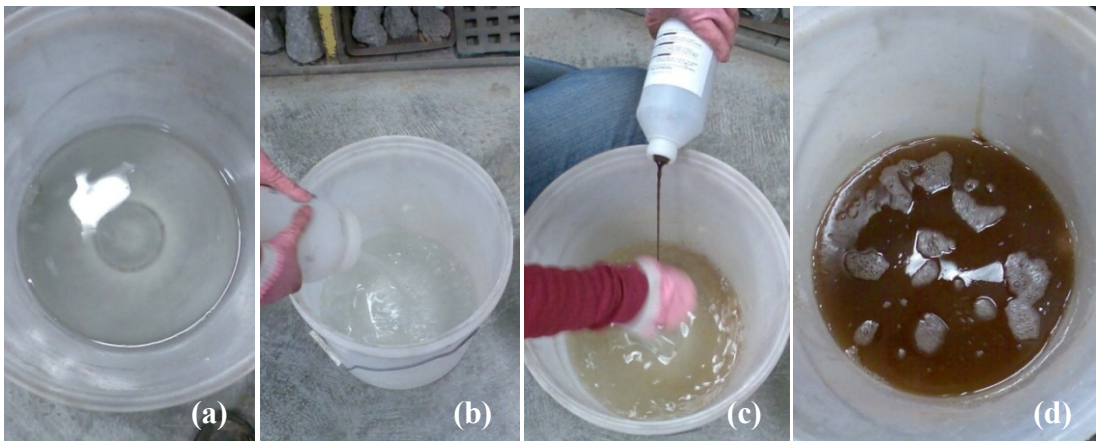

Figure 3-6 Alkaline solution mixing process: (a) sodium silicate, (b) sodium hydroxide was poured into the sodium silicate solution, (c) superplasticizer was poured into the solution, (d) alkaline solution was ready to be used.

3.7.2 Type and Size of Specimens

Specimens with different sizes meeting requirements of the testing procedure were used in this research. The detail of the specimen sizes is given in Table 3-15.

Table 3-15 Detail of the test specimen size

Type of test	Type of specimens	Size of specimens
Compressive strength	Cylinder	100x200mm
Tensile strength	Cylinder	150x300mm
Flexural strength	Beam	100x100x400mm
Young's Modulus	Cylinder	100x200mm
Drying Shrinkage/Length of Change	Prism	25x25x250mm
Water absorption and AVPV	Cylinder	100x50mm
Sorptivity	Cylinder	100x110mm
Water permeability	Cylinder	100x50mm
Chloride ion penetration	Cylinder	100x50mm
Concrete under wetting-drying cycles	Cylinder	100x200mm
Half-cell and Accelerated Corrosion test	Lollipop cylinder	100x200mm
Microbiologically Influenced Corrosion	Lollipop cylinder	50x100mm
SEM	Flat chip	20x10x1mm
pH measurement	Cylinder disc	100x50mm

Three specimens were produced for each test and the results were taken as the average of triplicate specimens. The half-cell potential and accelerated corrosion test using lollipop type specimens with a size of 100x200mm and a 16mm diameter of bar located centrally in the concrete. The Microbiologically Influenced Corrosion (MIC) test samples used a mild carbon steel rod with a 10mm diameter and 150mm length, embedded centrally in a concrete cylinder with 50mm in diameter and 100mm in height. The lollipop type specimen moulds are shown in Figure 3-7.

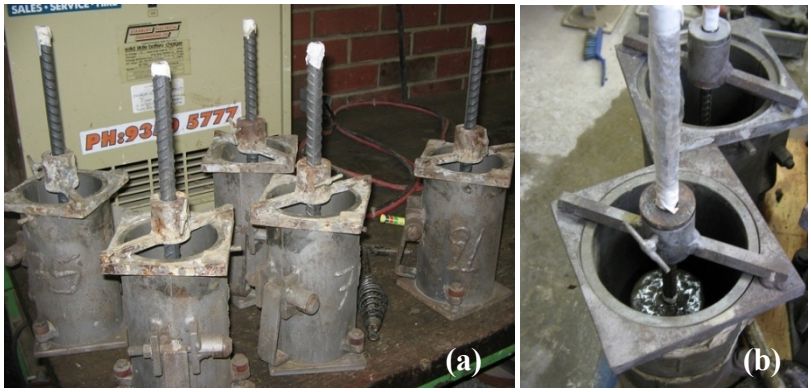

Figure 3-7 Lollipop sample type moulds: (a) ACT specimens, (b) MIC specimens.

Some tests required only the body of concrete cylinders to ensure homogeneity of specimens. The water absorption, water permeability and chloride ion penetration specimens were taken from no's 2 and 3 of the concrete as shown in Figure 3-8.

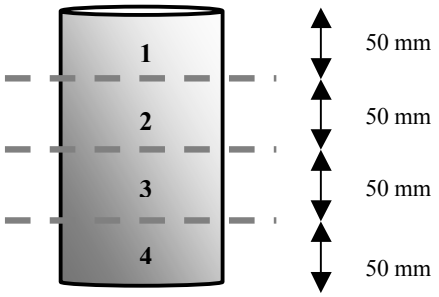

Figure 3-8 Slice of specimen taken for testing.

3.7.3 Concrete Casting, Curing, Demoulding and Storing

3.7.3.1 Geopolymer Concrete

The geopolymer concrete was produced using a procedure which involved mixing the dry aggregates with alkaline solutions. Initially the dry materials like aggregates and fly ash were mixed for 3 minutes until all materials were well combined. Then the alkaline solution was poured slowly into the mixture. The mixture was mixed for another 4 minutes to accelerate the reaction between the dry and liquid ingredients. The resulting mix has a dark grey colour and is cohesive. The fresh mixture was ready for a slump test and to be poured into the available moulds. The moulds were coated with Valsof water-based releasing agent to prevent the mix sticking to the mould. The specimens were covered with a steel cap to avoid excessive evaporation during the steam curing process.

The fresh mixtures have cured using high temperature steam to accelerate the geopolymerisation process and hardening of the concrete. The mixtures were steam cured for three different curing regimes. The preliminary trial mix specimens were cured at 60^0C for 24 hours. Samples of T4 and T10 were cured at 75^0C for 24 hours, while T7's samples were cured at 70^0C for 12 hours. After the curing process, the samples were left in the steam-curing chamber for at least 6 hours to prevent cracking due to a temperature shock between outside and inside the curing room. The samples were demoulded a day after the steam cured process finished. A demoulding day was counted as day 1 for the specimens. The samples were left to be air-cured in the curing room with a constant temperature of 24-25^0C. Figure 3-9 shows the arrangement of samples under the steam curing tent and steam curing equipment final set up.

Figure 3-9 Steam curing of specimens: (a) specimens underneath tent,
(b) steam curing final set up.

3.7.3.2 OPC Concrete

Ordinary Portland Cement (OPC) concrete was manufactured according to AS1012.2.[179] In the mixing process, the coarse and fine aggregates were initially mixed for about two minutes. The cement powder was then included in the dry mix. Water was poured slowly into in the dry mixture until it was combined uniformly. The pan mixer was still mixing for another two minutes before it was completely stopped. The workability measurement or slump test was carried out on the fresh OPC mixture. Then the fresh mix was poured into the moulds that had been coated with oil. The samples were left in the mould for one night. Demoulding of the OPC specimens took place on the following day. Then the specimens were stored directly into the water pond in the curing room. The day after that was counted as day 1 for the OPC samples. On day 28, those samples were removed from the water and placed in a dry pond. The samples were left to air cure until their testing date.

3.7.4 Workability Measurement

Workability of the OPC and geopolymer mixtures was measured by a standard slump test according to AS 1012.3.1.[180] The fresh concrete mix was placed in a first layer of one-third height of Abram's cone and 25 strokes were applied to it. The same procedure was repeated for the second layer and third layer. When the cone was filled with the compacted fresh mix, the cone was placed up-side down and the slump value was measured. Figure 3-10 shows the slump measurement of fly ash geopolymer concrete.

Figure 3-10 Slump of high strength fly ash geopolymer concrete.

3.8 Mechanical Properties, Drying Shrinkage and Water Penetrability

3.8.1 Preparation of Test Specimens

The mechanical properties, drying shrinkage and water penetrability were taken as the average of two or three specimens at each age. Details of the test program and the standard used for each test are presented in Table 3-16.

Table 3-16 Test program for hardened concrete

Type of test	Standard/Method	Test age (days)	Specimens number tested at each age
Compressive strength	AS 1012.9	7, 28, 91, 365	2, 3
Tensile strength	AS 1012.10	28, 91, 365	3
Flexural strength	AS 1012.11	28, 91, 365	3
Young's Modulus	AS 1012.17	28, 91, 365	3
Drying shrinkage	AS 1012.13	0, 7, 14, 28, 91, 112	3
Water absorption	ASTM C642	28, 91, 365	2
Sorptivity	GHD	28, 91, 365	2
Water permeability	GHD (DIN 1048)	91	2

3.8.2 Test Procedure for Mechanical Properties and Drying Shrinkage

3.8.2.1 Compressive Strength

Compressive strength of the specimens was determined in accordance with AS 1012.9.[181] Three specimens were tested at 7, 28, 91 and 365 days of concrete age. At the end faces of each specimen, a sulphur cap was applied to ensure uniform loading across the area during testing. The test was carried out using Multifunctional Computerised Control Console machine (MCC8). A loading rate of 0.33 MPa/min and sensitivity of 100 kN were set and maintained automatically in this machine during the test. The compressive strength was taken as a ratio of ultimate load and cross-sectional area of the specimen. The final result was the average of triplicate specimens. The specimen condition after compression failure is shown in Figure 3-11(a).

Figure 3-11 Strength specimens failure: (a) compressive strength test, (b) tensile strength test.

3.8.2.2 Tensile Strength

Brazilian splitting tensile strength was taken to determine the tensile strength of concrete specimens. The tests were taken at 28, 91 and 365 days and triplicate samples were used for each testing date. The splitting tensile strength was carried out in compliance with AS 1012.10.[182] The measurement was taken using a servo-controlled type machine (MCC8). The loading rate of 0.067 MPa/min and sensitivity of 80 kN were set and maintained by the machine during each specimen testing. The specimen was loaded by compressive force along the length of the cylinders. Tensile failure occurs on the plane with high compressive failure in the area around the applied load. Tensile strength was calculated by dividing the maximum load sustained with geometrical factors. The specimen condition after tension failure is shown in Figure 3-11(b).

3.8.2.3 Flexural Strength

A plain beam was used for flexural strength test at 28, 91 and 365 days. The flexural strength test was carried out in accordance with AS 1012.11.[183] The specimen was placed on support blocks at the MCC8 machine and two point load-applying blocks were applied to the specimen. The loading rate of 0.017 MPa/min with sensitivity of 5 kN was set and sustained by the computer during the test. The modulus of rupture or flexural strength could be calculated when the fracture started at the middle third of span length (maximum bending moment area). The flexural strength was determined from the ultimate load multiplied by the length and divided by geometrical factors. The test set-up for flexural strength is shown in Figure 3-12(a).

3.8.2.4 Young's Modulus of Elasticity and Poisson's Ratio

The test was carried out on a single cylinder at 28, 91 and 365 days for fly ash geopolymer and OPC concrete. Stress-strain ratio and a ratio of lateral to longitudinal strain of concrete were

determined to calculate Young's Modulus and Poisson's Ratio. Both values were obtained in accordance with AS 1012.17.[184] Both values are considered useful in designing the concrete size and calculating the reinforcement quantity in application. There were two strain-measuring pieces of equipment or LVDT attached around the cylinder to measure longitudinal strain. Another LVDT was placed horizontally to measure transverse strain. The arrangement of LVDT and specimen condition in the test is illustrated in Figure 3-12(b).

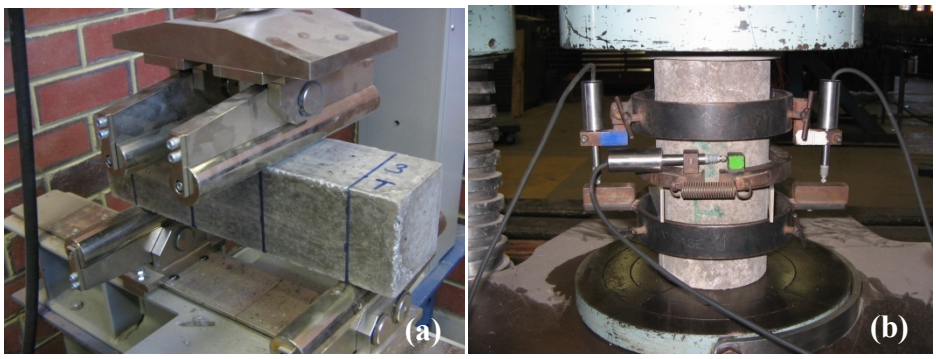

Figure 3-12 Test set up: (a) flexural strength, (b) Young's Modulus of Elasticity and Poisson's Ratio.

3.8.2.5 Drying Shrinkage

The length changes of specimens in air drying were determined by measuring drying shrinkage in accordance with AS 1012.13.[185] Prior to casting, the specimens were left in the curing room with a constant temperature of 23-25^{O}C and relative humidity of 40-60%. The measurement commenced on the third day after casting using a horizontal length comparator. The first measurement was taken as an initial day, and then the next day was considered as day 1 of shrinkage measurement. The measurement was continued every day for one week, after total periods of air-drying of 7, 14, 28, 56 days. The specimens measuring with horizontal comparator is shown in Figure 3-13.

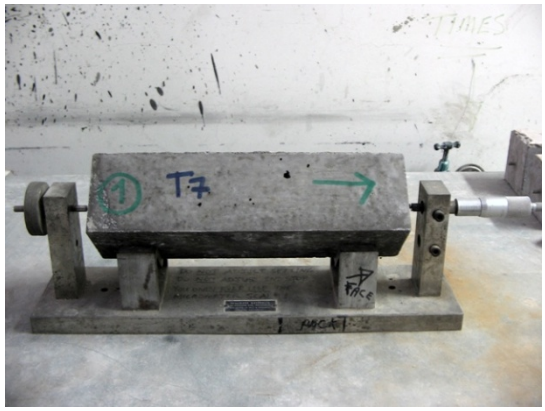

Figure 3-13 Drying shrinkage measurement by horizontal length comparator.

3.8.3 Test Procedure for Water Penetrability

3.8.3.1 Water Absorption and AVPV

Water absorption and volume of permeable voids determination were carried out according to ASTM C642.[186] Three specimens were cut into slices with maximum thickness of 50mm for each concrete mix. Water absorption values were measured by drying the specimens until constant mass was achieved, immersed them in water and measured the increase in mass as a percentage of dry mass. The Apparent Volume of Permeable Voids (AVPV) values were determined by boiling the concrete for at least 5 hours in a water bath, and were then weighed in water. Figure 3-14 shows the cut samples, immersed samples, boiled samples and water bath.

Figure 3-14 Water absorption and AVPV test: (a) cut samples, (b) immersed samples, (c) boiled samples, (d) water bath.

The water absorption and AVPV percentages were calculated by equations:

$$Water\ absorption = \left(\frac{Ms - Md}{Md}\right)x100 \tag{3.1}$$

$$AVPV = \left(\frac{g_2 - g_1}{g_2}\right)x100 \tag{3.2}$$

where M_s = mass of surface-dried sample (g), M_d = mass of oven dried sample (g), g_2 = apparent density (x 10^3 kg/m^3), g_1 = bulk density, dry (x 10^3 kg/m^3).

Based on the water absorption, the effective porosity of concrete can be calculated [187]:

Effective porosity (%) = (B-A)/V x 100 (3.3)

where A = mass of oven dried sample in air, B = saturated mass of the surface dry sample in air after immersion, V = bulk volume of the sample.

3.8.3.2 Sorptivity

Sorptivity is used to measure the rate of water absorption into the hardened concrete. The method used was an in house method developed by GHD (Determination of Sorptivity).[188] Triplicate cylinder specimens were prepared with a size of 50x110mm and a weight of at least 200g. The surface was cut perpendicular to the required direction of sorption. The specimens were dried at a temperature of 105^{O}C until constant mass. The specimens were supported by steel rods to allow free water movement in a tray of water of 20^{O}C. A selected face of concrete was placed to a depth of 1-2mm of water. Figure 3-15 illustrates the specimens' arrangement during the sorptivity test. The time of the test was recorded at intervals of 5, 10, 30, 60, 120, 180 and 240 minutes from the start of the test. At each increment, the specimens were removed from the tray, and dried off the surplus water was dried-off, the samples were weighed and returned to the tray. Then uptake of water per unit area of concrete surface I (g/mm) followed a linear relationship with the square root of time for the suction periods (t), hence:

$I = C + St^{0.5}$ (3.4)

where S, the sorptivity is the slope of the I vs $t^{0.5}$ plot and can be obtained by linear regression.

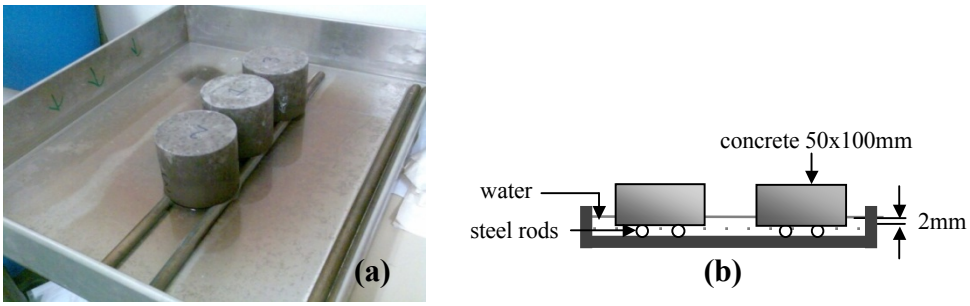

Figure 3-15 Sorptivity test: (a) side view photograph, (b) schematic diagram.

3.8.3.3 Water Permeability

The water permeability test was carried out based on the GHD Water Permeability method (previously Taywood Engineering Ltd).[188] These specimens were dried in the oven at 105^{0}C until constant mass. The specimens were coated with epoxy on the circular side to prevent water penetration from that side during the test. Figure 3-16 shows the epoxy-coated samples and water permeability test rig. A pressure of 850 kPa was applied to the samples at pressure head of 92.5 m. After the specimen was saturated, then the flow rate reading was taken using burette by measuring the changing of volume of water over time. The permeability defined by Darcy's Law as follows:

$$k = \frac{QL}{AH} \tag{3.5}$$

where k = permeability coefficients (m/s), Q = flow rate (m^3/s), A = area (m^2), L = depth of specimen (m), H = head of water (m).

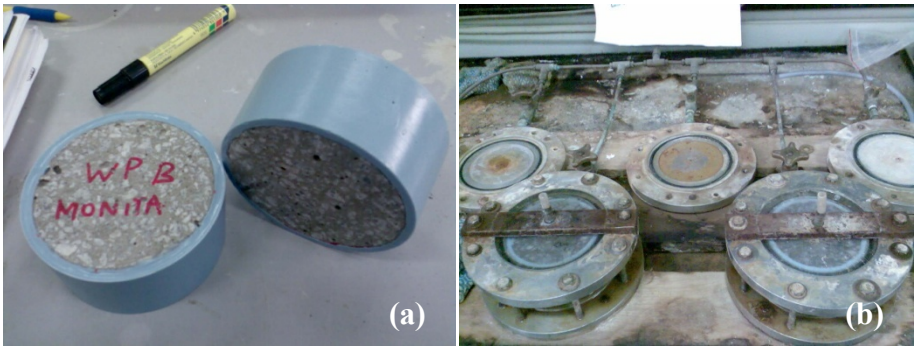

Figure 3-16 Water permeability test: (a) epoxy coated samples, (b) water permeability test rig.

3.9 Seawater Resistance

3.9.1 Preparation of Test Specimens

The seawater resistance was determined by investigating the chloride ion penetration into the concrete and concrete degradation caused by static immersion and wetting-drying cycles. The concrete degradation was identified through change in weight, change in compressive strength, change in Young's Modulus and length of change. The water absorption of the immersed specimens was also taken. Visual investigation was used to explain the degree of degradation caused by static and wetting-drying cycles. The details of the test program are shown in Table 3-17.

Table 3-17 Test program for seawater resistance

Type of test	Standard/Method	Test age (days)	Specimens number tested at each age
Chloride ion penetration	NT Build 443[189]	35	3
Static immersion	ASTM C267[190]	28, 91, 365	3
Wetting-drying cycles	Kasai & Nakamura[191]	28, 91, 200	3
Compressive strength	AS 1012.9[181]	7, 28, 91, 365	2, 3
Young's Modulus	AS 1012.17[184]	28, 91, 365	3
Length of change	AS 1012.13[185]	7, 28, 56, 91, 112	3
Water absorption	ASTM C642[186]	28, 91, 365	2
SEM		365	1

3.9.2 Chloride Ion Penetration

The chloride ion penetration of a hardened concrete was determined by Nordtest NT Build 443 (Concrete hardened accelerated chloride penetration).[189] Four samples were used, that is, three

discs (100mmx45-50mm thickness) for chloride penetration measurement and one disc for background chloride content. The discs with 45-50mm thickness were taken from the middle part of the concrete cylinders. Two discs were cut and exposed to sodium chloride solution, while one part of the remaining disc was used to determine the initial chloride content. Concrete needs to be dried in the oven until constant mass. The specimens were coated by epoxy paint except the test surface. This was to ensure one direction of chloride penetration into the concrete. The specimens were immersed in distilled water for the geopolymer concrete or lime ($Ca(OH)_2$) solution until the constant mass did not change by more than 0.1%. The immersed specimens are shown in Figure 3-17 (a). The specimens were placed in 165±1 gr NaCl per litre of water and exposed for 35 days in the control environment temperature. The ratio of area of specimens and volume of solution should be in a range of 20-80 to avoid carbonation. The container was closed tightly to reduce the chance of extreme liquid evaporation. The concrete surface was rinsed with water and the specimens were air-dried after 35 days. In this research, the specimens were grounded at the following depth: 0-15, 15-30, 30-45mm. The concrete powder was oven dried for 24 hours before the acid soluble chloride content was determined.

The acid soluble chloride content of concrete powder was carried out according to BS 1881: Part 124, Standard method for determination of chlorides in concrete. The powder was digested with 10ml nitric acid 70% w/w and 75ml hot deionised water. The chloride content was determined by using an automatic titrator that uses chloride ion selective and mercury/mercury sulphate electrodes. The volume of $AgNO_3$ used represents the available chloride in the solution. The auto titrator machine is shown in Figure 3-17 (b).

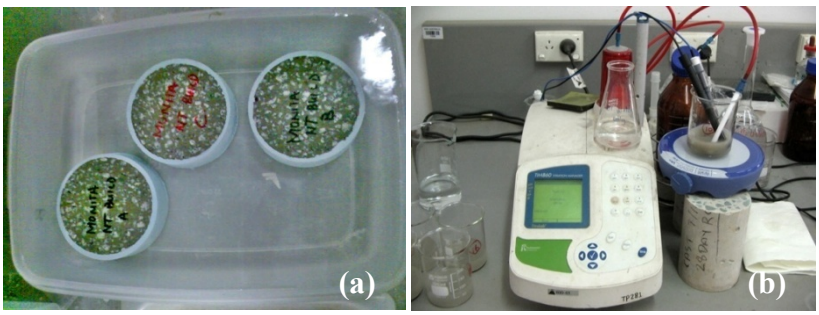

Figure 3-17 Chloride ion penetration test: (a) immersed and grounded specimens, (b) auto titrator machine to determine chloride content.

3.9.3 Concrete Resistance in Continuous Immersion and Accelerated Wetting-drying Cycles

3.9.3.1 Continuous Immersion

A seawater resistance test was carried out through a measurement of change in weight, compressive strength, Young's Modulus of Elasticity and length. The change in weight and compressive strength was calculated according to ASTM C 267.[190] In addition, an effective porosity was determined at 91 and 365 days. The 3.5% sodium chloride solution was used solely in the experiments and replaced once a month to maintain the salinity. The ratio of volume of container and volume of specimens is at least four to one.

The average weight from three cylinders was measured after certain exposure times. The weight change will be measured on 1, 7, 14, 21, 28, 42, 56, 84, 112, 140, 168, 196, 224, 252, 280, 380, 336, 364 days.

Weight change = [(W-C)/C] x 100 (3.6)

where C = conditioned weight of specimen (g), W = weight of specimen after immersion (g).

Change in compressive strength was determined on 28, 91, and 365 days. The Young's Modulus of Elasticity's change was taken at 91 and 365 days. The measurement was an average of three cylinders. These tests were used to evaluate the percentage decrease or increase in compressive strength of the specimen during immersion for each examination period. The values can be calculated using Equation 3.7; a similar principal was used to calculate the change in Young's Modulus of Elasticity:

Change in compressive strength = $[(S_2-S_1)/S_1] \times 100$ (3.7)

where S_1 = average compressive strength of a set of specimens following the conditioning period (MPa), S2 = average compressive strength of a set of specimens following the test period (MPa).

Three bars similar to drying shrinkage specimens have been used for measuring the change in length or expansion of geopolymer concrete in sodium chloride solution. The change in length was calculated as a drying shrinkage measurement. The reading was taken at 1, 2, 3, 4, 8, 13 and 15 weeks; 4, 6, 9, 12 months and if necessary, at 18 months.

3.9.3.2 Accelerated Wetting-drying Cycles

An accelerated wetting-drying cycle test was carried out according to Kasai & Nakamura[191] for investigating a resistance of mortar in synthetic salt water. The accelerated wetting-drying cycle was used to represent a seawater environment consisting of immersion of the specimens

in salt water with a concentration of 3.5% for 24 hours followed by drying for 24 hours in the oven at a temperature of 80^0C. Figure 3-18 illustrates the accelerated wetting-drying cycles.

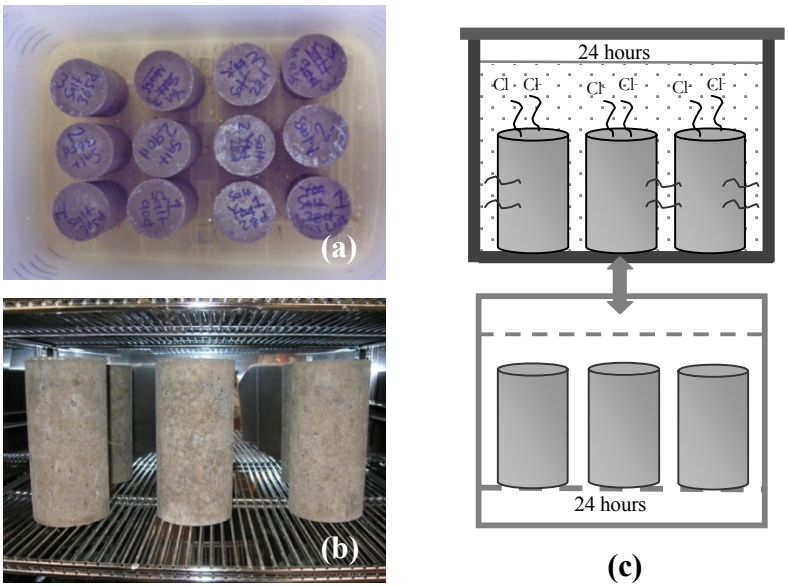

Figure 3-18 Accelerated wetting and drying cycles: (a) wetting immersion test, (b) drying in the oven test, (c) schematic diagram.

In this test, the specimens were immersed in the chloride solution immediately after the oven drying process. The solution was replaced after 15 cycles to maintain the salinity. The volume proportion of chloride solution to the specimens was one to four. The resistance of geopolymer concrete, in terms of change in mass, change in compressive strength, change in length and Young's Modulus were tested as per static immersion test. At 28, 91 and 200 days or 14, 45 and 100 cycles, the change in compressive strength, water absorption and Young's Modulus were carried out. The concrete was weighed after each wetting or drying to obtain a weight loss during the drying process and a total weight change. The weight loss during the drying process and total weight change can be calculated as follows:

$$d_n = \frac{w_{nw} - w_{nd}}{w_{nd}} x100 \tag{3.8}$$

where d_n = weight loss during the drying process at 'n' cycle (%), w_{nw} = weight of specimen at the end of immersion of 'n' cycle (kg), w_{nd} = weight of specimen at the end of drying of 'n' cycle (kg).

$$w = \frac{w_{nw}}{w_o} x100 \tag{3.9}$$

where w = total weight change (%), w_o = weight of specimen at before the accelerated test (kg).

3.10 Corrosion of Steel Reinforcement Bars

3.10.1 Preparation of Test Specimens

The corrosion performance of steel bars in fly ash geopolymer concrete was investigated through half-cell potential measurement, accelerated corrosion test by impressed voltage method and inclusion of microorganism causing Microbiologically Influenced Corrosion (MIC). The test program of corrosion specimens is presented in Table 3-18.

Table 3-18 Test program for corrosion resistance performance

Concrete type	Type of test/ method	Initial condition	Applied Voltage (V)	Specimens number tested at each age
T7	Half-cell measurement test (ASTM C876 [106])	dry	n/a	3
T10		dry	n/a	3
T4		dry	n/a	3
OPC		dry	n/a	3
T7	Accelerated corrosion test	dry, pre-immersion	5, 30	3
T10		dry, pre-immersion	5, 30	3
T4		pre-immersion	5, 30	3
OPC		dry, pre-immersion	5, 30	3
T7, T4, T10, OPC	pH[192]	dry	n/a	3

3.10.2 Half-cell Potential Measurement

The probability of steel corrosion at various stages can be measured with half-cell potential studies. Half-cell potential in this research was measured by silver/silver chloride (Ag/AgCl) reference electrode on 16mm diameter and 350mm long rebar in the lollipop samples. Reference electrode, Ag/AgCl with KCl solution (equals to SCE) was used to measure free corrosion potential of steel bar in the chamber. The procedure given in ASTM C876[106] for underwater measurement was followed for taking these potential readings. The half measurement set up was shown in Figure 3-19.

The samples were immersed in 3.5% sodium chloride. The readings were taken on 1, 3, 7, 14, 16, 21, 28, 56, 91, 120, 180, 365 days. The measurements were taken by connecting the steel bar and reference electrode to a high impedance digital multi meter. While taking the reading, a wire from rebar was connected to the positive terminal; the reference electrode was connected to the negative terminal. The tip surface of the reference electrode was in contact with the wet concrete surface. The reading was taken three times for each sample. There were triplicate specimens for each mix. The corrosion potential and pH values were reported as the average of three specimens.

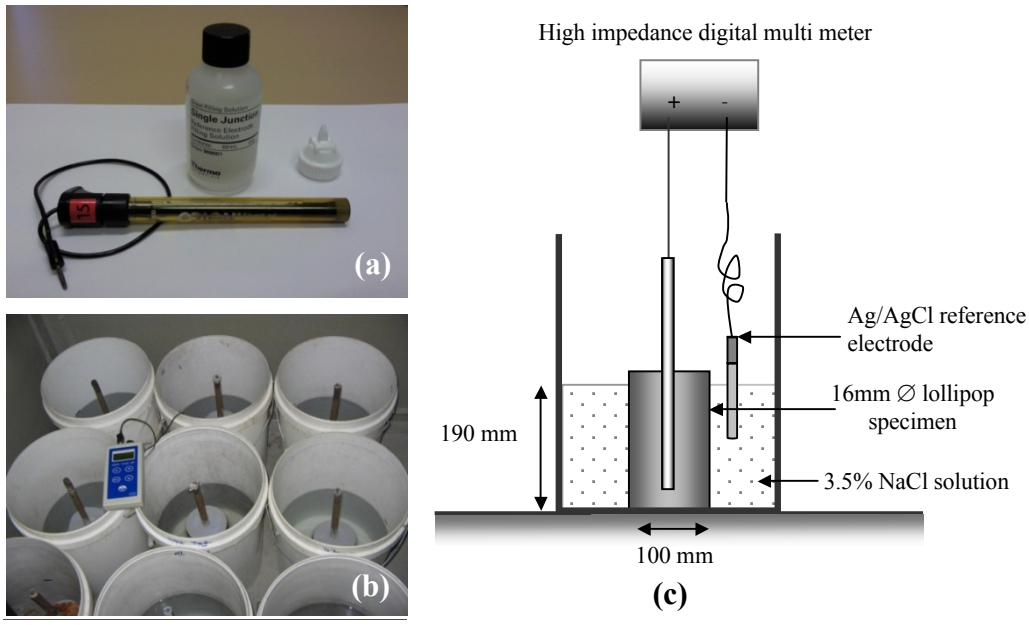

Figure 3-19 Half-cell potential measurements: (a) side view photograph, (b) top view photograph and (c) schematic diagram.

3.10.3 Accelerated Corrosion Test by Impressed Voltage Method

An impressed voltage system was used to accelerate the corrosion process. The corrosion test samples were 100x200mm cylinders with 16mm diameter steel bars located in the middle of specimen (lollipop). The same procedure was used by various researchers.[193,194] The system consisted of a power supply, resistor and data logger (Figure 3-20).

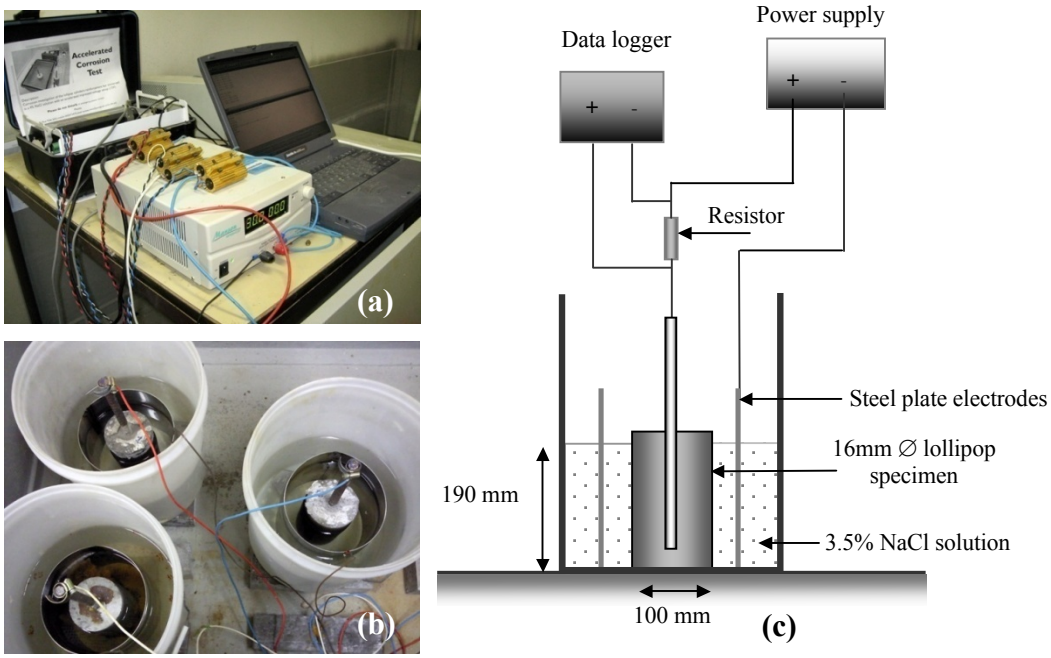

Figure 3-20 Accelerated corrosion test measurement: (a) power supply and data logger, (b) the arranged specimens, (c) schematic diagram.

A stainless steel plate was located around the specimens. The bar was connected to the positive terminal in the power supply, while the steel plate was connected to the negative terminal. The steel reinforcing bar acted as an anode, whereas the stainless plate was a cathode. The specimens were immersed in 3.5% sodium chloride solution for 3 days before the test date. After pre-immersion, the specimens were placed in a container contained chloride solution. A constant voltage of 5V and 30V was induced to the system.

The samples were split off at the end of every test. The pH by phenolphthalein method was carried out for one surface, and silver nitrate was sprayed for the other surface to measure chloride ion penetration. The steel bar, concrete surface, corrosion product location and type of crack were investigated by visual inspection. Mass loss of each bar specimen was taken as a difference between original mass and the final mass. The bars were cleaned up with mechanical technique using a wire brush and chemically washed with sodium hydroxide 2%.

3.10.4 Microbiologically Influenced Corrosion

The Microbiologically Influenced Corrosion (MIC) test incorporating algae as microorganism in the solution was carried out at Algae R&D, School of Biology and Environmental, Murdoch University. Fly ash geopolymer concrete specimens were prepared by mixing fly ash with alkaline solution to be cured in steam curing chamber for 24 hours at 75^{O}C. Mix T10 from optimization process and OPC control mix were used in this experiment. Microalgae used in the present research were *Pleurochrysis carterae* Braarud et Fagerland (MUR90) obtained from Algae R&D. The species was originally isolated from Salton Sea Salt Lake, California, USA. The algae were cultured in modified f/2 medium and show the best growth at pH 8.0. The *P. carterae* increases the pH to 8.1-9.9 in daylight and the pH decrease to 8.1 at night.[195] Filtered seawater from Hilary's Beach, Western Australia was used as modified f/2 medium (Guillard and Ryther, 1962) as summarized in Moheimani and Borowitzka.[196] The seawater was filtered from impurities and was stored in a tank at Algae R&D, Murdoch University. The seawater from the same source was also used as a control medium.

Reference electrode, Ag/AgCl with KCl solution (equals to SCE) was used to measure free corrosion potential of steel bars in the chamber. Measurement of corrosion potential versus time in all mediums was conducted twice. Data was taken with a data logger controlled with a computer. The potential measurement was taken at 10 minute increments. TPS pH meter was used to measure pH every hour for 8 hours a day three times a week. Cell densities measurement was carried out using Neubaeur haemocytometer^{TM} under microscope twice a day, three times a week. Figure 3-21 shows the Neubaeur slide and microscope used for counting cell number.

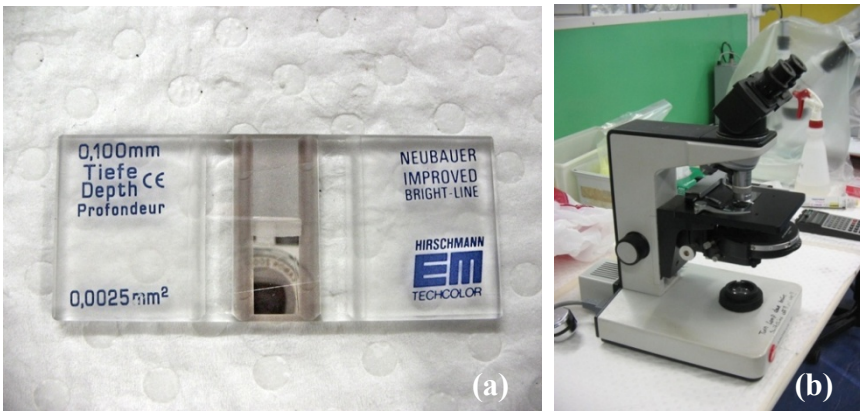

Figure 3-21 Apparatus for measuring cell number: (a) Neubauer counting slide, (b) Microscope.

Figure 3-22 shows the schematic diagram of the experimental apparatus. The electrochemical chamber test was a 1 L circular Teflon tube. The chamber was fitted with a transparent acrylic lid to allow light and oxygen into the chamber. The samples and chamber were chemically sterilized using sodium hypochlorite.[195] A fluorescent lamp was placed on top of the chamber to provide 50 µmol photons.m^{-2}.s^{-1}. The light/dark cycles were at 12 hours intervals. A mechanical stirrer was used to stir the solution inside the chamber. The operating volume of solution was 800ml for all media. Algae were inoculated into the system for every run with initial cell densities of approximately of 1.4x10^{5}cells/ml. Each run was carried out for 2 weeks.

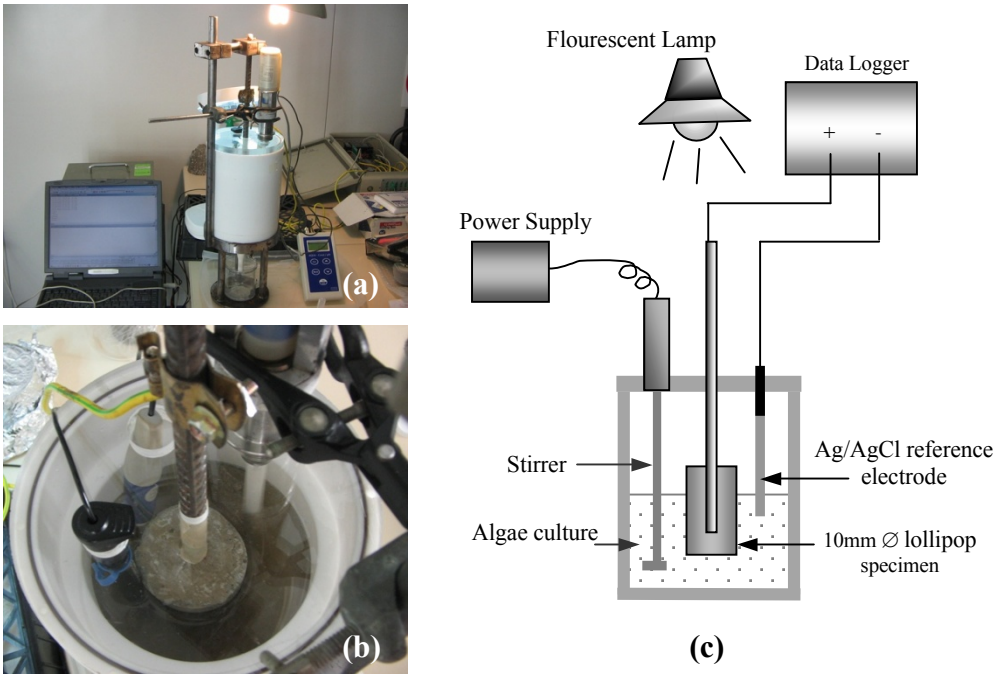

Figure 3-22 MIC test measurement: (a) side view photograph, (b) top view photograph and (c) schematic diagram.

3.10.5 pH Measurement

The pH of fresh concrete mixture was measured using a method that has been developed by Grubb, et al.[192] The fresh concrete paste (5g) was collected. The paste was mixed with 10ml of fresh distilled water at temperature of 22±1^{0}C using stirrer. The mixture was filtered using no 40 filter papers. The pH was taken by inserting the pH probe into the filtered mixture. The pH measurement is shown in Figure 3-23 (a).

Another pH indication was taken by spraying phenolphthalein solution into the concrete. Phenolphthalein is used to measure the pH of carbonated concrete.[197] Non-carbonated concrete turns red, while the carbonated concrete is colorless, as shown in Figure 3-23 (b). The same method was used to check the concrete pH by splitting the core of concrete and spraying it with the phenol solution.[198] The resulting red or pink color has pH in the range of 8.2-9.8.

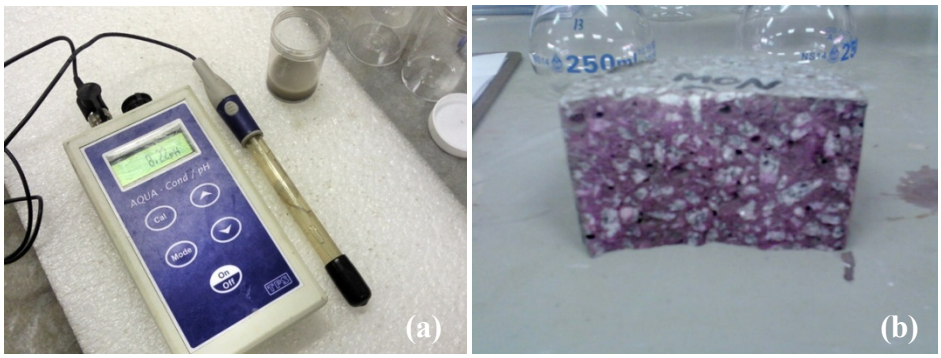

Figure 3-23 pH measurement: (a) pH meter, (b) phenolphtalein spray.

3.10.6 Microscopy Investigation

The Alicona Imaging GmbH microscope was used to observe a steel-concrete interface after exposure to the accelerated corrosion test. A microstructure study has been carried out by Scanning Electron Microscopy (SEM) to identify geopolymer concrete and corrosion product. Those samples were thinly cut using a saw blade approximately 1-2mm. Those samples were then stored in a vacuum dessiccator until it became time to coat it with platinum coating with a 4nm thickness. The microscope study was carried out to identify the microstructure and microstructure change of the concrete without any treatment and following corrosion test. The specimens in the stubs ready for platinum coating and Philips XL30 SEM machine are presented in Figure 3-24.

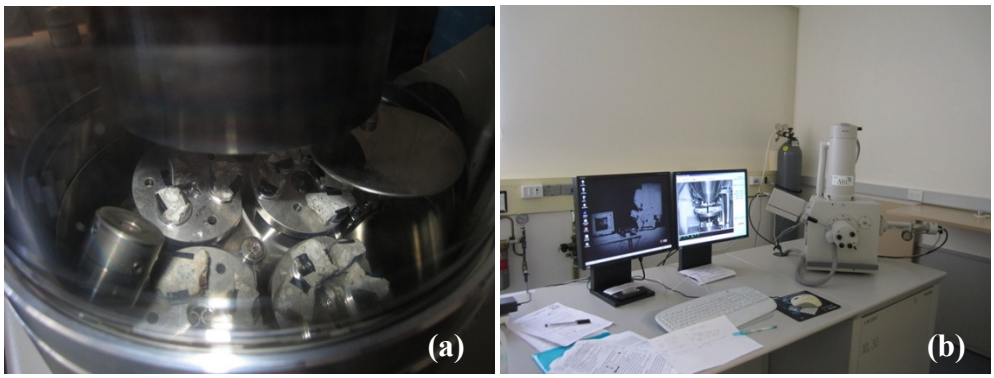

Figure 3-24 SEM investigation: (a) SEM specimens at platinum coating machine, (b) Philips XL30 SEM machine.

Chapter 4

RESULTS AND DISCUSSION

4.1 Introduction

This chapter presents results and discussion from the aggregate properties tests, a preliminary investigation, mixture optimization, mechanical properties and durability of the optimum mixtures and its control mix. The experimental method in Chapter 3 was followed to obtain data to achieve objectives outlined in Chapter 2. The development of concrete mixtures by the Taguchi method has resulted on three optimum mixtures. The mechanical properties, water absorption, sorptivity and drying shrinkage were obtained for each mixture. Durability was determined from seawater resistance and corrosion performance of the optimum geopolymer mixtures compared to the control mix. The effect of various parameters and correlation of the parameters are also discussed in this chapter.

4.2 Aggregate Properties

A combination of coarse aggregates with a maximum size of 20mm and fine aggregates was used in producing the fly ash geopolymer and OPC concrete mixtures. Physical properties and gradation of both types of the available aggregates were investigated to determine their suitability in the geopolymer concrete production.

4.2.1 Physical Properties

Coarse aggregate was crushed granites with diameter size of 7mm, 10mm, 14mm and maximum of 20mm. BGC Concrete and Asphalt supplied the coarse aggregates. The properties of coarse aggregates such particle density, oven dry specific gravity, SSD specific gravity, apparent specific gravity, absorption and moisture content of the aggregates are presented in Table 4-1 and 4-2.

Table 4-1 Physical properties of coarse aggregates

Property	Values			
	20mm	14mm	10mm	7mm
Particle density (x 10^3 kg/m^3)	2.67	2.70	2.65	2.64
Oven dry basis specific gravity	2.63	2.61	2.60	2.54
SSD basis specific gravity	2.65	2.65	2.62	2.58
Apparent specific gravity	2.67	2.71	2.65	2.65
Absorption (%)	0.58	1.42	0.74	1.60
SSD basis moisture content (%)*	0.3-0.4	0.3-0.4	0.3-0.4	0.5-0.7

*Recommended values in practice

Particle density of the aggregate determines a degree of packing in one unit volume that was useful in a concrete mix design calculation. The particle density of coarse aggregates studied was in the range of 2.64-2.70 t/m^3, which is less than 3.2 t/m^3 and greater than 2.1 t/m^3 specified by AS 2758.1 for normal weight concrete.[199] Compared to the oven-dried specific gravity, the Saturated Surface Dry (SSD) specific gravity is normally used in a concrete mix design calculation to represent an ideal condition of aggregate used in the mixture. The SSD specific values of coarse aggregate were 2.58-2.6. Coarse granite usually has SSD specific gravity of 2.6 to 3.0.[64] Absorption of coarse aggregates is related to porosity and indirectly to the final strength of concrete. The absorption of coarse aggregates varied in the range of 0.5-4.5%[64], while AS 2758.1 specifies value of less than 3% for an individual coarse aggregate. Since the absorption values of coarse aggregates were 0.58-1.60%, the coarse aggregates were found suitable for making specimens for durability testing purposes. In addition, a strict control was applied in the fly ash geopolymer production to use only SSD aggregates for controlling excessive water content in the mixture. Hence, a moisture content of aggregates was investigated to determine the amount of water after SSD treatment explained in Section 3.7.1.1. From the previous experiences, a recommended SSD moisture content was in the range of 0.3-0.4% for 10, 14 and 20mm aggregates.

Fine aggregate is uncrushed yellow sand and was supplied by Rocla. Table 4-2 presents the physical properties of fine aggregates used in this research. The yellow sand has a particle density of 1.86 t/m^3, which is in the range 2.1 to 3.2 t/m^3 specified by AS 2758.1. The SSD specific gravity of sand was 2.61, which is in the range of 2.6 to 3.0 for sand.[64] Given that the absorption was less than 2% as specified by AS 2758.1, yellow sand can be used for making the geopolymer concrete. From previous experiences, the recommend SSD moisture content was in the range of 0.5-0.7% for sand.

Table 4-2 Physical properties of fine aggregates

Property	Values
Particle density (x 10^3 kg/m^3)	1.86
Oven dry basis specific gravity	2.59
SSD basis specific gravity	2.61
Absorption (%)	0.8
SSD basis moisture content (%)*	0.5-0.7

*Recommended values in practice

4.2.2 Gradation

Aggregates grading determines the workability and water demand on concrete manufacturing. A good grading can optimize the usage of material to produce strong and durable concrete. Fly ash geopolymer concrete was designed by proportioning aggregate quantity based on a particle

size distribution through sieve analysis in compliance with AS 1141.11.1.[200] There were four aggregate grading combinations used in this research, i.e. 20:10:7mm: sand, 20:10mm: sand, 14:10:7mm: sand and 10:7mm: sand. The grading combination is shown in Figure 4-1, 4-2, 4-3 and 4-4. The combinations should comply with the grading requirement as outlined in BS 882.[64] Those figures indicate that the grading of different sizes of coarse and fine aggregates was within the limits specified by the BS 882.[64] Grading curves for single aggregate size are presented in Appendix C.

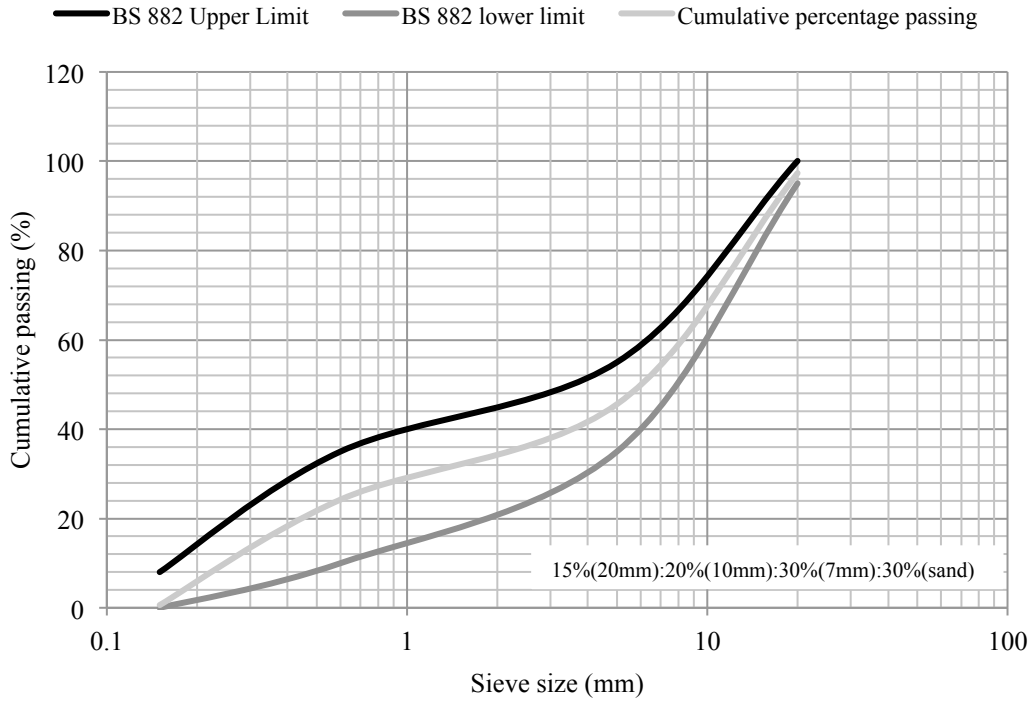

Figure 4-1 Grading of combined aggregates I (20:10:7mm: sand)

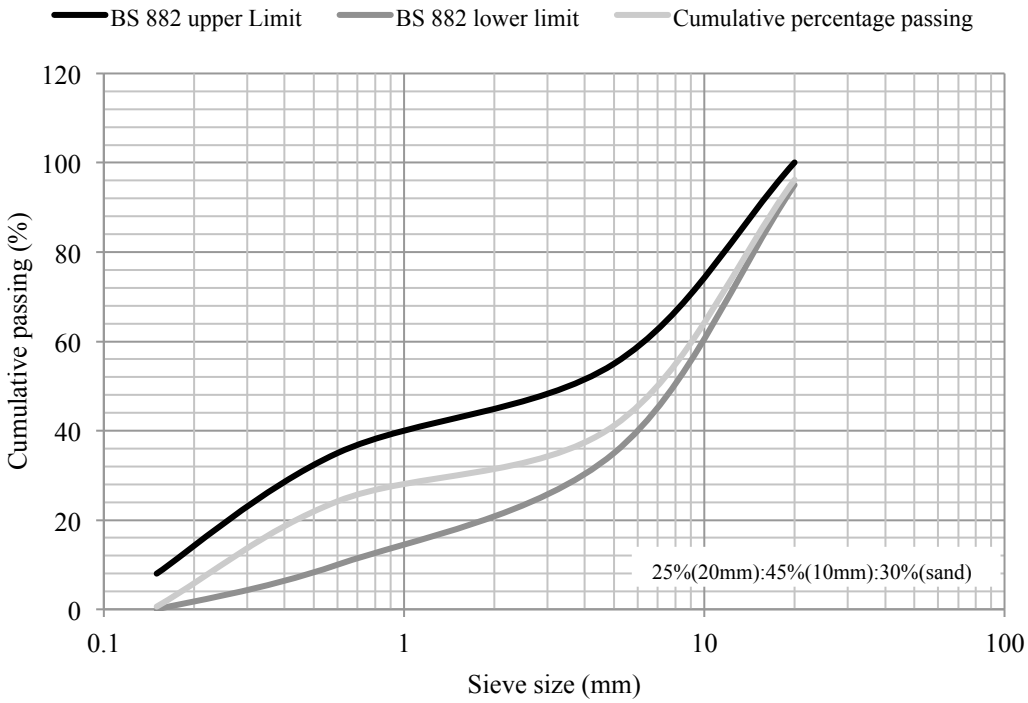

Figure 4-2 Grading of combined aggregates II (20:10mm: sand)

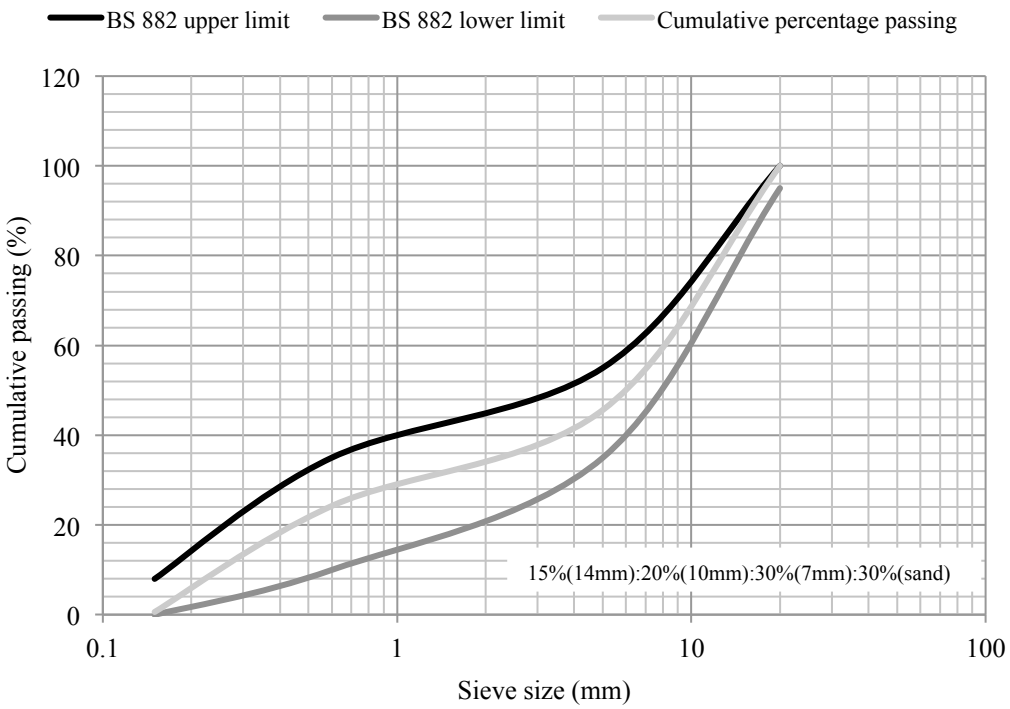

Figure 4-3 Grading of combined aggregates III (14:10:7mm: sand)

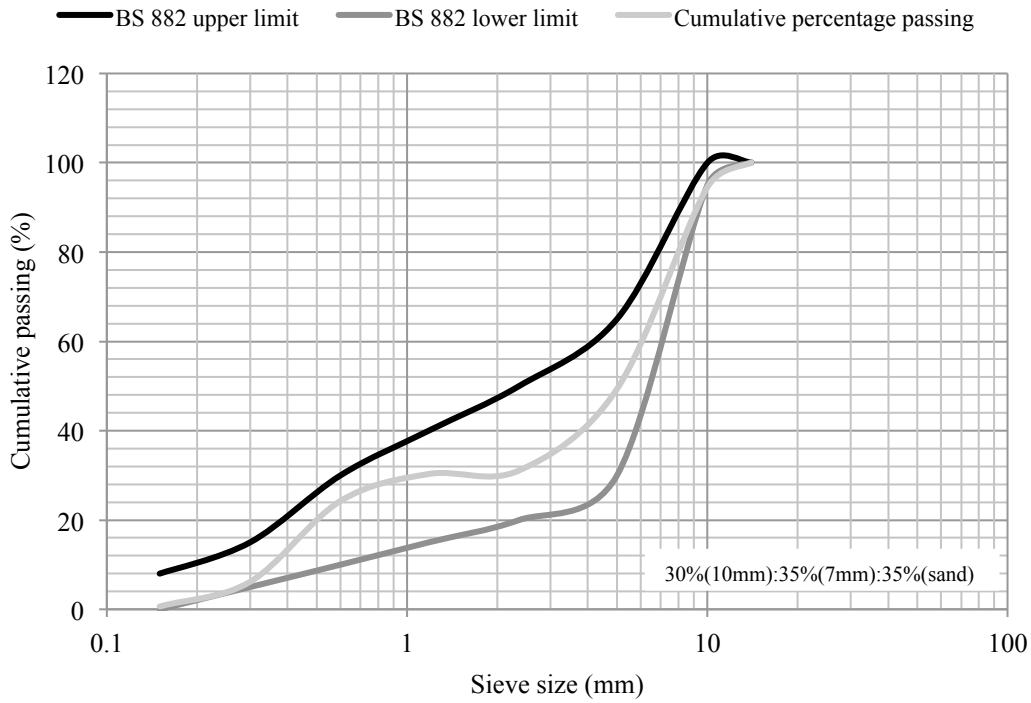

Figure 4-4 Grading of combined aggregates IV (10:7mm: sand)

A combined gradation is normally used to overcome restriction of particle size distribution of single-sized aggregate from various sources. The combined aggregate was found relevant especially for fine aggregates in Australia which has a very limited range of particle sizes.[201] The aggregate grading determines the water demand, voids content, voids distribution and packing of aggregates that can affect the final strength and durability of the concrete. The grading also influences the fresh properties of concrete such as slump, workability, pump ability, finishing, bleeding and segregation. In the case of geopolymer concrete, there was limited research on the impact of grading on the mixture workability or strength. Unlike the OPC concrete, the aggregate gradation in the geopolymer concrete does not determine the mixture's water demand or hardened concrete strength. It is more likely to influence the fresh properties such as slump and flow ability of the mixture.[16] Consequently, the aggregate gradation may affect the fresh properties of fly ash geopolymer concrete.

4.3 Preliminary Study

This section presents a preliminary study on some factors affecting the compressive strength, water absorption and water permeability of the fly ash geopolymer concrete. The parameters studied were water/solids ratio (w/s), aggregate/solids ratio (a/s), alkaline/fly ash ratio (alk/fa) and aggregate grading. One parameter was kept constant, while the other was changed to determine the influence of those combinations on geopolymer properties.

4.3.1 Slump, Density and Compressive strength

The average slump and density of the concretes at 28 days are presented in Table 4-3. The slump values of all geopolymer mixes were in the range 230-270 mm. Although slump values indicated a good workability, the actual fresh geopolymer workability was poor. The mixes were stiffer than the OPC concrete due to lack of water content and also cohesive sodium silicate used in the fly ash geopolymer system. Similar cohesive fresh geopolymer mixes have been confirmed by previous authors.[57, 70] The hardened geopolymer concrete density at 28 days was in the range 2248-2294 kg/m^3. The density of geopolymer is close to a density of normal weight concrete in practice, which varies in the range 2200-2600 kg/m^3.

Table 4-3 Slump and density of fly ash geopolymer concrete at 28 days

Mixture no	Slump (mm)	Density (kg/m^3) 28 days
GP1	260	2248.49
GP2	230	2294.55
GP3	270	2336.04
GP4	260	2281.61
GP5	240	2282.43
GP6	250	2288.71
GP7	250	2290.70
GP8	260	2289.01
GP9	240	2315.68

The average compressive strength at 7, 28 and 91 days are shown in Figure 4-5. Overall, it was noticed that the compressive strength of all mixes increased with concrete age. In the case of the water/solids ratios in Figure 4-5(a), GP3, with w/s 0.20, had the highest compressive strength of 76.00 MPa at 91 days. A decrease of compressive strength was observed as an increase of w/s ratio from 0.20 to 0.23. This data illustrates the effect of the w/s ratio on the geopolymer strength development, which is similar to OPC concrete. When low water content is used in the geopolymer mixes, the alkaline activator concentration tends to increase in the system. Thus, the available high alkalinity could accelerate the geopolymerisation process and increase the concrete's final strength.[71]

In the case of aggregate/solids ratios, a high compressive strength was shown by GP4 at 91 days. An increase of a/s ratios was observed to quite significantly decrease the compressive strength (Figure 4-5(b)). For example, at 28 days, the compressive strength of mixes with a/s ratios of 3.50 and 4.70 were 25.44 MPa and 48.06 MPa, respectively. This data clearly shows an increase of solids or dried alkaline activator, which is advantageous in producing more aluminosilicates bonds and in improving the final strength of the geopolymer concrete.[63]

The strength development of mix GP6 was slightly higher after 7 days and continued to gain strength after 28 days (Figure 4-5(c)). At an alkaline/fly ash ratio of 0.45, GP7 had not achieved the target strength of 35 MPa, but the strength gain after 28 days was comparatively high. A decrease of compressive strength was observed as the fly ash quantity increased in the mixture. A high amount of fly ash, with lack of alkaline activator to activate the ashes, produces aluminosilicates covering with a lot of unreacted fly ash. The unreacted fly ash failed to develop geopolymer bonds that could have a negative impact on the strength development. In the case of the aggregate grading variation, GP8 and GP9 obtained their target strength of 35 MPa at 28 days and both mixes were performing similarly (Figure 4-5(d)).

The results indicate there is no significant strength development of fly ash geopolymer concrete with variations of aggregate grading. Hence, among the parameters studied the water/solids ratios, aggregate/solids ratios, and alkaline/fly ash ratios were shown to improve the strength to a certain extent. A reduction of water content, aggregate and fly ash quantity were found more advantageous to enhance the geopolymer strength development.

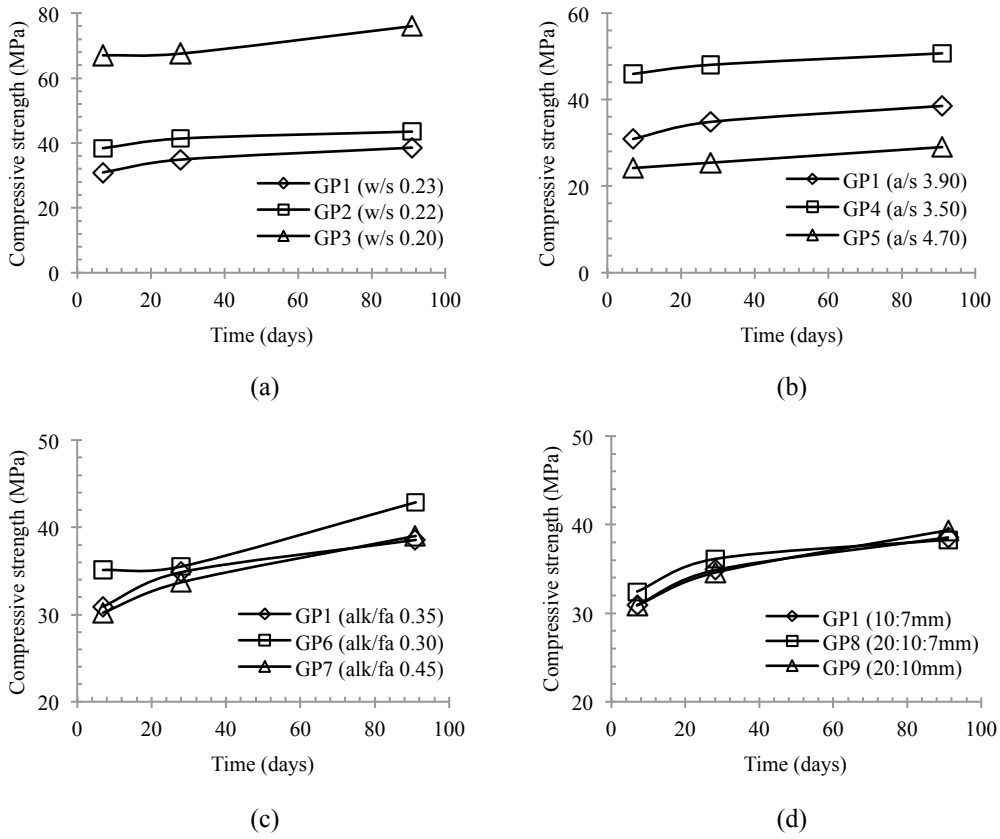

Figure 4-5 Strength development of concrete with various parameters: (a) water/solids ratio, (b) aggregate/solids ratio, (c) alkaline/fly ash ratio, (d) aggregate grading; at 7, 28 and 91 days.

4.3.2 Water Absorption and AVPV

A comparison of the water absorption of geopolymer concrete with different water/solids ratios, aggregate/solids ratios, alkaline/fly ash ratios and grading at 28 and 91 days is shown in Figure 4-6. Water absorption can be used to represent an open porosity of concrete paste. The measurement is taken by calculating the difference in specimen weight under oven-dried and fully saturated conditions. In general, various trends were observed from the water absorption of fly ash with various parameters. The low water/solids ratios, high aggregate/solids ratios and low alkaline/fly ash ratios were more significant in improving water absorption than the aggregate grading. The percentage of water absorption for all specimens and parameters varied in the range 3.63% to 4.90% at 28 and 91 days of the concrete age. The water absorption of fly ash geopolymer normally varies in the range 3-5%.[79, 145] Overall, a water absorption less than 5% is classified as 'low' according to VicRoads's standard specification.[133] BS 1881 specifies concrete with typical absorption values in the range 3-5% as "average" concrete.[105] This low water absorption level is a good indicator of limited open porosity that can inhibit the flow of water into the concrete.

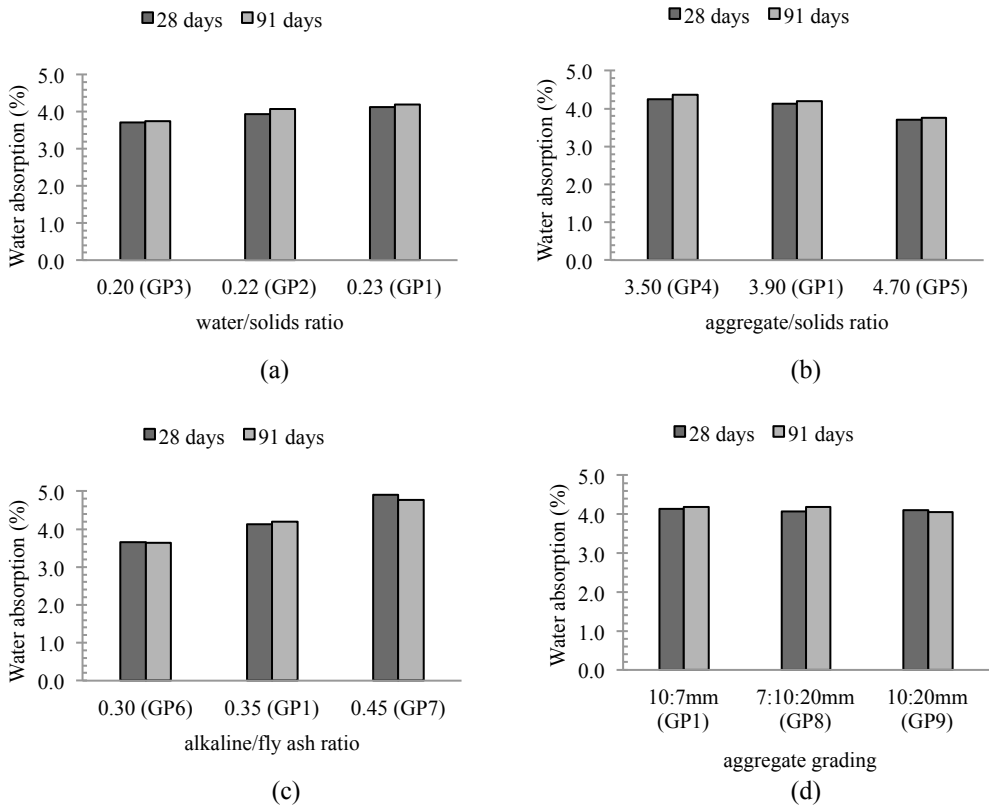

Figure 4-6 Water absorption of mixes with various: (a) water/solids ratio, (b) aggregate/solids ratio, (c) alkaline/fly ash ratio, (d) aggregate grading at 28 and 91 days.

Figure 4-7 illustrates the AVPV of concrete with various parameters. In general, the same trend with water absorption could be observed from this property. The AVPV, or closed porosity, is a percentage of pore space measured by boiling the saturated concrete. Overall, the AVPV of specimens was in the range 8.96% to 10.73%. An AVPV value of less than 12% is classified as 'good', according to VicRoads's standard specification.[133]

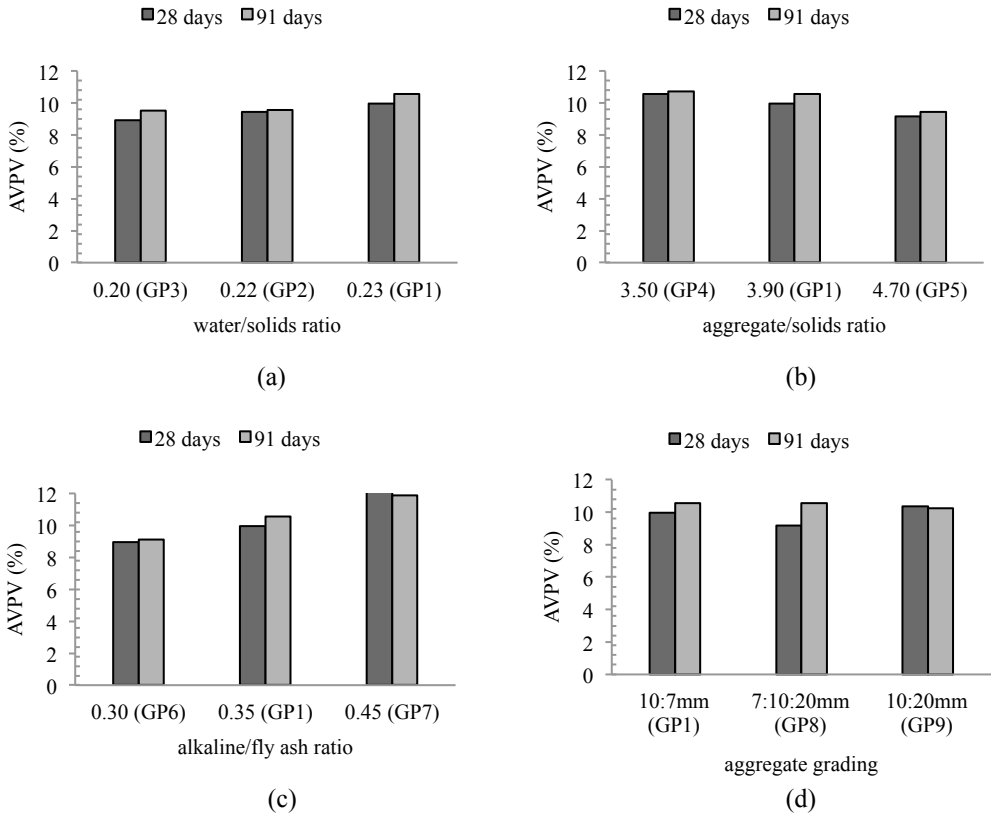

Figure 4-7 AVPV of mixes with various: (a) water/solids ratio, (b) aggregate/solids ratio, (c) alkaline/fly ash ratio, (d) aggregate grading at 28 and 91 days.

As indicated before, low water/solids ratios, high aggregate/solids ratios and low alkaline/fly ash ratios are significant in improving water absorption/AVPV. The reasons for the better improved performance of these ratios are as follows. Low water content in the mixture does not only increase the fly ash geopolymer concrete strength, but it also limits the pores size in the geopolymer paste. When water is included in the geopolymer mix, it is excluded from reaction and fills in the aluminosilicate gel pores.[202] Conversely, when high water content is used in the mix, the geopolymer produces large gel crystals with trapped water inside.[9] Once the water evaporates from the pores, the result is a highly porous geopolymer paste with high water absorption and low compressive strength, such as GP1.

The inclusion of high content aggregates favours a low water absorption/AVPV of concrete, due to less porosity, and results in a high aggregate mix, such as GP5. When more alkaline solution is added to the mixture, the water absorption/AVPV tends to increase. A mix with a high alkaline solution, such as the tacky sodium silicate, tends to produce a more porous geopolymer gel. The high amount of sodium silicate in the mix was found to produce concrete with large pore sizes.[49] This explained a tendency of some mixes, with a high alkaline content, to have higher porosity than mixes with a low alkaline/fly ash ratio, such as GP6. It was noticed that aggregate grading did not change the water absorption/AVPV values significantly. Perhaps the constant amounts of geopolymer paste, without any change in the aggregate quantity influence this behaviour.

A correlation between the water absorption/AVPV with compressive strength is presented in Figure 4-8. Current findings were compared with water absorption from the previous author who used a geopolymer mix with 10M NaOH concentration.[29] A linear correlation of AVPV with compressive strength shows a decrease in AVPV with an accompanying increase in compressive strength. It was observed that a minor change of water absorption with a higher compressive strength indicated that the open porosity was not only affected by compressive strength.

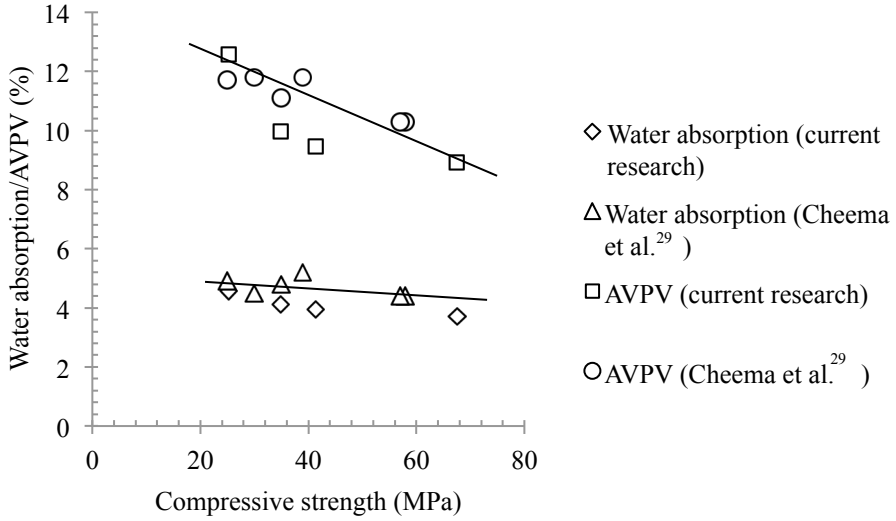

Figure 4-8 Correlation of water absorption/AVPV and compressive strength.

4.3.3 Water Permeability

Table 4-4 displays the average water permeability coefficient and the void content percentages of fly ash geopolymer concrete for selected mixes; i.e. GP1, GP2, GP3, GP4 and GP8. The coefficients obtained varied in the range from 2.46 $x10^{-11}$ to 4.67 $x10^{-11}$ m/s. The geopolymer concrete mixtures in this research can be classified as having an 'average' quality, judging by

the coefficient of permeability which is in the range of 10^{-11} to 10^{-12} m/s.[105] To ensure the water tightness of concrete cover in extreme environments under high water pressure, it is recommended to use concrete with a water permeability coefficient of less than $1x10^{-12}$ m/s.

Table 4-4 Water permeability coefficient of geopolymer concrete with different mixes

Mixture no	Parameter	Water permeability coefficient ($x10^{-11}$ m/s)	Void content (%)
GP1	w/s 0.23, a/s 3.90, 7:10mm	4.67	10.5
GP2	w/s 0.22	3.95	13
GP3	w/s 0.20	2.46	10.8
GP4	a/s 3.50	2.91	10
GP8	7:10:20mm	2.61	8.2

Mix GP1 showed the highest water permeability coefficient of any other concrete. Conversely, GP3 displayed the lowest coefficient. Except for GP1 and GP2, the final water permeability coefficients of other mixes were slightly similar. Void content was obtained during water permeability tests by measuring the difference between the dry and saturated weights of concrete before and after testing. From Table 4-4 it can be seen that the void varied from 8.2% to 13% which also confirms that all concrete has an 'average' quality.[105] There exists a nonlinear relation between the water permeability coefficient and the void content, since GP1 with a low void content has the highest permeability coefficient. Pore continuity, another aspect of porosity, was seen to be more influential in this flow rate measurement.

Water permeability is influenced by pore connectivity in the concrete paste. The pore development of concrete is dependent on parameters such as water content, binder content and the curing method. This is also the case for the fly ash geopolymer concrete. The low water permeability of GP3 was attributed to the denser paste and smaller pore interconnectivity. The increase of the aggregate content of GP4 contributes to a decrease in capillary pores volume and the water permeability coefficient.

A positive correlation exists between the water permeability coefficient and compressive strength (Figure 4-9). As the compressive strength increases, the permeability coefficient also increases. It can be seen that the water permeability coefficient of the current study was higher than Cheema et al.[29] This may be due to the geopolymer mixture composition and types of water permeability test carried out by both researchers.

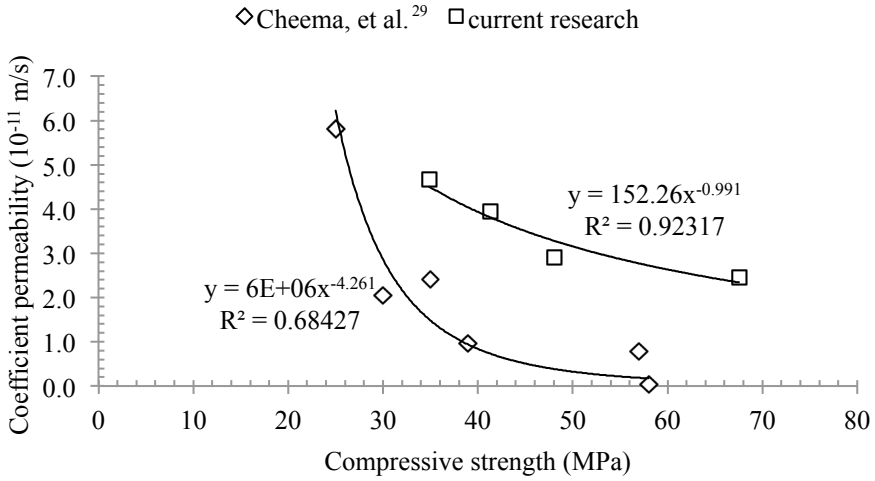

Figure 4-9 Correlation of water permeability coefficient and compressive strength.

The preliminary study was carried out to investigate the impact of some parameters such as water/solids ratios, aggregate/solids ratios, alkaline/fly ash ratios and aggregate grading, on the compressive strength, water absorption/AVPV and water permeability of fly ash geopolymer concrete. From this study, some conclusions can be made. First, the water/solids ratios are the most influential parameter, since the low water content increases the compressive strength and reduces the porosity of the concrete. Second, the alkaline/fly ash ratio of 0.30 is a second important parameter in producing a high strength and low porosity geopolymer concrete. Third, the optimum aggregate/binder ratio of 3.50 contributed to the strength of concrete; however, to obtain a low porosity of fly ash geopolymer, the ratio needs to be increased to 4.70. Thus, some parameters investigated in the preliminary study were considered useful in the next stage of designing the fly ash geopolymer concrete using the Taguchi method in the next section.

4.4 Taguchi Optimization of Geopolymer Concrete

Based on the Taguchi orthogonal array arrangement OA_9 (3^4) in section 3.5, nine concrete mixes were cast for this research. Each mix has a different variable but every combination of levels appears the same number of times. Mixture proportions according to Orthogonal Array (OA^9) are presented in Table 4-5.

Table 4-5 Mixture proportions design

Trial	Factors			
	Aggregate content (kg/m^3)	Alkaline/fly ash ratio	Ratio of Sodium Silicate/NaOH	Curing condition
T1	1752	0.3	1.5	24h 60^0C
T2	1752	0.35	2	12h 70^0C
T3	1752	0.4	2.5	24h 75^0C
T4	1800	0.3	2	24h 75^0C
T5	1800	0.35	2.5	24h 60^0C
T6	1800	0.4	1.5	12h 70^0C
T7	1848	0.3	2.5	12h 70^0C
T8	1848	0.35	1.5	24h 75^0C
T9	1848	0.4	2	24h 60^0C

A detailed proportion of geopolymer concrete with H_2O/Na_2O was kept constant at 12.50 to obtain workable mixes, and is presented in Table 4-6. The proportions were determined by a basic calculation of geopolymer concrete mixture (Section 3.3.2).

Table 4-6 Proportions of geopolymer concrete mixtures used in the study

Mix	T1	T2	T3	T4	T5	T6	T7	T8	T9
Fly ash (kg/m^3)	498.46	480.00	462.86	461.54	444.44	428.57	424.62	408.89	394.29
Aggregates (kg/m^3)	1752	1752	1752	1800	1800	1800	1800	1800	1848
NaOH 14M	59.82	56.00	52.90	46.15	44.44	68.57	36.40	57.24	52.57
Sodium silicate	89.72	112.00	132.24	92.31	111.11	102.86	90.99	85.87	105.14
Superplasticizer	6.1	6.1	6.1	6.1	6.1	6.1	6.1	6.1	6.1
Added water	26.47	23.65	21.23	18.61	18.55	28.51	15.97	24.46	21.47
SiO_2/Na_2O	0.85	0.97	1.05	0.86	0.96	0.92	0.85	0.82	0.93
SiO_2/Al_2O_3	3.76	3.86	3.96	3.79	3.89	3.87	3.82	3.81	3.92
Na_2O/Al_2O_3	0.42	0.48	0.54	0.46	0.51	0.51	0.49	0.50	0.56
H_2O/Na_2O (design)	12.50	12.50	12.50	12.50	12.50	12.50	12.50	12.50	12.50
H_2O/Na_2O (actual)	12.50	12.36	12.28	11.71	11.76	13.13	11.18	12.45	12.26

Some tests such as porosity, sorptivity and compressive strength, were carried out to justify the most optimum mixture that responds well with requirements for concrete in seawater environment. Table 4-7 displays the compressive strength of mixes T1-T9 at 1, 7 and 28 days.

Table 4-7 Compressive strength of trial geopolymer mixtures

Trial Mix	Combination	Compressive strength (MPa)		
		1 day	7 days	28 days
T1	A1B1C1D1	37.81	39.52	39.93
T2	A1B2C2D2	34.56	35.31	37.09
T3	A1B3C3D3	49.67	49.89	49.64
T4	A2B1C2D3	41.92	40.93	42.51
T5	A2B2C3D1	32.45	37.55	38.69
T6	A2B3C1D2	25.17	27.16	28.64
T7	A3B1C3D2	54.10	52.29	54.89
T8	A3B2C1D3	32.40	34.53	35.73
T9	A3B3C2D1	25.86	29.29	29.71

In general, the compressive strength increases with concrete age, except for T3 and T7. A slight reduction in the compressive strength at 28 days (T3) and at 7 days (T7) was observed.

The compressive strength of low calcium fly ash geopolymer varies until the concrete is 28 days old due to an extension of the geopolymerisation process.[136] The highest compressive strength was performed by T7 with 54.89 MPa at 28 days, while T9 showed the lowest strength properties of 29.71 MPa. Mix T7 contained the highest content of aggregate compared to the other geopolymer mixes. It is widely known that high aggregate content in the mixture could increase concrete strength substantially.[64] The inclusion of aggregate increases the geopolymer strength due to an improvement of bonding between aggregate in the presence of alkalis.[16]

Compressive strength was used in the initial evaluation of mixes using the Taguchi method in this experiment. Using the same principle with Signal/Noise (S/N) ratio analysis in section 2.5, a response index was determined in this experiment. The average contribution of each level of a factor to the final strength was calculated by adding the strength of mixtures corresponding to this level and dividing the sum by repeating the number of times for this level. A plot of compressive strength response index versus concrete age is presented in Figure 4-10. It can be seen that a combination of parameters of A1B1C3D3 produced the highest compressive strength. Thus, the yielded mix A1B1C3D3 was considered as T10 and used for further investigation.

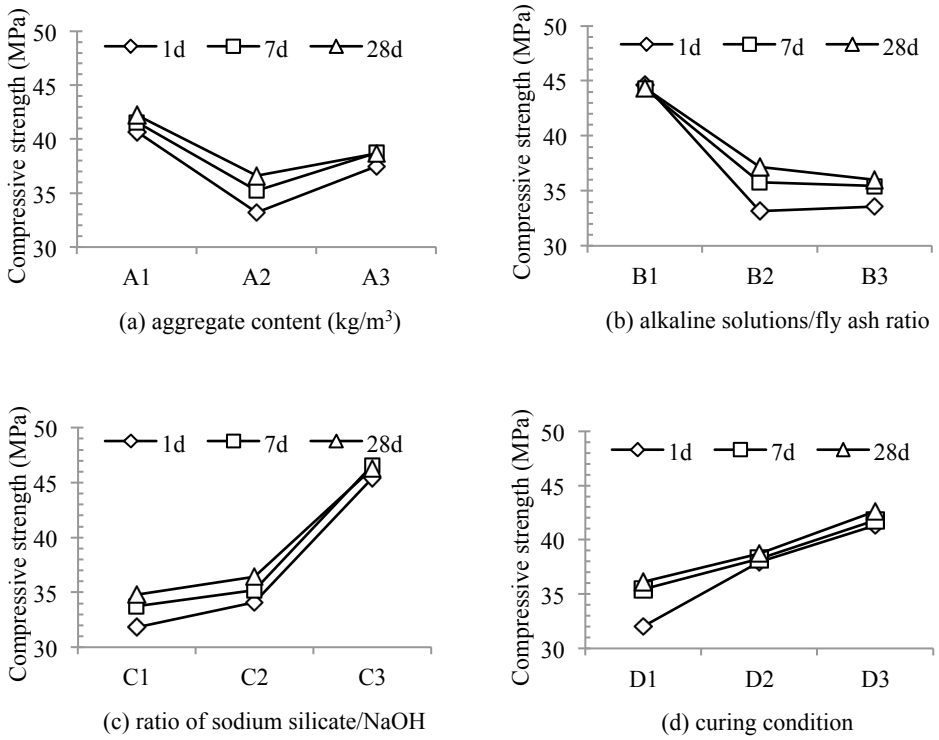

Figure 4-10 Relationship between compressive strength and variables at each value: (a) aggregate content, (b) alkaline solutions/fly ash ratio, (c) ratio of sodium silicate/NaOH, (d) curing condition.

The change in compressive strength, weight loss, total weight loss after wetting-drying cycles, sorptivity and AVPV results were displayed in Table 4-8. The response index method was applied for those properties as performance indicators of the pore structure[164], chloride resistance and porosity of bulk concrete[90], respectively, in the seawater environment.

Table 4-8 Test results of trial mixes

Trial Mix	Combination	Compressive strength after wetting-drying (MPa)	Change in compressive strength (%)	Weight loss during drying process (%)	Total weight change (%)	Sorptivity ($mm/min^{0.5}$)	AVPV (%)
T1	A1B1C1D1	52.62	33.15	2.65	101.51	0.1324	8.86
T2	A1B2C2D2	50.44	42.85	2.78	101.79	0.1344	9.54
T3	A1B3C3D3	59.48	19.22	2.80	101.14	0.1174	9.87
T4	A2B1C2D3	55.48	35.55	2.55	100.45	0.1034	8.33
T5	A2B2C3D1	47.87	27.48	2.59	101.54	0.1280	9.09
T6	A2B3C1D2	38.20	40.65	3.14	101.57	0.1806	9.95
T7	A3B1C3D2	69.81	33.51	1.97	101.04	0.0805	7.42
T8	A3B2C1D3	42.11	21.95	2.76	100.69	0.1538	8.96
T9	A3B3C2D1	37.92	29.46	2.92	101.73	0.1561	10.60

Figure 4-11 yielded the mixes with parameter combination of A3B1C3D2 (T7) and A1B1C3D3 (T10) performed the minimum weight loss during drying, AVPV and sorptivity values. The effect of variables on the mass loss, sorptivity and AVPV is explained as follows. From Figure 4-11(a), it can be seen that the optimal combination to getting a low value of mass loss is A3B1C3D2. This combination coincidently had a similar combination to T7. Mix T7 has the smallest mass loss of those mixes. Next, from Figure 4-11(b), the low value of sorptivity can be obtained using a combination of mix A1B1C3D3. It was found that the best combination for sorptivity had a similar proportion to those values proposed in determining high strength concrete. Figure 4-11(c) shows the effects of variables to concrete closed porosity, in terms of AVPV percentage. From the figure, the optimal combination to gaining low AVPV values is A3B1C3D2, which has a similar combination to T7. This means T7 can serve as a durable mix composition in seawater, since the mass loss and AVPV are low.

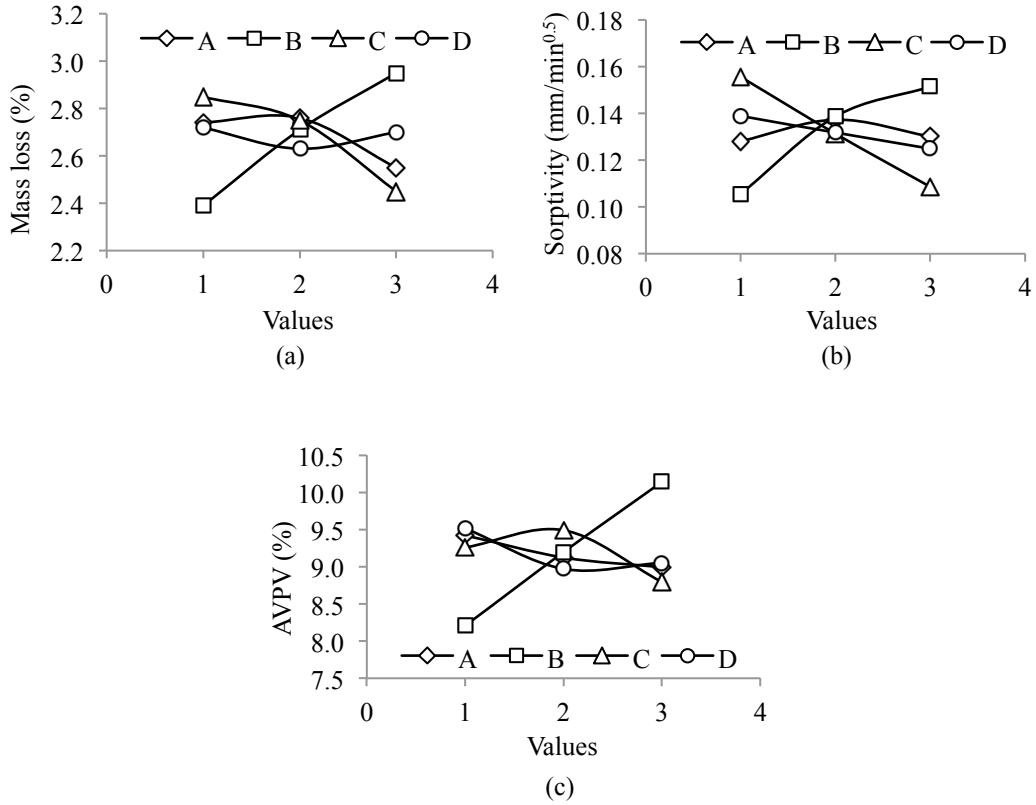

Figure 4-11 Relationship between: (a) weight loss, (b) sorptivity, (c) AVPV and variables at each value.

A new set of optimum mixtures is shown in Table 4-9 for further evaluation. Mix T7 has been chosen for its good properties in strength and durability. It also has a shorter curing duration, which is efficient for geopolymer concrete manufacturing. Mix T10 was yielded from a new combination A1B1C3D3 to obtain high strength concrete with low sorptivity. This mix needed to be evaluated to meet the durability standard of concrete in a marine environment. Mix T4 has a moderate strength but good workability and durability after T7. By reducing the H_2O/Na_2O ratio, a new high strength mix can be produced.

Table 4-9 Proposed optimum mixture proportion of fly ash geopolymer concrete

Mix	Combination	Component			
		Aggregate content (kg/m^3)	Alkaline/fly ash ratio	Ratio of Sodium Silicate/NaOH	Curing condition
T7	A3B1C3D2	1896	0.3	2.5	12h 70^{0}C
T10	A1B1C3D3	1800	0.3	2.5	24h 75^{0}C
T4	A2B1C2D3	1848	0.3	2.0	24h 75^{0}C

4.5 Mechanical Properties, Water Absorption, Sorptivity and Drying Shrinkage

The Taguchi mixture optimization of fly ash geopolymer in the previous section produced three mixtures, i.e. mix T4, T7 and T10. As already discussed, the optimization was intended to increase efficiency in durability study by using only three mixes with various characteristics. For example, T7 uses a high aggregate and NaOH quantities, while T10 uses more fly ash and the sodium silicate. To validate the optimum mixtures, the OPC concrete with an equivalent strength was used as a control mix. This section presents the characteristics, mechanical strength, water absorption, sorptivity and drying shrinkage of the optimum mixtures.

4.5.1 Fresh Concrete Characteristics

The fresh characteristics determined, namely slump, workability and pH of the fresh geopolymer are presented in Table 4-10. It can be seen that all geopolymer mixes have higher slump values than the OPC concrete. In fact, the geopolymer mixes were stiffer than the OPC. In terms of workability, mix T4 showed a considerable low workability, compared to the high workable OPC mix. Mix T7 with the highest aggregate content produced a very poor workability mix. Inclusion of high quantity of fly ash and sodium silicate of T10 has also created a very sticky and stiff mixture. It can be seen that the pH of the fresh geopolymer was higher than the fresh OPC mix. The fly ash geopolymer concrete usually has a considerably high pH in a fresh state. The high alkalinity from the chemical solution is essential to start the geopolymerisation process, since silica and alumina of fly ash can disintegrate in a very high pH environment.[41]

Table 4-10 Slump, workability description, and pH of fresh concrete

Mixtures	Slump (mm)	Workability	Fresh concrete pH
OPC	90	High	12.00
T7	180	Very stiff	12.12
T4	240	Low	12.30
T10	250	Sticky and stiff	12.27

Table 4-11 Density of OPC and geopolymer concrete at the age of 7, 28, 91 and 365 days

Mixture	Density (kg/m^3)			
	7 days	28 days	91 days	365 days
OPC	2392.95	2374.57	2294.77	2375.40
T4	2379.56	2385.42	2288.72	2310.24
T7	2362.93	2337.07	2326.64	2341.60
T10	2354.72	2358.53	2287.95	2299.12

The hardened concrete density is shown in Table 4-11. It can be seen that the fly ash geopolymer density was in the range of 2287.95 to 2385.42 kg/m^3. The density of the geopolymer mixes were in the range of normal concrete, i.e. 2200-2600 kg/m^3.[64]

4.5.2 Mechanical Properties

4.5.2.1 Compressive Strength

Figure 4-12 displays the average compressive strength and its standard error for the OPC and geopolymer concrete at day 28, 91 and 365. At 28 days, the compressive strength of the concrete was in the range 56.24 to 60.20 MPa. All mixes achieved a target strength of 55 MPa, which was higher than 50 MPa, as required for concrete in the seawater environment exposure class C.[129] It can be seen that the compressive strength increased with concrete age for all mixes. A gain in compressive strength of T4 continued until 91 days, before it slightly decreased at 365 days. Mix T7 showed a slow gain of strength until 91 days and reached the peak at 365 days. Mix T10 displayed a gradual increase of strength with concrete age and achieved the highest strength of 69.82 MPa in one year.

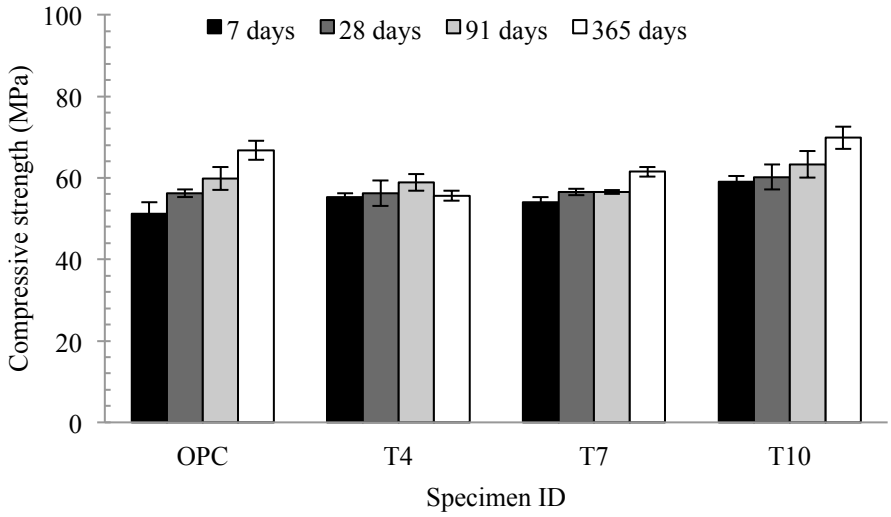

Figure 4-12 Compressive strength development of the optimum concrete mixtures.

The compressive strength of the OPC and fly ash geopolymer is influenced by different mechanisms occurring in the paste. A continuous hydration that keeps filling in the concrete pores was responsible for a strength gain in the OPC concrete. It was found that the fly ash geopolymer gained strength after 91 days when a slow reaction occurs to refill the gel structure and develop a crystalline phase in the system.[139] The geopolymer strength development depends upon the alkaline activators type and concentration, curing temperature and aggregate content. For example, a high sodium silicate concentration can increase a strength gain in T10 over time. This was confirmed in the previous studies that stated a mixture with high silicate concentration combined with sodium hydroxide with an optimum quantity yielded a high strength concrete.[78] Mix T7 performed a slow strength gain until 91 days. This might be due to a high quantity of aggregate with small alkaline solution left to react with the fly ash in the

mixture. A marginal strength reduction of T4 was observed at 365 days, which could be due to a variation of mix strength. Overall, the optimum mixture achieved a target compressive strength of 55 MPa, which is recommended for reinforced concrete structures in seawater environments.

4.5.2.2 Tensile Strength

Figure 4-13 displays the splitting tensile strength of OPC and geopolymer mixes at 28, 91 and 365 days. The tensile strength for all concrete at 28 days was in a range of 3.96-4.29 MPa. The highest level of tensile strength was performed by T7 at 365 days, while the OPC concrete showed the lowest value. Mix T7 gained a significant tensile strength after 91 days and following a similar trend for the compressive strength. Mix T4 and T10 tend to have a gradual increase on the tensile strength with concrete age; similar trend was reported by previous researchers.[78, 136] It was suggested that this high tensile strength was assumed from an improved bonding at the interface of the geopolymer paste and aggregates.[66, 137] The bonding between the aggregates and geopolymer paste was high as indicated by cut, not pull out on the aggregate grains like in the OPC concrete. A chemical interaction between the aggregate and alkaline solution was suggested to cause this behaviour.[16]

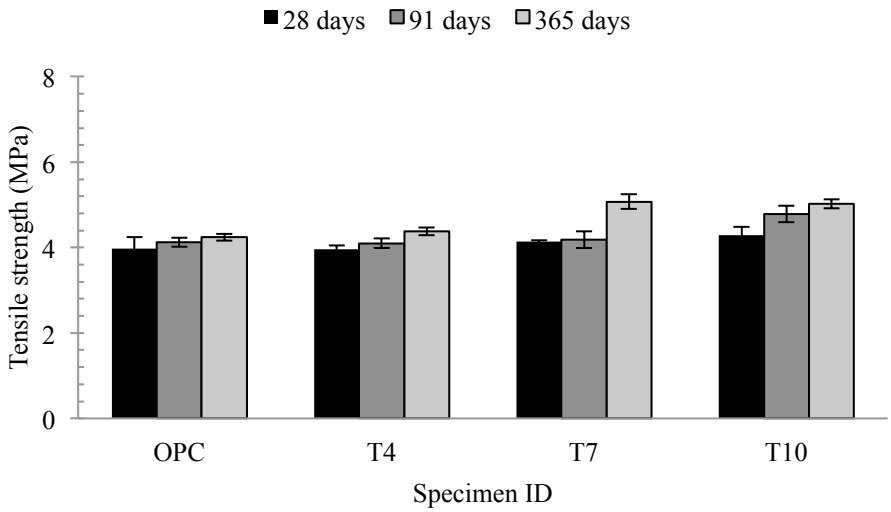

Figure 4-13 Tensile strength development of OPC and geopolymer concrete.

The tensile strength variation with the compressive strength is shown in Figure 4-14. As the strength increased, the tensile strength of OPC, T7 and T10 also has increased correspondingly. This trend was in agreement with the previous studies.[138] In contrast, T4 has an inverse relation between two parameters, since the tensile strength decreased as the compressive strength increased. It might be attributable to a decrease in compressive strength of T4 at 365 days as already discussed in the previous section.

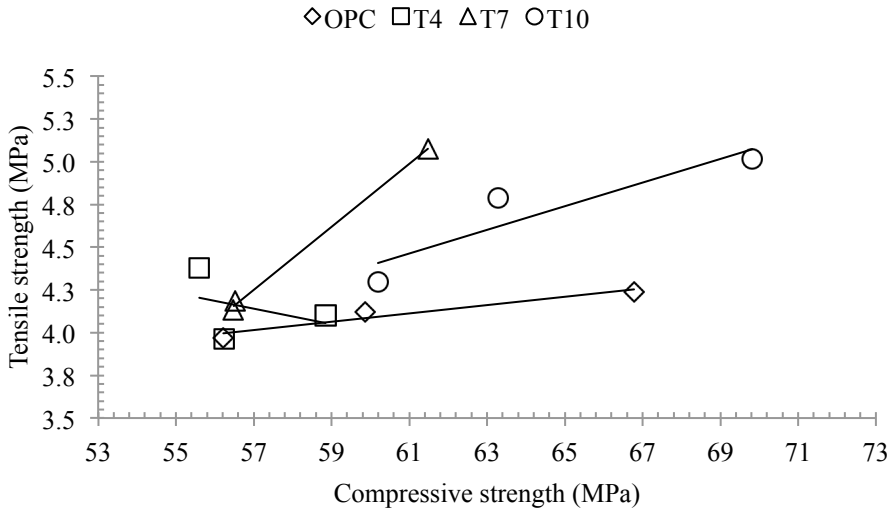

Figure 4-14 Variation of tensile strength with compressive strength.

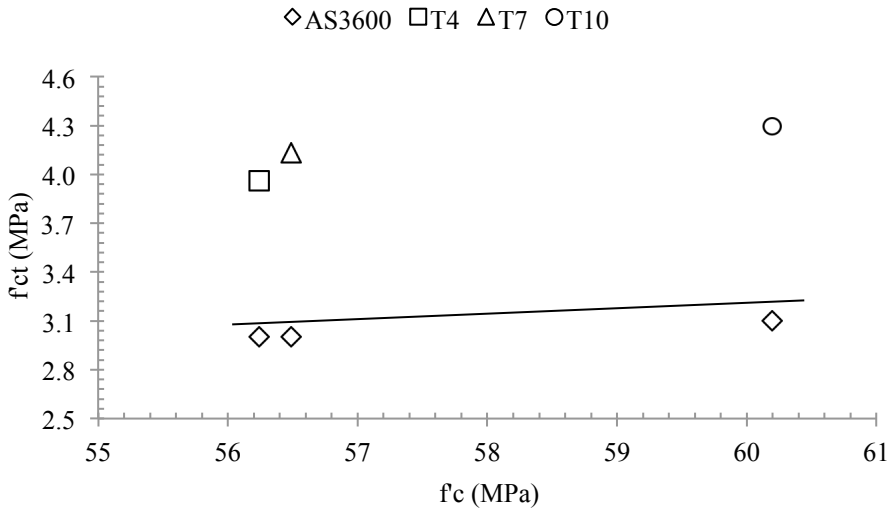

Figure 4-15 Tensile strength variation of geopolymer concrete at 28 days.

Figure 4-15 illustrates a tensile strength prediction that was plotted with values from the current research. The tensile strength for a design calculation can be predicted using an equation based on Australian Standard 3600[129] as follows:

$$f'ct = 0.4\sqrt{f'c} \quad (4.1)$$

where $f'ct$ = characteristics uniaxial tensile strength at 28 days (MPa), $f'c$ = characteristic compressive strength of concrete at 28 days (MPa). It was observed that the tensile strength of T4, T7, and T10 were higher than the AS3600 requirement for concrete with equal strength. This is favourable for reinforced concrete structures in the seawater environment. Low tensile strength assists the corrosion damage by developing tension or shrinkage cracks that can increase the moisture and oxygen penetration into the concrete. The high tensile strength can

decrease the rate and extent of concrete cover cracking because of corrosion of the steel reinforcement bars.[141] It can be seen that T10 performed the highest tensile strength among the other mixes. This is in agreement with a previous study[16] which found that mixes with high silicate content tend to produce a better bonding between the aggregates and geopolymer paste, thus the final tensile strength of concrete.

4.5.2.3 Flexural Strength

The average flexural strength of OPC and geopolymer concrete is presented in Figure 4-16. Overall, the values varied in the range of 7.02-9.91 MPa. It can be seen that the flexural strength of T4 and T7 tend to decrease at 365 days. The differences were probably due to a decrease of elasticity of specimens. For example, mix T7 contains a high quantity of aggregates that could change the elasticity of specimens, hence can have an adverse affect on the flexural strength in 365 days. This was confirmed by a change of Young's Modulus of Elasticity in Section 4.5.2.4. On the other hand, a considerable strength gain was displayed by T10 at 91 days before became steady at 365 days. This is because T10 contained more silicate than other mixes, thus became more elastic with the age of concrete. A different mixture composition between geopolymer and OPC certainly affects the flexural strength properties. In general, the geopolymer performed at a higher flexural strength than the OPC concrete. This was in agreement with previous findings[136]. It can be suggested that the silicate in geopolymer mix produced a better bonding between paste and aggregates, hence can influence the tension properties such as tensile and flexural strength. Concrete is known to be weak in tension and an additional increase in tension properties is advantageous for composite action between steel reinforcement bars and concrete.

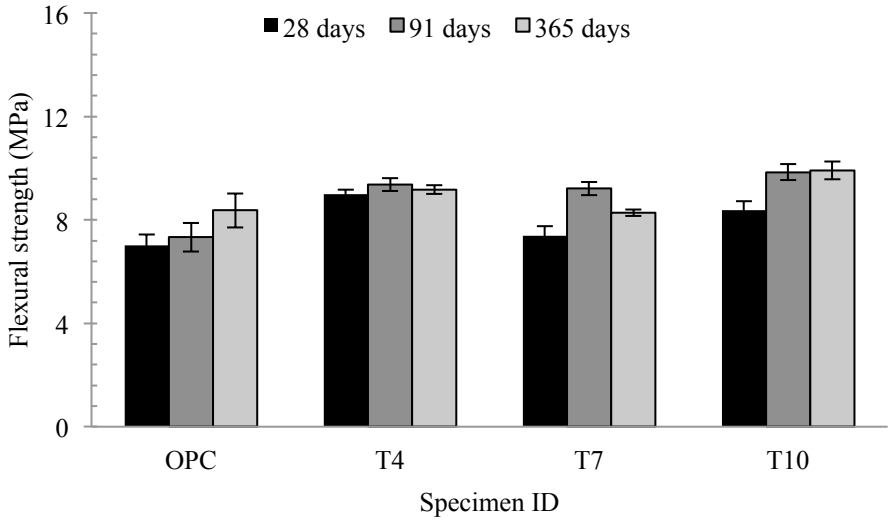

Figure 4-16 Flexural strength development of OPC and geopolymer concrete.

Figure 4-17 illustrates the flexural strength values from the experiment were plotted against a predicting model values from AS3600. The flexural strength for a design calculation can be predicted using equation based on Australian Standard 3600 as follows:

$$f'cf = 0.6\sqrt{f'c} \quad (4.2)$$

where $f'cf$ = characteristics flexural tensile strength of concrete at 28 days (MPa), $f'c$ = characteristic compressive strength of concrete at 28 days (MPa). Similar to the tensile strength, the flexural strength of the geopolymer concrete was higher than the model line prediction. Another study using the same AS 3600 equation reported a similar finding, where the flexural strength of geopolymer paste was high.[136] The high flexural strength demonstrated by the fly ash geopolymer concrete is very advantageous in decreasing the rate and extent of cracking due to the corrosion of reinforcement[141], especially in the seawater environment.

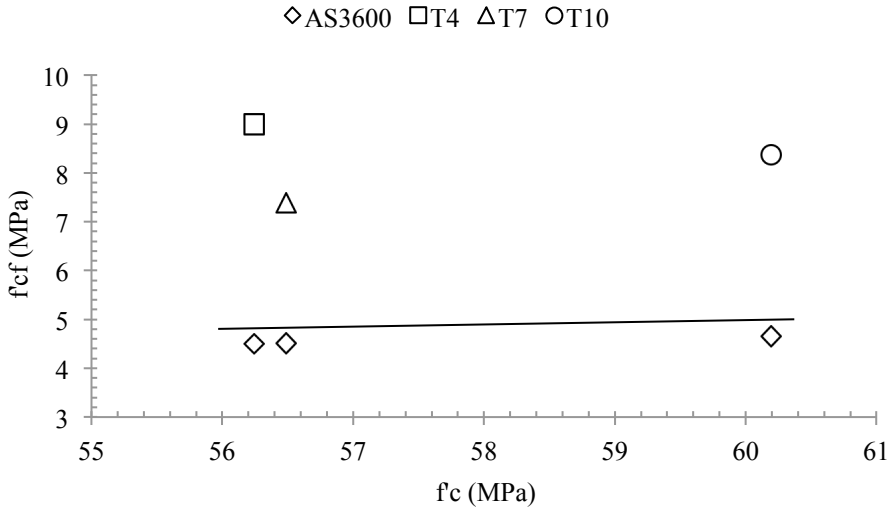

Figure 4-17 Variation of flexural strength with compressive strength at 28 days.

4.5.2.4 Young's Modulus of Elasticity and Poisson's Ratio

The average Young's modulus of elasticity at 28, 91 and 365 days for the OPC and geopolymer is shown in Figure 4-18. The modulus of elasticity of the geopolymer concrete varied between 25.33 to 31.26 GPa, while the OPC shows higher values in the range of 34.16-38.33 GPa. A normal weight concrete usually has a Young's Modulus in the range of 21-42 GPa. From the figure, it can be observed there was a gradual increase of Young's Modulus of the OPC, T4 and T7 with concrete age. In contrast, a decrease in modulus of elasticity was observed for T10 after 28 days. The presence of high silicate content in this mix might change the elastic nature and modulus elasticity evolution of T10.

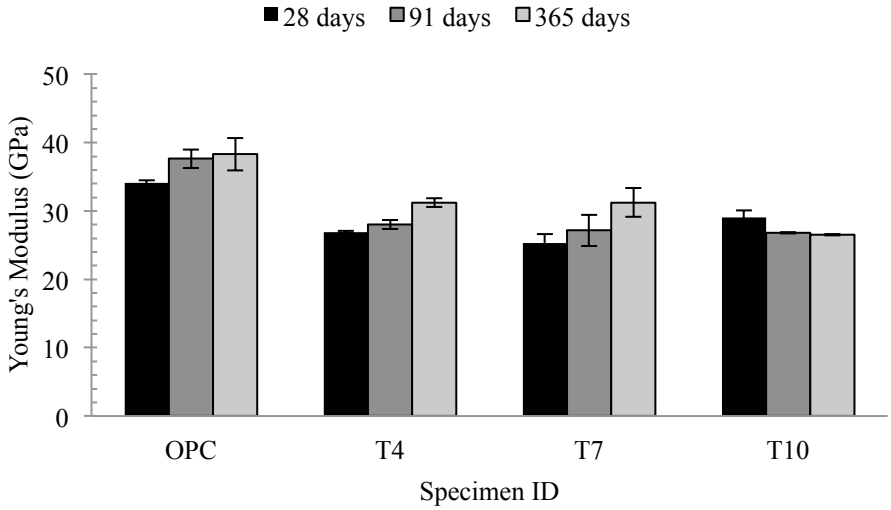

Figure 4-18 Young's Modulus of Elasticity of OPC and geopolymer concrete.

Geopolymer performed a lower modulus of elasticity than the OPC concrete that unlikely occurs in the OPC mixes with an equivalent compressive strength value. Similar behaviour has been confirmed by the previous authors using fly ash geopolymer paste.[78, 136] Previous studies suggested that a low density of geopolymer made from fly ash or slag and coarse aggregate such as granite influenced this behaviour.[138, 203] It seems that the modulus of elasticity of geopolymer is independent from the aggregates or fly ash type, but it mostly relies on geopolymer microstructure. This finding confirms factors such as an increase in homogeneity of geopolymer microstructures can improve the Young's Modulus, as stated by Duxson et al.[143]. Low modulus of elasticity is useful when the reinforced concrete structure's stiffness is not an issue. A low elastic modulus decreases the time of crack propagation in concrete cover due to volume expansion of corrosion product.[141]

The Young's Modulus of Elasticity of geopolymer concrete from the current investigation is plotted against the prediction using an equation from AS 3600 as shown in Figure 4-19. The following equation is used to predict Young's Modulus of Elasticity values for concrete with a compressive strength higher than 40 MPa:

$$Ecj = (\rho^{1.5}) \times (0.024\sqrt{f'c} + 0.12) \quad (4.3)$$

where Ecj = modulus of elasticity of concrete at the appropriate age (MPa), ρ = concrete density (kg/m^3), f'c = characteristic compressive strength of concrete at 28 days (MPa). It can be seen that the elastic modulus of geopolymer concrete was below the model line prediction of AS 3600. This could be due to the geopolymer paste composition (aluminosilicate), which is different than the OPC concrete.

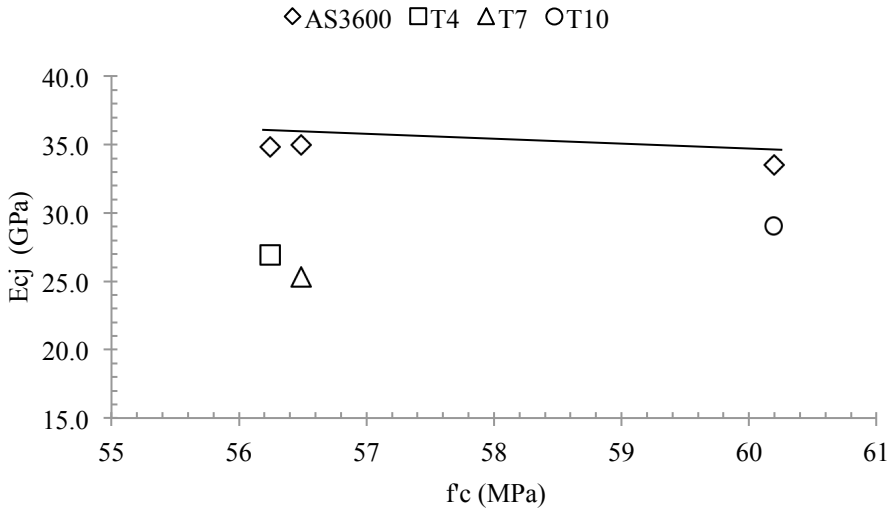

Figure 4-19 Variation of Young's Modulus of Elasticity with compressive strength at 28 days.

Poisson's ratio is determined together with the Young's modulus test. The property is used to describe the elastic behaviour of the material. Poisson's Ratio of the OPC and geopolymer concrete is presented in Figure 4-20. The average experimental values of the Poisson's Ratio of the geopolymer were in the range of 0.13 to 0.17, and are within the range observed for OPC concrete. These values were closed with previous findings of Poisson's Ratio's with a range of 0.12-0.16.[138] Poisson's Ratio of the geopolymer concrete in the current research was much lower than previous findings using geopolymer paste with a range of 0.23-0.26.[136] While the OPC showed a slightly higher value than the geopolymer in the range of 0.13-0.18. Poisson's Ratio is usually in the range of 0.15 for high strength and 0.22 for low strength concrete.[64] It normally taken as 0.2 for design purposes according to AS3600.[129]

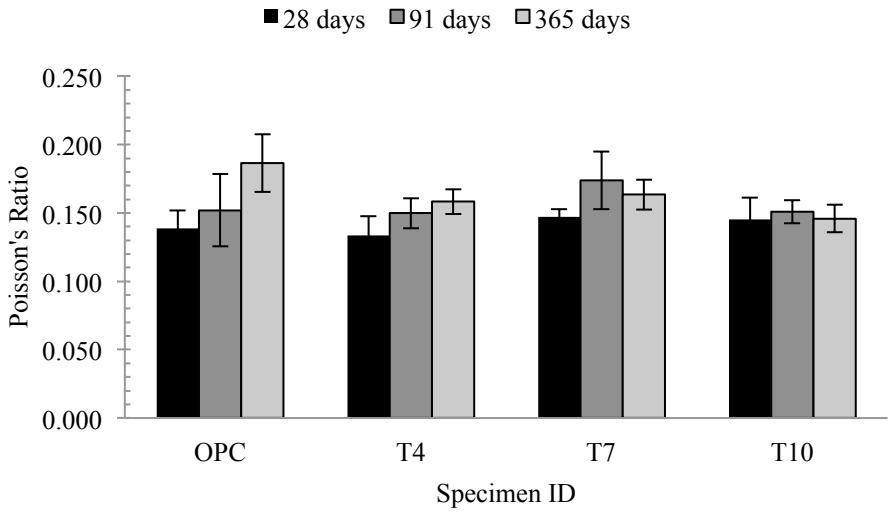

Figure 4-20 Poisson's Ratio of OPC and geopolymer concrete.

4.5.3 Water Absorption and AVPV

The water absorption for all concretes type is presented in Figure 4-21. Due to low water absorption of geopolymer concrete, the concrete can be classified as an 'excellent' concrete according to VicRoads.[133] There was a decline trend of the geopolymer concrete, showing a slight change in porosity. According to Llyod[139], a continuous reaction of the fly ash slowly refills the concrete pores with aluminosilicates producing denser pores. Therefore a change in concrete porosity could affect the water absorption of the concrete. Furthermore, T10 had the highest water absorption (4.05-4.32%) compared to other geopolymer mixes. It seems that the high sodium silicate amount in the system had an adverse impact for porosity, since it was responsible in producing porous aluminosilicate gel.[49] Water absorption of T4 decreased at 365 days, which showed a change of porosity in the concrete. Similar behaviour was also observed for T7, although a slight rise in the water absorption at 365 days. On the other hand, the OPC has higher water absorption than the geopolymer. There was no significant change in the porosity with concrete age, since water absorption values were in the range of 4.63-5.09%.

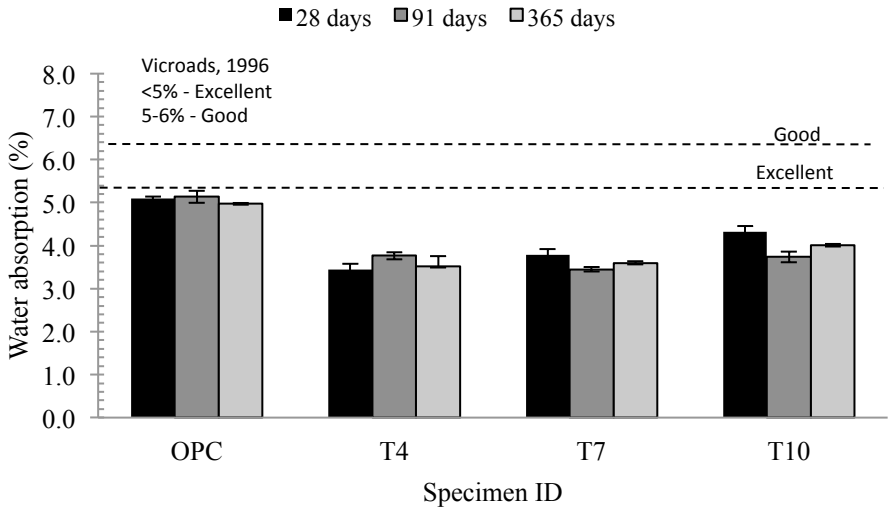

Figure 4-21 Water absorption of OPC and geopolymer concrete.

Figure 4-22 shows a variation of water absorption with the compressive strength. Water absorption of OPC decreases with an increase of the compressive strength. There was an inverse trend for T4 and T7 since water absorption tends to increase with compressive strength. A slight change in water absorption with compressive strength development was shown by T10. This clearly shows that the strength grade has a minor influence on the water absorption of geopolymer. The fact that pore development is more affected by mixture composition such as aggregates, alkaline solution and fly ash quantities than strength evolution. The geopolymer concrete performs unlimited pore refinement by aluminosilicates, unlike the OPC that has a continuous hydration process.

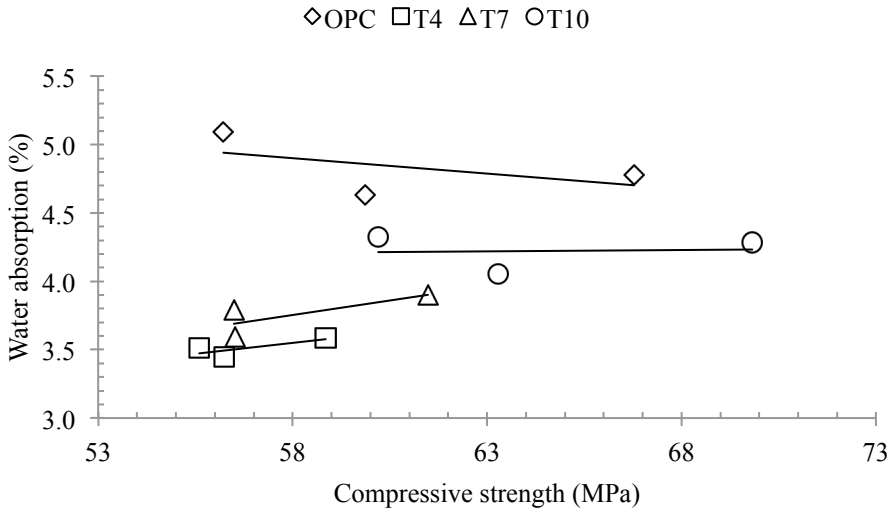

Figure 4-22 Variation of water absorption with compressive strength.

The Apparent Volume of Permeable Voids (AVPV) or the closed porosity of the OPC and geopolymer concrete are shown in Figure 4-23. In general, the AVPV of the geopolymer mixes followed a similar trend as shown by the water absorption in the previous section. The OPC concrete has AVPV varied in the range of 11.603-11.724%, while the geopolymer concrete indicate lower AVPV values in the range of 8.303-10.889%. The geopolymer can be classified as 'excellent' based on the limits specified by VicRoads.[133]

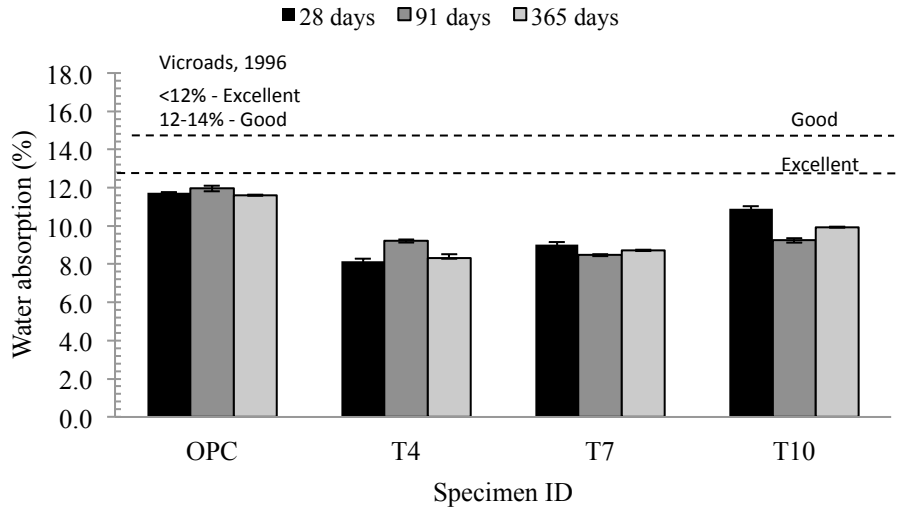

Figure 4-23 AVPV of OPC and geopolymer concrete.

Figure 4-24 presents a relation between water absorption and AVPV. Both parameters showing a linear correlation, as the water absorption increases the AVPV also increases correspondingly. The strong correlations were obtained because water absorption and AVPV varied similarly in spite of various mixture compositions. This suggests that the water

absorption can be predicted from AVPV for both types of concrete. Overall, based on water absorption and AVPV results, the geopolymer and OPC mixes in this research fulfilled the performance criteria for concrete in the seawater environment.

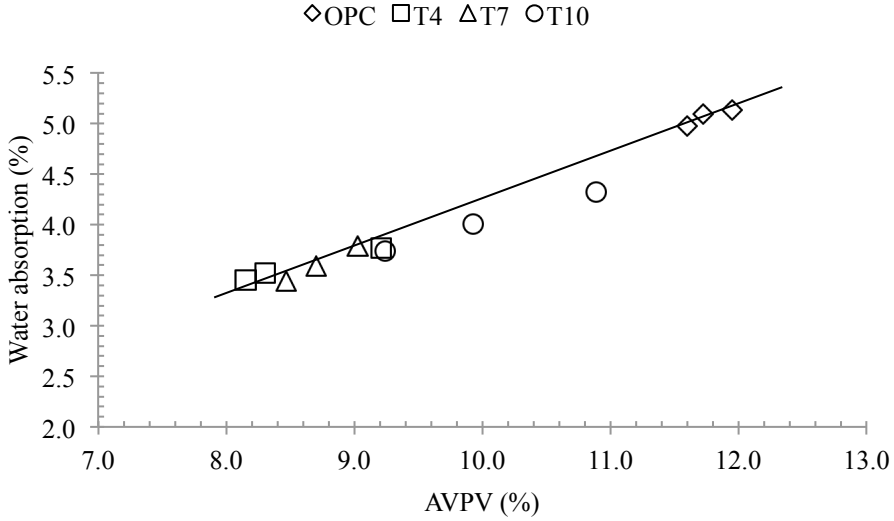

Figure 4-24 Variation of water absorption with AVPV.

4.5.4 Sorptivity

Another important indicator of transport properties is a rate of water absorption into the concrete through capillary pores or sorptivity. This is particularly important to evaluate the transport properties of concrete that governs the durability in the long term. In this research, only the initial sorptivity during the first four hours was measured. Figure 4-25 illustrates the variation of sorptivity for the OPC and geopolymer concrete. The sorptivity of the OPC samples varied in the range of 0.1888-0.2036 mm/min$^{0.5}$ while the geopolymer concrete has lower values in the range of 0.0813-0.1624 mm/min$^{0.5}$. Based on the experimental values, the geopolymer concrete in this research was classified as having an 'acceptable' quality. It was recommended to limit sorptivity index less than 0.2000 mm/ min$^{0.5}$ to maintain its water tightness.[132]

Geopolymer mixtures presented smaller sorptivity values than the OPC concrete. The same finding was also confirmed by previous research, where the fly ash geopolymer specimens performed a very low sorptivity compared to the alkali activated slag and GGBS blended cement [31]. That shows the geopolymer may have different capillary porosity network that can affect the rate of water absorption in the first four hours. This finding confirms the nonexistence of capillary pores in a well-reacted aluminosilicates using sodium silicate as stated by Llyod et al.[80]. It was suggested that aluminosilicates gel grows evenly through the geopolymer paste to develop a hardened binder structure. Hence, there is no capillary porosity

in the geopolymer paste that develops outward from the hydrating cement grains like in the OPC paste. This could explain the slow rate of water absorption into the geopolymer concrete since the pores are more distributed in paste. Interestingly, mix T7 and T10 showed a decrease of sorptivity index with time. Furthermore, the sorptivity of T7 was plunged into 0.0813 mm/ $min^{0.5}$ at 365 days. It probably reflects the porosity refinement of the gel particularly for this mixture. In the case of T10, it was found that the high sodium silicate content in the long term tended to fill the pores of geopolymer paste, making it less porous.[49] The gel porosity might be reduced by this mechanism.

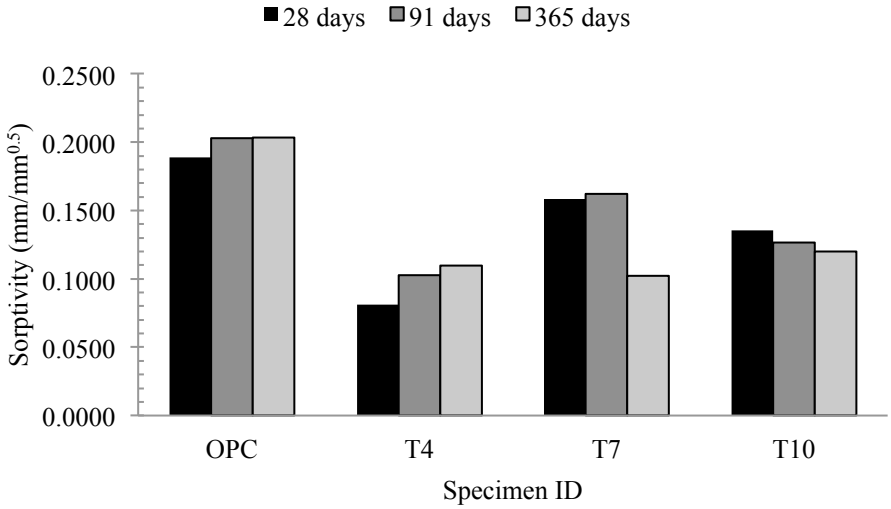

Figure 4-25 Sorptivity values of OPC and geopolymer concrete.

The variation of sorptivity with compressive strength is shown in Figure 4-26. It can be seen that only T10 showed a reduction of sorptivity with an increase in compressive strength. The same trend happened in mixtures T4 and T7. It can be concluded that sorptivity for both mixtures has no particular relation to the compressive strength. That shows how much mixture composition influences the transport properties in geopolymer concrete. On the other hand, the OPC mixture in this research showed a minor increase of sorptivity index with compressive strength. That behaviour is likely due to variation of specimens in the mixture. In fact, the mixtures produced in this research met the requirement for concrete in seawater environment since the sorptivity values were less than specified for concrete with exposure classification C2.[90]

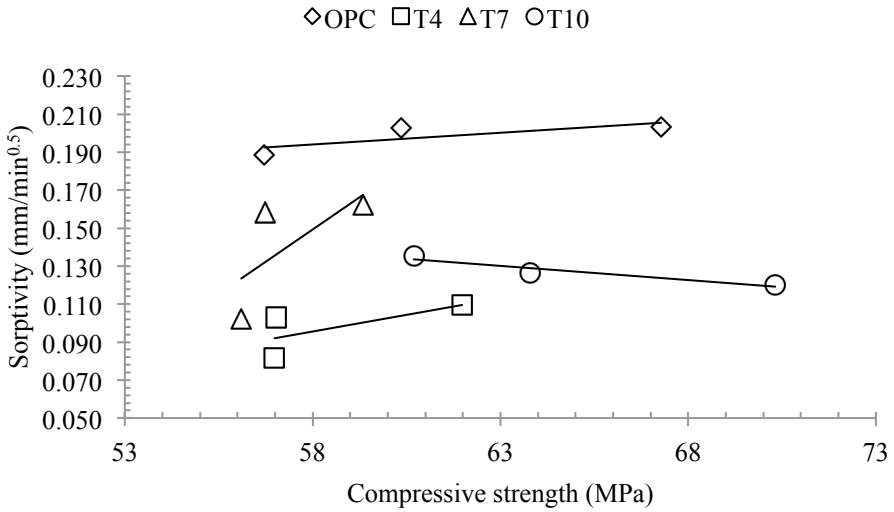

Figure 4-26 Variation of sorptivity with compressive strength.

4.5.5 Drying Shrinkage

Drying shrinkage of the geopolymer and control mix's specimen is presented in Figure 4-27. The negative reading refers to drying shrinkage and positive reading is an expansion/swelling. Mix T4 performed an expansion less than 200 micro strain (με) after being air-cured in the curing room with a relative humidity of 90%. A considerably steady and small expansion less than 4με were shown by T7. The OPC specimens performed a gradual rise in shrinkage to 500με at 91 days, before decreased to 384.39με at 115 days.

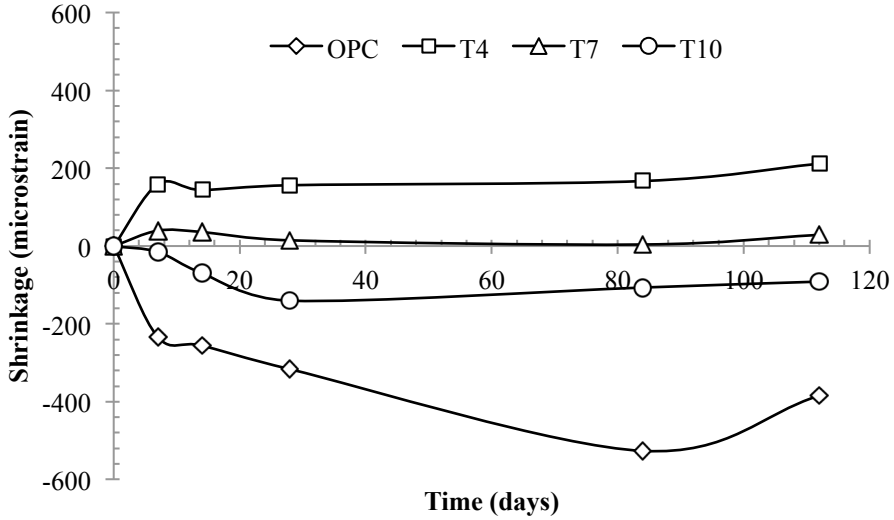

Figure 4-27 Drying shrinkage of OPC and geopolymer concrete.

The aluminosilicates in the geopolymer mix has a low water content that was unaffected by water loss during geopolymerisation. In contrast, the aluminosilicate is more prone to absorb moisture from humidity in the atmosphere, which is the case of T4.[78] High aggregate content might be a reason of the lowest values performed by T7, as the aggregate has restraining effect on the shrinkage.[64] It can be seen, T10 was the only geopolymer mixture that experienced shrinkage in this research. The value was less than 200 με, which was considerably low compared to the OPC concrete. Similar behaviour was confirmed in the previous studies.[21, 78]

In fact, there was no water loss during geopolymerisation or after steam curing due to low water content in the geopolymer mixtures. This low shrinkage is related to the high tensile and flexural strength as discussed previously. There were no cracks due high drying shrinkage such as in the OPC samples that can lead to a reduction of tensile strength. It can increase concrete degradation causing cracks that act as a rapid pathway for water penetration and other harmful ions. Hence, it was found that the fly ash geopolymer has a low shrinkage that is suitable to be used for concrete in seawater environment.

4.5.6 Microstructure of Fly Ash Geopolymer Concrete

The surface image of mix T4 observed using SEM were presented in this section. Typical fly ash geopolymer consists predominantly of aluminosilicate gel or geopolymer paste, unreacted fly ash and voids (Figure 4-28).

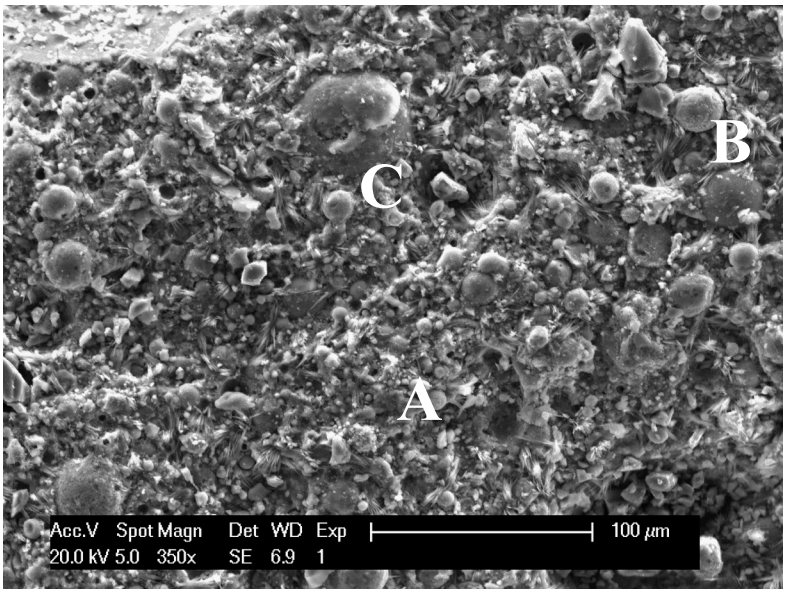

Figure 4-28 Typical microstructure of fly ash geopolymer concrete:
A: aluminosilicates/geopolymer paste; B: unreacted fly ash; C: partially reacted fly ash.

Similar results were reported by various authors.[49, 63] The aluminosilicate gel has an irregular shape, and the unreacted fly ash still exists in a spherical form. The reactivity of the system changed the resulted geopolymer paste. Coarser gel indicates a moderate reactivity of the geopolymer. Concrete cured in low temperature or ambient temperature might have coarser microstructure with high porosity gel. An increase of silicate content could increase the reactivity, providing a denser microstructure in the microstructure. The unreacted fly ash, according to mechanism discussed in Section 2.2.5, is unavoidable although high alkaline concentration and curing temperature were used in the system.[37] In this research, it was found that the geopolymer gel has small pores, which can influence the water absorption and permeability values.

Figure 4-29 displays the aggregate-gel interface of fly ash geopolymer concrete. As can be seen that there is no clear boundary between the geopolymer gel and aggregate such as Interfacial Transition Zone (ITZ) in the OPC system. A strong chemical bonding between the geopolymer gel and aggregate was observed under SEM.[63] A chemical reaction between aggregate and alkali, or mechanical interlocking between the geopolymer gel and coarse surface of the aggregate could be a reason for the high tensile and flexural strength of the fly ash geopolymer concrete observed in the previous section.[65]

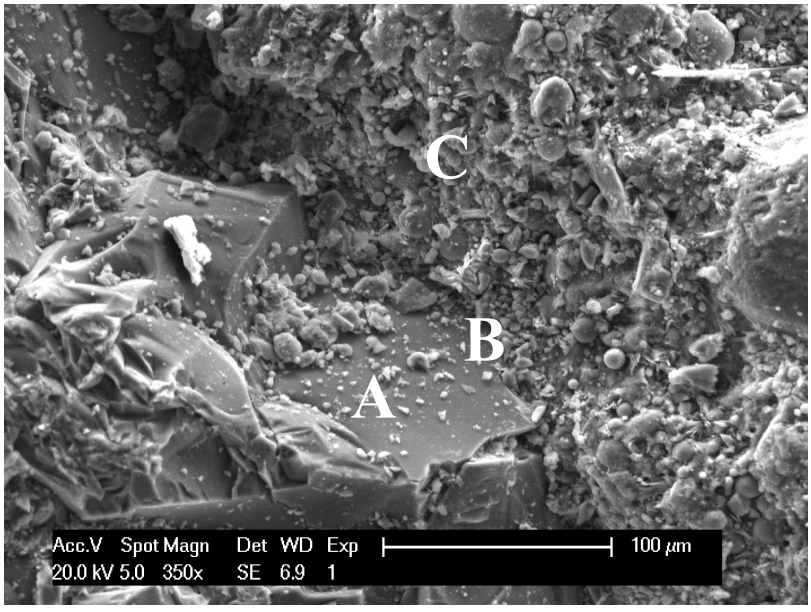

Figure 4-29 Aggregate-gel interface of fly ash geopolymer concrete: A: aggregate; B: interface between gel and aggregate; C: geopolymer paste.

4.6 Seawater Resistance

4.6.1 Chloride Ion Penetration

The chloride content of specimens without exposure to the NaCl solution was presented in Figure 4-30. The geopolymer samples contained chloride ions in the range of 0.010-0.012%, which was slightly higher than the OPC concrete sample. The only source of chloride of the geopolymer concrete is sodium hydroxide. The OPC concrete contained sodium chloride from calcium chloride that is usually added for accelerating the time of setting. The risk of chloride-induced corrosion of steel reinforcing bars in concrete is insignificant within the range. Mix T10 has the highest background chloride content compared to the other geopolymer mixes due to the high sodium hydroxide in the mixture.

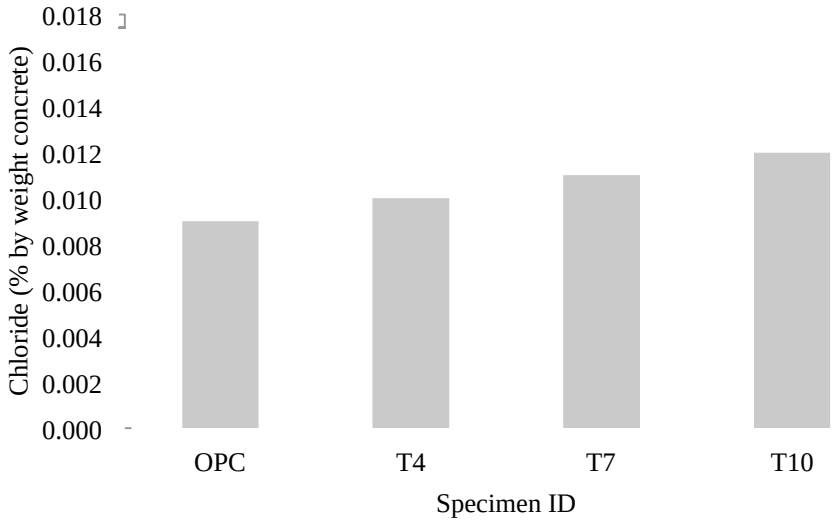

Figure 4-30 Chloride content background of OPC and geopolymer concrete.

The chloride content of the specimens at depth 0-15mm, 15-30mm and 30-45 mm are presented in Figure 4-31. The OPC concrete displayed a high chloride percentage with a sharp decrease for the 30-45mm concrete depth. A good concrete mix has normally had a decline trend of chloride profile with an increasing depth. The geopolymer concrete showed the same trend for all cover depth. The chloride content at 0-15mm depth was quite high. The geopolymer concrete performed high chloride content with a range of 0.35-0.46% at 0-15mm depth. There was a reduction of chloride content at 15-30mm depth, with a range of 0.28-0.35%. Chloride content of the geopolymer concrete at 30-45mm depth was 0.22-0.27%. The lowest chloride concentration among the geopolymer mixes was performed by T7. This could be due to a decrease of porosity at 91 days that can reduce the ingress of chloride as shown by water absorption/AVPV. It should be noted that the chloride content of the solution used was 16.5%, which is 4.7 times higher than normal chloride in a seawater environment (3.5%). The purpose was to accelerate the chloride ion penetration; hence, these values from this

experiment cannot be used to determine the chloride threshold on the concrete to quantify a corrosion risk.

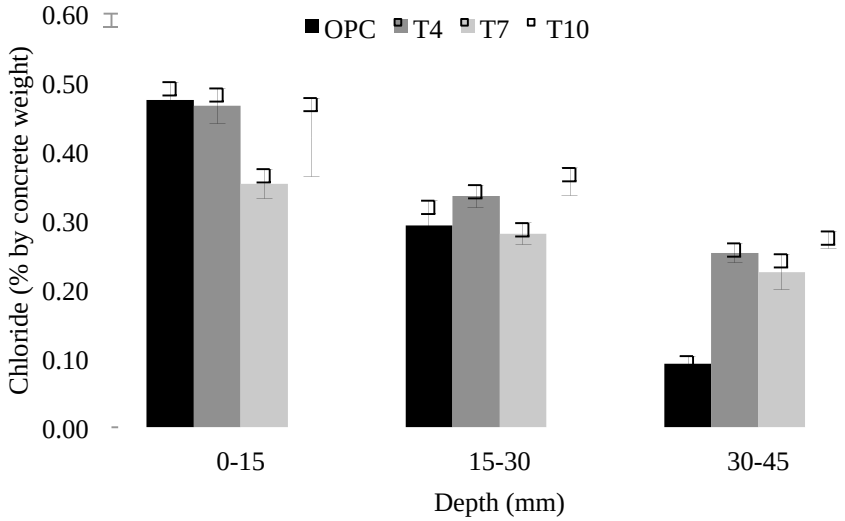

Figure 4-31 Chloride ion penetration for depth of 0-15mm, 15-30mm and 30-45mm.

It can be seen that there are two possible reasons for the high chloride concentration in the geopolymer matrix. First, the low calcium fly ash geopolymer concrete has no C_3A that could enable a chloride binding to minimize chloride ion penetration in the concrete paste. The chloride binding ability is an important mechanism that can reduce the chloride content in the OPC system, as discussed in Section 2.6.3.1. Second, there is no continuous hydration mechanism such as in the OPC concrete when the specimens were immersed under an aqueous medium. Continuous hydration under water is generally useful for concrete paste to refill pores that can reduce porosity and minimize ingress from harmful ions such as chloride. When the fly ash geopolymer concrete cured in the aqueous medium, there was no significant pore improvement due to this mechanism. Instead, there was leaching of alkalis from the aluminosilicates pore network, which can change the geopolymer microstructure.[204] There is a risk of an increase of porosity that can increase a rate of chloride ingress in the concrete.

4.6.2 Concrete Resistance in Continuous Immersion and Wetting-drying Cycles

The seawater resistance of OPC and geopolymer concrete subjected to continuous immersion and wetting-drying cycles in 3% NaCl was determined through a change in compressive strength, effective porosity, weight loss and length of specimens. All data were compared with similar properties from specimens cured at room temperature.

4.6.2.1 Change in Compressive Strength

The compressive strength of specimens exposed to different exposures is presented in Table 4-12. It can be seen that the compressive strength of concrete subjected to continuous immersion has a similar behaviour pattern with the specimens cured at room temperature. The lower strength of T7 at 28 and 91 days might be due to a slow geopolymer process under water immersion that inhibited strength development during the earlier time frame. Mix T4 and T10 showed no significant change of the strength up to 91 days under full immersion.

Table 4-12 Compressive strength of concrete subjected to different exposure

Test age (days)	Compressive strength (MPa)			
	OPC	T4	T7	T10
Curing at room temperature (23-25^{O}C)				
28	56.22	56.49	56.24	60.20
91	59.86	58.85	56.51	63.29
365	66.78	55.60	61.48	69.82
Continuous immersion at 23-25^{O}C in 3% NaCl solution				
28	58.88	56.12	49.26	60.29
91	60.87	61.68	48.43	64.00
365	64.06	59.42	56.29	65.78
Wetting-drying cycles: 24 hours drying at 80^{O}C in oven, 24 hours immersion at 23-25^{O}C in 3% NaCl solution				
28	59.78	68.95		
91	57.09	72.03		
200	56.55	62.26		

When the compressive strength of specimens cured at room temperature and continuous immersion were compared in Figure 4-32, the OPC and T10 showed an approximate strength loss of 4-6% at 365 days. In reverse, the continuous immersion has also increased compressive strength of T4 and T7 by 6% at 365 days. The strength losses in the OPC was marginal and could be due to leaching of portlandite or $Ca(OH)_2$, which slightly change the microstructure. When the chloride diffuses into the OPC, the hydroxide ions leach out to maintain the electro neutrality of paste which results in the portlandite solubility and a decrease of concrete strength.[127, 128] An increase of strength was observed for T4, which could be due to crystallization of aluminosilicates for mixtures with a high alkali content.[139, 162] In the case of T10, leaching of alkalis that alter the integrity of aluminosilicates network might contribute to a decrease of strength. This confirms the effect of alkalis leaching in the compressive strength of geopolymer from a previous study.[151] There was a decrease of strength of mix T7 at concrete age 91 days and a gradual increase at 365 days for mix T7. This mix has a high aggregate content and less alkaline activator than was needed to react with the available silica and alumina from the fly ash, which may delay the increase of compressive strength. The same behaviour was observed for mixtures with a small amount of alkaline activators in the

geopolymer fly ash mixed with rice husk ash, since lack of geopolymer binder contributed to that behaviour.[140] It can be concluded that there was a variation of strength change for the geopolymer specimens cured in chloride solution that depends on the mixture composition.

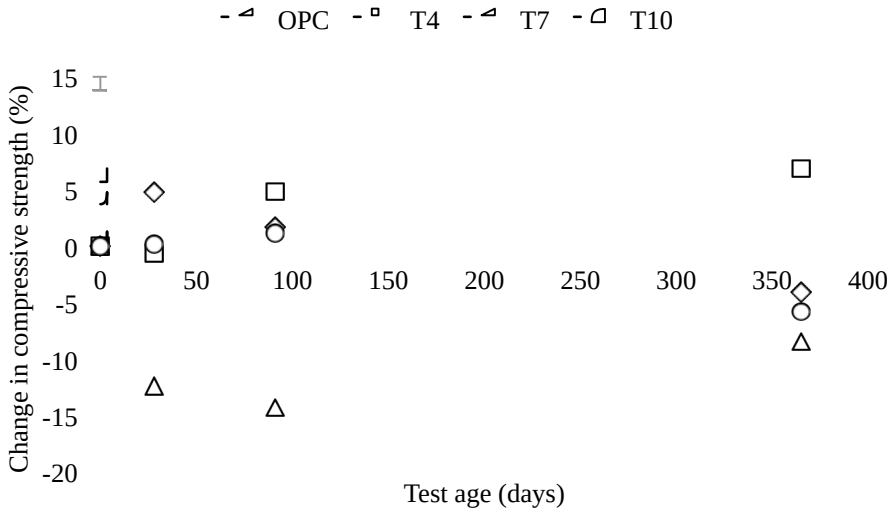

Figure 4-32 Change in compressive strength subjected to continuous immersion.

When subjected to wetting-drying cycles, the OPC concrete showed similar behaviour with the geopolymer concrete (Table 4-12). It can be seen also in Figure 4-33; the compressive strength initially increased and began to decrease at the end of the wetting-drying cycles. There was a 15% decrease of strength at 100 cycles or 200 days. In contrast, compressive strength of the geopolymer increased to 22% at 28 days before eventually decreasing to 11% at 200 days. The decrease of OPC strength was mainly due to an extreme temperature during exposure to accelerated wetting-drying cycles. A repetitive wetting and evaporation during drying in the NaCl solution resulted in salt crystals accumulation in the concrete pores.[64] The accumulative salt crystals in the pores could generate micro cracks in the paste and eventually the concrete cover. In fact, a decrease of strength was more dominant for the OPC, which might be due to the extreme temperature difference. It seems an increase of hydration rate during the wetting-drying cycles had an adverse impact compared to the physical attack of temperature difference.

The cyclic exposure was adversely affecting the geopolymer concrete strength. It was known that the geopolymer is a ceramic material that performs well under high temperature heating.[4] The repetitive exposure to the high temperature during drying cycles slightly increased the geopolymer strength. This is attributable to a faster crystallization process in the geopolymer concrete. A decrease of strength was observed at 100 cycles, which might be due to a faster rate of degradation on the concrete paste than the crystallization. Overall, it can be assumed

that there was no significant change in compressive strength in the fly ash geopolymer subjected to wetting-drying cycles. This is certainly beneficial for geopolymer concrete applications in tidal and splash zones.

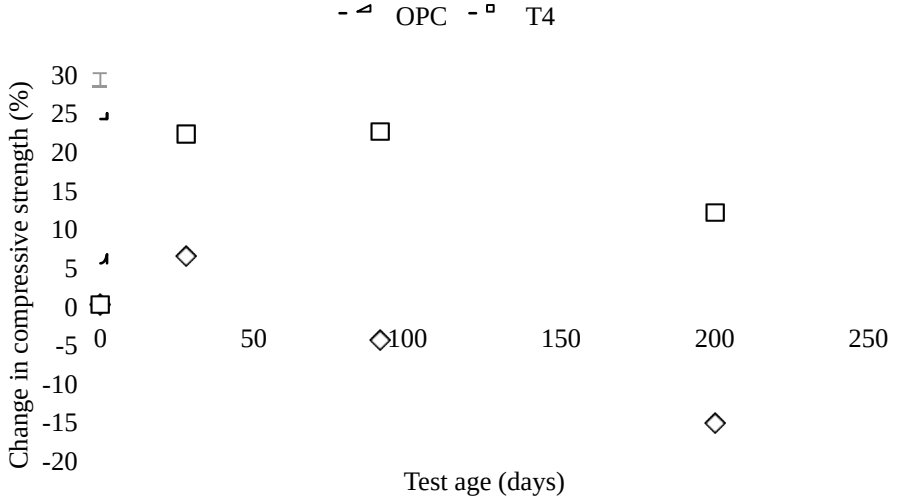

Figure 4-33 Change in compressive strength subjected to wetting-drying cycles.

4.6.2.2 Change in Young's Modulus of Elasticity

A change in Young's Modulus of Elasticity was observed for different exposures. Young's Modulus of Elasticity is sensitive in a changing environment, hence this property is usually used to measure a stiffness of material under certain exposures.[64] As can be seen in Table 4-13, all mixtures, except T4 displayed similar behaviour, elastic modulus decreased by 25% under continuous immersion at 365 days. A change in modulus elasticity of T7 and T10 was considered marginal, varied between 0.6-6% at 365 days (Figure 4-34). This proves that chloride ions have a minor effect on modulus elasticity of T7 and T10. There was a reduction of the Young's Modulus of Elasticity of the OPC concrete at 91 days. Similar finding was observed, which was probably due to ettringite and gypsum formation that decrease OPC's strength and stiffness.[205] In the case of low calcium fly ash geopolymer concrete that do not contain high $Ca(OH)_2$, immersed samples in sodium solution produces traces of ettringite and gypsum, which did not significantly have an adverse impact on the modulus of elasticity.[153] A decrease of stiffness was observed in T4 under fully immersion, but an increase of modulus of elasticity was observed for specimens in air-cured conditions. From the results, it can be seen that mixes T7 and T10 performed a small change in modulus of elasticity caused by chloride in the continuous immersion. This behaviour is favourable for reinforced structures in a submerged zone.

Table 4-13 Young's Modulus of Elasticity of concrete subjected to different exposure

Test age (days)	Modulus of Elasticity (GPa)			
	OPC	T4	T7	T10
Curing at room temperature (23-25^{O}C)				
28	34.16	26.95	25.33	29.05
91	37.64	28.03	27.18	26.80
365	38.33	31.23	31.26	26.54
Continuous immersion at 23-25^{O}C in 3% NaCl solution				
28	34.16	26.95	25.33	29.05
91	33.96	32.61	27.08	26.68
365	39.50	28.59	31.47	28.16
Wetting-drying: 24 hours drying at 80^{O}C in oven, 24 hours immersion at 23-25^{O}C in 3% NaCl solution				
28	34.16	26.95		
91	28.40	32.61		
200	32.59	32.09		

When subjected to wetting-drying cycles (Figure 4-35), the geopolymer concrete (mix T4) showed a decrease in elastic modulus by 14% at 365 days. This behaviour was similar when this particular mix was subjected to the continuous immersion. Another research on mechanical properties such as flexural and modulus of elasticity of fly ash geopolymer confirmed those values was much smaller than the OPC concrete after 50 cycles of wet/dry.[206] In contrast, the OPC displayed a decrease of modulus of elasticity by 25%, before increasing to 14%. The effect of wetting-drying cycles was significant in the geopolymer stiffness, which could be a problem for reinforced concrete carrying loads in tidal and splash zones in the long term.

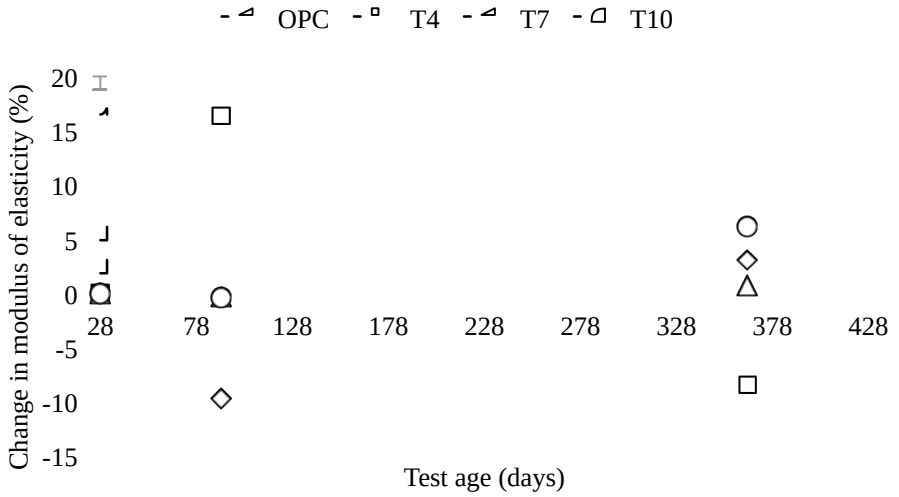

Figure 4-34 Change in Young's Modulus of Elasticity subjected to continuous immersion.

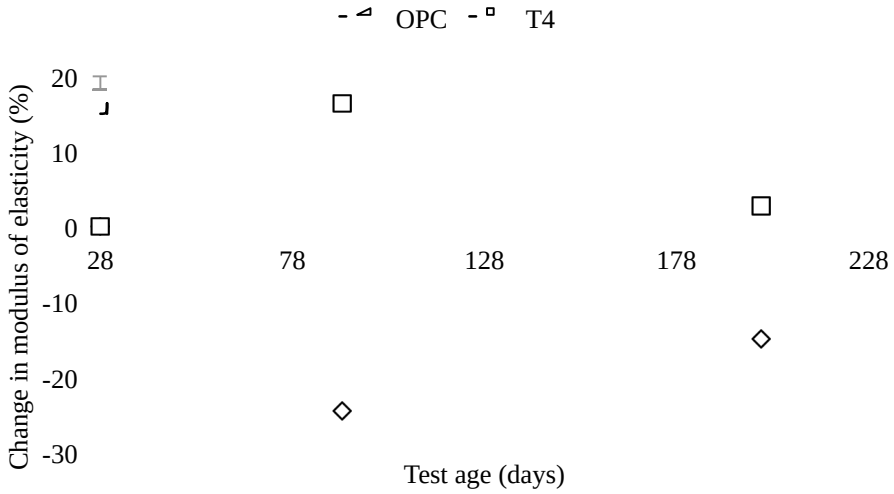

Figure 4-35 Change in Young's Modulus of Elasticity subjected to wetting-drying cycles.

4.6.2.3 Change in Effective Porosity

The effective porosity was calculated from water absorption values and the results are presented in Table 4-14. In general, the effective porosity of mixes T4, T10 and OPC increased with concrete age. The result was consistent with the earlier results of water absorption, where the fly ash geopolymer mixtures have lower water absorption than the OPC concrete. Plain cement is more porous than blended cement concrete and the geopolymer concrete. An increase in porosity of the OPC concrete under continuous immersion might be due to the microstructure alteration after portlandite leaching from concrete pores as already discussed in Section 2.6.3.4. Similar trends were observed for the geopolymer. This was due to alkalis leaching from aluminosilicates that change the microstructure and increase the porosity.

Table 4-14 Effective porosity of concrete subjected to different exposure

Test age (days)	Effective porosity (%)			
	OPC	T4	T7	T10
Curing at room temperature (23-25^{O}C)				
28	11.73	8.59	8.71	9.76
91	11.57	8.02	8.31	8.42
365	10.65	7.28	8.06	8.96
Continuous immersion at 23-25^{O}C in 3% NaCl solution				
28	11.73	8.59	8.71	9.76
91	11.46	8.30	8.32	9.14
365	12.34	8.42	7.91	10.07
Wetting-drying: 24 hours drying at 80^{O}C in oven, 24 hours immersion at 23-25^{O}C in 3% NaCl solution				
28	11.73	8.59		
91	10.35	9.59		
200	0.367	8.11		

There was a reverse trend for T7 with a decrease of porosity in Figure 4-36. This might be due to two reasons. First, there was a porosity improvement that has a positive effect on the compressive strength after being subjected in the chloride solution. Second, it could be due to a very low rate of alkalis leaching in the T7 paste, as this mix has a high aggregate content. From this finding, it can be concluded the alkalis leaching in the mixes with high aluminosilicate content such as T10 and T4 change the porosity of fly ash geopolymer concrete during continuous immersion. It needs to be investigated further whether this porosity change could affect the integrity of geopolymer structures in full immersion zones in the long term.

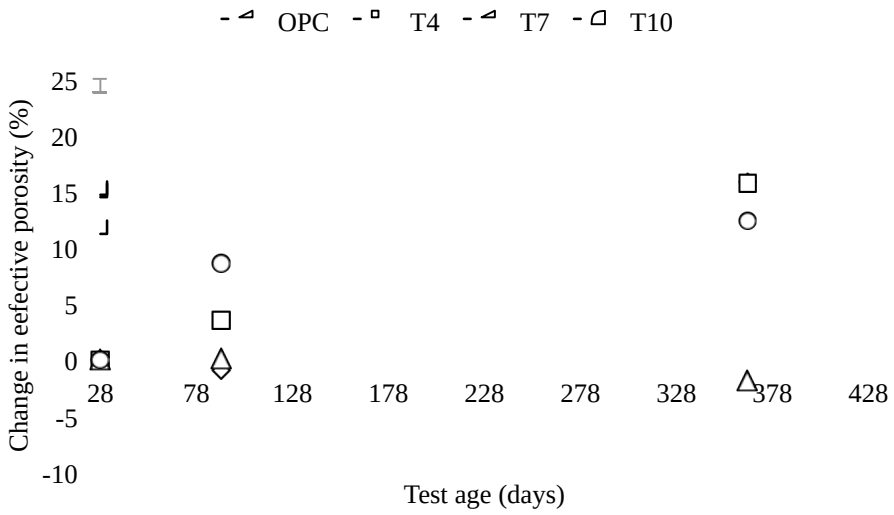

Figure 4-36 Change in effective porosity subjected to continuous immersion.

The most significant result is a decrease of the OPC porosity by 96% after 365 days subjected to wetting/drying cycles (Figure 4-37). This might be attributable to an accelerated hydration that reduced the concrete porosity and the damaging effect from repetitive wetting-drying cycles. This confirms similar behaviour from a previous study of wetting-drying in sulphate attack medium.[205] On the other hand, the porosity of geopolymer from the cyclic wetting-drying exposure was quite similar to the initial porosity at 28 days. There was no significant change in concrete porosity, such as in the OPC concrete. Due to low calcium content in the geopolymer paste, there was no replenishment of the pores due from continuous hydration, except the aluminosilicates crystallization. This crystallization seemed to be affecting the mechanical strength more than geopolymer porosity under wetting-drying cycles. This is certainly advantageous when the concrete to be used is subjected to wetting-drying conditions.

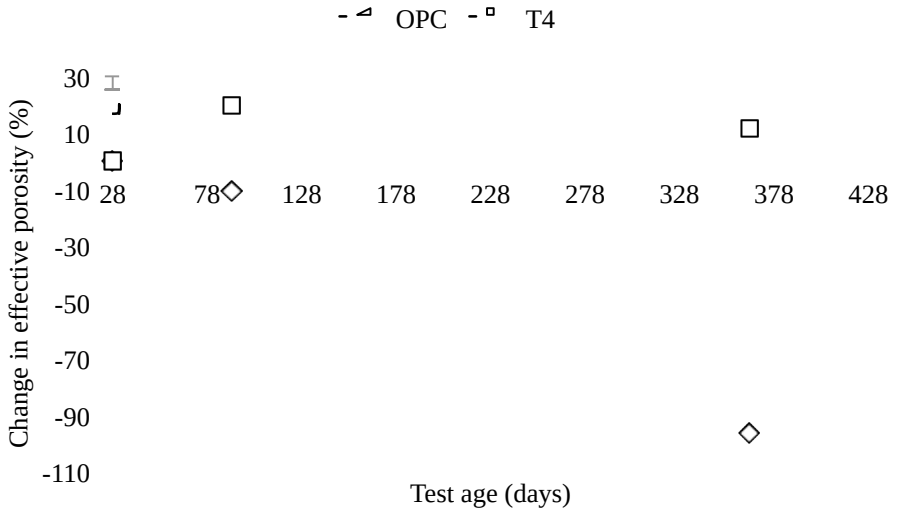

Figure 4-37 Change in effective porosity subjected to wetting-drying cycles.

4.6.2.4 Change in Weight

Figure 4-38 displays the weight changes of concrete subjected to continuous immersion in NaCl 3.5%. The geopolymer concrete performed a steady weight change, although it started with a considerable high value of 1%. There was a steady trend of weight change for all geopolymer concrete. Mix T4 has low weight change percentages compared to T7 and T10, indicating no sign of chloride accumulation in the specimens. All mixtures showed a constant change in weight with time, revealing that a marginal microstructure alteration occurred in the specimens.

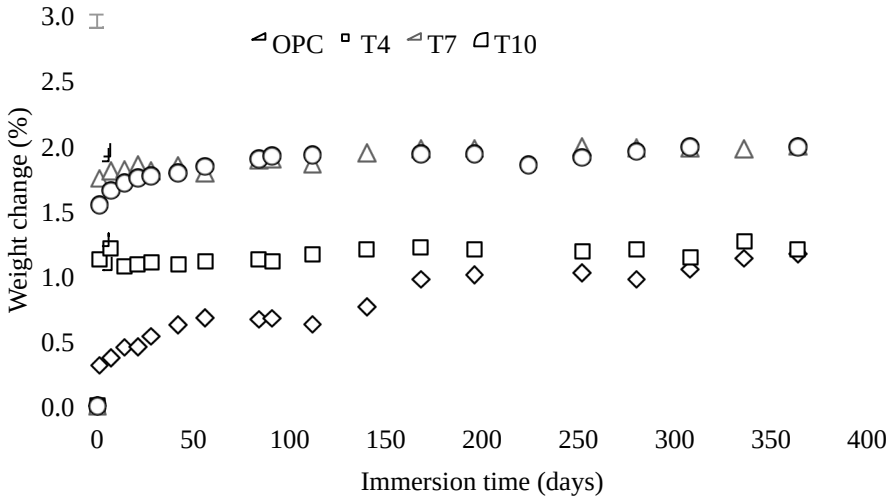

Figure 4-38 Weight changes of concrete subjected to continuous immersion.

In contrast, the OPC concrete showed a gradual increase in the percentage of weight change with time. This might be due to the chloride crystal accumulation into the concrete pores that

was bound by the paste and which increases the final concrete mass. Since there is no chloride accumulation in the geopolymer concrete paste this could be related to the high change of porosity in Section 4.6.2.3. Hence, it can be concluded that the change in weight of the fly ash geopolymer concrete is minor in the continuous immersion related to the increase of porosity.

Figure 4-39 presents the weight losses for both geopolymer and OPC concrete subjected to the wetting-drying cycles. There was a substantial initial weight loss of 2.4% for the geopolymer concrete up to 60 cycles before it decreased slightly at 100 cycles. There was a high initial weight loss for the OPC before it went down gradually by 0.5% at 100 cycles. The sudden increase of weight loss in the first days for both concrete mixes indicated higher water absorption than evaporation in the early stages of wetting and drying cycles. The elevated weight loss of the fly ash geopolymer can be attributed to the high pores interconnectivity that allows rapid chloride ion movements from the outer to inner side of concrete. Moreover, constant values indicated no sign of repetitive chlorides crystallization formed in the fly ash geopolymer pores. Chlorides crystallization in the pores was more noticeable on the OPC concrete as there was a gradual reduction of weight percentage over time.

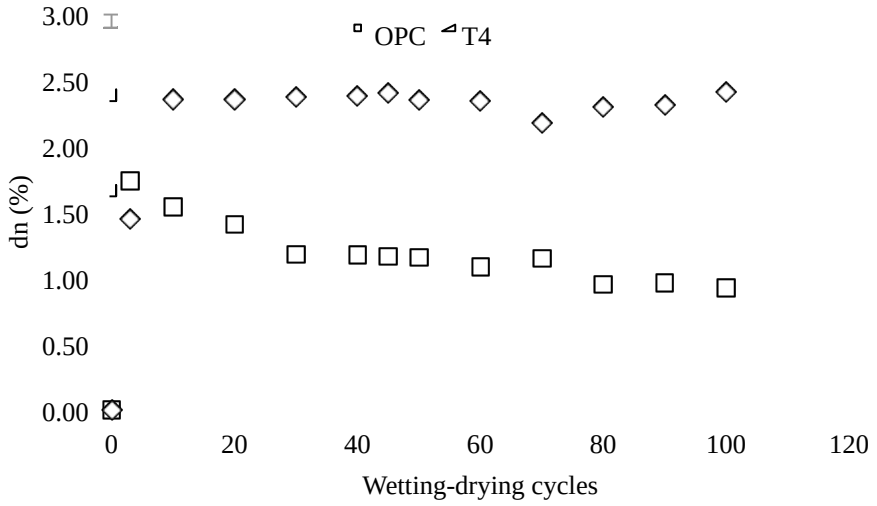

Figure 4-39 Weight losses during the drying process of concrete subjected to wetting-drying cycles.

A change in total weight of concrete during wetting-drying cycles is presented in Figure 4-40. There was a decrease in total weight of the geopolymer concrete because of paste degradation during wetting cycles. As indicated in the previous section, the fly ash geopolymer concrete was more prone to paste structural degradation in aqueous medium because of alkalis leaching, which can disrupt the final microstructure.[204] Visual examination shows a high disturbance of geopolymer concrete cover with visible holes and loss of fine aggregates (Figure 4-41(f)). In

application, the disintegration of fly ash geopolymer concrete cover after wetting-drying cycles up to 100 cycles could significantly affect its protection from corrosion of reinforced steel bar in seawater environment, particularly in tidal and splash regions. Chloride ions penetrate at a faster rate and oxygen diffuses through the disrupted pore network, which eventually increasing the corrosion rate. On the other hand, the OPC concrete showed an increase of total weight as a result of chloride crystallization in the pores during the drying process and semi-continuous hydration during wetting. The accelerated hydration refines the capillary pores, thus reducing the chloride penetration in the pores. When the pores cannot store any more salt crystals, the crystals will appear as salt scaling on the concrete surface.[205]

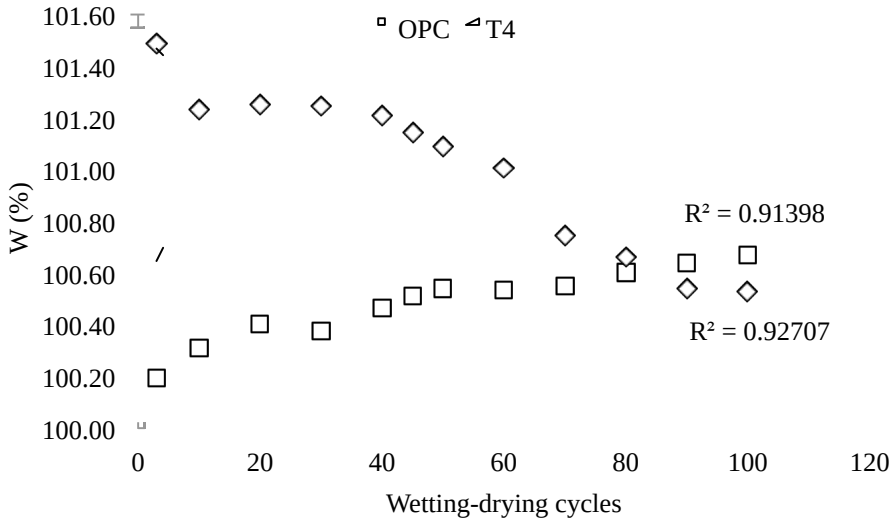

Figure 4-40 Change in total weight of concrete subjected to wetting-drying cycles.

Figure 4-41 (a-f) shows the surface appearance of both type of concrete subjected to three different exposures, i.e. air-cured, continuous immersion and a cyclic wetting-drying at 365 days. There was no significant change in the OPC and T4 surface after air-curing at 365 days (Figure 4-41 (a, b)). It can be seen in Figure 4-41 (b) that there was a crystallization of sodium chloride in the OPC concrete surface that contributes to the gradual weight change. The geopolymer concrete in Figure 4-41 (d), on the other hand showed no sign of chloride crystal growth in the concrete surface. The OPC concrete seemed to be more prone to ettringite formation due a reaction between chloride and calcium from cement. The crystal, formed in the concrete surface changed the weight quite significantly and influenced the microstructure of the concrete. After being exposed to wetting-drying cycles for 100 cycles, the OPC concrete in Figure 4-41 (c) demonstrated surface degradation. The concrete paste was damaged and some voids became more apparent. High surface degradation can be seen in T4 after 100 cycles

wetting-drying in Figure 4-41 (f). Geopolymer paste was highly disintegrated, more voids were distributed and the fine particles were eroded from the concrete surface.

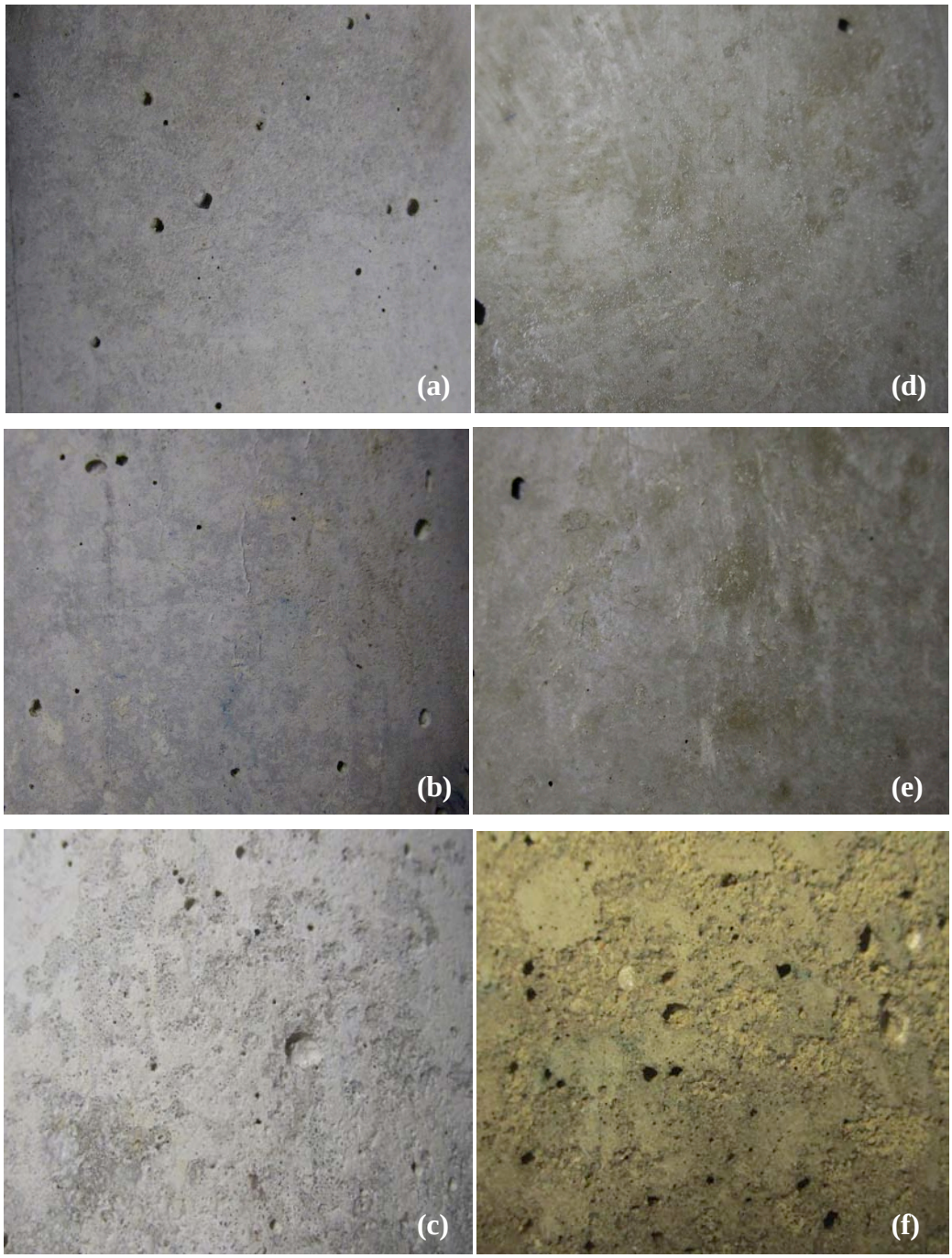

Figure 4-41 Surface appearance of the OPC and geopolymer concrete subjected to air-cured, continuous immersion and wetting-drying cycles, up to down: (a): OPC after 365 days air-cured, (b) OPC after 365 days continuous immersion, (c): OPC after 100 cycles of wetting-drying; (d) T4 after 365 days air-cured, (e) T4 after 365 days continuous immersion; (f) T4 after 100 cycles of wetting-drying.

4.6.2.5 Change in Length

A change in length of the concrete subjected to continuous immersion and wetting-drying cycles was represented by shrinkage or expansion. As can be seen in Figure 4-42, there was a very high expansion by the OPC concrete of approximately 2650 μ ε at 112 days. The expansion of OPC was related to swelling in the pores due to chloride ion penetration and continuous hydration in the long term. On the other hand, mix T7 and T10 recorded much smaller expansions that were mainly in the range of 461-527 με at 112 days. This is likely due to a smaller accumulation of salt crystals in the tiny aluminosilicates pores. In contrast, T4 experienced shrinkage, of approximately 700 με during the immersion period. A change of state of T4 was unique, since this type of concrete performed expansion during air-curing and shrinkage in continuous immersion. This matter certainly needs more investigation in the future.

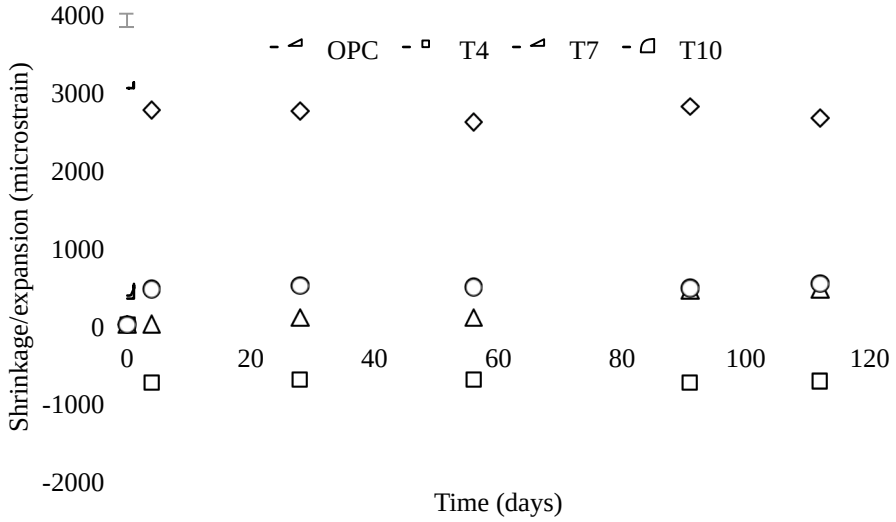

Figure 4-42 Length of change subjected to static immersion.

The change in length of OPC and geopolymer concrete under wetting-drying cycles was reported separately in Figure 4-43. It can be noted that considerable shrinkage was observed from the OPC specimens after wetting and drying cycles. There was a high initial shrinkage of 3000 με, before it began to decrease to 3700 με at 112 days. On the other hand, there was a gradual increase of shrinkage up to 56 days, which slightly rose before it went down at 112 days. This significant change in length resulted from extreme conditions during repetitive wetting-drying that could have caused micro cracks in the specimens to expand. The shrinkage cracks influences the tensile strength and modulus of elasticity of OPC concrete subjected to wetting-drying condition.

In contrast, the geopolymer T4 performed a small and steady trend of expansion and shrinkage during the wetting-drying testing period. Geopolymer showed an expansion during drying cycles, and shrinkage during wetting cycles. Overall, this indicated the geopolymer resistance to an extreme and repetitive temperature changes during wetting-drying cycles. This could be due to microstructure alteration that also affected porosity and modulus of elasticity discussed in the previous section. Compared to the OPC, the geopolymer concrete was found more tolerant to the extreme temperature difference during wetting-drying cycles. This is advantageous for reinforced concrete structures in the tidal and splash zones because there was no damage from tensile strength due to shrinkage cracks.

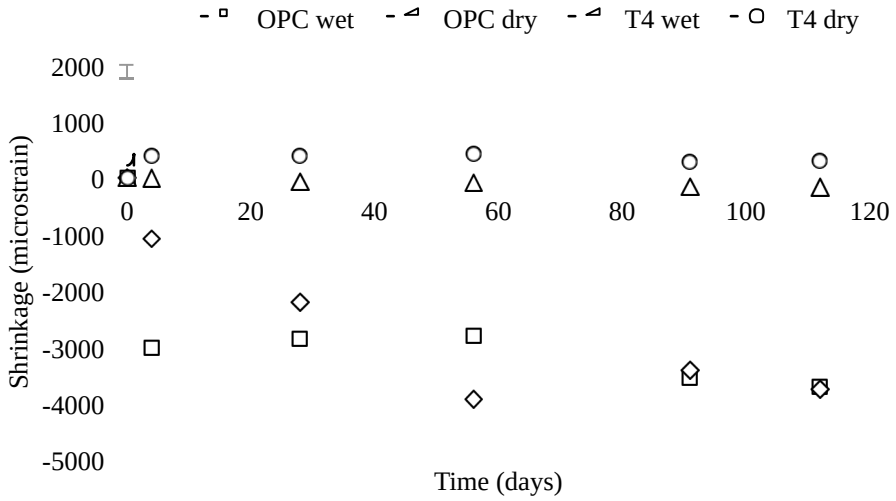

Figure 4-43 Length of change OPC and T4 after exposed to wetting-drying cycles.

4.6.2.6 Microstructure of Specimen under Continuous Immersion

Figure 4-44 displays the SEM image of fly ash geopolymer concrete T10 after continuous immersion at 365 days. It can be seen that the actual geopolymer microstructure could hardly be seen since it was covered with crystals. It was revealed that a formation of large amounts of chloride crystals in the concrete pores in the long term could increase the expansion and attack the microstructure of geopolymer. Previous research stated that the salt contamination in the added water for the geopolymer mixture reduced mechanical strength and affected the durability of specimens.[207] Since there is no EDX analysis for this specimen, the actual elements formed in the reaction between geopolymer and salt cannot be analysed further. This matter certainly needs more investigation in the future.

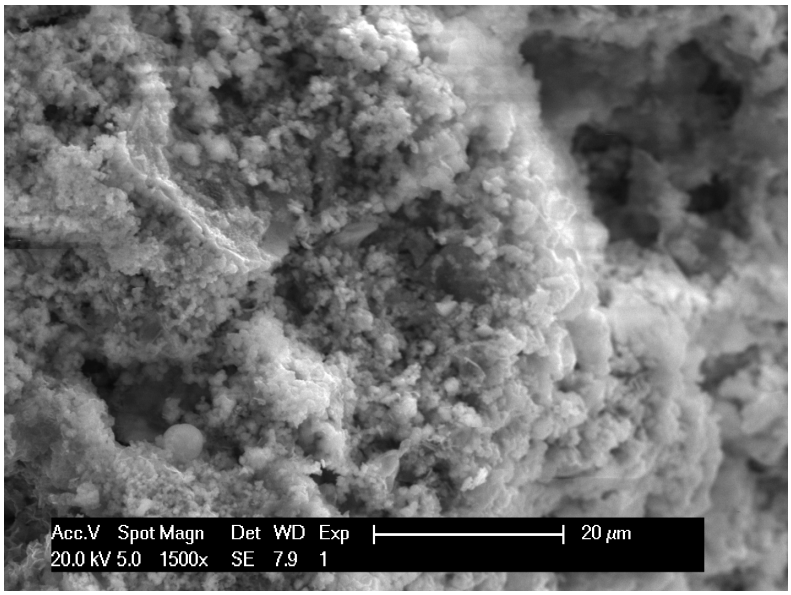

Figure 4-44 SEM image of fly ash geopolymer concrete (mix T10) after continuous immersion.

4.7 Corrosion of Steel Reinforcement Bars

4.7.1 Half-cell Potential Measurement

The corrosion potential measurement was carried out using Ag/AgCl reference electrode for lollipop samples immersed in 3.5% NaCl solution. An average value of three specimens is shown in Figure 4-45.

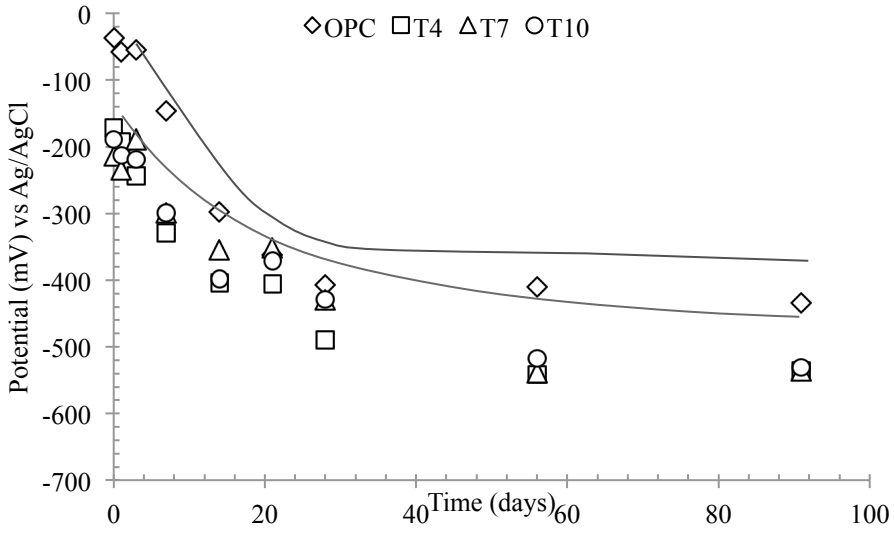

Figure 4-45 Change in half-cell corrosion potentials with respect to time.

A gradual decrease in the case of OPC was noticed up to 28 days, after this the potentials were differed. It can be seen that compared to OPC concrete, all geopolymer showed more negative

potentials at 91 days with almost similar values. According to ASTM C876, the corrosion potential higher than -404 mV vs Ag/AgCl, indicated a high risk of corrosion.[208] It seems that there was unstable passive film formed on the reinforcement bar, so the passive film does not form to protect the rebar. Hence, the chloride ion depassivated the protective film earlier than the OPC concrete and crossed the threshold limit of a high corrosion risk at less than 91 days.

The pH of aqueous solution measured during half-cell potential measurement is displayed in Figure 4-46. From this is noticed that there was no significant variation for different geopolymer mixtures. The pH of geopolymer was lower than the threshold value of 9.5 for depassivation.[209] This could be a reason for more negative potentials measured by half-cell. It was observed in the early measurement; the OPC concrete had pH of 10.5 and decreased to approximately 9.5. Concrete alkalinity measured by pH is critical to maintain the passive film existence to protect the steel reinforcement bar. With regard to initial alkalinity less than 9.5 such in the figure, the chloride ion could depassivate the steel bar in fly ash geopolymer concrete almost immediately.

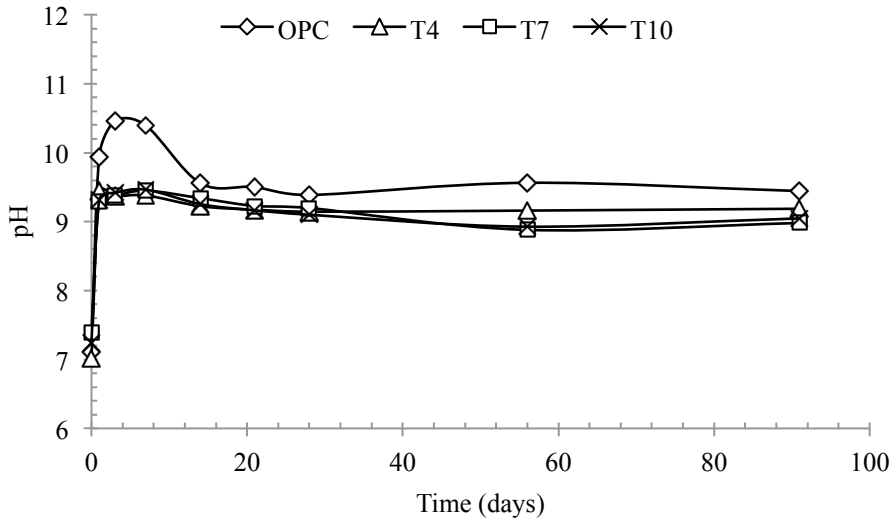

Figure 4-46 Variation of pH of aqueous solution for half-cell potential test with respect to time.

Table 4-15 shows the average steel bar mass loss, corrosion mass loss and corrosion rate of OPC and geopolymer concrete specimens. The percentage of corrosion mass loss was determined as the difference of initial and final mass. The mass loss can be used to calculate corrosion rate of steel bar after 91 days immersion in NaCl solution. From the mass loss, the corrosion rate can calculated according to ASTM G1[210]:

Corrosion rate = (K x W)/(A x T x D) (4.3)

where K = a constant (see clause 8.1.2 ASTM G1), T = time of exposure (hours), A = area (cm^2), W = mass loss (grams) and D = density (g/cm^3, see Appendix X1 ASTM G1).

Table 4-15 Steel bar mass loss and corrosion rate

Mixtures	Initial weight (g)	Mass loss		Corrosion mass loss		Corrosion rate	
		W (g)	SD	W (%)	SD	L (mm/year)	SD
OPC	539.34	3.87	0.341	0.717	0.061	2.573	0.178
T4	540.53	0.17	0.006	0.031	0.001	0.102	0.009
T7	535.30	0.42	0.080	0.079	0.014	0.260	0.055
T10	539.31	0.04	0.010	0.007	0.002	0.025	0.006

As can be seen from the table, the mass loss and, subsequently the corrosion rate of the geopolymer were generally lower than the OPC concrete. The corrosion rates obtained for geopolymer were about 48 to 97 times lower than OPC concrete. The OPC concrete had corrosion rates of higher than 0.1016 mm/year or 'very high' according to the assessment criteria from Bertolini et al.[211]. Mix T10 showed corrosion rates between 0.0101-0.0500 mm/year, which comes under the category 'intermediate', while T4 and T7 performed corrosion rates of 0.102 and 0.260 mm/year, respectively, according to the same assessment criteria comes under the category 'high'.

The compressive strength of concrete had a minimal effect on the corrosion rates of fly ash geopolymer as can be seen in Figure 4-47. There was a very minor decline of the corrosion rates of geopolymer concrete as the compressive strength of concrete increases. Interestingly, the OPC concrete with strength of more than 55 MPa at 91 days performed higher corrosion rates than the geopolymer concrete. This figure also clearly displays that the binder type certainly influences the corrosion rate for all mixtures. The improved corrosion resistance of fly ash geopolymer concrete can be due to the sodium silicate inclusion in the system that acts like a corrosion inhibitor[212] that can decrease the corrosion rate of steel reinforcement. The effect of using a high quantity of sodium silicate can be seen in the strength development of mix T10. Another possible theory is a competing action between alkalis that diffuse out from geopolymer with chloride ion in concrete.[151] This has a significant bearing on the corrosion rate of reinforcement after depassivation in fly ash geopolymer system. This clearly suggested that the mixture composition of fly ash geopolymer concrete governs the corrosion rate of steel reinforcement bars rather the oxygen availability and concrete cover thickness.

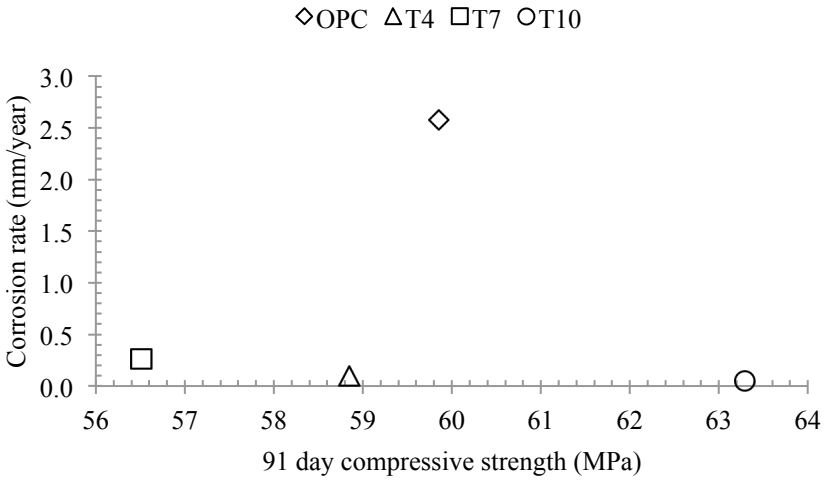

Figure 4-47 Variation of corrosion rate with compressive strength.

4.7.2 Accelerated Corrosion Test by Impressed Voltage Method

The accelerated corrosion test by an impressed voltage was used to determine the evolution of current with time and time to failure of OPC and fly ash geopolymer concrete. The constant voltage of 30V was induced to a system in 3.5% NaCl solution served as electrolyte.

4.7.2.1 Investigation of Preconditioning Effect on Specimen's Failure

In the initial experimental run, air-dried specimens were placed directly without any treatment in the corrosion test set up impressed by 30V. It took more than 200 days to accomplish one run since the specimens did not fail as early as the specimens in the literature suggested.[193, 194, 213] Initially, it was suspected that a very low porosity of geopolymer that might influence the behaviour.[214] However, the mixture composition of the geopolymer that contains various ions might decelerate the corrosion activity. The dry pores might influence the rate of current flow from anode to cathode then it can prolong the testing time. Previous findings reported the influence of this geopolymer composition on the corrosion process induced by the accelerated corrosion set up. Hence, in order to accelerate the corrosion process, a preconditioning of the specimens before placing them in the corrosion system is necessary. The specimens then were immersed for at least 3 days in 3% NaCl solution to make it saturated.[215] It can be seen a preconditioning of specimens gave a significant difference on test length about 3 times shorter than without preconditioning. The samples with preconditioning failed within 28 days than the samples without the treatment. The corrosion current-time relationships with different initial preconditioning treatment are shown in Figure 4-48.

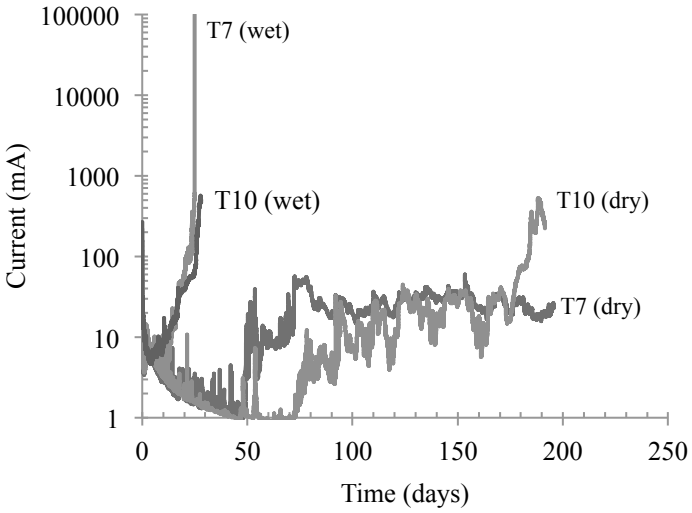

Figure 4-48 Corrosion current-time relationships of geopolymer concrete at constant voltage of 30V without preconditioning.

However, similar behaviour was not observed in the OPC system (Figure 4-49). The specimens without preconditioning (dry) failed less than 25 days, or 8 days more than the wet specimens. It seems the rich calcium OPC binder has a role in this behaviour, which highlighted a significant difference of this binder for preconditioning. Hence, to shorten the time needed for observation, it is recommended for the geopolymer specimens to be immersed in the electrolyte solution for at least 3 days.

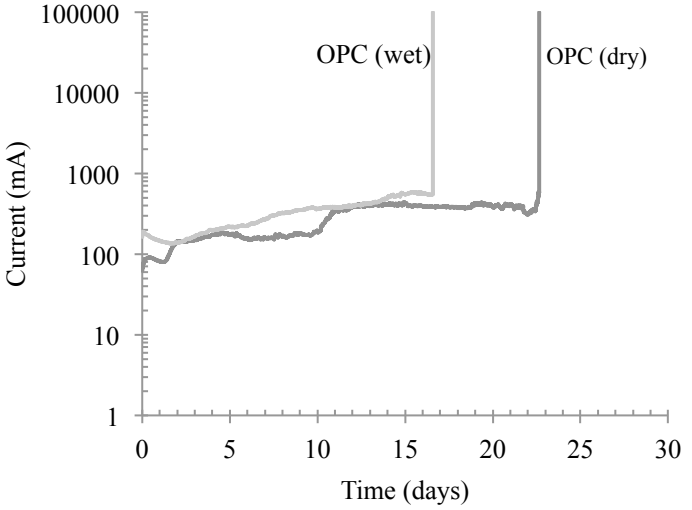

Figure 4-49 Corrosion current-time relationship of OPC concrete at constant voltage of 30V with and without preconditioning.

4.7.2.2 Corrosion Current-time Relationship

The corrosion current-time relationship of OPC and geopolymer specimens exposed to impressed voltage of 5V and 30V are presented in Figure 4-50 and 4-51. It is noticed that the corrosion currents of the geopolymer specimens decreased with time, showing a lower corrosion activity than the OPC concrete. Furthermore, there was no significant change for this activity for both types of binder up to 28 days.

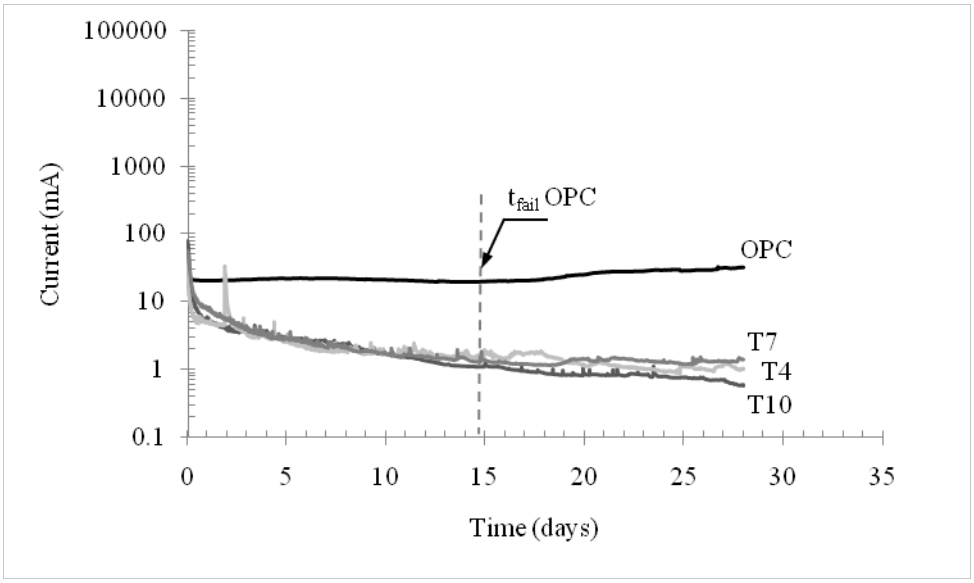

Figure 4-50 Corrosion current-time relationships of concrete at constant voltage of 5V.

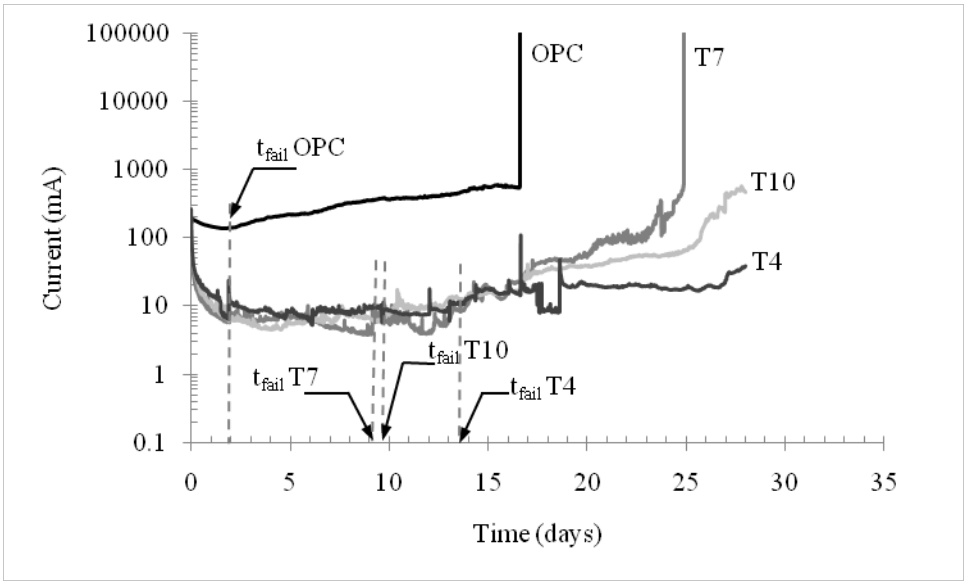

Figure 4-51 Corrosion current-time relationships of concrete at constant voltage of 30V.

Figure 4-51 displays the corrosion current-time relationships for specimens impressed by a constant voltage of 30V. In general, the fly ash geopolymer concrete performed smaller currents with respect to time than the OPC concrete such as in the system impressed with 5V.

According to the previous researchers[160, 216], the recorded current of the geopolymer was always smaller than the OPC binder that closely aligns with this findings. It was suggested that the role of binder influences the corrosion resistance performance. There was a gradual increase on the currents for the OPC concrete, before the specimens reach active corrosion potentials and crack under impressed voltage. The cracks allowed oxygen and chloride ions to ingress in the concrete and accelerate the corrosion that was marked with very high currents.

The time to failure (t_{fail}) for both type of concrete specimens is defined as time corresponding to the onset of a large increase in currents.[217] Using Figure 4-50, 4-51 and Table 4-16, the deterioration occurrence time or time to failure can be compared. The summary of corrosion current and time to failure values is presented in Table 4-16. Both type of concrete has notable differences on the initial and final current level.

Table 4-16 Current reading and time to failure of samples at constant voltage of 5V and 30V

Mix	Initial current (mA)		Final current (mA)		Time to failure (days)	
	5V	30V	5V	30V	5V	30V
OPC (Control)	23.79	163.64	32.43	99999.99	14.7	2.27
T7	31.38	218.04	1.04	99999.99	n/a	8.77
T4	51.79	259.87	1.39	38.14	n/a	12.94
T10	76.54	268.02	0.17	66.33	n/a	9.22

It can be observed from Figure 4-51 and Table 4-16 that specimens made from OPC had failed earlier at 2.27 days than those made with geopolymer. On the other hand, the geopolymer specimens displayed longer deterioration occurrence time than the OPC, which follows the order: T4>T10>T7. The geopolymer T7, T10 and T4 had failed at 8.7, 9.2 and 12.9 days, respectively. However, time to failure was not apparent for both geopolymer samples with a constant voltage of 5V, except for the OPC specimens since it was longer than the specimens exposed to 30V.

It is interesting to note the geopolymer paste could delay the effect of impressed voltage to accelerate the corrosion process, although the presence of chloride ions was obvious to depassivate the protective film of the embedded steel bar faster than the OPC concrete. It was suggested that partially immersed specimens such as in this test influences a low corrosion activity. This is related to low oxygen levels under water that influences the cathodic reaction and the subsequent corrosion rate. The second possibility might be due to uniform corrosion formed of the steel bar surface under the accelerated impressed voltage method. This uniform corrosion prevented further active corrosion by acting as a barrier around the steel bar.

It was found that the value of impressed voltage used in the accelerated corrosion system was useful to induce corrosion activity at a different rate. The fly ash geopolymer specimens still had a very low corrosion activity in this type of test, despite the impressed voltage value charged to the system. That means the binder type could significantly influence the corrosion resistance performance of concrete in an accelerated corrosion test.

4.7.2.3 Average Daily Resistance (ADR)

The average daily resistances of OPC and geopolymer samples were calculated from Ohm's Law are presented in Figure 4-52 and 4-53. Based on the recorded current (DC), the theoretical Average Daily Resistance (ADR) can be determined by Ohm's Law[217]:

$$R_{avg} = \frac{V_{constant}}{I_{avg}} \tag{4.4}$$

where $V_{constant}$ = the voltage; and I_{avg} = the recorded current (DC).

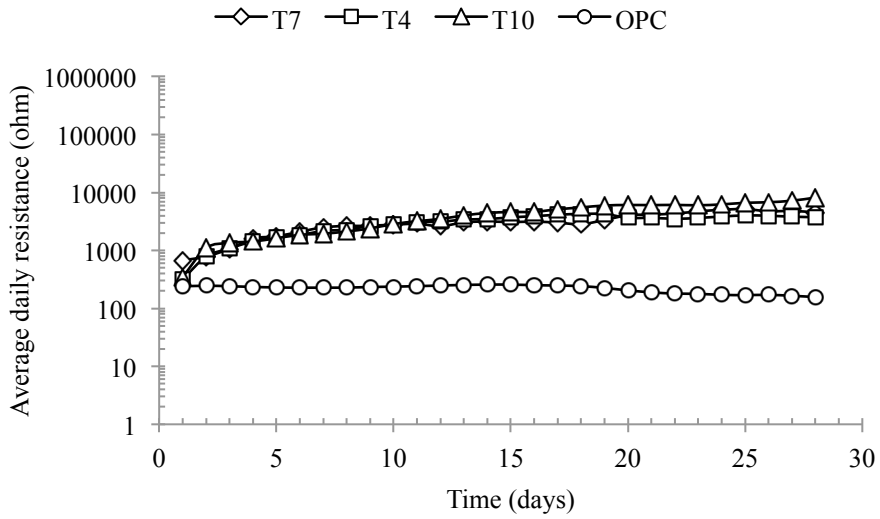

Figure 4-52 Average Daily Resistance of concrete specimens at constant voltage of 5V.

Both figures illustrate the ADR trend for concrete charging with 5V and 30V, respectively. In reverse to the currents, the geopolymer performed higher ADR than the OPC concrete. In the system with applied voltage of 5V, the ADR of geopolymer concrete varied in the range of 317-8159 ohm. The geopolymer showed a higher ADR in the range of 1036-2016 ohm for 15 days, before a decline at 28 days.

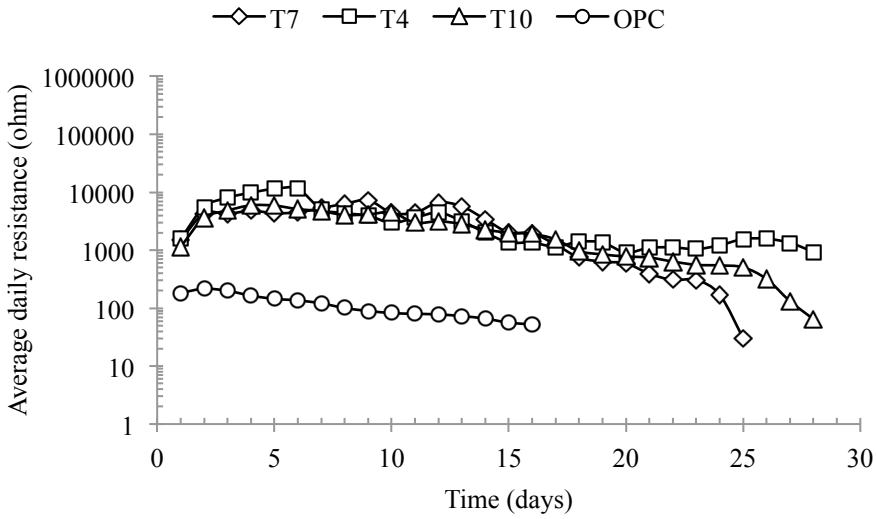

Figure 4-53 Average Daily Resistance of concrete specimens at constant voltage of 30V.

Table 4-17 Times to failure vs average daily resistance of specimens

Mixtures	Time to failure (days)	ADR (k-ohm) 30V
OPC	2.27	0.14
T4	12.94	9.42
T7	8.77	4.25
T10	9.22	6.22

The value of ADR at the time to failure could be seen in Table 4-17. The average daily resistance values are related to the electrical resistance of material or resistivity. Both graphs demonstrate that a higher electrical resistance of fly ash geopolymer concrete than the OPC concrete when the time to failure was achieved. As previously discussed in Section 4.7.2.2, the type of binder and composition could be a reason for this behaviour. It was found that concrete resistivity had a positive impact on a reduction of corrosion rate and time to failure of embedded steel on the blended cement concrete.[215] Blended cement in concrete can delay the chloride-induced corrosion because of high chloride penetration resistance, higher electrical resistivity and subsequently causing lower corrosion rates.[104]

Similar to blended cement, the geopolymer concrete in this research contains fly ash and alkaline activators with various ions in the pore solution that tend to increase electrical resistance. This finding was indicated by Morris and Hodges; Zhang, et al.[154, 218] that highlighted the geopolymer composition might increase the concrete resistivity and corrosion rates. A positive impact from the high electrical resistance of concrete in the steel bar is a decline on a rate of charge-carrying ionic species flow.[104] It was stated that the mixture composition governs the corrosion rate of blended cement, which explained a similar

behaviour performed by the fly ash geopolymer concrete. However, the same resistance was not found on the OPC concrete since the factor influencing its corrosion rate are the oxygen availability and cover depth.[101]

The variation of time to failure with tensile strength is displayed in Figure 4-54. Tensile strength is closely related to concrete's resistance to inhibit crack due to a volume expansion of corrosion product in the pores. It can be seen that there is no specific correlation between specimen failure and tensile strength for the geopolymer concrete. The geopolymer specimens indicated a higher time to failure than the OPC as discussed in the previous section. Mix T10 showed a high deviation because the time to failure depends not only on the tensile strength but also on the mixture composition. The high silicate content seemed to be favourable to increase the tensile strength of concrete, but on the other hand it slightly reduced the concrete's resistance under the impressed voltage method. Overall, the high tensile strength gives a positive contribution on the delay of deterioration such as cracking that occurred in the corrosion of steel bar in fly ash geopolymer concrete.

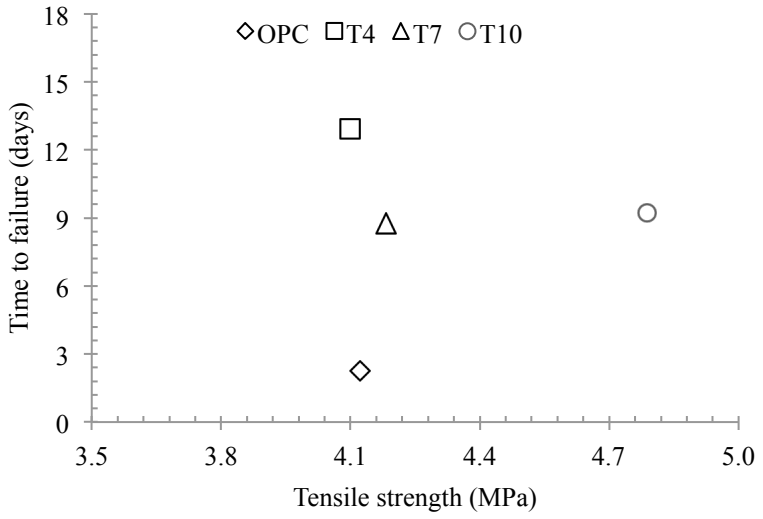

Figure 4-54 Variation of time to failure with tensile strength of concrete at 90 days.

4.7.2.4 Mass Loss of Steel Reinforcement Bar

Table 4-18 presents average mass loss percentages of steel bar specimens tested with the applied voltage of 5 and 30V. The data was taken as the average of triplicate specimens cleaned mechanically after testing. The original mass loss was measured based on the procedure given in ASTM G1.[210] The theoretical mass loss was calculated based on Faraday's Law as follows:

$$\Delta w = (AIt)/ZF \quad (4.5)$$

where: A = atomic weight of iron (56 grams), I = corrosion current (amp), t = time elapsed (seconds), Z = the valency of the reacting electrode (2 for iron), F = Faraday's constant (96,500 amp-sec).

Table 4-18 Mass loss percentages at different levels of applied voltage

Mixture	Applied voltage			
	5V		30V	
	Original (%)	Theoretical (%)	Original (%)	Theoretical (%)
OPC	0.49	4.25	20.53	38.23
T4	0.42	0.18	2.52	5.10
T7	0.23	0.14	0.83	23.08
T10	0.38	0.02	7.80	60.17

Table 4-18 showed a high mass loss performed by the OPC specimens after imposed to a constant voltage of 30V. It can be seen that the original mass loss of the steel bar in geopolymer was lower than rebar in the OPC concrete, but not at relatively high values or less than 1%. The highest loss of cross sectional area was demonstrated by rebar in T10, followed by T4 and T7 at 7.8, 2.5 and 0.8%, respectively. A difference on the mass loss of steel bar in fly ash geopolymer with the OPC corresponding control mix shown was indicated by the slow corrosion activity at 28 days. There was no significant difference between the theoretical mass loss of OPC and the geopolymer, which is probably due to very small amount of electricity charging into the system. This small theoretical mass loss might be due to a low corrosion rate performed by the geopolymer than the OPC concrete.

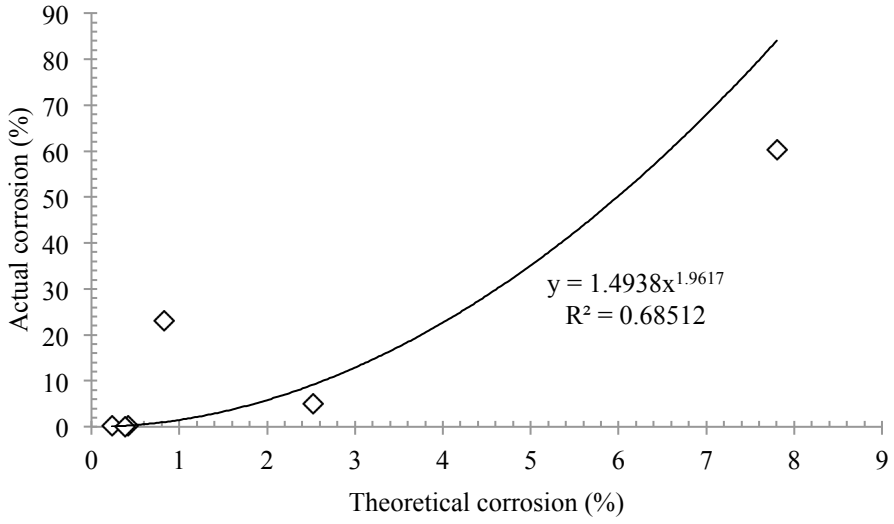

Figure 4-55 Relationship of actual and theoretical corrosion of geopolymer concrete.

A variation of actual corrosion with theoretical corrosion is illustrated in Figure 4-55. Although there was some scattering of the points, the actual corrosion increased with an increase of the

theoretical corrosion percentage. The relationship did not correspond with earlier studies.[216] This might be due to non-linearity factor on the fly ash geopolymer characteristics, such as water permeability, chloride's flow path into the concrete, steel bar geometrical heterogeneity and porosity of the specimens. [219, 220] An aggressive nature of the accelerated corrosion test by impressed voltage method could also become a reason of the mass loss difference. It was suggested that the oxygen and chloride was prevented by the corrosion deposition on cracks and voids around the steel bar.[158] The presence of various ions in the concrete pore solution also could distort the accelerated corrosion test mechanism such as in rapid chloride permeability test, as already discussed by previous authors on fly ash geopolymer concrete.[148] This could explain the influence of geopolymer concrete binder to corrosion resistance performance that certainly needs further investigation.

4.7.2.5 Visual Inspection

The samples were split off at the end of the each test session. The condition of concrete surface and interface of steel-concrete were observed. Figure 4-56 showed the OPC concrete sample with a typical wide crack on the top shortly after exposure to applied voltage of 30. Some deposits from a high degradation of paste and mass loss of steel bar were found on the concrete surface. This condition illustrated that a severe condition occurred on the specimen such as OPC under the accelerated condition test.

Figure 4-56 Visual inspection of typical OPC concrete sample with applied voltage of 30V.

As can be seen in Figure 4-57 (a), brown rust covered the crack surface. There was a thick corrosion product covering the steel bar in Figure 4-57 (b). The steel bar showed a high loss of the cross section. When the phenolphthalein indicator was sprayed, there was a strong pink colour on the concrete surface and no sign of alkalinity reduction during the corrosion test on the uncracked paste as shown in Figure 4-57 (c). Chloride ions have penetrated deeply into the steel bar from uniform white precipitation as indicated by spraying the $AgNO_3$ solution (Figure

4-57 (d)). The wide crack increased the chloride penetration into the concrete, induced more corrosion and increased the corrosion rate.

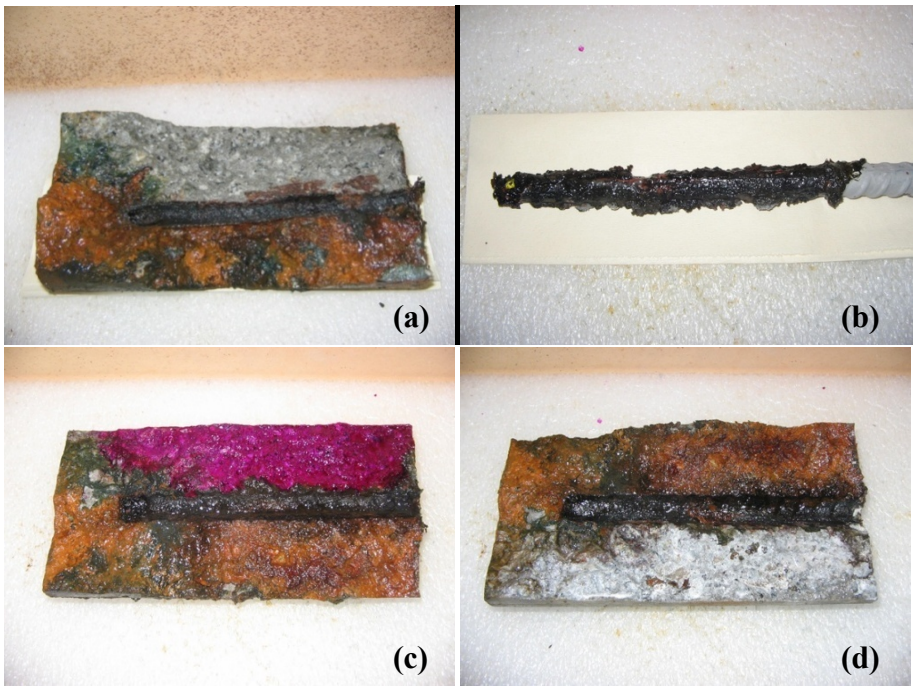

Figure 4-57 Steel and OPC concrete specimens after exposure to the accelerated corrosion test with applied voltage of 30V.

Figure 4-58 displays the geopolymer specimens (mix T10) after exposure to the accelerated corrosion with applied voltage of 30V. The corrosion product was observed near the steel interface of the specimen surface. As can be seen the corrosion product migrated through concrete pores reducing a pressure to start a wide crack. Unlike the OPC concrete, small cracks were observed on the surface of fly ash geopolymer concrete.

Figure 4-58 Visual inspection of typical geopolymer concrete sample (mix T7) with applied voltage of 30V.

Figure 4-59 illustrates the area near the rebar of T7 specimen and its trace after dissection revealed some local sites where a corrosion product was available. There was no sign of bonding between steel and concrete in Figure 4-59 (a). As seen in Figure 4-59 (b), a black thick product covered the steel bar, which soon turned to brown rust when in contact with air. There was alkalinity reduction around the steel bar as indicated by phenolphthalein spray in Figure 4-59 (c). Chloride had penetrated deeply into concrete-steel bar interface as indicated by $AgNO_3$ solution. The light grey area in Figure 4-59 (d) showed a precipitation of silver chloride.

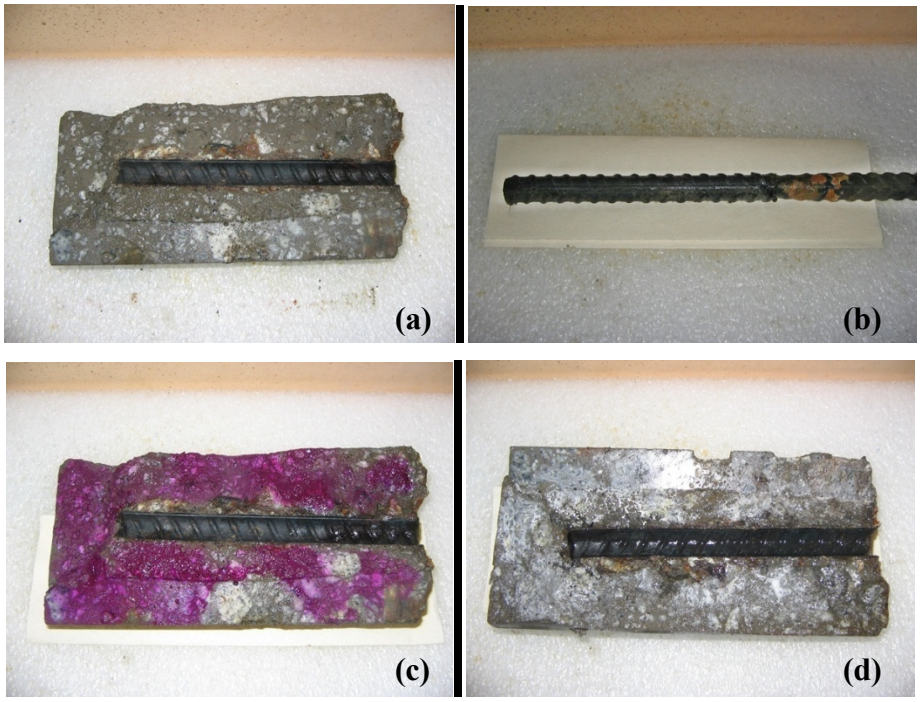

Figure 4-59 Steel and geopolymer concrete specimens (Mix T10) after exposure to the accelerated corrosion test with applied voltage of 30V.

Visual inspection revealed the effect of two different binders used in the corrosion process under the accelerated corrosion test. The accelerated corrosion test is used to reduce the time needed for chloride ion to penetrate into the steel reinforcement bars in the concrete. The initiation period as already discussed in Section 2.6.3.2 could be reduced with high voltage. Hence, normally there is severe corrosion in the system due to fast energy to induce the corrosion process. There is a high ion movement in the system, since chloride migrates to the steel surface, and iron migrate to the outer surface of specimens.[159] The ions in the concrete paste are also affected; hence calcium leaching in the case of OPC concrete is normally observed in the accelerated corrosion test. A combination of ion migration could deteriorate the concrete very quickly, once the propagation period has commenced.

4.7.2.6 General Discussion

Corrosion resistance performance of steel bars in fly ash geopolymer concrete certainly become an interesting issue for durability, in particular areas such as seawater environment. Some interesting findings were revealed in the previous section that highlighted the geopolymer strength and weaknesses regarding the corrosion. This section is presented to discuss the relation of current findings with some related properties that has a serious implication in durability of geopolymer in seawater environment.

A principal issue that needed to be highlighted was the pore solution and porosity of the fly ash geopolymer concrete. It was revealed that the alkalis tend to leach out from the fly ash geopolymer paste with time. When chloride is present in the system, the alkalis leaching become higher in order maintain the electro neutrality in the pores.[151] The alkalinity loss cannot be replenished in the low calcium fly ash geopolymer system, due to lack of calcium content. In contrast, the OPC binder has portlandite, an indispensable element that is responsible in maintaining the paste alkalinity in the long term. This self-healing mechanism is also responsible for porosity reduction in the OPC paste. Without a similar mechanism, there is a high risk of corrosion for reinforced geopolymer structures in the seawater environment. Furthermore, a more precise method such as Wood's intrusion porosimetry, which was carried out to identify the fly ash geopolymer concrete porosity and pores distribution[80], found that the pore system of fly ash geopolymer is highly heterogeneous. The capillary porosity is not continuous such as in the OPC concrete, but consists of several pores connected by fine networks in the geopolymer paste. Besides, the high amount of pore volume resulted from fully reacted fly ash grains in the paste also contributing to a high risk of chloride-induced corrosion of the steel reinforcement bar.

It was found that a high amount of chloride started to depassivate the steel bar in the geopolymer concrete in a very short time. The initiation phase where chloride depassivates the steel reinforcement bar in concrete in Tuuti model[107], occurred in a relatively short time. Slowly, the small amount of corrosion product initially filled the nearest voids in the embedded steel and paste interface section, causing a total loss of bonding. This is the free expansion stage, mentioned by Liu and Weyers[109]. Gradually, the corrosion product filled the concrete pores around the steel bar and stress build-up stage was reached. However, generally small cracks were spotted on the geopolymer concrete surface after exposure to the set-up for 28 days. A delay in crack propagation in the geopolymer is normally due to the high void spaces in the concrete that can accommodate the corrosion product without generating high pressure around the steel bar. This condition is not favourable in real applications because corrosion

activity can be extended in order to generate significant pressure, thus, will result in an abrupt high overall loss of the steel bar.[221]

Corrosion of steel reinforcement bar in fly ash geopolymer concrete in seawater environment is the most detrimental in the durability issue. Based on the findings from the corrosion performance study, it can be seen that without low porosity and high alkalinity in the concrete pores, then it is difficult to propose this material to be applied in seawater environments. On the other hand, low drying shrinkage, high compressive and tensile strength and the slow corrosion rate of geopolymer binder can be considered as a counterbalance to minimize deterioration such as such as concrete cover crack or high loss of steel cross section area due to corrosion. Furthermore, it is suggested that further research is needed in improving the porosity, strength and workability to improve the fly ash geopolymer in overcoming the basic problem in durability. In the mean time, some precautionary measures such as using epoxy coating for the steel bar, adding water inhibitor and polymer into the mixture or applying cathodic protection can be applied to ensure the corrosion resistance of fly ash geopolymer concrete in a seawater environment.

4.7.2.7 Microstructure of Corroded Specimen

A typical interface of geopolymer paste and steel bar are shown in Figure 4-60. The specimen was taken after testing at 28 days. It can be seen that the interface between the geopolymer and steel bar was dark indicating intense corrosion product. The edge around the steel bar was filled by rust precipitation which influences bonding between steel and geopolymer paste in Figure 4-60(a). It was reported the carbon steel and geopolymer paste has a good chemical bonding as does the OPC concrete.[222] However, the bond was destroyed by uniform corrosion product around the steel bar. Loss of bond between the specimens could lead into reduction of tensile strength capacity of reinforced concrete. Figure 4-60(b) showed small pitting near the steel interface. Corrosion product around the concrete steel is displayed in Figure 4-60(c). Thick black rust was precipitated in the area where bonding of steel and paste should take place. Once the steel bar corroded, some of the liquid corrosion product filled the pores and voids around the concrete. The corrosion product also penetrated into the pores, indicated by the yellow area near the grey aggregates in Figure 4-60(d).

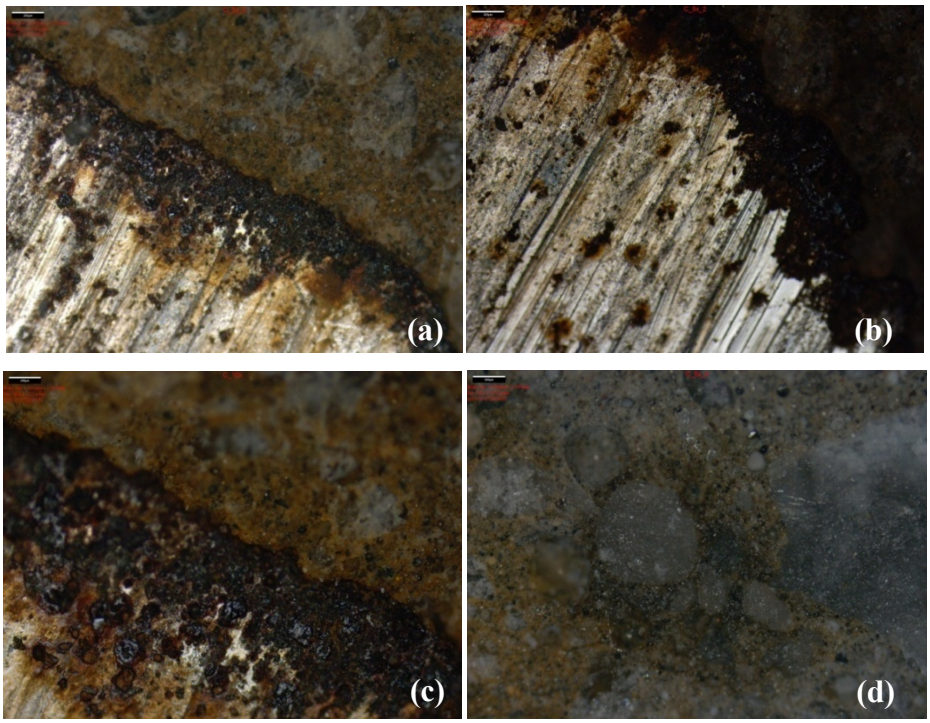

Figure 4-60 Typical interface of geopolymer paste and steel bar after corrosion test, (a) steel and concrete interface, (b) pitting of steel bar near interface, (c) corrosion product around the steel bar, (d) corrosion product spreading over the concrete paste.

The typical microstructure of geopolymer concrete after being exposed to the accelerated corrosion is displayed in Figure 4-61. The microstructure of geopolymer without the corrosion product was filled with a needle shape and irregular crystal formation. The original microstructure could barely be observed, due to a thick layer of the salt crystals. The passive film of steel reinforcement bar cannot be formed, since a high amount of chloride fills the concrete pores and reduces the alkalinity of the paste.

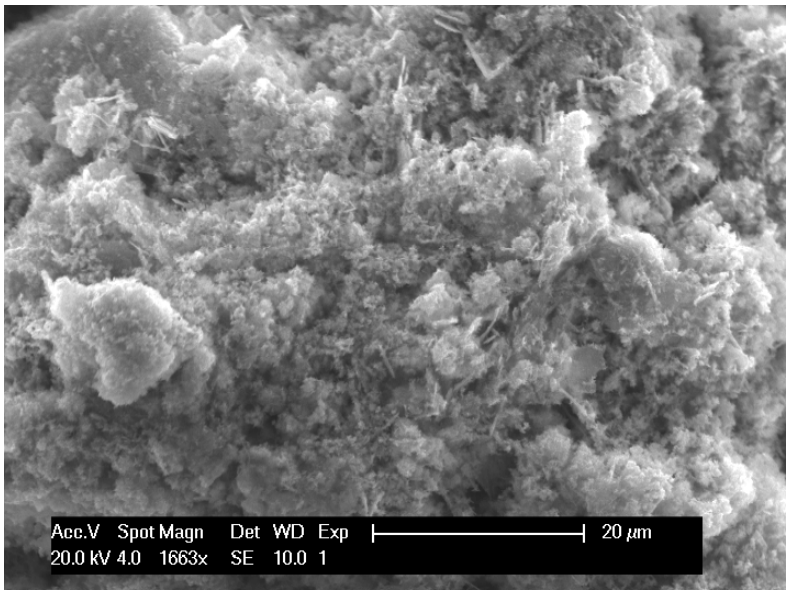

Figure 4-61 SEM image of geopolymer paste after exposure to chloride during the accelerated corrosion test.

The specimen filled with corrosion product was taken near the steel bar in Figure 4-62. The corrosion product totally altered the geopolymer microstructure. There is no sign of the original geopolymer microstructure, since the rust covered and reacted with the elements in the geopolymer paste. This deteriorating geopolymer microstructure might damage the concrete performance in the long term. The resulting elements are unknown since EDX characterisation was not carried out in this research.

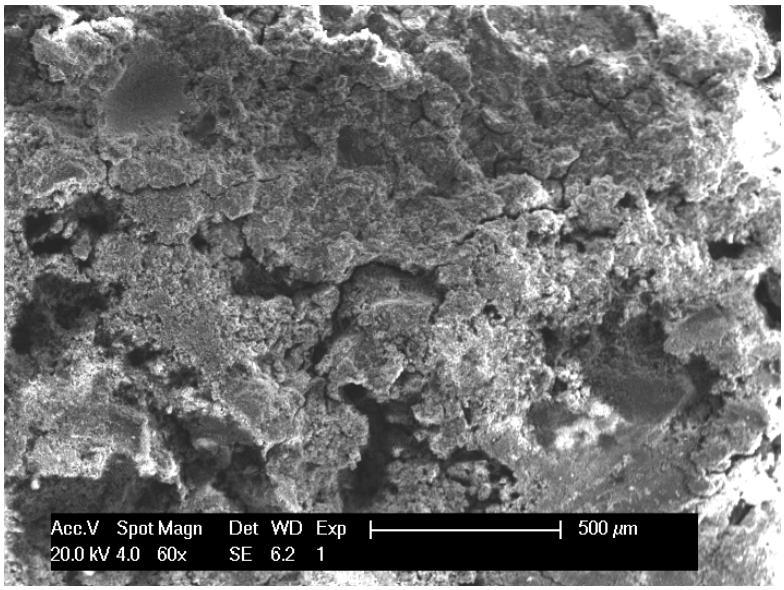

Figure 4-62 SEM image of geopolymer paste after being exposed to the corrosion product.

4.7.3 Microbiologically Influenced Corrosion

This section describes the corrosion performance of steel reinforcement bar in fly ash geopolymer concrete under Microbiological Influenced Corrosion (MIC). This new area has never been investigated by any researcher and made it a novel contribution to the durability study of fly ash geopolymer concrete.

4.7.3.1 Corrosion Potential

Figure 4-63 shows the corrosion potential of geopolymer and OPC concrete samples exposed to the testing environments (f/2 medium and seawater). The corrosion potential of the OPC concrete was generally steady at -55mV. Some oscillations occurred with increasing exposure time. At day 7, the potential shifted into a negative reading before changing back in a more positive direction. The same trend was not observed with the geopolymer concrete where there was a gradual decrease of the potential reading heading to negative potential before it plunged to -270mV at day 12. Gradually, after this, the corrosion potential started to shift in a positive direction. The corrosion potential of geopolymer concrete in the f/2 medium and seawater are also plotted in this figure. Shortly after immersion in the f/2 medium, the potential drifted to -250 mV and then levelled off to a steady value. In a seawater medium, the potential drifted gradually, shifting to more positive values until day 14.

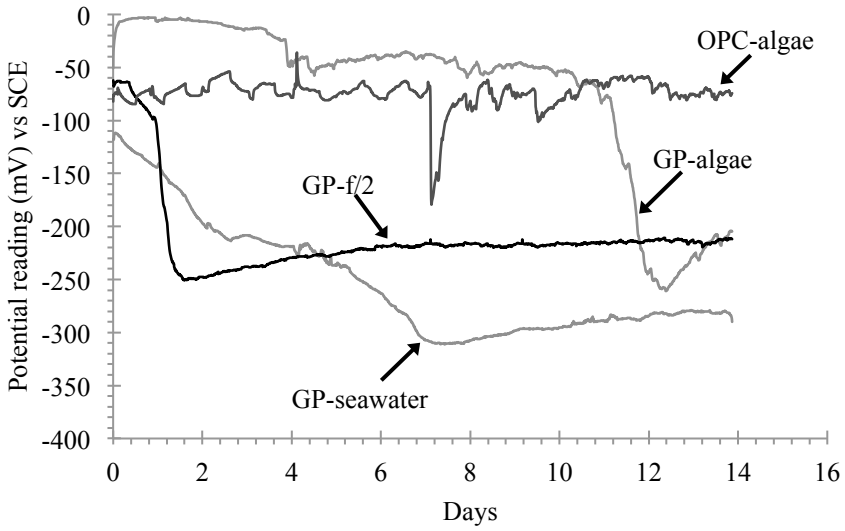

Figure 4-63 Variation of potential with time for geopolymer (GP) and OPC concrete in the biotic (algae+f/2 medium) and abiotic (seawater and f/2 medium alone) testing environments.

The corrosion of steel bars is controlled by the environment. Temperature, pH, oxygen availability and biofouling are some important factors that influence corrosion thermodynamics

and kinetics in aqueous environments.[223] The present study has shown that microalgae were responsible for the electrochemical behaviour of steel bars in fly ash geopolymer concrete. The presence of microalgae colonizing the metal surface was believed to be a factor in altering the oxygen reduction process.[224] Alga is a phototropic microorganism that uses light for photosynthesis. During photosynthesis, algae produce oxygen, and they consume oxygen by respiration in the dark. This pattern could change the oxygen content in the surface of the steel bars during the light/dark cycle. Photosynthetic and respiratory activities produce and consume oxygen. A differential aeration cells from these activities can create varying oxygen partial pressures to facilitate corrosion.[161] This cyclic effect was probably responsible for producing the observed oscillations in the corrosion potential when a biofilm of *P. carterae* was present on the steel bar surface. In contrast, no periodic oscillation was detected in the f/2 medium or seawater system. In the geopolymer system with *P. carterae*, the potential decreased gradually and there was a sudden change in the negative direction after 12 days. According to Dexter et al.[225], high oscillations or sudden changes in the active or negative direction are a typical behaviour of the onset of localized pitting. This was also found in the geopolymer algae-inoculated system, where the potentials shifted to being more positive after the incubation period of 12 days. The OPC concrete in the present of algae indicated a steady state potential with periodic oscillations. A sudden change was observed in the active direction after 7 days as an initial attack on the steel bar. The microalgae presence and photosynthesis activities also influenced the potential reading but only until the 7th day.

The sterile medium (f/2) and the seawater had different effects on the potential reading of the geopolymer concrete. The corrosion potential was steady after an initial decrease of -250mV in the f/2 medium, which is in essence autoclaved filtered seawater with chemical compounds addition and no microorganism. It is generally known that the presence of passive film can protect the steel bars of concrete against corrosion. A study of stainless steel in filtered seawater by Dexter and Gao[226], indicated that there was passivation on the steel surface compared to samples in natural seawater. Seawater has higher chloride content than the f/2 medium, and so the initial attack seems to be caused mostly by chlorides. The corrosion potential decreases gradually before the steady state is achieved. However, once the chloride depassivates the steel bar, then the corrosion potential drifts to being more negative showing the initiation of corrosion.

4.7.3.2 pH of Concrete in Testing Medium

The pH measurement in Figure 4-64 indicated that the OPC concrete increased the pH of algae-inoculated medium by 2 units. The geopolymer concrete increased the pH by 0.5 units after dropping by 0.5 units on day 2. The mean pH of the algae medium with the OPC concrete

was 10.2, while the mean pH of the algae medium with the geopolymer concrete was 8.5. In general, there was a change of pH in the f/2 medium after the geopolymer samples were immersed in the algae-inoculated medium. The pH of the medium was stable with mean values of 9.2 for the f/2 medium and 9.0 for the seawater. The control medium (algae) showed a fairly stable pH at 9.0 for six days before it dropped to less than pH 7.0 at 14 days.

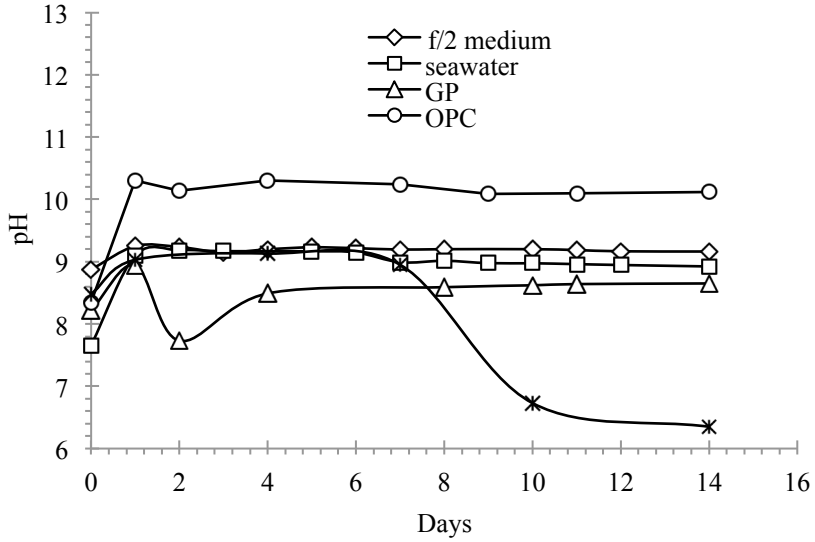

Figure 4-64 Variation of pH with time of the geopolymer (GP) and OPC concrete.

Some marine algae can increase the pH to as high as 10.0, as a result of photosynthetic CO_2 uptake, and a decrease in the pH values when they decay.[227] The control medium (algae) showed the same trend, with high pH in the early days of growth and quite low pH after six days due to the dead cells. The high alkalinity environment from the OPC concrete system is an ideal chemical barrier to reducing the possibility of corrosion. Once the pH decreases, the chloride ion is able to depassivate the concrete steel bar and induce corrosion. The geopolymer concrete in algae culture has a pH of less than 9.0, which was sufficient enough to prevent corrosion in the short term. The condition was quite stable for 12 days, considering the passive film (biofilm) was being established on the steel surface and this temporarily inhibited localized corrosion. The pH of geopolymer in the f/2 medium was approximately 9.0 with the potential reading being nearly steady, indicating that the chloride ions were not active enough to induce corrosion and thus ruin the passive film formed on the steel bar by the geopolymer. On the other hand, although the passive film seems rather stable for the geopolymer in a seawater environment, after day 14, due to depassivation, the potential was plunged into more negative readings, which may be interpreted as a sign of corrosion occurring in the steel bar.

Algae growth in the chamber was mainly influenced by the concrete pH. The ideal pH for growing microorganisms such as bacteria and algae is 7-8[228]. It seemed the OPC concrete has too high a pH level, in comparison with the geopolymer concrete for algae growth in the system. It was interesting to note that the geopolymer concrete could provide a pH lower than the OPC system, so the algae still grew until day 14. Slag and fly ash geopolymer mortars have been used to study algae attachment in freshwater and brackish water environments.[119] It is likely that, in the present study, the highly porous paste of the concrete and low pH/high carbonation levels were among the factors contributing to the attachment of algae to the geopolymer concrete.

4.7.3.3 Cell Densities

Cell densities of microalgae species in the cultures were also determined (Figure 4-65). *Pleurochrysis carterae* doubling time was 3.5 days when grown under controlled conditions. On the other hand, both geopolymer and OPC concrete resulted in a lowering of the cell densities. However, as shown in Figure 4, OPC grown *P. carterae* declined at a much faster rate (6 days) compared to geopolymer grown *P. carterae* (14 days).

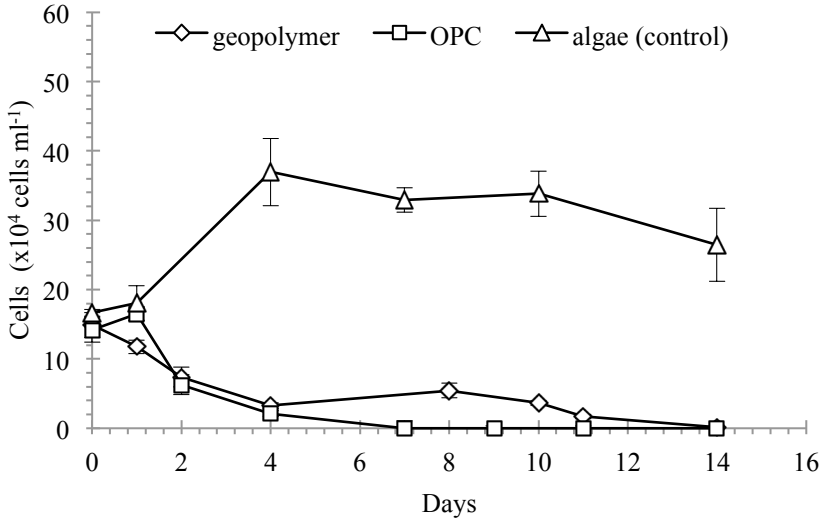

Figure 4-65 Cell densities vs time of the geopolymer (GP) and OPC concrete in algae medium.

A correlation between corrosion potential and cell densities of the OPC and geopolymer concrete are shown in Figure 4-66 and 4-67. There was no change in the corrosion potential with increasing time corresponding to the cell densities of the algae culture (Figure 4-66). The cell densities did not correlate with the potential reading at any time. However, a decrease in cell densities in the algae-inoculated with time was accompanied by a gradual shift in the

negative direction of corrosion potential of the geopolymer concrete (Figure 4-67). Although there was a small increase in cell densities at day 8, the potential reading kept shifting in a negative direction.

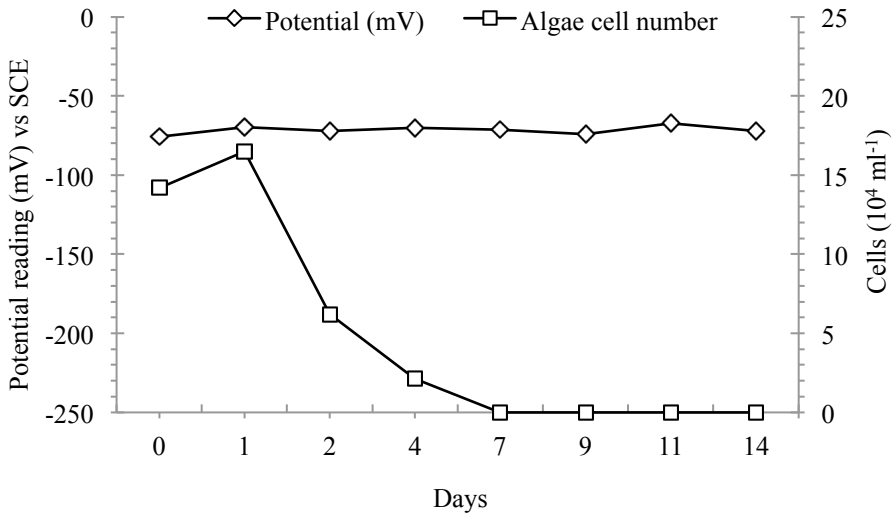

Figure 4-66 Potential vs cell densities at particular time for the OPC concrete.

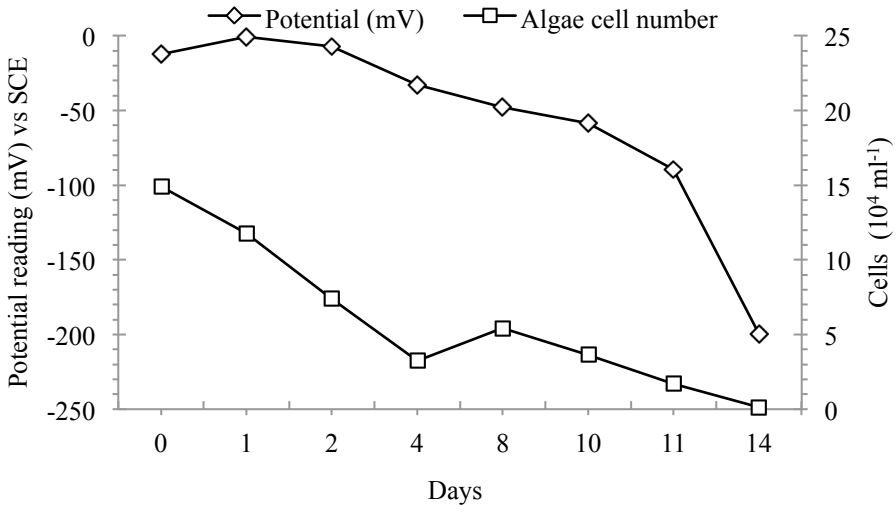

Figure 4-67 Potential vs cell densities at particular time for the OPC concrete.

Cell densities indicated no sign of significant contribution to the electrochemical effect for the OPC sample in the *P. carterae* culture. It was a different trend for the geopolymer concrete because cell densities had a positive correlation with the potential reading. The significant influence of cell densities was on the production of biofilm, which could change the pattern of potential reading in a positive direction. In addition, the cell densities might directly influence the local pH on the metal surface by accelerating the cathodic reduction of dissolved oxygen

[229]. Although this might not be the single cause of a potential shift towards a negative direction, the cell densities could be responsible for observing such effects on the electrochemical behaviour of the geopolymer concrete. On the other hand, the OPC concrete also showed the same trend. There was probably a formation of biofilm after the potential reading declined in a negative direction.

Judging from the above results, there was a risk of corrosion of steel bar in fly ash geopolymer in the micro algae medium. A tolerable pH was provided by fly ash geopolymer causing a considerable algae growth in the concrete pores. Corrosion potential decreased with a decrease of micro algae densities. The cell densities change the electrochemical of steel bar through a production of biofilm. Another mechanism involved, photosynthesis of micro algae raises the corrosion rate by providing more oxygen and increasing the cathode reaction. It can be concluded that the microorganism environment has a considerable effect on the corrosion performance of steel reinforcement bar in fly ash geopolymer.

4.7.3.4 Visual Investigation and Microstructure

Figure 4-68 shows the geopolymer concrete that was dissected along the plane of the top reinforcing bar revealing the corrosion product on the concrete and steel bar surfaces. Some black, thick corrosion product/rust can be observed on the steel surface of the geopolymer concrete.

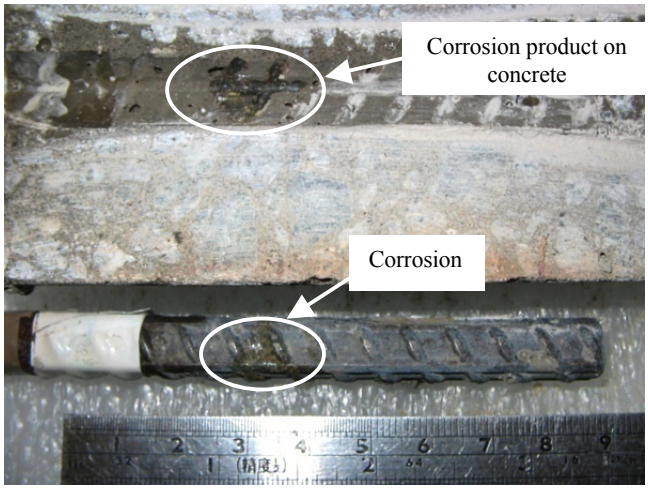

Figure 4-68 Photograph of geopolymer concrete specimen that was dissected after corrosion test.

SEM investigation was carried out to observe the microstructure of steel bar embedded in fly ash geopolymer paste after exposure to the micro algae environment (Figure 4-69). The sample in Figure 4-68 was cut, fixed and analysed under SEM.

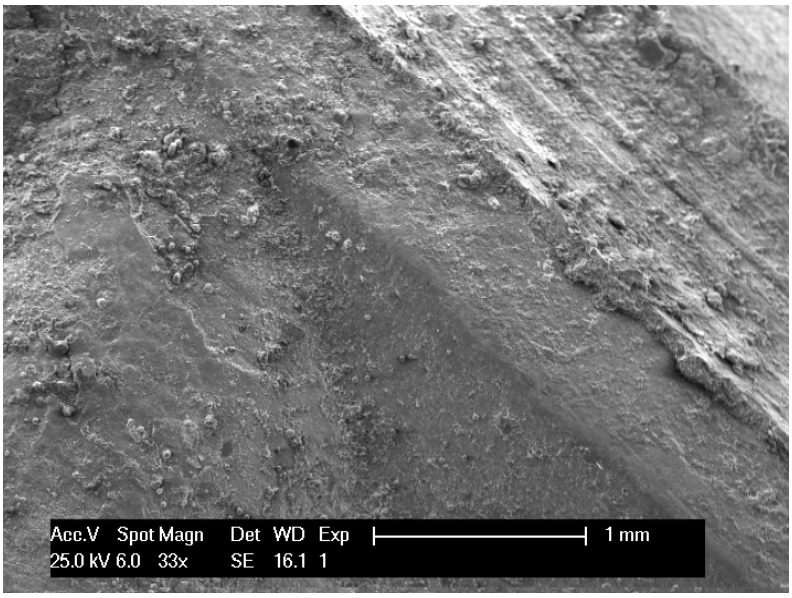

Figure 4-69 SEM image of steel bar embedded in fly ash geopolymer concrete after exposure to micro algae medium.

The microstructure of geopolymer paste following exposure to the micro algae medium is presented in Figure 4-70. It can be seen in Figure 4-70 some spongy particles indicating some hydrated organic matters were embedded in the microstructure. It also demonstrates the abundant deposits of corrosion products and microorganisms embedded in biofilm. This certainly needs further investigation by EDX to reveal the elements covering the microstructure of fly ash geopolymer in algae medium.

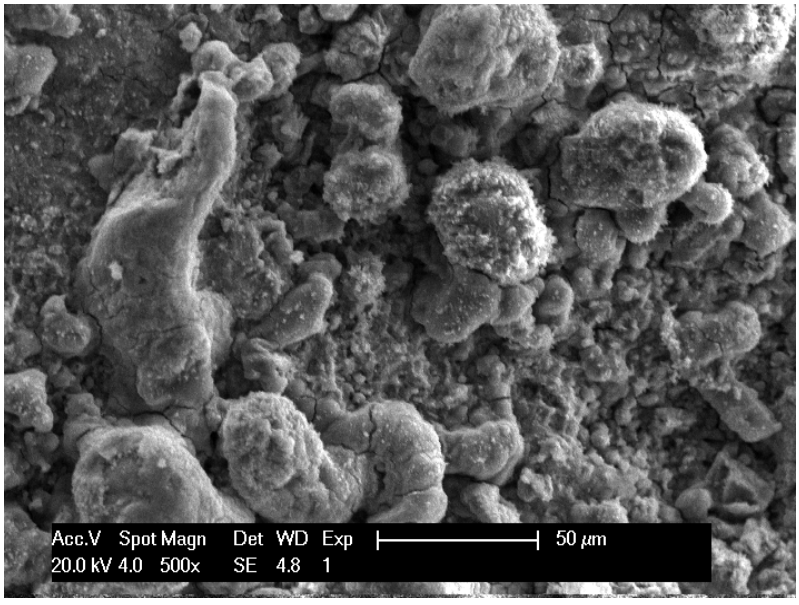

Figure 4-70 SEM image of fly ash geopolymer paste after exposure to micro algae medium.

Chapter 5

CONCLUSIONS AND RECOMMENDATIONS

5.1 Introduction

This chapter concludes the research findings on strength and durability of fly ash geopolymer concrete in Chapter 4 and provides recommendations for future study. The present research has contributed to the present status of knowledge on the durability of fly ash geopolymer concrete in the seawater environment. The preliminary study is useful in determining the important parameters for further evaluation in this research. Mix design development of fly ash geopolymer concrete using the Taguchi optimization method increases efficiency when designing a mixture with various parameters involved. The strength, elastic modulus, water penetrability development of the optimum mixes until 365 days of the concrete age were revealed. The chloride ion penetration, and the strength, elastic modulus, porosity development, of concrete in continuous immersion and accelerated wetting-drying cycles were reported. This study also investigated the corrosion performance of fly ash geopolymer concrete using natural immersion and accelerated corrosion tests. The corrosion of steel bars in fly ash geopolymer concrete exposed to microorganism environment, which were firstly reported in this area, is an important step to elaborate on the effect of Microbiologically Influenced Corrosion (MIC) on this particular concrete. The main findings are given below.

5.2 Conclusions

Preliminary Study

a. Strength of fly ash geopolymer concrete was improved to a certain extent by decreasing water/solids ratio, aggregate/solids ratio and alkaline to fly ash ratio. The aggregate grading showed marginal influence in a strength development of fly ash geopolymer concrete.
b. Water absorption of fly ash geopolymer in average was less than 5%, which can be classified ‘low’. The water absorption decreased by decreasing the water/solids ratio, increasing the aggregate/solids ratio and increasing the alkaline/fly ash ratio. The aggregate grading showed a marginal change in water absorption in accordance with the age of the concrete.
c. The overall percentage of Apparent Volume of Permeable Voids (AVPV) was less than 12% and was classified as ‘good’. The same trend of water absorption was applied to AVPV. The values can be improved by decreasing the water/solids ratio, increasing the aggregate/solids ratio and increasing the alkaline/fly ash ratio. The

aggregate grading was not a significant parameter, since there was little change in AVPV with the concrete age.

d. The water permeability test revealed the concrete has 'average' quality, judging from the coefficient permeability in the range of $2.46x10^{-11}$ to $4.67x10^{-11}$ m/s. The void content measured from the test, showed similar 'average' criteria applied with void varied from 8.2-13%.
e. It can be inferred that the water/solids ratio is the most influential parameter to increase strength, decrease the water absorption/AVPV and water permeability. The alkaline/fly ash ratio of 0.30 can increase strength and reduce porosity significantly. The optimum aggregate/binder ratio of 3.50 contributed to a high strength of concrete, however to obtain a low porosity of fly ash geopolymer, the ratio needs to be increased to 4.70.

Taguchi Optimization of Geopolymer Concrete

a. The Taguchi orthogonal array method was found to be well suited in the optimisation of fly ash geopolymer concrete mixtures. This method can reduce the number of trial batches needed to achieve a durable geopolymer concrete with special requirements.
b. Nine mixes based on Taguchi Orthogonal Array OA_9 (3^4) was used in fly ash geopolymer concrete with various parameters ranging from aggregate content, alkaline/fly ash ratio, ratio of sodium silicate/NaOH and curing conditions.
c. Three optimum mixes were yielded from nine studied mixes. Mix T7 has been proposed for further investigation due to its strength and durable characteristics. Second, mix T10 has been proposed due to a combination of high strength and low sorptivity. Three, mix T4 was proposed as it has suitable workability, produced moderate strength and durability, second to mix T7.

Mechanical Properties, Water Absorption, Sorptivity and Drying Shrinkage

a. The fly ash geopolymer concrete has high slump values but low workability due to the nature of the sticky and stiff mixture.
b. The pH of fresh concrete is somewhat higher than the OPC concrete.
c. The density of the optimum fly ash geopolymer concrete was in the range of 2287 to 2385.42 kg/m^3. The values were still in the range of normal concrete, that is, 2200-2600 kg/m^3.
d. The optimum mixtures, that is mixes T4, T7 and T10, and the control mix OPC reached a target compressive strength of 55 MPa, which is recommended for reinforced concrete structures in a seawater environment. At 28 days the concrete

strength was in the range of 56.24-60.20 MPa. The highest strength was achieved by Mix T10, followed by mix T7 and T4.

e. The tensile strength of mix T7 was highest after at 365 days of concrete age. In general, all geopolymer mixes showed higher tensile strength than the OPC mix. As the strength increases the tensile strength of mix T7 and T10 increases correspondingly. Mix T4 demonstrated an inverse trend, where tensile strength decreases as the compressive strength increases. In general, the tensile strength value from all geopolymer concrete was higher than the tensile strength prediction of AS3600.

f. The flexural strength of fly ash geopolymer was higher than the OPC concrete mix. This might be due to an enhanced bonding between aggregate and geopolymer paste. Those values were also higher than the flexural strength prediction of AS3600.

g. The Young's Modulus of Elasticity of the fly ash geopolymer varied in the range of 25.33-31.26 GPa, which was smaller than the OPC concrete. This could be due to inclusion of sodium silicate in the mixture, which changes the microstructure and reduces the stiffness of the concrete. The low stiffness or elastic modulus could reduce the time of crack propagation due to corrosion product volume expansion of steel reinforcement bars.

h. The water absorption of all mixes was lower than 5%, which can be classified as 'excellent'. There was a positive correlation between water absorption of mix T10 and the OPC concrete. The water absorption decreased as the compressive strength increased. MixT4 and T7 showed an inverse trend, i.e. the water absorption increased as the strength increased. Irrespective of the strength grade, water absorption is dependent on the mixture composition and curing. A linear correlation of water absorption and AVPV was observed. It was depicted that the OPC has the highest water absorption and AVPV.

i. Sorptivity of fly ash geopolymer was in the range of 0.0813-01624 mm/min$^{0.5}$. Those values were lower than the OPC with sorptivity varying between 0.1888-02036 mm/min$^{0.5}$. It can be seen that the geopolymer has lower capillary porosity than the OPC. A positive correlation between sorptivity and compressive strength was shown by mix T10 and OPC. Mix T4 and T7 showed a reverse trend. As long as the values were less than 0.2000 mm/min$^{0.5}$, the mixes remained acceptable for concrete in the seawater environment.

j. Mix T10 performed a drying shrinkage less than 200 με, while the OPC showed a higher drying shrinkage of approximately 500 με. Mix T4 experienced an expansion when cured in the air. Instead of shrinkage, the geopolymer tended to absorb moisture

from humidity, making it expand. Low expansion or shrinkage of mix T7 might be due to a high aggregate content in the mixture.

k. Geopolymer microstructure consists of irregular shapes of geopolymer, unreacted fly ash in a spherical form and voids. There is no clear boundary between the aggregate and geopolymer gel such as ITZ in the OPC concrete. This chemical reaction/bonding between aggregate and alkali could increase mechanical properties such as tensile and flexural strength of fly ash geopolymer concrete.

Seawater Resistance

a. Chloride ion penetration of fly ash geopolymer was higher than the OPC concrete. A high risk of chloride-induced corrosion of steel reinforcement bar is possible for concrete in a seawater environment. This could be due to no chloride binding mechanism such as in cement with C_3A. It also caused no continuous hydration in the fly ash geopolymer to reduce porosity.
b. There is no significant change in strength for the geopolymer following continuous immersion in the chloride environment for one year. It was also observed that there is no significant degradation of the fly ash geopolymer compressive strength under the wetting-drying cycles that represents the tidal and splash zones.
c. Mix T7 and T10 could resist the stiffness degradation caused by chloride in the continuous immersion such as reinforced structures in a submerged zone. Nevertheless, it seems the wetting-drying cycles caused quite a significant effect on geopolymer stiffness in this research, which is not beneficial for concrete in tidal and splash zones.
d. The alkalis leaching in the mixes with high aluminosilicate content could change the porosity of fly ash geopolymer concrete during continuous immersion. However, there is no significant change on the low calcium fly ash porosity under the wetting-drying cycles.
e. The change in weight of the fly ash geopolymer concrete is marginal in the continuous immersion that related to the change in porosity. A gradual increase in OPC concrete was probably due to chloride penetration that has been bound into the paste to increase the concrete density. A constant weight was demonstrated by the fly ash geopolymer mix after being exposed to wetting-drying cycles. On the other hand, chloride crystallization in the OPC pores was noticeable due to a gradual reduction of weight percentage over time.
f. A visual investigation revealed a significant change in the surface appearance for both OPC and geopolymer concrete after exposure to wetting-drying cycles. A surface degradation was shown by the geopolymer, which could increase the concrete porosity

and resistance to chloride ion penetration in that condition. On the other hand, thin salt crystals covered the surface of OPC and geopolymer under continuous immersion. There was no significant change in their appearance or crystallization.

g. After being immersed continuously, there was an expansion of OPC, mix T7 and T7. In contrast, mix T4 experienced shrinkage after the immersion. Expansion of OPC related to swelling in the pores due to chloride ion penetration and continuous hydration in the long term. A significant shrinkage of the OPC was observed after exposure to wetting-drying cycles. A very small expansion and shrinkage was observed for the geopolymer dry and wet that indicated the fly ash geopolymer resistance to a repetitive temperature change after wetting-drying.
h. Microstructure of geopolymer after continuous immersion of 365 days revealed a formation of chloride crystals in the concrete pores. Those crystals could be accumulated and increase the chance of expansion of specimens.

Corrosion of Steel Reinforcement Bar

a. Corrosion potential of fly ash geopolymer was lower than -270mV vs Ag/AgCl, which indicates a high risk of corrosion of steel reinforcement bar. In contrast, the OPC concrete specimens performed a slight lower risk of corrosion than the geopolymer. The pH of both concrete mixes in the aqueous medium was steady around 9.2 and considered low to maintain the passive film availability to protect the steel bar. Based on the steel weight loss calculation, the fly ash geopolymer has a lower corrosion rate than the OPC concrete. This might be due to sodium silicate in the pore system or a competing action between alkalis and chloride in the geopolymer system.
b. A preconditioning of fly ash geopolymer specimen in a testing medium for 3 days is essential to cut time for chloride ion penetration into the concrete pores. High temperature of the applied voltage induced a high electrical resistance of specimens, which could prolong the specimen failure during the accelerated corrosion test.
c. Corrosion activity based on current versus the time of geopolymer in the applied voltage of 30V setup was higher than specimens exposed to a similar system with a lower voltage of 5V. The fly ash geopolymer showed a lower corrosion activity than the OPC concrete after exposure to both voltages. The time to failure was higher for mix T4, followed by mix T10 and T7 compared to the OPC concrete.
d. The fly ash geopolymer has higher electrical resistance than the OPC, which could reduce the corrosion rate of steel reinforcement bar. Mix T4 has the highest time to failure compared to the geopolymer mixes. The OPC has the lowest electrical resistance. It was found that there was no specific correlation between time to failure and tensile strength of the geopolymer concrete.

e. Mass loss of steel reinforcement bar in the OPC was higher than the geopolymer concrete after exposure to the accelerated corrosion test. There was a considerable difference between the percentages of original mass loss with theoretical mass loss calculated with Faraday's Law. Non-linear characteristics of geopolymer concrete such as water permeability, flow path of chlorides, steel bar geometric heterogeneity, porosity of specimens and the aggressive nature of the accelerated corrosion test could be the reasons for this behaviour.

f. Visual investigation revealed a wide crack was normally observed from the OPC concrete after exposure to the 30V system. There was a high steel bar mass loss, loss of alkalinity and chloride ion penetration into the concrete due to the wide crack. On the other hand, the fly ash geopolymer concrete showed smaller crack and steel bar mass loss. There was alkalinity reduction around the steel bar and high chloride penetration into the matrix.

g. The corrosion product covered the steel reinforcement bar causing loss of the strong bonding between the geopolymer and carbon steel. Corrosion products tend to penetrate into the concrete pores sometimes to the outer surface of concrete. The geopolymer paste filled with salt crystals. The geopolymer paste contaminated with corrosion product had a damaged microstructure.

h. It can be concluded that the unique porosity characteristics of the geopolymer paste can lead to a high risk of corrosion on the system. Alkalis leach out from the paste and have a high penetration of chloride due to porous capillary porosity can increase the damage of reinforced structures in seawater environment. Although the corrosion rate was low due to low expansion and porous pore structure of geopolymer, the corrosion activity can be extended in order to generate significant pressure. A very high steel mass loss due to this process in the long term that could sacrifice the concrete integrity and serviceability.

Microbiologically Influenced Corrosion

a. The corrosion potential of geopolymer in micro algae testing medium was more negative than the OPC, showing a risk of corrosion of steel reinforcement bar. The biofilm produced by micro algae and photosynthetic influence the corrosion potential of steel embedded in fly ash geopolymer concrete.

b. The pH of geopolymer concrete in micro algae medium was less than the OPC concrete, causing a tolerable environment for algae growth. This could add a risk to a prolonged existence of micro algae in the geopolymer system.

c. Low cell densities representing a small growth of micro algae was observed for both types of concrete. However, the geopolymer concrete was a more tolerable environment increasing the algae growth marginally.
d. A positive correlation between cell densities of micro algae with corrosion potential was observed. The corrosion potential became more negative as the cell densities decreased. In contrast, the corrosion potential of the OPC concrete was independent of the micro algae density.
e. It can be concluded that the microorganism environment has a considerable effect on the corrosion performance of steel reinforcement bars in fly ash geopolymer.
f. Microstructure of steel embedded in fly ash geopolymer concrete revealed a formation of corrosion product and dehydrated microorganism in the geopolymer surface.

5.3 Recommendations

There are some areas that were not investigated in the present study. The following recommendations are given:

a. An optimization using particle packing density to reduce fly ash geopolymer porosity is recommended.
b. The effect of alkali and silica content in the fly ash geopolymer mixtures need to be investigated with similar fly ash, aggregate, water content and curing temperature.
c. A model of service life of fly ash geopolymer concrete should be investigated for various parameters and composition.
d. The corrosion rate of fly ash geopolymer using LPR device should be examined and compared with steel bar mass loss under a natural immersion test.
e. The effect of bacteria in corrosion of fly ash geopolymer concrete needs to be carried out to model a system in sewer pipes.
f. The accelerated corrosion test using impressed current should be investigated and compared with the impressed voltage system.
g. Bond between steel reinforcement bars and geopolymer after corrosion need to be investigated to ensure the strong bonding still exists.
h. A systematic approach to investigate the microstructure change after corrosion and characterisation of corrosion product is needed.
i. A correlation between the mechanical strength and durability properties needs to be investigated to fulfil requirements in application.
j. Sulphate resistance in the continuous and wetting-drying cycles need to be studied and compared with the chloride resistance of the fly ash geopolymer.

REFERENCES

1. ADAA Statistics Page [Internet]. Wollongong: Ash Development Association of Australia; 2009 [updated 2009 October 15; cited 2010 May 20]. Available from: http://www.adaa.asn.au/statistics.htm
2. Bakharev T. Resistance of geopolymer materials to acid attack. Cement and Concrete Research. 2005; 35(4):658-670.
3. Bakharev T. Durability of geopolymer materials in sodium and magnesium sulfate solutions. Cement and Concrete Research. 2005; 35(6):1233-1246.
4. Kong DLY, Sanjayan JG, Sagoe-Crentsil K. Comparative performance of geopolymers made with metakaolin and fly ash after exposure to elevated temperatures. Cement and Concrete Research. 2007; 37(12):1583-1589.
5. Davidovits J Davidovits J, Orlinski J, editors. Geopolymer chemistry and properties. Geopolymer'88; 1988; Saint-Quentin (France): Institut Geopolymere; 1988.
6. Davidovits J. Geopolymers: inorganic polymeric new materials. Journal of Thermal Analysis. 1991; 37(8):1633-1656.
7. Davidovits J. Geopolymer Chemistry & Applications. Saint-Quentin: Institut Geopolymere; 2008.
8. Alonso S, Palomo A. Alkaline activation of metakaolin and calcium hydroxide mixtures: influence of temperature, activator concentration and solids ratio. Materials Letters. 2001; 47(1-2):55-62.
9. Van Jaarsveld JGS, Van Deventer JSJ, Lukey GC. The effect of composition and temperature on the properties of fly ash- and kaolinite-based geopolymers. Chemical Engineering Journal. 2002; 89(1-3):63-73.
10. Barbosa VFF, MacKenzie KJD, Thaumaturgo C. Synthesis and characterisation of materials based on inorganic polymers of alumina and silica: sodium polysialate polymers. International Journal of Inorganic Materials. 2000; 2(4):309-317.
11. Palomo A, Blanco-Varela MT, Granizo ML, Puertas F, Vazquez T, Grutzeck MW. Chemical stability of cementitious materials based on metakaolin. Cement and Concrete Research. 1999; 29(7):997-1004.
12. Cioffi R, Maffucci L, Santoro L. Optimization of geopolymer synthesis by calcination and polycondensation of a kaolinitic residue. Resources, Conservation and Recycling. 2003; 40(1):27-38.
13. Swanepoel JC, Strydom CA. Utilisation of fly ash in a geopolymeric material. Applied Geochemistry. 2002; 17(8):1143-1148.
14. Roy DM. Alkali-activated cements: Opportunities and challenges. Cement and Concrete Research. 1999; 29(2):249-254.
15. Van Deventer J, Provis J, Duxson P, Brice D. Chemical Research and Climate Change as Drivers in the Commercial Adoption of Alkali Activated Materials. Waste and Biomass Valorization. 2010; 1(1):145-155.
16. Pacheco-Torgal F, Castro-Gomes J, Jalali S. Investigations about the effect of aggregates on strength and microstructure of geopolymeric mine waste mud binders. Cement and Concrete Research. 2007; 37(6):933-941.
17. Detphan S, Chindaprasirt P. Preparation of fly ash and rice husk ash geopolymer. International Journal of Minerals, Metallurgy and Materials. 2009; 16(6):720-726.

18. Wimpenny D Gilbert I, editor. Low carbon concrete- options for the next generation of infrastructure. Concrete 09; 2009; Sydney (Australia): Concrete Institute of Australia.

19. Day KW. Concrete Mix Design, Quality Control and Specification. 3rd ed. New York: Taylor & Francis; 2006.

20. Bakharev T. Geopolymeric materials prepared using Class F fly ash and elevated temperature curing. Cement and Concrete Research. 2005; 35(6):1224-1232.

21. Wallah SE. Drying shrinkage of heat-cured fly ash-based geopolymer concrete. Modern Applied Science. 2009; 3(12):14-21.

22. Davidovits J, Comrie DC, Paterson JH, Ritcey DJ. Geopolymeric concretes for environmental protection. Concrete International 1990:30-40.

23. Gourley JT, Johnson GB Davidovits J, editor. Developments in geopolymer precast concrete. World Congress Geopolymer 2005, Geopolymer, Green Chemistry and Sustainable Development Solutions; 2005; Saint-Quentin (France): Institut Geopolymere.

24. Amalfi C. A path that's more than it's cracked up to be [Internet]. Perth: Scitech & Government of Western Australia; 2008 [cited 2010 June 20]. Available from: http://www.geopolymers.com.au/publications/demonstration-projects/curtin-university-footpath.

25. Montes C, Allouche E Ohji T, editor. Applications of geopolymer concrete in the rehabilitation of wastewater conveyance systems in extreme environments. 32nd International Conference on Advanced Ceramics and Composites; 2008; Florida (USA): Wiley.

26. Song XJ, Marosszeky M, Brungs M, Munn R Chevalier J-L, editor. Durability of fly ash based geopolymer concrete against sulphuric acid attack. 10DBMC International Conference on Durability of Building Materials and Components; 2005; Lyon (France): Centre Scientifique et Technique du Batiment.

27. Kong DLY, Sanjayan JG. Effect of elevated temperatures on geopolymer paste, mortar and concrete. Cement and Concrete Research. 2010; 40(2):334-339.

28. Temuujin J, Minjigmaa A, Rickard W, Lee M, Williams I, van Riessen A. Fly ash based geopolymer thin coatings on metal substrates and its thermal evaluation. Journal of Hazardous Materials. 2010; 180(1-3):748-752.

29. Cheema DS, Llyod NA, Rangan BV Tam CT, Ong KG, Teng S, Zhang MH, editors. Durability of geopolymer concrete box culverts- a green alternative. 34th Conference on Our World in Concrete & Structures; 2009; Singapore: CiPremier.

30. Llyod NA, Rangan BV Naik TR, Canpolat F, Claisse P, Ganjian E, editors. Geopolymer concrete with fly ash. Second International Conference on Sustainable Construction Materials and Technologies; 2010; Ancona (Italy): UWM Center for By-Products Utilization.

31. Adam AA, Molyneaux TK, Patnaikuni I, Law DW. Strength, sorptivity and carbonation of geopolymer concrete. In: Ghafoori N, editor. Challenges, Opportunities and Solutions in Structural Engineering and Construction. Boca Raton: CRC Press; 2010.

32. Olivia M, Nikraz HR. Corrosion performance of embedded steel in fly ash geopolymer concrete by impressed voltage method. In: Fragomeni S, Venkatesan S, Lam NTK, Setunge S, editors. Incorporating Sustainable Practice in Mechanics of Structures and Materials. Boca Raton: CRC Press; 2011.

33. Bastidas DM, Fernández-Jiménez A, Palomo A, González JA. A study on the passive state stability of steel embedded in activated fly ash mortars. Corrosion Science. 2008; 50(4):1058-1065.

34. Van Jaarsveld JGS, Van Deventer JSJ, Schwartzman A. The potential use of geopolymeric materials to immobilise toxic metals: Part II. Material and leaching characteristics. Minerals Engineering. 1999; 12(1):75-91.

35. Chaudhary D, Liu H. Influence of high temperature and high acidic conditions on geopolymeric composite material for steel pickling tanks. Journal of Materials Science. 2009; 44(16):4472-4481.

36. Temuujin J, van Riessen A. Effect of fly ash preliminary calcination on the properties of geopolymer. Journal of Hazardous Materials. 2009; 164(2-3):634-639.

37. Shindunata. A Conceptual Model of Geopolymerisation. Melbourne: The University of Melbourne; 2006.

38. Juenger MCG, Winnefeld F, Provis JL, Ideker JH. Advances in alternative cementitious binders. Cement and Concrete Research. 2010; In Press, Corrected Proof.

39. Fernandez-Jimenez A, Palomo A, Criado M. Microstructure development of alkali-activated fly ash cement: a descriptive model. Cement and Concrete Research. 2005 [cited February 19, 2007]; 35(6):1204-1209.

40. Duxson P, Fernández-Jiménez A, Provis J, Lukey G, Palomo A, van Deventer J. Geopolymer technology: the current state of the art. Journal of Materials Science. 2007; 42(9):2917-2933.

41. Jo B-W, Park S-K, Park M-S. Strength and hardening characteristics of activated fly ash mortars. Magazine of Concrete Research. 2007; 59(2):121-129.

42. Sear LKA. The Properties and Use of Coal Fly Ash. London: Thomas Telford Publisher; 2001.

43. Van Jaarsveld JGS, Van Deventer JSJ, Lukey GC. The characterisation of source materials in fly ash-based geopolymers. Materials Letters. 2003; 57(7):1272-1280.

44. Diaz EI, Allouche EN, Eklund S. Factors affecting the suitability of fly ash as source material for geopolymers. Fuel. 2010; 89(5):992-996.

45. Ness J, Heeley P. Production and handling of coal combustion products. In: Gurba L, Heidrich C, Ward C, editors. Coal Combustion Products Handbook. Kenmore: Cooperative Research Centre for Coal in Sustainable Development; 2007.

46. French D, Riley K, Ward C. Characterisation, classification and properties of coal combustion products. In: Gurba L, Heidrich C, Ward C, editors. Coal Combustion Products Handbook. Kenmore: Cooperative Research Centre for Coal in Sustainable Development; 2007.

47. Fernández-Jiménez A, Palomo A. Characterisation of fly ashes. Potential reactivity as alkaline cements. Fuel. 2003; 82(18):2259-2265.

48. Temuujin J, Williams RP, van Riessen A. Effect of mechanical activation of fly ash on the properties of geopolymer cured at ambient temperature. Journal of Materials Processing Technology. 2009; 209(12-13):5276-5280.

49. Shindunata, van Deventer JSJ, Lukey GC, Xu H. Effect of curing temperature and silicate concentration on fly ash based geopolymerization. Industrial & Engineering Chemistry Research. 2006; 45(10):3559-3568.

50. Xu H, Lukey GC, van Deventer JSJ Malhotra VM, editor. The activation of class C, class F fly ash and blast furnace slag using geopolymerisation. Eighth CANMET/ACI

International Conference on Fly Ash, Silica Fume, Slag, and Natural Pozzolans in Concrete; 2004; Las Vegas (USA): CANMET/ACI.

51. Temuujin J, van Riessen A, Williams R. Influence of calcium compounds on the mechanical properties of fly ash geopolymer pastes. Journal of Hazardous Materials. 2009; 167(1-3):82-88.

52. Winnefeld F, Leemann A, Lucuk M, Svoboda P, Neuroth M. Assessment of phase formation in alkali activated low and high calcium fly ashes in building materials. Construction and Building Materials. 2010; 24(6):1086-1093.

53. Yip CK, Lukey GC, Provis JL, van Deventer JSJ. Effect of calcium silicate sources on geopolymerisation. Cement and Concrete Research. 2008; 38(4):554-564.

54. Guo X, Shi H, Dick WA. Compressive strength and microstructural characteristics of class C fly ash geopolymer. Cement and Concrete Composites. 2010; 32(2):142-147.

55. Fan Y, Yin S, Wen Z, Zhong J. Activation of fly ash and its effects on cement properties. Cement and Concrete Research. 1999; 29(4):467-472.

56. Buchwald A, Ch. K, M. H Alkali-activated binders and pozzolan cement binders-compete binder reaction or two sides of the same story? Proceedings of the 11th International Congress on the Chemistry of Cement (ICCC). Cement's contribution to the development in the 21st century.; 2003; Durban (South Africa): ICCC.

57. Rangan BV. Low calcium fly ash based geopolymer concrete. In: Nawy EG, editor. Concrete Construction Engineering Handbook. Second ed. Boca Raton: CRC Press; 2008.

58. Kriven WM, Bell JL. Effect of alkali choice of geopolymer properties. In: The American Ceramic Society, editor. Ceramic Engineering and Sciences Proceedings. New York: Wiley; 2004.

59. Palomo A, Grutzeck MW, Blanco MT. Alkali-activated fly ashes: A cement for the future. Cement and Concrete Research. 1999; 29(8):1323-1329.

60. Arjunan P, Silsbee MR, Roy DM Chemical activation of low calcium fly ash. Part 1: Identification of suitable activators and their dosage. 2001 International Ash Utilization Symposium; 2001; Kentucky (USA): University of Kentucky: Center for Applied Energy Research.

61. Provis JL. Activating solution chemistry for geopolymers. In: Provis JL, Deventer JSJv, editors. Geopolymers, structure, processing, properties and industrial applications. Oxford: Woodhead Publishing Limited; 2009.

62. Ravikumar D, Peethamparan S, Neithalath N. Structure and strength of NaOH activated concretes containing fly ash or GGBFS as the sole binder. Cement and Concrete Composites. 2010; 32(6):399-410.

63. Fernandez-Jimenez A, Palomo A. Composition and microstructure of alkali activated fly ash binder: Effect of the activator. Cement and Concrete Research. 2005; 35(10):1984-1992.

64. Neville AM. Properties of concrete. Essex: Longman Group Limited; 1995.

65. Temuujin J, van Riessen A, MacKenzie KJD. Preparation and characterisation of fly ash based geopolymer mortars. Construction and Building Materials. 2010; 24(10):1906-1910.

66. Lee WKW, van Deventer JSJ. The interface between natural siliceous aggregates and geopolymers. Cement and Concrete Research. 2004; 34(2):195-206.

67. Palacios M, Puertas F. Effect of superplasticizer and shrinkage-reducing admixtures on alkali-activated slag pastes and mortars. Cement and Concrete Research. 2005; 35(7):1358-1367.

68. Bakharev T, Sanjayan JG, Cheng YB. Effect of admixtures on properties of alkali-activated slag concrete. Cement and Concrete Research. 2000; 30(9):1367-1374.

69. Hardjito D, Wallah SE, Sumajouw DMJ, Rangan BV. On the development of fly ash-based geopolymer concrete. ACI Materials Journal. 2004; 101(6):467-472.

70. Chindaprasirt P, Chareerat T, Sirivivatnanon V. Workability and strength of coarse high calcium fly ash geopolymer. Cement and Concrete Composites. 2007; 29(3):224-229.

71. Panias D, Giannopoulou IP, Perraki T. Effect of synthesis parameters on the mechanical properties of fly ash-based geopolymers. Colloids and Surfaces A: Physicochemical and Engineering Aspects. 2007; 301(1-3):246-254.

72. Songpiriyakij S, Kubprasit T, Jaturapitakkul C, Chindaprasirt P. Compressive strength and degree of reaction of biomass- and fly ash-based geopolymer. Construction and Building Materials. 2010; 24(3):236-240.

73. Álvarez-Ayuso E, Querol X, Plana F, Alastuey A, Moreno N, Izquierdo M, et al. Environmental, physical and structural characterisation of geopolymer matrixes synthesised from coal (co-)combustion fly ashes. Journal of Hazardous Materials. 2008; 154(1-3):175-183.

74. Kumar S, Kumar R. Mechanical activation of fly ash: Effect on reaction, structure and properties of resulting geopolymer. Ceramics International. 2011; 37(2):533-541.

75. Rattanasak U, Chindaprasirt P. Influence of NaOH solution on the synthesis of fly ash geopolymer. Minerals Engineering. 2009; 22(12):1073-1078.

76. Komljenovic M, Bascarevic Z, Bradic V. Mechanical and microstructural properties of alkali-activated fly ash geopolymers. Journal of Hazardous Materials. 2010; 181(1-3):35-42.

77. Duxson P, Provis JL, Lukey GC, van Deventer JSJ. The role of inorganic polymer technology in the development of `green concrete'. Cement and Concrete Research. 2007; 37(12):1590-1597.

78. Fernandez-Jimenez A, Palomo A, Lopez-Hombrados. C. Engineering properties of alkali-activated fly ash concrete. ACI Materials Journal. 2006; 103(2):106-112.

79. Song X. Development and performance of class F fly ash based geopolymer concretes against sulphuric acid attack. Sydney: University of New South Wales; 2007.

80. Lloyd RR, Provis JL, Smeaton KJ, van Deventer JSJ. Spatial distribution of pores in fly ash-based inorganic polymer gels visualised by Wood's metal intrusion. Microporous and Mesoporous Materials. 2009; 126(1-2):32-39.

81. Provis JL, Duxson P, van Deventer JSJ. The role of particle technology in developing sustainable construction materials. Advanced Powder Technology. 2010; 21(1):2-7.

82. Wu Z, Naik TR. Chemically activated blended cements. ACI Materials Journal. 2003; 100(5):434-440.

83. Ozbay E, Oztas A, Baykasoglu A, Ozbebek H. Investigating mix proportions of high strength self compacting concrete by using Taguchi method. Construction and Building Materials. 2009; 23(2):694-702.

84. Türkmen I, Gül R, Çelik C. A Taguchi approach for investigation of some physical properties of concrete produced from mineral admixtures. Building and Environment. 2008; 43(6):1127-1137.

85. Ross PJ. Taguchi techniques for quality engineering. New York: McGraw-Hill; 1988.

86. Mather B. Concrete durability. Cement and Concrete Composites. 2004; 26(1):3-4.

87. CEB. Durable Concrete Structures Design Guide. Lausanne: Comite Euro-International Du Beton; 1992.

88. Liu P. Damage to concrete structures in a marine environment. Materials and Structures. 1991; 24(4):302-307.

89. Hunkeler F. Corrosion in reinforced concrete: processes and mechanisms. In: Bohni H, editor. Corrosion in Reinforced Concrete Structures. Boca Raton: CRC Press; 2005.

90. Cement Concrete & Aggregates Australia. Chloride Resistance of Concrete. Perth: Cement Concrete & Aggregates Australia; 2009.

91. Costa A, Appleton J. Chloride penetration into concrete in marine environment-Part II: Prediction of long term chloride penetration. Materials and Structures. 1999; 32(5):354-359.

92. Chalee W, Jaturapitakkul C, Chindaprasirt P. Predicting the chloride penetration of fly ash concrete in seawater. Marine Structures. 2009; 22(3):341-353.

93. Neville A. Chloride attack of reinforced concrete: an overview. Materials and Structures. 1995; 28(2):63-70.

94. Morris W, Vico A, Vázquez M. Chloride induced corrosion of reinforcing steel evaluated by concrete resistivity measurements. Electrochimica Acta. 2004; 49(25):4447-4453.

95. Bickley J, Hooton RD, Hover KC. Preparation of a Performance-based Specification for Cast-In-Place Concrete. Portsmouth: RMC Research Foundation; 2006.

96. Cheewaket T, Jaturapitakkul C, Chalee W. Long term performance of chloride binding capacity in fly ash concrete in a marine environment. Construction and Building Materials. 2010; 24(8):1352-1357.

97. Dhir RK, El-Mohr MAK, Dyer TD. Developing chloride resisting concrete using PFA. Cement and Concrete Research. 1997; 27(11):1633-1639.

98. Gowripalan N, Mohamed HM. Chloride-ion induced corrosion of galvanized and ordinary steel reinforcement in high-performance concrete. Cement and Concrete Research. 1998; 28(8):1119-1131.

99. Baweja D, Roper H, Sirivivatnon V. Chloride induced steel corrosion in concrete: Part I- Corrosion rates, corrosion activity, and attack areas. ACI Materials Journal. 1998; 95(3):207-217.

100. Dehwah HAF, Austin SA, Maslehuddin M. Chloride-induced reinforcement corrosion in blended cement concretes exposed to chloride sulphate environments. Magazine of Concrete Research. 2002; 54(5):355-364.

101. Scott A, Alexander MG. The influence of binder type, cracking and cover on corrosion rates of steel in chloride-contaminated concrete. Magazine of Concrete Research. 2007; 59(7):435-505.

102. Ahmad S. Reinforcement corrosion in concrete structures, its monitoring and service life prediction--a review. Cement and Concrete Composites. 2003; 25(4-5):459-471.

103. González J, Feliú S, Rodríguez P, Ramírez E, Alonso C, Andrade C. Some questions on the corrosion of steel in concrete—Part I: when, how and how much steel corrodes. Materials and Structures. 1996; 29(1):40-46.

104. Bentur A, Diamond S, Berke NS. Steel Corrosion in Concrete. London: E&FN Spon; 1997.

105. Rendell F, Jauberthie R, Grantham M. Deteriorated Concrete, Inspection and physicochemical analysis. London: Thomas Telford; 2002.

106. ASTMC876. Standard Test Method for Corrosion Potentials of Uncoated Reinforcing Steel in Concrete. Philadelphia: ASTM International; 2009.

107. Tuutti K Malhotra VM, editor. Service life of structures with regard to corrosion of embedded steel. International Conference on Performance of Concrete in Marine Environment; 1982; St Andrews (Canada): CANMET/ACI.

108. Weyers RE. Service life model for concrete structures in chloride laden environments. ACI Materials Journal. 1998; 95(4):445-453.

109. Liu Y, Weyers RE. Modeling the time to corrosion cracking in chloride contaminated reinforced concrete structures. ACI Materials Journal. 1998; 95(6):675-681.

110. El Maaddawy T, Soudki K. A model for prediction of time from corrosion initiation to corrosion cracking. Cement and Concrete Composites. 2007; 29(3):168-175.

111. De Belie N, Monteny J, Beeldens A, Vincke E, Van Gemert D, Verstraete W. Experimental research and prediction of the effect of chemical and biogenic sulfuric acid on different types of commercially produced concrete sewer pipes. Cement and Concrete Research. 2004; 34(12):2223-2236.

112. Mori T, Nonaka T, Tazaki K, Koga M, Hikosaka Y, Noda S. Interactions of nutrients, moisture and pH on microbial corrosion of concrete sewer pipes. Water Research. 1992; 26(1):29-37.

113. Javaherdashti R. Microbiologically Influenced Corrosion- An Engineering Insight. London: Springer-Verlag; 2008.

114. Diercks M, Sand W, Bock E. Microbial corrosion of concrete. Cellular and Molecular Life Sciences. 1991; 47(6):514-516.

115. Alum A, Rashid A, Mobasher B, Abbaszadegan M. Cement-based biocide coatings for controlling algal growth in water distribution canals. Cement and Concrete Composites. 2008; 30(9):839-847.

116. Gaylarde PM, Gaylarde CC. Algae and cyanobacteria on painted buildings in Latin America. International Biodeterioration & Biodegradation. 2000; 46(2):93-97.

117. Tiller AK The Metals Society, editor. Electrochemical aspects of microbial corrosion: an overview. Microbial Corrosion; 1983; London (UK): The Metals Society.

118. Jayakumar S, Saravanane R. Biodeterioration of coastal concrete structures by Macro algae - Chaetomorpha antennina. Materials Research. 2009; 12:465-472.

119. Guilbeau BP, Harry FP, Gambrell RP, Knopf FC, Dooley KM. Algae attachment on carbonated cements in fresh and brackish waters--preliminary results. Ecological Engineering. 2003; 20(4):309-319.

120. Edyvean RGJ, Terry LA, editors. The influence of micro-algae on corrosion of structural steels used in the North Sea. Chichester: John Wiley and Sons; 1983.

121. Terry LA, Edyvean RGJ. Microalgae and corrosion. Botanica Marina. 1981; 24:177-183.

122. Little B, Wagner P, Mansfeld F. An overview of microbiologically influenced corrosion. Electrochimica Acta. 1992; 37(12):2185-2194.

123. Bastidas-Arteaga E, Sánchez-Silva M, Chateauneuf A, Silva MR. Coupled reliability model of biodeterioration, chloride ingress and cracking for reinforced concrete structures. Structural Safety. 2008; 30(2):110-129.

124. Bassuoni MT, Nehdi ML. Durability of self-consolidating concrete to sulfate attack under combined cyclic environments and flexural loading. Cement and Concrete Research. 2009; 39(3):206-226.

125. Aïtcin PC. The durability characteristics of high performance concrete: a review. Cement and Concrete Composites. 2003; 25(4-5):409-420.

126. Rilem Technical Committee 32-RCA. Seawater attack on concrete and precautionary measures. Materials and Structures. 1985; 18(3):223-226.

127. Delagrave A, Pigeon M, Revertégat É. Influence of chloride ions and pH level on the durability of high performance cement pastes. Cement and Concrete Research. 1994; 24(8):1433-1443.

128. Gégout P, Revertégat E, Moine G. Action of chloride ions on hydrated cement pastes: Influence of the cement type and long time effect of the concentration of chlorides. Cement and Concrete Research. 1992; 22(2-3):451-457.

129. AS3600. Concrete Structures [standard online]. 2009 [cited 2008 December 05]; AS 3600-2009. Available from: Standard Australia Online.

130. Concrete Institute of Australia. Recommended Practice Performance Criteria for Concrete in Marine Environments. Crows Nest: Concrete Institute of Australia; 2001.

131. Ho DWS, Chirgwin GJ. A performance specification for durable concrete. Construction and Building Materials. 1996; 10(5):375-379.

132. Papworth F, Grace W Designing for concrete durability in marine environs. Concrete 85,; 1985; Brisbane: Concrete Institute of Australia.

133. Vicroads. Test methods for the assessment of durability of concrete- Technical Note [Internet]. Melbourne: Vicroads; 2007 [updated 2007 October; cited 2008 March 09]. Available from: http://docs.google.com/viewer?a=v&q=cache:Xab6xJBE-7YJ:www.bookshop.vicroads.vic.gov.au/redirectpdf/redirectpdf.aspx%3Faddr%3Dpdfs/tn89.pdf+Test+methods+for+the+assessment+of+durability+of+concrete-+Technical+Note&hl=en&gl=au&pid=bl&srcid=ADGEESgNTHypHf9aD_3u4VgG8OvlkDpZEyA7O7ioW33sAWsSe-BdPVvXBdQvHNIdF9fWeojAu5cta-3oHZ6pk_9ROg7BK8tzXUMECT6ZsW9hv4wjBA-xTq0IeU3ZdYBrQG0dNnlk1vRB&sig=AHIEtbR6YX6S3YUPMEFTsIyTb2NJ8kgnPQ.

134. ASTMC1202. Standard Test Method for Electrical Indication of Concrete's Ability to Resist Chloride Ion Penetration. Philadelphia: ASTM International; 2010.

135. Chang ZT, Marosszeky M Malhotra VM, editor. Chloride penetration and water absorption into P.C., fly ash and slag concrete under different curing conditions. Fourth CANMET/ACI International Conference on Durability of Concrete; 1997; Sydney: CANMET/ACI p. 349-362.

136. Sofi M, van Deventer JSJ, Mendis PA, Lukey GC. Engineering properties of inorganic polymer concretes (IPCs). Cement and Concrete Research. 2007; 37(2):251-257.

137. Rangan BV. Engineering properties of geopolymer concrete. In: Provis JL, van Deventer JSJ, editors. Geopolymers, structure, processing, properties and industrial applications. Oxford: Woodhead Publishing Limited; 2009.

138. Hardjito D. Studies on Fly-Ash Based Geopolymer Concrete. Perth: Curtin University of Technology; 2005.

139. Llyod RR. Accelerated ageing of geopolymers. In: Provis JL, van Deventer JSJ, editors. Geopolymers, structure, processing, properties and industrial applications. Oxford: Woodhead Publishing Limited; 2009.

140. Wongpa J, Kiattikomol K, Jaturapitakkul C, Chindaprasirt P. Compressive strength, modulus of elasticity, and water permeability of inorganic polymer concrete. Materials & Design. 2010; 31(10):4748-4754.

141. Popovics S, Simeonov Y, Bozhinov G, Barovsky N Crane AP, editor. Durability of reinforced concrete in sea water. Corrosion of reinforcement in concrete construction; 1983; London: Ellish Horwood Limited.

142. Hardjito D, Wallah SE, Sumajouw DMJ, Rangan BV. Fly ash-based geopolymer concrete. Australian Journal of Structural Engineering. 2005; 6(1):77-84.

143. Duxson P, Provis JL, Lukey GC, Mallicoat SW, Kriven WM, van Deventer JSJ. Understanding the relationship between geopolymer composition, microstructure and mechanical properties. Colloids and Surfaces A: Physicochemical and Engineering Aspects. 2005; 269(1-3):47-58.

144. Skvara F, Kopecky L, Nemecek J, Bittnar Z. Microstructure of geopolymer materials based on fly ash. Ceramics-Silikaty. 2006; 50(4):208-215.

145. Sathia R, Babu KG, Santhanam M Uomoto T, Nga TV, Dich NT, Long LD, Hoang TM, Hung LV, et al., editors. Durability study of low calcium fly ash geopolymer concrete. The 3rd ACF International Conference-ACF/VCA 2008; 2008; Ho Chi Minh City: Vietnam Institute for Building Materials.

146. Thokchom S, Ghosh P, Ghosh S. Effect of water absorption, porosity and sorptivity on durability of geopolymer mortars. ARPN Journal of Engineering and Applied Sciences. 2009; 4(7):28-32.

147. Mishra A, Choudhary D, Jain N, Kumar M, Sharda N, Dutt D. Effect of concentration of alkaline liquid and curing time on strength and water absorption of geopolymer concrete. ARPN Journal of Engineering and Applied Sciences. 2008; 3(1):14-18.

148. Adam AA, Molyneaux TK, Patnaikuni I, Law DW Gilbert I, editor. Chloride penetration and carbonation in blended OPC-GGBS, alkali activated slag and fly ash based geopolymer concrete. Concrete Solutions 09; 2009; Sydney (Australia): Concrete Institute of Australia.

149. Muntingh Y. Durability and diffusive behaviour evaluation of geopolymeric material: University of Stellenbosch; 2006.

150. Ahmed MS, Kayali O, Anderson W. Chloride penetration in binary and ternary blended cement concretes as measured by two different rapid methods. Cement and Concrete Composites. 2008; 30(7):576-582.

151. Lloyd RR, Provis JL, van Deventer JSJ. Pore solution composition and alkali diffusion in inorganic polymer cement. Cement and Concrete Research. 2010; 40(9):1386-1392.

152. Wallah SE, Hardjito D, Sumajouw DMJ, Rangan BV Stewart MG, Dockrill B, editors. Sulfate and acid resistance of fly ash-based geopolymer concrete. Australian Structural Engineering Conference; 2005; Newcastle (Australia): Engineers Australia.

153. Thokchom S, Ghosh P, Ghosh S. Performance of fly ash based geopolymer mortars in sulphate solution. Journal of Engineering Science and Technology Review. 2010; 3(1):36-40.

154. Morris J, Hodges S Davidovits J, editor. Corrosion of metals in fly ash based geopolymers. World Congress Geopolymer 2005: Geopolymer, Green Chemistry and Sustainable Development Solutions; 2005; Saint-Quentin (France): Institute Geopolymere.

155. Miranda JM, Fernández-Jiménez A, González JA, Palomo A. Corrosion resistance in activated fly ash mortars. Cement and Concrete Research. 2005; 35(6):1210-1217.

156. Davidovits J Davidovits J, editor. Geopolymer chemistry and sustainable development. The poly(sialate) terminology: a very useful and simple model for the promotion and understanding of green-chemistry. World Congress Geopolymer 2005: Geopolymer, Green Chemistry and Sustainable Development Solutions; 2005; Saint-Quentin (France): Institut Geopolymere.

157. Mukhin V, Khatri R, Dumitru I Some limitations of geopolymer concrete. Concrete 07; 2007; Adelaide (Australia): Concrete Institute of Australia.

158. Graeff AG, Torres AS, Filho LCPS Biondini F, Frangopol DM, editors. Comparison of corrosion accelerated tests performed in reinforced concrete structures using voltage and current induction. Life Cycle Civil Engineering; 2008; Lake Como (Italy): CRC Press.

159. Caré S, Raharinaivo A. Influence of impressed current on the initiation of damage in reinforced mortar due to corrosion of embedded steel. Cement and Concrete Research. 2007; 37(12):1598-1612.

160. Yodmunee S, Yodsujai W Study on corrosion of steel bar in fly ash based geopolymer concrete. International Conference on Pozzolan, Concrete and Geopolymer; 2006; Khon Kaen (Thailand): Sustainable Infrastructure Research and Development Center.

161. Javaherdashti R, Nikraz H, Borowitzka M, Moheimani N, Olivia M. On the impact of algae on accelerating the biodeterioration/biocorrosion of reinforced concrete: a mechanistic review. European Journal of Scientific Research. 2009; 36(3):394-406.

162. Fernandez-Jimenez A, García-Lodeiro I, Palomo A. Durability of alkali-activated fly ash cementitious materials. Journal of Materials Science. 2007; 42(9):3055-3065.

163. Skvara F, Jilek T, Kopecky L. Geopolymer materials based on fly ash. Ceramics-Silikaty. 2005; 49:194-204.

164. Hong K, Hooton RD. Effects of cyclic chloride exposure on penetration of concrete cover. Cement and Concrete Research. 1999; 29(9):1379-1386.

165. AS3972. Portland and blended cements [standard online]. 1997 [cited 2008 April 09]; AS 3972-1997. Available from: Standard Australia Online.

166. ASTMC150. Standard Specification for Portland Cement. Philadelphia: ASTM International; 2009.

167. Cavanagh KJ, Guirguis S. Cements. In: Ryan WG, Samarin A, editors. Australian Concrete Technology. Melbourne: Longman; 1996.

168. Bye GC. Portland Cement. London: Thomas Telford; 1999.

169. Rapp P. Effect of calcium chloride on Portland Cements and Concretes. Highway Research Board Proceedings. 1934.

170. ASTMC618. Standard Specification for Coal Fly Ash and Raw or Calcined Natural Pozzolan for Use in Concrete. Philadelphia: ASTM International; 2008.

171. AS3582.1. Supplementary cementitious materials for use with portland and blended cements- Fly ash [standard online]. 1998 [cited 2009 October 02]. Available from: Standard Australia Online.

172. Hardjito D, Wallah SE, Sumajouw DMJ, Rangan BV Malhotra VM, editor. Properties of Geopolymer Concrete with Fly Ash as Source Material: Effect of Mixture Composition. Seventh CANMET/ACI International Conference on Recent Advances in Concrete Technology; 2004; Las Vegas (USA): CANMET/ACI.

173. AS1141.6.1. Methods for sampling and testing aggregates. Method 6.1: Particle density and water absorption of coarse aggregate- Weighing-in-water method [standard online]. 2000 [cited 2008 June 20]. Available from: Standard Australia Online.

174. AS1141.5. Method for sampling and testing aggregates. Method 5: Particle density and water absorption of fine aggregate [standard online]. 2000 [cited 2009 April 24]. Available from: Standard Australia Online.

175. ASTMC127. Standard Test Method for Density, Relative Density (Specific Gravity), and Absorption of Coarse Aggregate. Philadelphia: ASTM International; 2007.

176. ASTMC128. Standard Test Method for Density, Relative Density (Specific Gravity), and Absorption of Fine Aggregate. Philadelphia: ASTM International; 2007.

177. ASTMC566. Standard Test Method for Total Evaporable Moisture Content of Aggregate by Drying. Philadelphia: ASTM International; 2004.

178. Teychenne DC, Franklin RE, Erntory HC. Design of Normal Concrete Mixes. Watford: Department of Environment; 1988.

179. AS1012.2. Methods of testing concrete- Preparation of concrete mixes in the laboratory [standard online]. 1994 [cited 2008 June 10]. Available from: Standards Australia Online.

180. AS1012.3.1. Methods of testing concrete- Determination of properties related to the consistency of concrete- Slump test [standard online]. 1998 [cited 2007 March 20]. Available from: Standard Australia Online.

181. AS1012.9. Method of testing concrete- Determination of the compressive strength of concrete specimens [standard online]. 1999 [cited 2007 April 15]. Available from: Standard Australia Online.

182. AS1012.10. Methods of testing concrete- Determination of indirect tensile strength of concrete cylinders (Brasil or splitting test) [standard online]. 2000 [cited 2007 July 16]. Available from: Standard Australia Online.

183. AS1012.11. Methods of testing concrete- Determination of the modulus of rupture [standard online]. 2000 [cited 2008 September 13]. Available from: Standard Australia Online.

184. AS1012.17. Methods of testing concrete- Determination of the static chord modulus of elasticity and Poisson's ratio of concrete specimens [standard online]. 1997 [cited 2009 October 09]. Available from: Standard Australia Online.

185. AS1012.13. Methods of testing concrete- Determination of the drying shrinkage of concrete for samples prepared in the field or in the laboratory [standard online]. 1993 [cited 2007 March 19]. Available from: Standard Australia Online.

186. ASTMC642. Standard Test Method for Density, Absorption and Voids in Hardened Concrete. Philadelphia: ASTM International; 2006.

187. Saraswathy V, Song H-W. Corrosion performance of rice husk ash blended concrete. Construction and Building Materials. 2007; 21(8):1779-1784.

188. Peek AM, Nguyen N, Wong T Australia Corrosion Association, editor. Durability planning and compliance testing of concrete in construction projects. Corrosion Control 007; 2007; Sydney (Australia): Australia Corrosion Association; 25-28 November 2007.

189. NTBuild443. Concrete, Hardened: Accelerated Chloride Penetration. Espoo: Nordtest; 1995.

190. ASTMC267. Standard Test Methods for Chemical Resistance of Mortars, Grouts, and Monolithic Surfacings and Polymer Concretes. Philadelphia: ASTM International; 2006.

191. Kasai Y, Nakamura N Malhotra VM, editor. Accelerated test method for durability of cement mortars in sea water. International Conference on Performance of Concrete in Marine Environment; 1980; St. Andrews (Canada): CANMET/ACI.

192. Grubb JA, Limaye HS, Kakade AM. Testing pH of concrete. Concrete International 2007:78-83.

193. Güneyisi E, Özturan T, Gesoglu M. A study on reinforcement corrosion and related properties of plain and blended cement concretes under different curing conditions. Cement and Concrete Composites. 2005; 27(4):449-461.

194. Sakr K. Effect of cement type on the corrosion of reinforcing steel bars exposed to acidic media using electrochemical techniques. Cement and Concrete Research. 2005; 35(9):1820-1826.

195. Moheimani N. The culture of Coccolithophorid Algae for carbondioxide bioremediation. Perth: Murdoch University; 2005.

196. Moheimani N, Borowitzka M. The long-term culture of the coccolithophore Pleurochrysis carterae (Haptophyta) in outdoor raceway ponds. Journal of Applied Phycology. 2006; 18(6):703-712.

197. Rilem Recommendations TC56-MHM Hydrocarbon Materials. CPC-18 Measurement of hardened concrete carbonation depth. Materials and Structures. 1988; 21(6):453-455.

198. Mattila JS, Pentti MJ Page C, Bamforth P, Figg J, editors. Re-alkalisation of carbonated concrete by cement-based coatings. Fourth International Symposium on Corrosion of Reinforcement in Concrete Construction; 1996; Cambridge: The Royal Society of Chemistry.

199. AS2758.1. Aggregate and rock for engineering purposes, Part 1: Concrete aggregates [standard online]. 1998 [cited 2009 August 31]. Available from: Standard Australia Online.

200. AS1141.11.1. Methods for sampling and testing aggregates- Particle size distribution-Sieving method [standard online]. 2009 [cited 2009 September 02]. Available from: Standard Australia Online.

201. Munn RL. Concrete Aggregates. In: Ryan WG, Samarin A, editors. Australian Concrete Technology. Melbourne: Addison Wesley Longman Australia 1996.

202. Provis JL. Introduction to geopolymers. In: Provis JL, van Deventer JSJ, editors. Geopolymers, structure, processing, properties and industrial applications. Oxford: Woodhead Publishing Limited; 2009. p. 1-11.

203. E-Crete Engineering Summary [Internet]. Somerton: Zeobond; 2008 [updated February 2008; cited 2010 April 12]. Available from: http://www.zeobond.com/downloads/Zeobond_Engineering_Summary.pdf.

204. Ly L, Vance ER, Perera DS, Aly Z, Olufson K. Leaching of geopolymers in deionised water. Advances in Technology of Materials and Materials Processing Journal. 2006; 8(2):236-247.

205. Sahmaran M, Erdem TK, Yaman IO. Sulfate resistance of plain and blended cements exposed to wetting-drying and heating-cooling environments. Construction and Building Materials. 2007; 21(8):1771-1778.

206. Puertas F, Amat T, Fernández-Jiménez A, Vázquez T. Mechanical and durable behaviour of alkaline cement mortars reinforced with polypropylene fibres. Cement and Concrete Research. 2003; 33(12):2031-2036.

207. Lee WKW, van Deventer JSJ. The effects of inorganic salt contamination on the strength and durability of geopolymers. Colloids and Surfaces A: Physicochemical and Engineering Aspects. 2002; 211(2-3):115-126.

208. Masoud S, Soudki K. Evaluation of corrosion activity in FRP repaired RC beams. Cement and Concrete Composites. 2006; 28(10):969-977.

209. Hobbs DW. Carbonation of concrete containing pfa. Magazine of Concrete Research. 1988; 40(143):69-78.

210. ASTMG1. Standard Practice for Preparing, Cleaning, and Evaluating Corrosion Test Specimens. Philadelphia: ASTM International; 2003.

211. Bertolini L, Elneser B, Pedeferri P, Polder RB. Corrosion of Steel in Concrete-Prevention, Diagnosis, Repair. Weinheim: Wiley; 2004.

212. Yuan M-r, Lu J-t, Kong G. Effect of SiO2:Na2O molar ratio of sodium silicate on the corrosion resistance of silicate conversion coatings. Surface and Coatings Technology. 2010; 204(8):1229-1235.

213. Topçu IB, Boga AR. Effect of ground granulate blast-furnace slag on corrosion performance of steel embedded in concrete. Materials & Design. 2010; 31(7):3358-3365.

214. Olivia M, Nikraz H Wang P, Zhong S, editors. Corrosion of low calcium fly ash geopolymer concrete: a preliminary analysis. 6th Asian Symposium on Polymers in Concrete; 2009; Shanghai: Tongji University Press.

215. Cabrera JG. Deterioration of concrete due to reinforcement steel corrosion. Cement and Concrete Composites. 1996; 18(1):47-59.

216. Kriven WM, Gordon M, Ervin BL, Reis H Kriven WM, editor. Corrosion protection assessment of concrete reinforcing bars with a geopolymer coating. 30th International Conference on Advanced Ceramics and Composites; 2007; Daytona Beach (USA): ICACC.

217. FM5-522. Floride method of test for an accelerated laboratory method for corrosion testing of reinforced concrete using impressed current (FM 5-522) [Internet]. Florida; 2000 [updated 2000 September 1; cited 2008 June 12]. Available from: http://www.dot.state.fl.us/statematerialsoffice/administration/library/publications/fstm/methods/fm5-522.pdf

218. Zhang Y, Li Z, Sun W, Li W. Setting and Hardening of Geopolymeric Cement Pastes Incorporated with Fly Ash. ACI Materials Journal. 2009; 106(5):405-412.

219. Auyeung Y, Balaguru P, Chung L. Bond behavior of corroded reinforcement bars. ACI Materials Journal. 2000; 97:214-220.

220. Austin SA, Lyons R, Ing MJ. Electrochemical behavior of steel-reinforced concrete during accelerated corrosion testing. Corrosion. 2004; 60(2):203-215.

221. Allan ML. Probability of corrosion induced cracking in reinforced concrete. Cement and Concrete Research. 1995; 25(6):1179-1190.

222. Sofi M, van Deventer J, Mendis P, Lukey G. Bond performance of reinforcing bars in inorganic polymer concrete (IPC). Journal of Materials Science. 2007; 42(9):3107-3116.

223. American Society for Metals. Metals Handbook. 9th ed. Ohio: American Society for Metals; 1989.

224. Scotto V, Cintio RD, Marcenaro G. The influence of marine aerobic microbial film on stainless steel corrosion behaviour. Corrosion Science. 1985; 25(3):185-194.

225. Dexter SC, Duquette DJ, Siebert OW, Videla HA. Use and limitations of electrochemical techniques for investigating microbial corrosion. Corrosion. 1991; 47:308-319.

226. Dexter SC, Gao GY. Effect of seawater biofilms on corrosion potential and oxygen reduction of stainless steel. Corrosion. 1988; 44:717-723.

227. Terry LA, Edyvean RGJ. Recent investigations into the effects of algae on corrosion. In: Evans EL, Hoagland KD, editors. Algal Biofouling. Amsterdam: Elsevier; 1986. p. 211-239.

228. Aviam O, Bar-nes G, Zeiri Y, Sivan A. Accelerated biodegradation of cement by sulfur-oxidizing bacteria as a bioassay for evaluating immobilization of low-level radioactive waste. Applied and Environmental Microbiology. 2004; 70(10):6031-6036.

229. Little B, Ray R, Wagner P, Lewandowski Z, Lee WC, Characklis WG, et al. Impact of biofouling on the electrochemical behaviour of 304 stainless steel in natural seawater. Biofouling: The Journal of Bioadhesion and Biofilm Research. 1991; 3(1):45 - 59.

APPENDICES

APPENDIX A - CONCRETE MIX DESIGN FORM

Stage	Item		Reference		Values		
I	1.1	Characteristic strength	Specified	45 N/mm^2	at	28	days
	1.2	Standard deviation	Fig 3	N/mm^2	or no data		N/mm^2
	1.3	Margin	C1	n/a			N/mm^2
	1.4	Target mean strength	C2	= 45 + 10	=	55	N/mm^2
	1.5	Cement type	Specified			OPC	
	1.6	Aggregate type: coarse				Crushed	
		Aggregate type: fine				Uncrushed	
	1.7	Free/water cement ratio	Tab 2, Fig 4			0.45	
2	2.1	Slump	Specified			10-30mm	
	2.2	Maximum aggregate size	Specified			20mm	
	2.3	Free water content	Tab 3			190	kg/m^3
3	3.1	Cement content	C3	= 190/0.45	=	422.23	kg/m^3
	3.2	Maximum cement content	Specified	n/a			
	3.3	Minimum cement content	Specified	n/a			
	3.4	Modified free/water cement ratio		n/a			
4	4.1	Specific gravity of aggregate				2.65	
	4.2	Concrete density	Fig 5			2400	kg/m^3
	4.3	Total aggregate content	C4	= 2400-422.3-190	=	1787.70	kg/m^3
5	5.1	Grading of fine aggregate					
	5.2	Proportion of fine aggregate				30%	
	5.3	Fine aggregate content	C5	= 1787.7 x 0.3	=	536.49	kg/m^3
	5.4	Coarse aggregate content		= 1787.7-536.49	=	1251.21	kg/m^3

Final Quantities				
	cement		422.23	kg/m^3
	water		190.00	kg/m^3
	fine aggregate		536.49	kg/m^3
	coarse aggregate	20mm (15%)	313.00	kg/m^3
		10mm (20%)	375.60	kg/m^3
		7mm (30%)	563.40	kg/m^3

APPENDIX B - MOLAR RATIO CALCULATION OF THE TAGUCHI OPTIMIZATION MIXTURES

Mix design specification:

Compressive strength = 55 MPa

H_2O/Na_2O = 12

Superplasticizer = 1.5 %

NaOH = 14 M

Sodium silicate = 2 Ms

Concrete unit weight = 2400 kg/m^3

Mix	Combination	Variables			
		Aggregate content (kg/m^3)	alkaline/ fly ash ratio	Sodium silicate/NaOH ratio	Curing regime (hours, degree)
T1	A1B1C1D1	1752	0.3	1.5	24h60deg
T2	A1B2C2D2	1752	0.35	2	10h85deg
T3	A1B3C3D3	1752	0.4	2.5	4h30deg, 24h75deg
T4	A2B1C2D3	1800	0.3	2	4h30deg, 24h75deg
T5	A2B2C3D1	1800	0.35	2.5	24h60deg
T6	A2B3C1D2	1800	0.4	1.5	10h85deg
T7	A3B1C3D2	1848	0.3	2.5	10h85deg
T8	A3B2C1D3	1848	0.35	1.5	4h30deg, 24h75deg
T9	A3B3C2D1	1848	0.4	2	24h60deg

Chemical compounds of Fly ash

SiO_2	50.5
Al_2O_3	26.57
Na_2O	0.45

Chemical composition of sodium silicate

SiO_2	29.4
Na_2O	14.7
H_2O	55.9

% of NaOH flakes in various molarity

NaOH solutio	Flakes	H_2O
8M	26.23	
10M	31.37	
12M	36.09	63.91
14M	40.43	59.57

Molecular weight of some oxides

SiO_2	60.09
Al_2O_3	101.96
Na_2O	61.98
H_2O	18
NaOH	39.99

Mix	NaOH	Fly ash			Sodium silicate			NaOH solution			Added water	Total moles per m^3				Molar ratio						
								Flakes														
		SiO_2	Al_2O_3	Na_2O	SiO_2	Na_2O	H_2O	Na_2O	H_2O	H_2O	H_2O	Na_2O	SiO_2	Al_2O_3	H_2O	Na_2O/SiO_2	SiO_2/Al_2O_3	H_2O/Na_2O	Na_2O/Al_2O_3	SS/Na	SiO_2/Na_2O	water/fly ash
1	14M	4189.10	1298.95	36.19	438.98	212.80	2786.40	302.37	302.37	1979.56	1547.96	551.36	4628.09	1298.95	6616.29	0.119	3.563	12.00	0.424	1.5	0.852	0.239
2	14M	4033.95	1250.84	34.85	547.98	265.63	3478.22	283.08	283.08	1853.29	1388.19	583.56	4581.93	1250.84	7002.78	0.127	3.663	12.00	0.467	2.0	0.999	0.263
3	14M	3889.88	1206.17	33.61	647.03	313.65	4106.94	267.40	267.40	1750.63	1250.89	614.65	4536.91	1206.17	7375.86	0.135	3.761	12.00	0.510	2.5	1.114	0.287
4	14M	3878.80	1202.73	33.51	451.63	218.93	2866.67	233.31	233.31	1527.44	1046.11	485.75	4330.43	1202.73	5673.53	0.112	3.600	11.68	0.404	2.0	0.999	0.221
5	14M	3735.14	1158.19	32.27	543.63	263.53	3450.62	224.67	224.67	1470.86	1099.39	520.46	4278.77	1158.19	6245.54	0.122	3.694	12.00	0.449	2.5	1.114	0.253
6	14M	3601.74	1116.82	31.12	503.25	243.95	3194.29	346.63	346.63	2269.33	1650.09	621.70	4104.99	1116.82	7460.34	0.151	3.676	12.00	0.557	1.5	0.852	0.313
7	14M	3568.49	1106.52	30.83	445.18	215.80	2825.71	183.98	183.98	1204.49	996.20	430.61	4013.67	1106.52	5210.39	0.107	3.627	12.10	0.389	2.5	1.114	0.221
8	14M	3436.33	1065.53	29.69	420.12	203.65	2666.64	289.37	289.37	1894.47	1422.05	522.71	3856.44	1065.53	6272.53	0.136	3.619	12.00	0.491	1.5	0.852	0.276
9	14M	3313.60	1027.48	28.63	514.43	249.37	3265.27	265.75	265.75	1739.82	1254.12	543.75	3828.03	1027.48	6524.96	0.142	3.726	12.00	0.529	2.0	0.999	0.298
10	14M	4189.10	1298.95	36.19	522.60	253.33	3317.14	215.98	215.98	1413.97	1048.14	505.50	4711.70	1298.95	5995.22	0.107	3.627	11.86	0.389	2.5	1.114	0.216

APPENDIX C - COARSE AGGREGATE PARTICLE SIZE DISTRIBUTION BY SIEVE ANALYSIS

Appendix C-1 20mm Coarse Aggregate

Sample weight (g): 1030.60

Sieve size (mm)	Mass Retained (g)	Mass retained (%)	Cumulative retained (%)	Cumulative passing (%)
26.5	0	0	0	100
19	160.12	16	16	84.46
13.2	729.1	71	86	13.71
9.5	135.06	13.11	99	0.60
6.7	4.84	0.47	100	0.13
4.75	0	0.00	100	0.13
2.36	0.25	0.02	100	0.11
1.18	0.04	0.00	100	0.11
0.6	0	0.00	100	0.11
0.425	0	0.00	100	0.11
0.3	0	0.00	100	0.11
0.15	0	0.00	100	0.11
0.075	0	0.00	100	0.11
pan	1.1	0.11	100	0
Total	1030.51	100.00	1200.20	

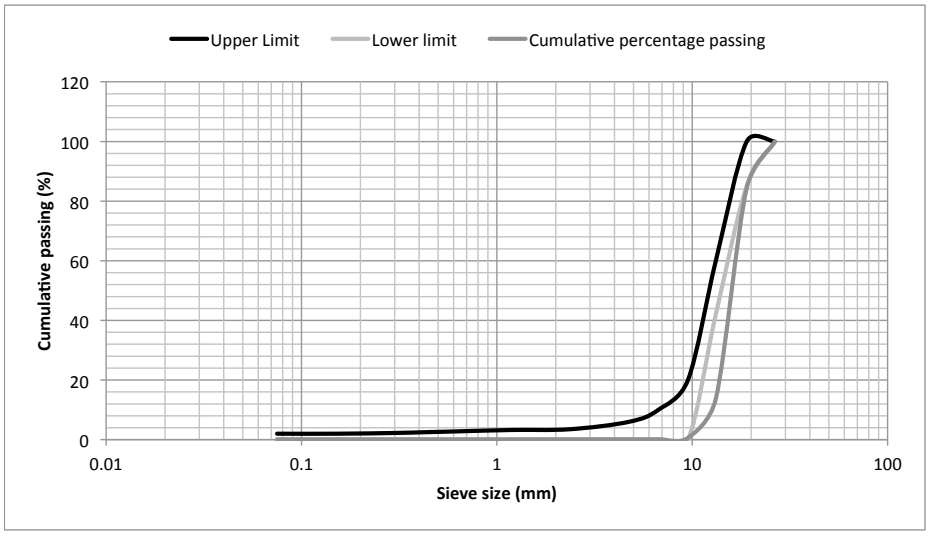

APPENDIX C - COARSE AGGREGATE PARTICLE SIZE DISTRIBUTION BY SIEVE ANALYSIS

Appendix C-2 14mm Coarse Aggregate

Sample weight (g): 550.29

Sieve size (mm)	Mass Retained (g)	Mass retained (%)	Cumulative retained (%)	Cumulative passing (%)
26.5	0	0	0	100
19	0	0	0	100.00
13.2	108.02	20	20	80.10
9.5	411.55	75.83	96	4.27
6.7	21.34	3.93	100	0.34
4.75	0.52	0.10	100	0.25
2.36	0.23	0.04	100	0.20
1.18	0.06	0.01	100	0.19
0.6	0.06	0.01	100	0.18
0.425	0	0.00	100	0.18
0.3	0	0.00	100	0.18
0.15	0	0.00	100	0.18
0.075	0.08	0.01	100	0.17
pan	0.9	0.17	100	0
Total	542.76	100.00	1113.76	

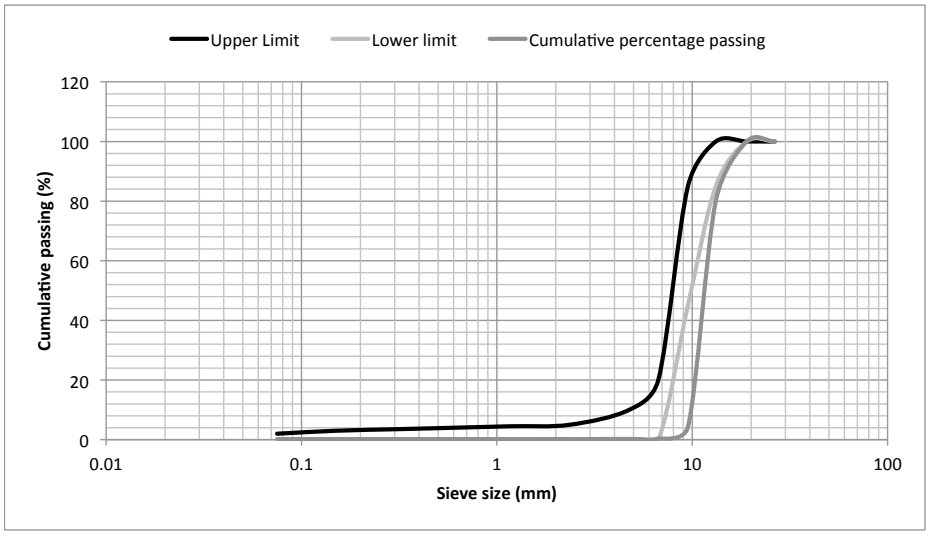

APPENDIX C - COARSE AGGREGATE PARTICLE SIZE DISTRIBUTION BY SIEVE ANALYSIS

Appendix C-3 10mm Coarse Aggregate

Sample weight (g): 533.06

Sieve size (mm)	Mass Retained (g)	Mass retained (%)	Cumulative retained (%)	Cumulative passing (%)
26.5	0	0	0	100
19	0	0	0	100
13.2	0	0	0	100
9.5	92.49	17.36	17	82.64
6.7	309.82	58.14	75	24.50
4.75	104.62	19.63	95	4.87
2.36	22.28	4.18	99	0.69
1.18	2.02	0.38	100	0.31
0.6	0.04	0.01	100	0.30
0.425	0.02	0.00	100	0.30
0.3	0.02	0.00	100	0.29
0.15	0.1	0.02	100	0.28
0.075	0.45	0.08	100	0.19
pan	1.02	0.19	100	0
Total	532.88	100.00	985.62	

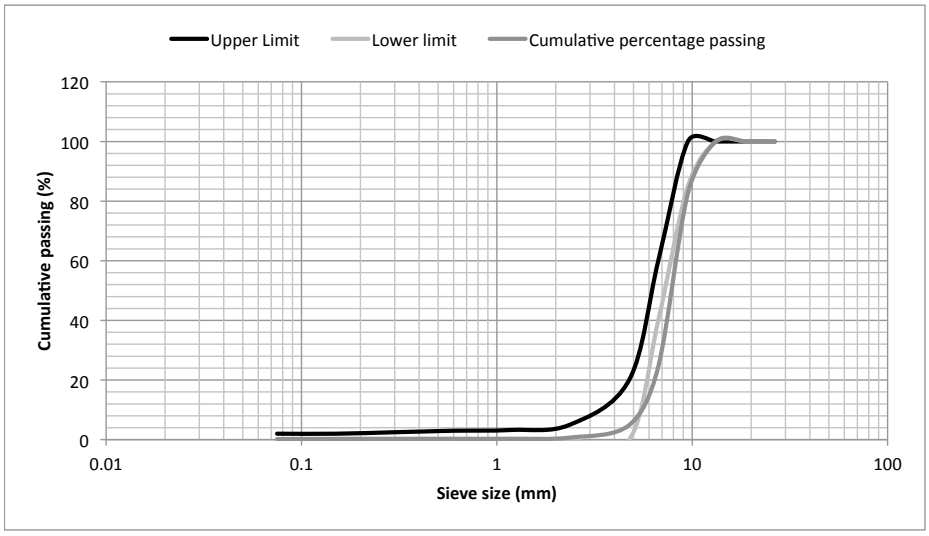

APPENDIX C - COARSE AGGREGATE PARTICLE SIZE DISTRIBUTION BY SIEVE ANALYSIS

Appendix C-4 7mm Coarse Aggregate

Sample weight (g): 674.99

Sieve size (mm)	Mass Retained (g)	Mass retained (%)	Cumulative retained (%)	Cumulative passing (%)
26.5	0	0	0	100
19	0	0	0	100
13.2	0	0	0	100
9.5	0	0.00	0	100.00
6.7	40.43	5.99	6	94.01
4.75	321.52	47.65	54	46.36
2.36	296.19	43.90	98	2.46
1.18	11.53	1.71	99	0.75
0.6	2.34	0.35	100	0.40
0.425	0.45	0.07	100	0.34
0.3	0.23	0.03	100	0.30
0.15	0.36	0.05	100	0.25
0.075	0.5	0.07	100	0.17
pan	1.18	0.17	100	0
Total	674.73	100.00	854.96	

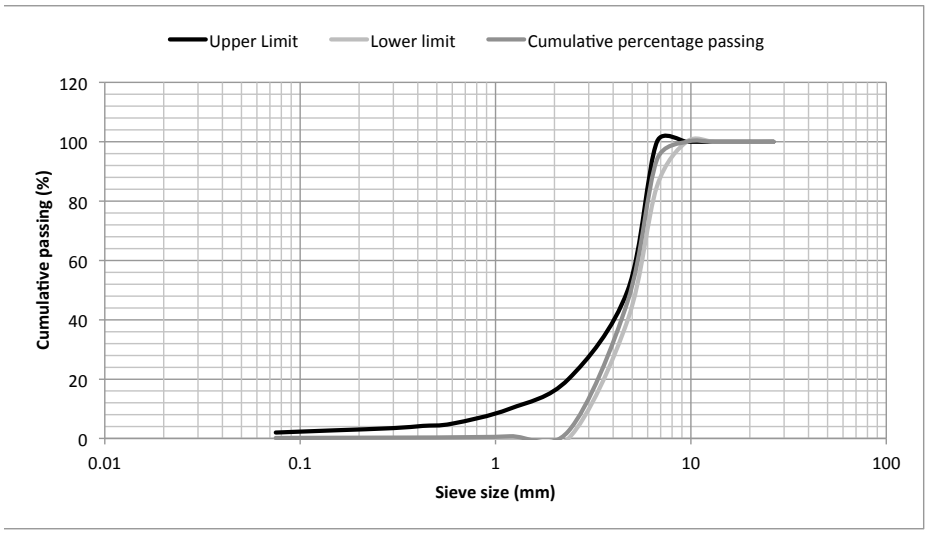

APPENDIX C - FINE AGGREGATE PARTICLE SIZE DISTRIBUTION BY SIEVE ANALYSIS

Appendix C-5 Fine Aggregate

Sample weight (g): 352.13

Sieve size (mm)	Mass Retained (g)	Mass retained (%)	Cumulative retained (%)	Cumulative passing (%)
26.5	0	0	0	100
19	0	0	0	100
13.2	0	0	0	100
9.5	0	0.00	0	100.00
6.7	0	0.00	0	100.00
4.75	0	0.00	0	100.00
2.36	0	0.00	0	100.00
1.18	0.24	0.07	0	99.93
0.6	69.2	19.69	20	80.24
0.425	115.66	32.91	53	47.34
0.3	96.48	27.45	80	19.89
0.15	64.52	18.36	98	1.53
0.075	4.98	1.42	100	0.12
pan	0.41	0.12	100	0
Total	351.49	100.00	450.95	

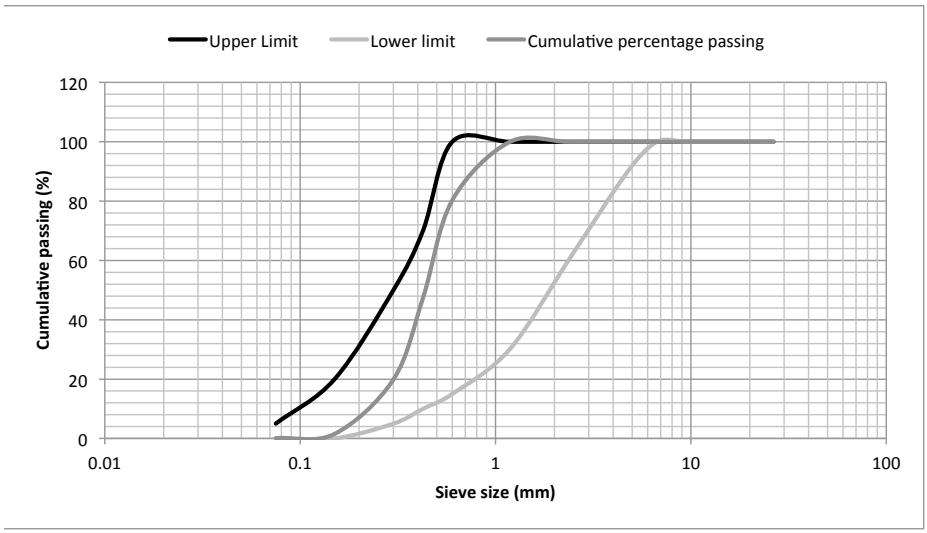

APPENDIX D - MECHANICAL PROPERTIES, WATER ABSORPTION, SORPTIVITY, DRYING SHRINKAGE OF THE OPTIMUM MIXTURES

Appendix D-1 Compressive strength

Mixture	Age (days)	Sample	Diameter (mm)	Height (mm)	Weight (g)	Density (kg/m^3)	Load (kN)	Compressive Strength (MPa)	Average (MPa)	SD	SQRT	ERROR BAR
OPC	7	1	99.97	200.73	3770.60	2408.98	412.10	52.53	51.23	4.94	1.73	2.85
		2	100.18	200.46	3789.90	2428.22	360.60	45.77				
		3	99.29	197.76	3686.60	2289.00	428.70	55.40				
	28	1	100.02	199.44	3696.60	2348.87	445.10	56.68	56.22	1.63	1.73	0.94
		2	99.41	196.62	3697.70	2288.18	446.60	57.57				
		3	99.74	197.43	3667.00	2293.68	424.90	54.41				
	91	1	99.97	199.00	3696.70	2341.41	493.20	62.87	59.86	4.88	1.73	2.82
		2	99.89	200.00	3697.40	2349.85	489.40	62.48				
		3	100.10	198.74	3679.50	2333.53	426.50	54.22				
	365	1	100.00	198.99	3717.80	2356.07	550.40	70.11	66.78	4.09	1.73	2.36
		2	99.22	200.10	3694.80	2317.96	480.80	62.22				
		3	98.32	197.26	3661.10	2223.33	516.20	68.02				
T7	7	1	99.60	200.20	3776.70	2388.72	430.90	55.33	54.04	1.83	1.41	1.29
		2	99.75	200.12	3780.20	2397.18	412.00	52.75				
		3	N/A					N/A				
	28	1	99.73	200.47	3723.70	2364.54	452.50	57.96	56.49	1.28	1.73	0.74
		2	99.74	200.36	3718.00	2360.10	436.80	55.93				
		3	99.75	202.52	3761.70	2414.06	434.10	55.58				
	91	1	99.70	201.50	3657.30	2332.90	444.31	56.94	56.51	0.78	1.73	0.45
		2	99.80	201.50	3729.00	2383.41	445.50	56.98				
		3	99.60	202.00	3717.60	2372.48	433.10	55.62				
	365	1	99.74	201.20	3676.80	2343.73	483.30	61.89	61.48	2.04	1.73	1.18
		2	100.10	200.50	3682.30	2355.98	497.70	63.27				
		3	99.62	200.10	3738.70	2364.46	461.70	59.26				
T4	7	1	99.66	200.44	3733.30	2366.95	423.10	54.27	55.27	1.42	1.41	1.01
		2	99.83	200.78	3738.20	2382.18	440.30	56.28				
		3	N/A					N/A				
	28	1	100.07	201.91	3715.61	2392.58	417.40	53.10	56.24	4.45	1.41	3.14
		2	99.84	201.63	3715.57	2378.26	464.70	59.39				
		3	N/A					N/A				
	91	1	99.49	201.63	3695.54	2348.89	435.70	56.07	58.85	3.48	1.73	2.01
		2	99.86	201.13	3684.88	2353.71	491.20	62.75				
		3	99.26	201.14	3657.89	2308.60	446.40	57.72				
	365	1	100.02	201.03	3649.30	2337.30	446.10	56.81	55.60	1.71	1.41	1.21
		2	99.97	201.90	3703.30	2379.77	426.70	54.39				
		3	N/A									
T10	7	1	99.69	199.68	3621.19	2288.54	471.50	60.44	59.08	1.92	1.41	1.36
		2	99.54	200.36	3639.47	2300.99	449.00	57.73				
		3	N/A					N/A				
	28	1	99.91	200.95	3615.47	2309.62	428.40	54.67	60.20	5.40	1.73	3.12
		2	99.88	200.68	3613.56	2303.92	512.60	65.46				
		3	99.42	200.16	3575.12	2252.61	469.10	60.46				
	91	1	99.96	201.00	3613.53	2311.27	460.20	58.67	63.29	5.62	1.73	3.24
		2	99.83	202.61	3598.79	2314.25	544.10	69.55				
		3	99.82	201.52	3681.78	2354.41	482.30	61.66				
	365	1	99.95	200.36	3630.10	2314.01	538.70	68.69	69.82	4.72	1.73	2.72
		2	99.20	200.68	3608.30	2269.34	579.30	74.99				
		3	99.56	200.90	3595.90	2280.49	511.70	65.76				

APPENDIX D - MECHANICAL PROPERTIES, WATER ABSORPTION, SORPTIVITY, DRYING SHRINKAGE OF THE OPTIMUM MIXTURES

Appendix D-2 Tensile strength

Mixture	Age (days)	Sample	Load (kN)	Tensile Strength (MPa)	Average (MPa)	SD	SQRT	ERROR BAR
OPC	28	1	280.60	3.97	3.97	0.49	1.73	0.28
		2	246.00	3.48				
		3	314.90	4.46				
	91	1	289.00	4.09	4.12	0.18	1.73	0.11
		2	305.40	4.32				
		3	279.6	3.96				
	365	1	288.7	4.09	4.24	0.13	1.73	0.08
		2	305.60	4.33				
		3	304.3	4.31				
T7	28	1	294.1	4.16	4.13	0.07	1.73	0.04
		2	295.5	4.18				
		3	286.4	4.05				
	91	1	298.5	4.23	4.18	0.34	1.73	0.20
		2	317.9	4.50				
		3	270.1	3.82				
	365	1	356.1	5.04	5.08	0.29	1.73	0.17
		2	339.2	4.80				
		3	380.6	5.39				
T4	28	1	285.70	4.04	3.96	0.16	1.73	0.09
		2	266.70	3.77				
		3	287.00	4.06				
	91	1	294.50	4.17	4.10	0.19	1.73	0.11
		2	299.80	4.24				
		3	274.40	3.88				
	365	1	297.70	4.21	4.38	0.15	1.73	0.09
		2	310.40	4.39				
		3	319.40	4.52				
T10	28	1	277.60	3.93	4.29	0.32	1.73	0.19
		2	321.40	4.55				
		3	311.20	4.40				
	91	1	357.20	5.06	4.79	0.33	1.73	0.19
		2	311.80	4.41				
		3	345.90	4.90				
	365	1	364.7	5.16	5.02	0.18	1.73	0.10
		2	340.5	4.82				
		3	358.7	5.08				

APPENDIX D - MECHANICAL PROPERTIES, WATER ABSORPTION, SORPTIVITY, DRYING SHRINKAGE OF THE OPTIMUM MIXTURES

Appendix D-3 Flexural strength

Mixture	Age (days)	Sample	Load (kN)	Flexural Strength (MPa)	Average (MPa)	SD	SQRT	ERROR BAR
OPC	28	1	15.92	6.37	7.02	0.74	1.73	0.43
		2	19.55	7.82				
		3	17.19	6.88				
	91	1	21.06	8.42	7.33	0.96	1.73	0.55
		2	17.23	6.89				
		3	16.67	6.67				
	365	1	17.85	7.14	8.37	1.15	1.73	0.66
		2	21.35	8.54				
		3	23.55	9.42				
T7	28	1	17.28	6.91	7.39	0.63	1.73	0.36
		2	17.87	7.15				
		3	20.26	8.10				
	91	1	23.72	9.49	9.21	0.43	1.73	0.25
		2	21.78	8.71				
		3	23.55	9.42				
	365	1	20.90	8.36	8.27	0.21	1.73	0.12
		2	21.05	8.42				
		3	20.06	8.02				
T4	28	1	23.18	9.27	8.99	0.30	1.73	0.17
		2	22.57	9.03				
		3	21.70	8.68				
	91	1	23.40	9.36	9.36	0.44	1.73	0.25
		2	24.50	9.80				
		3	22.31	8.92				
	365	1	22.69	9.08	9.18	0.29	1.73	0.17
		2	23.77	9.51				
		3	22.36	8.94				
T10	28	1	22.57	9.03	8.38	0.58	1.73	0.34
		2	20.51	8.20				
		3	19.75	7.90				
	91	1	25.04	10.02	9.85	0.53	1.73	0.30
		2	23.14	9.26				
		3	25.66	10.26				
	365	1	24.01	9.60	9.91	0.59	1.73	0.34
		2	26.47	10.59				
		3	23.85	9.54				

APPENDIX D - MECHANICAL PROPERTIES, WATER ABSORPTION, SORPTIVITY, DRYING SHRINKAGE OF THE OPTIMUM MIXTURES

Appendix D-4 Young's Modulus of Elasticity & Poisson's Ratio

Mixture	Age (days)	Sample	YM (GPa)	Average (GPa)	SD	SQRT	ERROR BAR	Poisson's Ratio	Average (GPa)	SD	SQRT	ERROR BAR
OPC	28	1	34.0389	34.16	0.54	1.73	0.31	0.1124	0.139	0.02	1.73	0.01
		2	34.7518					0.1516				
		3	33.6970					0.1519				
	91	1	39.3219	37.64	2.34	1.73	1.35	0.2045	0.152	0.05	1.73	0.03
		2	34.9681					0.1304				
		3	38.6364					0.1208				
	365	1	42.8539	38.33	4.14	1.73	2.39	0.2202	0.187	0.04	1.73	0.02
		2	37.4213					0.1472				
		3	34.7289					0.1921				

Mixture	Age (days)	Sample	YM (GPa)	Average (GPa)	SD	SQRT	ERROR BAR	Poisson's Ratio	Average (GPa)	SD	SQRT	ERROR BAR
T7	28	1	27.9492	25.33	2.27	1.73	1.31	0.1506	0.147	0.01	1.73	0.01
		2	23.8329					0.1365				
		3	24.2209					0.1550				
	91	1	22.9532	27.18	3.98	1.73	2.30	0.1486	0.174	0.04	1.73	0.02
		2	30.8486					0.2158				
		3	27.7283					0.1569				
	365	1	28.6358	31.26	3.72	1.73	2.15	0.1445	0.164	0.02	1.73	0.01
		2	29.6299					0.1827				
		3	35.5182					0.1634				

Mixture	Age (days)	Sample	YM (GPa)	Average (GPa)	SD	SQRT	ERROR BAR	Poisson's Ratio	Average (GPa)	SD	SQRT	ERROR BAR
T4	28	1	27.0453	26.95	0.32	1.73	0.18	0.1428	0.134	0.02	1.73	0.01
		2	26.5909					0.1522				
		3	27.2074					0.1059				
	91	1	29.3655	28.03	1.16	1.73	0.67	0.1311	0.150	0.02	1.73	0.01
		2	27.3591					0.1492				
		3	27.3570					0.1693				
	365	1	32.0806	31.23	1.10	1.73	0.64	0.1687	0.158	0.02	1.73	0.01
		2	31.6319					0.1663				
		3	29.9900					0.1402				

Mixture	Age (days)	Sample	YM (GPa)	Average (GPa)	SD	SQRT	ERROR BAR	Poisson's Ratio	Average (GPa)	SD	SQRT	ERROR BAR
T10	28	1	27.1198	29.05	1.74	1.73	1.01	0.1516	0.145	0.03	1.73	0.02
		2	30.5069					0.1149				
		3	29.5379					0.1692				
	91	1	26.6871	26.80	0.22	1.73	0.13	0.1480	0.151	0.01	1.73	0.01
		2	26.6646					0.1669				
		3	27.0598					0.1377				
	365	1	26.7631	26.54	0.22	1.73	0.13	0.1282	0.146	0.02	1.73	0.01
		2	26.3188					0.1462				
		3	26.5482					0.1632				

APPENDIX D - MECHANICAL PROPERTIES, WATER ABSORPTION, SORPTIVITY, DRYING SHRINKAGE OF THE OPTIMUM MIXTURES

Appendix D-5 Water absorption, AVPV, Effective Porosity

Concrete mix: OPC, T7, T4, T10
Age of specimen at commencement of test: 28, 91, 365 days

Method of compaction: manual stroke
Description of specimen (moulded, cut, cored, broken, irregular, etc): regular cut

Specimen dimension:

Slices	Radius (mm)			Height (mm)			Volume (mm^3)	Volume (cm^3)
	1	2	average	1	2	average		
OPC-28D-1	99.22	99.22	99.22	52.89	52.89	52.89	408734.85	408.73
OPC-28D-2	99.43	99.43	99.43	50.36	50.36	50.36	390832.13	390.83
OPC-91D-1	99.67	99.68	99.68	46.14	46.17	46.16	359812.43	359.81
OPC-91D-2	99.71	99.75	99.73	51.39	51.42	51.41	401075.11	401.08
OPC-365D-1	99.05	99.05	99.05	50.00	50.00	50.00	385077.92	385.08
OPC-365D-2	99.05	99.05	99.05	51.30	51.30	51.30	395089.95	395.09

Specimen dimension:

Slices	Radius (mm)			Height (mm)			Volume (mm^3)	Volume (cm^3)
	1	2	average	1	2	average		
T7-28D-1	99.85	99.90	99.88	52.02	52.07	52.05	407132.85	407.13
T7-28D-2	99.55	99.60	99.58	53.23	53.28	53.26	414103.26	414.10
T7-91D-1	99.72	99.74	99.73	51.98	51.90	51.94	405761.16	405.76
T7-91D-2	99.39	99.42	99.41	49.15	52.10	50.63	381134.76	381.13
T7-365D-1	100.02	100.02	100.02	51.90	51.90	51.90	407577.98	407.58
T7-365D-2	99.80	99.80	99.80	52.16	52.16	52.16	407819.81	407.82

Slices	Radius (mm)			Height (mm)			Volume (mm^3)	Volume (cm^3)
	1	2	average	1	2	average		
T4-28D-1	99.71	99.76	99.74	52.11	52.11	52.11	406694.37	406.69
T4-28D-2	99.75	99.75	99.75	48.80	48.80	48.80	381166.99	381.17
T4-91D-1	99.18	98.63	98.91	47.11	47.11	47.11	363773.42	363.77
T4-91D-2	99.53	99.32	99.43	57.30	57.30	57.30	445586.77	445.59
T4-365D-1	99.70	99.65	99.68	50.74	50.82	50.78	395922.73	395.92
T4-365D-2	99.91	99.91	99.91	50.81	50.81	50.81	398140.88	398.14

Slices	Radius (mm)			Height (mm)			Volume (mm^3)	Volume (cm^3)
	1	2	average	1	2	average		
T10-28D-1	99.49	99.48	99.49	49.26	49.26	49.26	382756.81	382.76
T10-28D-2	100.03	100	100.02	50.44	50.44	50.44	396191.61	396.19
T10-91D-1	100.26	100.26	100.26	52.27	52.27	52.27	412455.94	412.46
T10-91D-2	99.86	99.86	99.86	51.27	51.27	51.27	401343.37	401.34
T10-365D-1	99.53	99.53	99.53	53.77	53.77	53.77	418136.14	418.14
T10-365D-2	99.54	99.54	99.54	52.41	52.41	52.41	407642.16	407.64

Slices	M (g)	A (g)	B (g)	Absorption after immersion	C (g)	D (g)	Absorption after boiling (%)	Bulk density, dry (Mg/m^3)	Bulk density after immersion	Bulk density after boiling ($x10^3$ kg/m^3)	Apparent density (Mg/m^3)	Volume of permeable voids (%)	Bulk volume of the sample	Effective porosity (%)
OPC-28D-1	945.40	902.41	947.93	5.04	947.98	557.11	5.05	2.31	2.43	2.43	2.61	11.66	408.73	11.14
OPC-28D-2	982.95	937.20	985.36	5.14	985.40	576.55	5.14	2.29	2.41	2.41	2.60	11.79	390.83	12.32
Average				5.09			5.10					11.72		11.73
OPC-91D-1	840.36	801.44	841.47	4.99	841.93	494.03	5.05	2.30	2.42	2.42	2.61	11.64	359.81	11.13
OPC-91D-2	959.20	912.34	960.51	5.28	961.45	560.97	5.38	2.28	2.40	2.40	2.60	12.26	401.08	12.01
Average				5.14			5.22					11.95		11.57
OPC-365D-1	931.70	898.76	940.03	4.59	941.36	551.70	4.74	2.31	2.41	2.42	2.59	10.93	385.08	10.72
OPC-365D-2	950.24	916.60	958.42	4.56	959.76	562.68	4.71	2.31	2.41	2.42	2.59	10.87	395.09	10.58
Average				4.98								11.60		10.65

T7-28D-1	935.10	916.05	951.97	3.92	952.34	557.20	3.96	2.32	2.41	2.41	2.55	9.18	407.13	8.82
T7-28D-2	990.20	973.70	1009.31	3.66	1010.51	595.76	3.78	2.35	2.43	2.44	2.58	8.88	414.10	8.60
Average				3.79			3.87					9.03		8.71
T7-91D-1	971.54	953.96	986.35	3.40	987.75	579.87	3.54	2.34	2.42	2.42	2.55	8.28	405.76	7.98
T7-91D-2	959.20	942.46	975.41	3.50	977.34	574.09	3.70	2.34	2.42	2.42	2.56	8.65	381.13	8.65
Average				3.45			3.62					8.47		8.31
T7-365D-1	932.97	920.93	952.93	3.47	954.76	557.05	3.67	2.32	2.40	2.40	2.53	8.51	407.58	7.85
T7-365D-2	961.05	948.65	982.40	3.56	983.88	575.58	3.71	2.32	2.41	2.41	2.54	8.63	407.82	8.28
Average				3.59								8.70		8.06

Slices	M (g)	A (g)	B (g)	Absorption after immersion	C (g)	D (g)	Absorption after boiling (%)	Bulk density, dry (Mg/m^3)	Bulk density after immersion	Bulk density after boiling (Mg/m^3)	Apparent density (Mg/m^3)	Volume of permeable voids (%)	Bulk volume of the sample	Effective porosity (%)
T4-28D-1	1044.14	1022.60	1059.14	3.57	1060.00	615.20	3.66	2.30	2.38	2.38	2.51	8.41	406.69	8.98
T4-28D-2	958.68	939.84	971.06	3.32	971.90	565.72	3.41	2.31	2.39	2.39	2.51	7.89	381.17	8.19
Average				3.45			3.53					8.15		8.59
T4-91D-1	848.22	837.93	870.19	3.85	872.63	506.35	4.14	2.29	2.38	2.38	2.53	9.47	363.77	8.87
T4-91D-2	879.10	868.64	900.61	3.68	902.50	524.20	3.90	2.30	2.38	2.39	2.52	8.95	445.59	7.17
Average				3.77			4.02					9.21		8.02
T4-365D-1	928.10	916.25	948.20	3.49	950.28	553.78	3.71	2.31	2.39	2.40	2.53	8.58	395.92	8.07
T4-365D-2		853.24	879.09	3.03	874.03	512.75	2.44	2.36	2.43	2.42	2.51	5.75	398.14	6.49
Average				3.52			3.08					8.30		7.28

T10-28D-1	879.22	859.67	897.99	4.46	903.33	520.15	5.08	2.24	2.34	2.36	2.53	11.39	382.76	10.01
T10-28D-2	915.93	898.38	936.07	4.20	939.39	544.45	4.56	2.27	2.37	2.38	2.54	10.38	396.19	9.51
Average				4.33			4.82					10.89		9.76
T10-91D-1	947.57	933.76	967.49	3.61	970.82	563.61	3.97	2.29	2.38	2.38	2.52	9.10	412.46	8.18
T10-91D-2	914.88	901.14	935.88	3.86	938.21	543.20	4.11	2.28	2.37	2.38	2.52	9.38	401.34	8.66
Average				3.73			4.04					9.24		8.42
T10-365D-1	970.75	955.34	993.22	3.97	995.26	579.35	4.18	2.30	2.39	2.39	2.54	9.60	418.14	9.06
T10-365D-2	937.95	924.73	960.86	3.91	963.17	557.26	4.16	2.28	2.37	2.37	2.52	9.47	407.64	8.86
Average				4.01			4.17					9.93		8.96

APPENDIX D - MECHANICAL PROPERTIES, WATER ABSORPTION, SORPTIVITY, DRYING SHRINKAGE OF THE OPTIMUM MIXTURES

Appendix D-6 Sorptivity OPC

Concrete mixture: OPC					Sample age: 28 days
Standard: GHD Method					Conditioning: N/A
Sample conditioning: Oven dried					
Diameter (mm):	A:	100.08	B:	99.85	Curing history: wet cured 28 days, air cured
Thickness (mm):	A:	107.95	B:	109.32	Type of compaction: Manual stroke
Water/room temperature: 18deg/23deg					

t	$m^{1/2}$	mass (g)		Dmass (g)		Area (mm^2)		I (mm)	
		A	B	A	B	A	B	A	B
0	0	1945.14	1971.6	0.00	0.00	7862.57	7826.47	0.0000	0.0000
60s	0.71	1946.95	1973.79	1.81	2.19	7862.57	7826.47	0.2302	0.2798
5min	2.24	1949.13	1976.05	3.99	4.45	7862.57	7826.47	0.5075	0.5686
10min	3.16	1950.23	1977.21	5.09	5.61	7862.57	7826.47	0.6474	0.7168
20min	4.47	1952.43	1979.58	7.29	7.98	7862.57	7826.47	0.9272	1.0196
30min	5.48	1953.47	1980.81	8.33	9.21	7862.57	7826.47	1.0595	1.1768
60min	7.75	1956.70	1984.54	11.56	12.94	7862.57	7826.47	1.4703	1.6534
2h	10.95	1961.94	1990.47	16.80	18.87	7862.57	7826.47	2.1367	2.4110
3h	13.42	1964.22	1993.2	19.08	21.60	7862.57	7826.47	2.4267	2.7599
4h	15.49	1966.92	1996.11	21.78	24.51	7862.57	7826.47	2.7701	3.1317

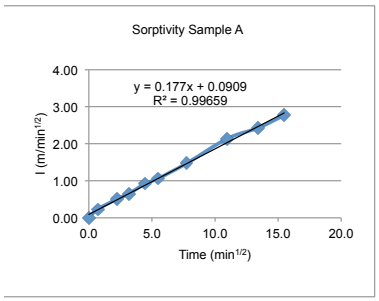

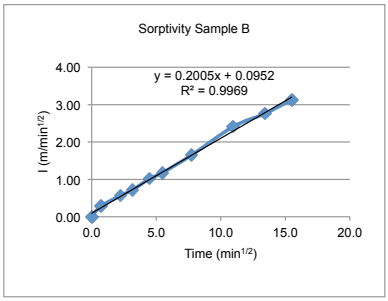

Result	S ($mm/min^{1/2}$)	R^2
Sample A	0.177	0.9966
Sample B	0.2005	0.9969
average	0.1888	0.9968

SORPTIVITY (MIX OPC)

Concrete mixture: T7					Sample age: 91 days
Standard: GHD Method					Conditioning: N/A
Sample conditioning: Oven dried					
Diameter (mm):	A:	99.75	B:	99.91	Curing history: wet cured 28 days, air cured
Thickness (mm):	A:	110.88	B:	109.65	Type of compaction: Manual stroke
Water/room temperature: 18deg/23deg					

t	$m^{1/2}$	mass (g)		Dmass (g)		Area (mm^2)		I (mm)	
		A	B	A	B	A	B	A	B
0	0	1995.71	1995.06	0.00	0.00	7810.80	7835.88	0.0000	0.0000
60s	0.71	1998.30	1997.63	2.59	2.57	7810.80	7835.88	0.3316	0.3280
5min	2.24	2000.33	1999.46	4.62	4.40	7810.80	7835.88	0.5915	0.5615
10min	3.16	2001.98	2001.11	6.27	6.05	7810.80	7835.88	0.8027	0.7721
20min	4.47	2004.09	2003.21	8.38	8.15	7810.80	7835.88	1.0729	1.0401
30min	5.48	2005.73	2004.83	10.02	9.77	7810.80	7835.88	1.2828	1.2468
60min	7.75	2011.32	2010.59	15.61	15.53	7810.80	7835.88	1.9985	1.9819
2h	10.95	2013.72	2014.38	18.01	19.32	7810.80	7835.88	2.3058	2.4656
3h	13.42	2017.56	2017.06	21.85	22.00	7810.80	7835.88	2.7974	2.8076
4h	15.49	2020.63	2020.19	24.92	25.13	7810.80	7835.88	3.1905	3.2070

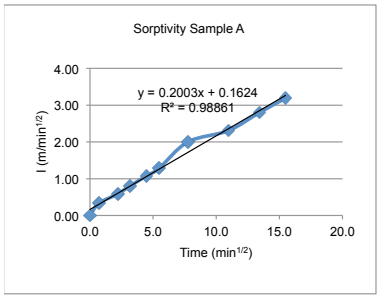

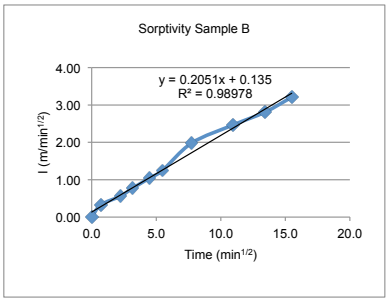

Result	S ($mm/min^{1/2}$)	R^2
Sample A	0.2003	0.9886
Sample B	0.2051	0.9898
average	0.2027	0.9892

SORPTIVITY (MIX OPC)

Concrete mixture: OPC					Sample age: 365 days	
Standard: GHD Method					Conditioning:	N/A
Sample conditioning: Oven dried						
Diameter (mm):	A:	99.05	B:	99.05	Curing history: wet cured 28 days, air cured	
Thickness (mm):	A:	110.11	B:	110.08	Type of compaction: Manual stroke	
Water/room temperature: 18deg/23deg						

t	$m^{1/2}$	mass (g)		Dmass (g)		Area (mm^2)		I (mm)	
		A	B	A	B	A	B	A	B
0	0	2031.93	1988.34	0.00	0.00	7701.56	7701.56	0.0000	0.0000
60s	0.71	2036.11	1992.71	4.18	4.37	7701.56	7701.56	0.5427	0.5674
5min	2.24	2037.33	1993.77	5.40	5.43	7701.56	7701.56	0.7012	0.7051
10min	3.16	2038.61	1995.04	6.68	6.70	7701.56	7701.56	0.8674	0.8700
20min	4.47	2040.52	1996.95	8.59	8.61	7701.56	7701.56	1.1154	1.1180
30min	5.48	2042.50	1998.8	10.57	10.46	7701.56	7701.56	1.3724	1.3582
60min	7.75	2045.59	2002.00	13.66	13.66	7701.56	7701.56	1.7737	1.7737
2h	10.95	2051.77	2008.81	19.84	20.47	7701.56	7701.56	2.5761	2.6579
3h	13.42	2054.08	2011.17	22.15	22.83	7701.56	7701.56	2.8760	2.9643
4h	15.49	2056.93	2014.1	25.00	25.76	7701.56	7701.56	3.2461	3.3448

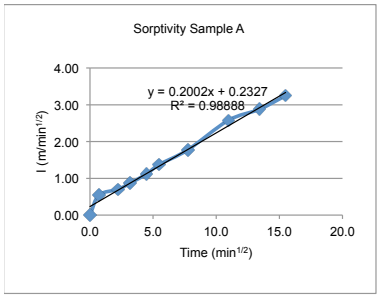

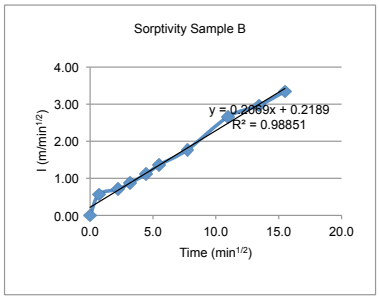

Result	S ($mm/min^{1/2}$)	R^2
Sample A	0.2002	0.9889
Sample B	0.2069	0.9885
average	0.2036	0.9887

S = coefficient of sorptivity

w/c ratio 0.4 ----- 0.09mm/$min^{1/2}$	**Neville**
w/c ratio 0.6 ----- 0.17mm/$min^{1/2}$	**Neville**
w/c ratio 0.46-0.53 ------ 0.14-0.17 mm/$min^{1/2}$	**GHD**
w/c ratio 0.4-0.5 0.094-0.12 mm/$min^{1/2}$	**Hall**

APPENDIX D - MECHANICAL PROPERTIES, WATER ABSORPTION, SORPTIVITY, DRYING SHRINKAGE OF THE OPTIMUM MIXTURES

Appendix D-7 Sorptivity T4

Concrete mixture: T4					Sample age: 28 days
Standard: GHD Method					Conditioning: N/A
Sample conditioning: Oven dried					
Diameter (mm):	A:	99.74	B:	99.75	Curing history: steam curing 24h 75deg C
Thickness (mm):	A:	118.97	B:	112.84	Type of compaction: Manual stroke
Water/room temperature: 18deg/23deg					

t	$m^{1/2}$	mass (g)		Dmass (g)		Area (mm^2)		I (mm)	
		A	B	A	B	A	B	A	B
0	0	2174.42	2051.02	0.00	0.00	7809.23	7810.80	0.0000	0.0000
60s	0.71	2175.61	2052.46	1.19	1.44	7809.23	7810.80	0.1524	0.1844
5min	2.24	2176.26	2053.17	1.84	2.15	7809.23	7810.80	0.2356	0.2753
10min	3.16	2176.79	2053.92	2.37	2.90	7809.23	7810.80	0.3035	0.3713
20min	4.47	2177.53	2054.77	3.11	3.75	7809.23	7810.80	0.3982	0.4801
30min	5.48	2178.14	2055.52	3.72	4.50	7809.23	7810.80	0.4764	0.5761
60min	7.75	2179.43	2057.10	5.01	6.08	7809.23	7810.80	0.6415	0.7784
2h	10.95	2181.38	2059.13	6.96	8.11	7809.23	7810.80	0.8913	1.0383
3h	13.42	2182.89	2060.68	8.47	9.66	7809.23	7810.80	1.0846	1.2367
4h	15.49	2184.05	2061.85	9.63	10.83	7809.23	7810.80	1.2332	1.3865

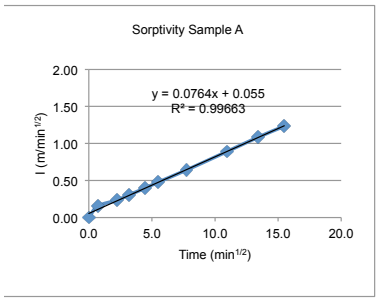

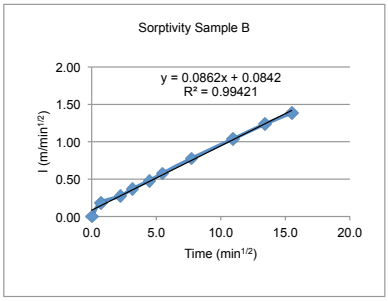

Result	S ($mm/min^{1/2}$)	R^2
Sample A	0.0764	0.9966
Sample B	0.0862	0.9942
average	0.0813	0.9954

SORPTIVITY (MIX T4)

Concrete mixture: T4					Sample age: 91 days
Standard: GHD Method					Conditioning: N/A
Sample conditioning: Oven dried					
Diameter (mm):	A:	98.91	B:	99.43	Curing history: steam curing 24h 75deg C
Thickness (mm):	A:	109.32	B:	112.41	Type of compaction: Manual stroke
Water/room temperature: 18deg/23deg					

t	$m^{1/2}$	mass (g)		Dmass (g)		Area (mm^2)		I (mm)	
		A	B	A	B	A	B	A	B
0	0	1918.64	2006.89	0.00	0.00	7679.80	7760.77	0.0000	0.0000
60s	0.71	1920.01	2008.60	1.37	1.71	7679.80	7760.77	0.1784	0.2203
5min	2.24	1920.99	2009.48	2.35	2.59	7679.80	7760.77	0.3060	0.3337
10min	3.16	1921.79	2010.26	3.15	3.37	7679.80	7760.77	0.4102	0.4342
20min	4.47	1922.81	2011.29	4.17	4.40	7679.80	7760.77	0.5430	0.5670
30min	5.48	1923.68	2012.00	5.04	5.11	7679.80	7760.77	0.6563	0.6584
60min	7.75	1925.44	2013.69	6.80	6.80	7679.80	7760.77	0.8854	0.8762
2h	10.95	1928.13	2016.08	9.49	9.19	7679.80	7760.77	1.2357	1.1842
3h	13.42	1930.22	2017.84	11.58	10.95	7679.80	7760.77	1.5079	1.4109
4h	15.49	1931.86	2019.31	13.22	12.42	7679.80	7760.77	1.7214	1.6004

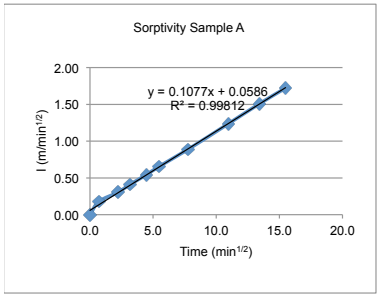

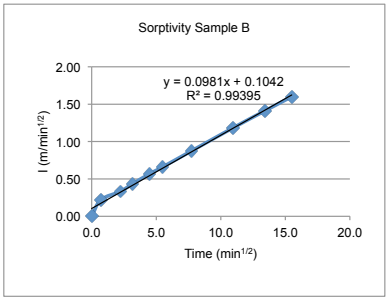

Result	S ($mm/min^{1/2}$)	R^2
Sample A	0.1077	0.9981
Sample B	0.0981	0.9940
average	0.1029	0.9961

SORPTIVITY (MIX T4)

Concrete mixture: T4					Sample age: 365 days
Standard: GHD Method					Conditioning: N/A
Sample conditioning: Oven dried					
Diameter (mm):	A:	100.45	B:	99.37	Curing history: steam curing 24h 75deg C
Thickness (mm):	A:	111.43	B:	111.89	Type of compaction: Manual stroke
Water/room temperature: 18deg/23deg					

t	$m^{1/2}$	mass (g)		Dmass (g)		Area (mm^2)		I (mm)	
		A	B	A	B	A	B	A	B
0	0	2020.72	2027.55	0.00	0.00	7920.81	7751.40	0.0000	0.0000
60s	0.71	2023.58	2028.95	2.86	1.40	7920.81	7751.40	0.3611	0.1806
5min	2.24	2024.34	2030.45	3.62	2.90	7920.81	7751.40	0.4570	0.3741
10min	3.16	2025.18	2031.26	4.46	3.71	7920.81	7751.40	0.5631	0.4786
20min	4.47	2026.14	2032.14	5.42	4.59	7920.81	7751.40	0.6843	0.5922
30min	5.48	2026.77	2033.04	6.05	5.49	7920.81	7751.40	0.7638	0.7083
60min	7.75	2028.44	2035.26	7.72	7.71	7920.81	7751.40	0.9746	0.9947
2h	10.95	2031.73	2037.61	11.01	10.06	7920.81	7751.40	1.3900	1.2978
3h	13.42	2033.81	2039.81	13.09	12.26	7920.81	7751.40	1.6526	1.5816
4h	15.49	2034.43	2041.9	13.71	14.35	7920.81	7751.40	1.7309	1.8513

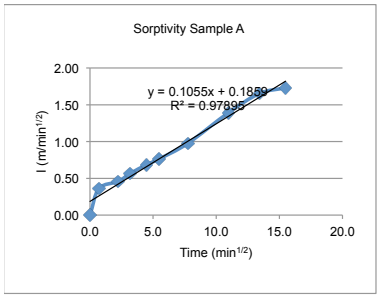

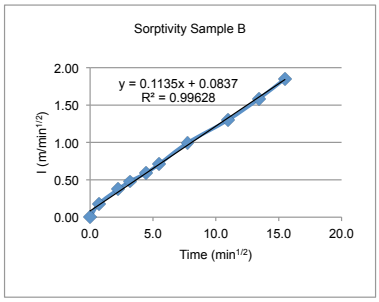

Result	S ($mm/min^{1/2}$)	R^2
Sample A	0.1055	0.9790
Sample B	0.1135	0.9963
average	0.1095	0.9877

S = coefficient of sorptivity

w/c ratio 0.4 ----- 0.09mm/$min^{1/2}$	**Neville**
w/c ratio 0.6 ----- 0.17mm/$min^{1/2}$	**Neville**
w/c ratio 0.46-0.53 ------ 0.14-0.17 mm/$min^{1/2}$	**GHD**
w/c ratio 0.4-0.5 0.094-0.12 mm/$min^{1/2}$	**Hall**

APPENDIX D - MECHANICAL PROPERTIES, WATER ABSORPTION, SORPTIVITY, DRYING SHRINKAGE OF THE OPTIMUM MIXTURES

Appendix D-8 Sorptivity T7

Concrete mixture: T7				Sample age: 28 days	
Standard: GHD Method				Conditioning:	N/A
Sample conditioning: Oven dried					
Diameter (mm):	A:	99.84	B: 99.85	Curing history: steam curing 12h 70deg C	
Thickness (mm):	A:	113.08	B: 108.07	Type of compaction: Manual stroke	
Water/room temperature: 18deg/23deg					

t	$m^{1/2}$	mass (g)		Dmass (g)		Area (mm^2)		I (mm)	
		A	B	A	B	A	B	A	B
0	0	2089.77	1980.89	0.00	0.00	7824.90	7826.47	0.0000	0.0000
60s	0.71	2092.58	1982.89	2.81	2.00	7824.90	7826.47	0.3591	0.2555
5min	2.24	2094.44	1984.24	4.67	3.35	7824.90	7826.47	0.5968	0.4280
10min	3.16	2095.98	1985.26	6.21	4.37	7824.90	7826.47	0.7936	0.5584
20min	4.47	2097.89	1986.53	8.12	5.64	7824.90	7826.47	1.0377	0.7206
30min	5.48	2099.59	1987.61	9.82	6.72	7824.90	7826.47	1.2550	0.8586
60min	7.75	2103.13	1990.08	13.36	9.19	7824.90	7826.47	1.7074	1.1742
2h	10.95	2107.19	1993.29	17.42	12.40	7824.90	7826.47	2.2262	1.5844
3h	13.42	2110.87	1996.61	21.10	15.72	7824.90	7826.47	2.6965	2.0086
4h	15.49	2111.83	1997.49	22.06	16.60	7824.90	7826.47	2.8192	2.1210

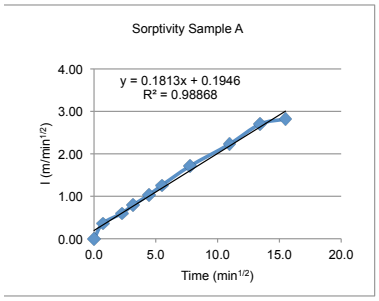

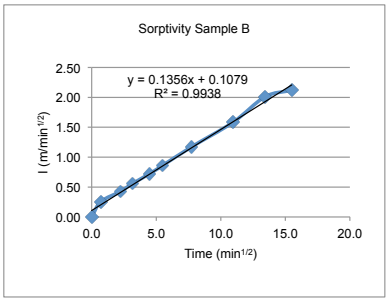

Result	S ($mm/min^{1/2}$)	R^2
Sample A	0.1813	0.9887
Sample B	0.1356	0.9938
average	0.1585	0.9913

SORPTIVITY (MIX T7)

Concrete mixture: T7				Sample age: 91 days	
Standard: GHD Method				Conditioning:	N/A
Sample conditioning: Oven dried					
Diameter (mm):	A:	99.47	B: 99.72	Curing history: steam curing 12h 70deg C	
Thickness (mm):	A:	111.17	B: 108.97	Type of compaction: Manual stroke	
Water/room temperature: 18deg/23deg					

t	$m^{1/2}$	mass (g)		Dmass (g)		Area (mm^2)		I (mm)	
		A	B	A	B	A	B	A	B
0	0	2017.25	1974.92	0.00	0.00	7767.01	7806.10	0.0000	0.0000
60s	0.71	2018.73	1976.59	1.48	1.67	7767.01	7806.10	0.1905	0.2139
5min	2.24	2019.79	1977.6	2.54	2.68	7767.01	7806.10	0.3270	0.3433
10min	3.16	2020.65	1978.52	3.40	3.60	7767.01	7806.10	0.4377	0.4612
20min	4.47	2021.77	1979.62	4.52	4.70	7767.01	7806.10	0.5819	0.6021
30min	5.48	2022.60	1980.5	5.35	5.58	7767.01	7806.10	0.6888	0.7148
60min	7.75	2025.42	1983.25	8.17	8.33	7767.01	7806.10	1.0519	1.0671
2h	10.95	2026.94	1984.68	9.69	9.76	7767.01	7806.10	1.2476	1.2503
3h	13.42	2028.48	1986.19	11.23	11.27	7767.01	7806.10	1.4459	1.4437
4h	15.49	2030.06	1987.74	12.81	12.82	7767.01	7806.10	1.6493	1.6423

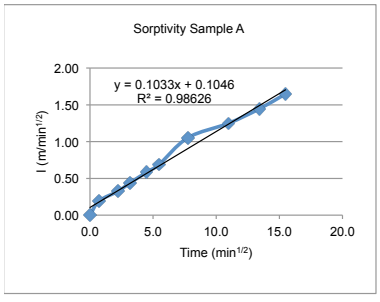

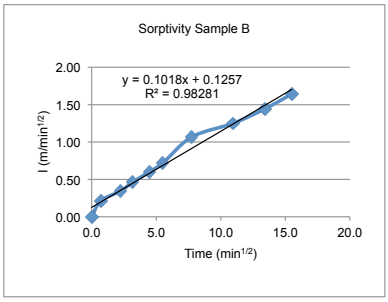

Result	S ($mm/min^{1/2}$)	R^2
Sample A	0.1715	0.9939
Sample B	0.1533	0.9903
average	0.1624	0.9921

SORPTIVITY (MIX T7)

Concrete mixture: T7					Sample age: 365 days	
Standard: GHD Method					Conditioning:	N/A
Sample conditioning: Oven dried						
Diameter (mm):	A:	100.02	B:	99.8	Curing history: steam curing 12h 70deg C	
Thickness (mm):	A:	109.07	B:	110.05	Type of compaction: Manual stroke	
Water/room temperature: 18deg/23deg						

t	$m^{1/2}$	mass (g)		Dmass (g)		Area (mm^2)		I (mm)	
		A	B	A	B	A	B	A	B
0	0	2010.28	1998.42	0.00	0.00	7853.14	7818.63	0.0000	0.0000
60s	0.71	2013.08	2001.29	2.80	2.87	7853.14	7818.63	0.3565	0.3671
5min	2.24	2013.68	2001.94	3.40	3.52	7853.14	7818.63	0.4329	0.4502
10min	3.16	2014.50	2002.41	4.22	3.99	7853.14	7818.63	0.5374	0.5103
20min	4.47	2015.46	2003.36	5.18	4.94	7853.14	7818.63	0.6596	0.6318
30min	5.48	2016.74	2004.49	6.46	6.07	7853.14	7818.63	0.8226	0.7764
60min	7.75	2018.35	2005.74	8.07	7.32	7853.14	7818.63	1.0276	0.9362
2h	10.95	2021.57	2008.85	11.29	10.43	7853.14	7818.63	1.4376	1.3340
3h	13.42	2022.65	2009.98	12.37	11.56	7853.14	7818.63	1.5752	1.4785
4h	15.49	2024.07	2011.54	13.79	13.12	7853.14	7818.63	1.7560	1.6780

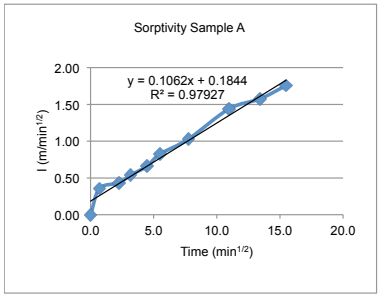

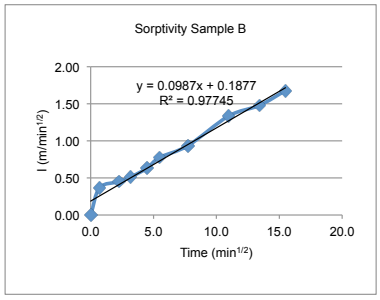

Result	S ($mm/min^{1/2}$)	R^2
Sample A	0.1062	0.9793
Sample B	0.0987	0.9774
average	0.1025	0.9784

S = coefficient of sorptivity

w/c ratio 0.4 ----- 0.09mm/$min^{1/2}$	**Neville**
w/c ratio 0.6 ----- 0.17mm/$min^{1/2}$	**Neville**
w/c ratio 0.46-0.53 ------ 0.14-0.17 mm/$min^{1/2}$	**GHD**
w/c ratio 0.4-0.5 0.094-0.12 mm/$min^{1/2}$	**Hall**

APPENDIX D - MECHANICAL PROPERTIES, WATER ABSORPTION, SORPTIVITY, DRYING SHRINKAGE OF THE OPTIMUM MIXTURES

Appendix D-9 Sorptivity T10

Concrete mixture: T10					Sample age: 28 days
Standard: GHD Method					Conditioning: N/A
Sample conditioning: Oven dried					
Diameter (mm):	A:	99.49	B:	100.00	Curing history: steam curing 24h 75deg C
Thickness (mm):	A:	108.84	B:	109.32	Type of compaction: Manual stroke
Water/room temperature: 18deg/23deg					

t	$m^{1/2}$	mass (g)		Dmass (g)		Area (mm^2)		I (mm)	
		A	B	A	B	A	B	A	B
0	0	1921.71	1949.41	0.00	0.00	7770.13	7850.00	0.0000	0.0000
60s	0.71	1923.91	1951.49	2.20	2.08	7770.13	7850.00	0.2831	0.2650
5min	2.24	1925.14	1952.65	3.43	3.24	7770.13	7850.00	0.4414	0.4127
10min	3.16	1925.88	1953.37	4.17	3.96	7770.13	7850.00	0.5367	0.5045
20min	4.47	1927.45	1954.69	5.74	5.28	7770.13	7850.00	0.7387	0.6726
30min	5.48	1928.49	1955.90	6.78	6.49	7770.13	7850.00	0.8726	0.8268
60min	7.75	1930.76	1958.22	9.05	8.81	7770.13	7850.00	1.1647	1.1223
2h	10.95	1934.08	1961.74	12.37	12.33	7770.13	7850.00	1.5920	1.5707
3h	13.42	1936.60	1964.44	14.89	15.03	7770.13	7850.00	1.9163	1.9146
4h	15.49	1938.66	1966.62	16.95	17.21	7770.13	7850.00	2.1814	2.1924

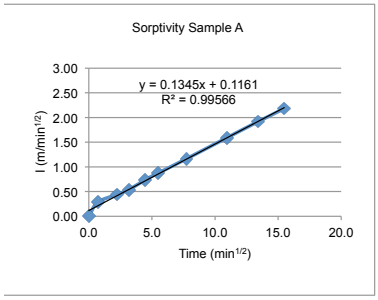

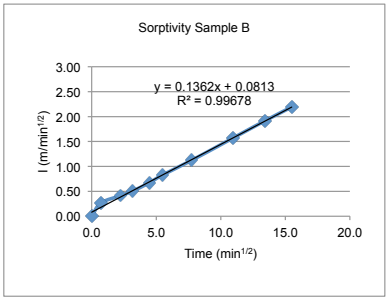

Result	S ($mm/min^{1/2}$)	R^2
Sample A	0.1345	0.9957
Sample B	0.1362	0.9968
average	0.1354	0.9963

SORPTIVITY (MIX T10)

Concrete mixture: T7					Sample age: 91 days
Standard: GHD Method					Conditioning: N/A
Sample conditioning: Oven dried					
Diameter (mm):	A:	99.75	B:	100.12	Curing history: steam curing 24h 75deg C
Thickness (mm):	A:	113.3	B:	112.88	Type of compaction: Manual stroke
Water/room temperature: 18deg/23deg					

t	$m^{1/2}$	mass (g)		Dmass (g)		Area (mm^2)		I (mm)	
		A	B	A	B	A	B	A	B
0	0	2000.23	1995.53	0.00	0.00	7810.80	7868.85	0.0000	0.0000
60s	0.71	2001.91	1997.40	1.68	1.87	7810.80	7868.85	0.2151	0.2376
5min	2.24	2003.17	1998.43	2.94	2.90	7810.80	7868.85	0.3764	0.3685
10min	3.16	2004.00	1999.33	3.77	3.80	7810.80	7868.85	0.4827	0.4829
20min	4.47	2005.33	2000.61	5.10	5.08	7810.80	7868.85	0.6529	0.6456
30min	5.48	2006.28	2001.56	6.05	6.03	7810.80	7868.85	0.7746	0.7663
60min	7.75	2008.64	2004.02	8.41	8.49	7810.80	7868.85	1.0767	1.0789
2h	10.95	2011.63	2007.1	11.40	11.57	7810.80	7868.85	1.4595	1.4704
3h	13.42	2013.88	2009.42	13.65	13.89	7810.80	7868.85	1.7476	1.7652
4h	15.49	2016.04	2011.64	15.81	16.11	7810.80	7868.85	2.0241	2.0473

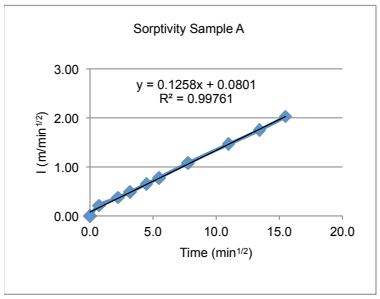

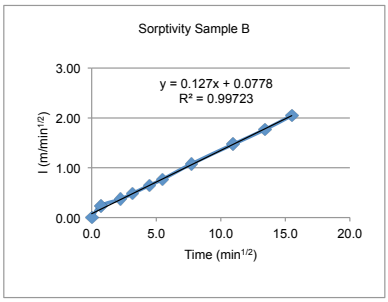

Result	S ($mm/min^{1/2}$)	R^2
Sample A	0.1258	0.9976
Sample B	0.1270	0.9972
average	0.1264	0.9974

SORPTIVITY (MIX T10)

Concrete mixture: OPC					Sample age: 365 days
Standard: GHD Method					Conditioning: N/A
Sample conditioning: Oven dried					
Diameter (mm):	A:	99.29	B:	99.5	Curing history: steam curing 24h 75deg C
Thickness (mm):	A:	110.95	B:	110.23	Type of compaction: Manual stroke
Water/room temperature: 18deg/23deg					

t	$m^{1/2}$	mass (g)		Dmass (g)		Area (mm^2)		I (mm)	
		A	B	A	B	A	B	A	B
0	0	1999.74	1968.68	0.00	0.00	7738.93	7771.70	0.0000	0.0000
60s	0.71	2001.27	1970.36	1.53	1.68	7738.93	7771.70	0.1977	0.2162
5min	2.24	2002.33	1971.52	2.59	2.84	7738.93	7771.70	0.3347	0.3654
10min	3.16	2003.08	1972.4	3.34	3.72	7738.93	7771.70	0.4316	0.4787
20min	4.47	2004.21	1973.6	4.47	4.92	7738.93	7771.70	0.5776	0.6331
30min	5.48	2005.19	1974.68	5.45	6.00	7738.93	7771.70	0.7042	0.7720
60min	7.75	2007.23	1976.82	7.49	8.14	7738.93	7771.70	0.9678	1.0474
2h	10.95	2010.18	1980.03	10.44	11.35	7738.93	7771.70	1.3490	1.4604
3h	13.42	2012.24	1982.18	12.50	13.50	7738.93	7771.70	1.6152	1.7371
4h	15.49	2014.02	1984.07	14.28	15.39	7738.93	7771.70	1.8452	1.9803

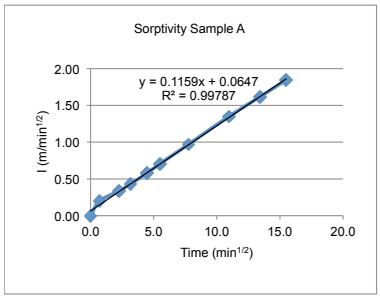

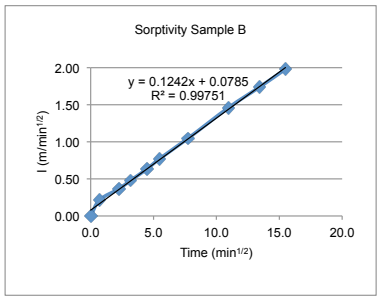

Result	S ($mm/min^{1/2}$)	R^2
Sample A	0.1159	0.9979
Sample B	0.1242	0.9975
average	0.1201	0.9977

S = coefficient of sorptivity

w/c ratio 0.4 ----- 0.09mm/$min^{1/2}$	**Neville**
w/c ratio 0.6 ----- 0.17mm/$min^{1/2}$	**Neville**
w/c ratio 0.46-0.53 ------ 0.14-0.17 mm/$min^{1/2}$	**GHD**
w/c ratio 0.4-0.5 0.094-0.12 mm/$min^{1/2}$	**Hall**

APPENDIX D - MECHANICAL PROPERTIES, WATER ABSORPTION, SORPTIVITY, DRYING SHRINKAGE OF THE OPTIMUM MIXTURES

Appendix D-10 Drying Shrinkage OPC

Date	Temp.	Ref. Bar			Sample 1	Sample 3
30/11/09	21.5deg C	before (in)	0.2003	Reading 1	0.5531	0.5961
(Day 0)		after (in)	0.2005	Reading 2	0.5530	0.5960
		avg. (in)	0.2004	Reading 3	0.5531	0.5960
				Raw average	0.5531	0.5960
				Real average	0.3527	0.3956
7/12/09	21.5deg C	before (in)	0.2006	Reading 1	0.5508	0.5940
(Day 7)		after (in)	0.2006	Reading 2	0.5509	0.5941
		avg. (in)	0.2006	Reading 3	0.5509	0.5940
				Raw average	0.5509	0.5940
				Real average	0.3503	0.3934
				Shrinkage	-0.0024	-0.0022
				Avg.	-0.0023	
				Avg. (mstrain)	-233.68	
14/12/09	21.5deg C	before (in)	0.2004	Reading 1	0.5508	0.5930
(Day 14)		after (in)	0.2003	Reading 2	0.5508	0.5932
		avg. (in)	0.2004	Reading 3	0.5510	0.5931
				Raw average	0.5509	0.5931
				Real average	0.3505	0.3928
				Shrinkage	-0.0021	-0.0029
				Avg.	-0.0025	
				Avg. (mstrain)	-255.69333	
28/12/09	21.5deg C	before (in)	0.2003	Reading 1	0.5507	0.5920
(Day 28)		after (in)	0.2003	Reading 2	0.5507	0.5919
		avg. (in)	0.2003	Reading 3	0.5507	0.5920
				Raw average	0.5507	0.5920
				Real average	0.3504	0.3917
				Shrinkage	-0.0023	-0.0040
				Avg.	-0.0031	
				Avg. (mstrain)	-316.65333	
22/02/10	21.5deg C	before (in)	0.2004	Reading 1	0.5478	0.5909
(Day 84)		after (in)	0.2003	Reading 2	0.5478	0.5909
		avg. (in)	0.2004	Reading 3	0.5477	0.5908
				Raw average	0.5478	0.5909
				Real average	0.3474	0.3905
				Shrinkage	-0.0053	-0.0051
				Avg.	-0.0052	
				Avg. (mstrain)	-526.62667	
22/03/10	21.5deg C	before (in)	0.2	Reading 1	0.5489	0.5921
(Day 112)		after (in)	0.2001	Reading 2	0.5489	0.5919
		avg. (in)	0.2001	Reading 3	0.5488	0.5919
				Raw average	0.5489	0.5920
				Real average	0.3488	0.3919
				Shrinkage	-0.0038	-0.0037
				Avg.	-0.0038	
				Avg. (mstrain)	-384.38667	

APPENDIX D - MECHANICAL PROPERTIES, WATER ABSORPTION, SORPTIVITY, DRYING SHRINKAGE OF THE OPTIMUM MIXTURES

Appendix D-11 Drying Shrinkage T4

Date	Temp.	Ref. Bar			Sample 1	Sample 2	Sample 3
29/03/09	21.5deg C	before (in)	0.2004	Reading 1	0.7769	0.7795	0.7941
(DAY 0)		after (in)	0.2003	Reading 2	0.7773	0.7993	0.7938
		avg. (in)	0.2004	Reading 3	0.7775	0.7991	0.7936
				Raw average	0.7772	0.7926	0.7938
				Real average	0.5769	0.5923	0.5935
5/04/09		before (in)	0.2002	Reading 1	0.7769	0.7985	0.7930
(DAY 7)		after (in)	0.2006	Reading 2	0.7769	0.7988	0.7930
		avg. (in)	0.2004	Reading 3	0.7770	0.7985	0.7930
				Raw average	0.7769	0.7986	0.7930
				Real average	0.5765	0.5982	0.5926
				Shrinkage	-0.0003	0.0059	-0.0009
				Avg.	0.0016		
				Avg. (mstrain)	158.60889		
12/04/09		before (in)	0.2004	Reading 1	0.7766	0.7986	0.7925
(DAY 14)		after (in)	0.2002	Reading 2	0.7768	0.7981	0.7926
		avg. (in)	0.2003	Reading 3	0.7766	0.7988	0.7928
				Raw average	0.7767	0.7985	0.7926
				Real average	0.5764	0.5982	0.5923
				Shrinkage	-0.0005	0.0059	-0.0011
				Avg.	0.0014		
				Avg. (mstrain)	143.93333		
26/04/09		before (in)	0.2005	Reading 1	0.7766	0.7987	0.7930
(DAY 28)		after (in)	0.2003	Reading 2	0.7767	0.7989	0.7933
		avg. (in)	0.2004	Reading 3	0.7767	0.7987	0.7928
				Raw average	0.7767	0.7988	0.7930
				Real average	0.5763	0.5984	0.5926
				Shrinkage	-0.0006	0.0061	-0.0008
				Avg.	0.0015		
				Avg. (mstrain)	156.35111		
14/06/09		before (in)	0.2004	Reading 1	0.7771	0.7989	0.7928
(DAY 84)		after (in)	0.2005	Reading 2	0.7772	0.7990	0.7930
		avg. (in)	0.2005	Reading 3	0.777	0.7989	0.7929
				Raw average	0.7771	0.7989	0.7929
				Real average	0.5767	0.5985	0.5925
				Shrinkage	-0.0002	0.0062	-0.0010
				Avg.	0.0016		
				Avg. (mstrain)	167.07556		
26/06/09		before (in)	0.2002	Reading 1	0.7770	0.7989	0.7937
(DAY 112)		after (in)	0.2002	Reading 2	0.7771	0.7986	0.7937
		avg. (in)	0.2002	Reading 3	0.7771	0.7986	0.7938
				Raw average	0.7771	0.7987	0.7937
				Real average	0.5769	0.5985	0.5935
				Shrinkage	0.0000	0.0062	0.0000
				Avg.	0.0021		
				Avg. (mstrain)	211.66667		

APPENDIX D - MECHANICAL PROPERTIES, WATER ABSORPTION, SORPTIVITY, DRYING SHRINKAGE OF THE OPTIMUM MIXTURES

Appendix D-12 Drying Shrinkage T7

Date	Temp.	Ref. Bar			Sample 1	Sample 2	Sample 3	
27/03/09	21.5deg C	before (in)	0.2006	Reading 1	0.7782	0.8231	0.7774	
(DAY 0)		after (in)	0.2004	Reading 2	0.7784	0.8225	0.7776	
		avg. (in)	0.2005	Reading 3	0.7784	0.8224	0.7779	v
				Raw average	0.7783	0.8227	0.7776	
				Real average	0.5778	0.6222	0.5771	
3/04/09		before (in)	0.2003	Reading 1	0.7776	0.8233	0.7783	
(DAY 7)		after (in)	0.2001	Reading 2	0.7772	0.8232	0.7781	
		avg. (in)	0.2002	Reading 3	0.7774	0.8234	0.7782	v
				Raw average	0.7774	0.8233	0.7782	
				Real average	0.5772	0.6231	0.5780	
				Shrinkage	-0.0006	0.0009	0.0009	
				Avg.	0.0004			
				Avg. (mstrain)	39.5111			
10/04/09		before (in)	0.2004	Reading 1	0.7776	0.8232	0.7784	
(DAY 14)		after (in)	0.2002	Reading 2	0.7775	0.8232	0.7782	
		avg. (in)	0.2003	Reading 3	0.7776	0.8231	0.7785	v
				Raw average	0.7776	0.8232	0.7784	
				Real average	0.5773	0.6229	0.5781	
				Shrinkage	-0.0006	0.0007	0.0009	
				Avg.	0.0004			
				Avg. (mstrain)	36.1244			
24/04/09		before (in)	0.2005	Reading 1	0.7775	0.8233	0.7785	
(DAY 28)		after (in)	0.2005	Reading 2	0.7775	0.8232	0.7782	
		avg. (in)	0.2005	Reading 3	0.7775	0.8234	0.7781	v
				Raw average	0.7775	0.8233	0.7783	
				Real average	0.5770	0.6228	0.5778	
				Shrinkage	-0.0008	0.0006	0.0006	
				Avg.	0.0001			
				Avg. (mstrain)	14.6756			
12/06/09		before (in)	0.2004	Reading 1	0.7777	0.8233	0.7776	
(DAY 84)		after (in)	0.2003	Reading 2	0.7776	0.8235	0.7775	
		avg. (in)	0.2004	Reading 3	0.7774	0.8232	0.7771	v
				Raw average	0.7776	0.8233	0.7774	
				Real average	0.5772	0.6230	0.5771	
				Shrinkage	-0.0006	0.0008	-0.0001	
				Avg.	0.0000			
				Avg. (mstrain)	3.9511			
Date	**Temp.**	**Ref. Bar**			**Sample 1**	**Sample 2**	**Sample 3**	
26/06/09		before (in)	0.2004	Reading 1	0.7778	0.8231	0.7783	
(DAY 112)		after (in)	0.2005	Reading 2	0.7776	0.8233	0.7784	
		avg. (in)	0.2005	Reading 3	0.7775	0.8234	0.7786	v
				Raw average	0.7776	0.8233	0.7784	
				Real average	0.5772	0.6228	0.5780	
				Shrinkage	-0.0007	0.0007	0.0009	
				Avg.	0.0003			
				Avg. (mstrain)	28.7867			

APPENDIX D - MECHANICAL PROPERTIES, WATER ABSORPTION, SORPTIVITY, DRYING SHRINKAGE OF THE OPTIMUM MIXTURES

Appendix D-13 Drying Shrinkage T10

Date	Temp.	Ref. Bar			Sample 1	Sample 2	Sample 3	
28/03/09	21.5deg C	before (in)	0.2004	Reading 1	0.5816	0.5973		
(Day 0)		after (in)	0.2001	Reading 2	0.5818	0.5972		
		avg. (in)	0.2003	Reading 3	0.5817	0.5970		
				Raw average	0.5817	0.5972		
				Real average	0.3815	0.3969		
4/04/09		before (in)	0.2001	Reading 1	0.5815	0.5977		v
(Day 7)		after (in)	0.2004	Reading 2	0.5816	0.5966		
		avg. (in)	0.2003	Reading 3	0.5816	0.5967		
				Raw average	0.5816	0.597		
				Real average	0.3813	0.3968		
				Shrinkage	-0.0001	-0.0002		
				Avg.	-0.0001			
				Avg. (mstrain)	-15.2400			
11/04/09		before (in)	0.2003	Reading 1	0.5813	0.5963		
(Day 14)		after (in)	0.2000	Reading 2	0.5810	0.5961		
		avg. (in)	0.2002	Reading 3	0.5811	0.5961		v
				Raw average	0.5811	0.5962		
				Real average	0.3810	0.3960		
				Shrinkage	-0.0005	-0.0009		
				Avg.	-0.0007			
				Avg. (mstrain)	-69.4267			
25/04/09		before (in)	0.2001	Reading 1	0.5796	0.5957		
(Day 28)		after (in)	0.2002	Reading 2	0.5800	0.5961		
		avg. (in)	0.20015	Reading 3	0.5800	0.5963		v
				Raw average	0.5799	0.5960		
				Real average	0.3797	0.3959		
				Shrinkage	-0.0017	-0.0010		
				Avg.	-0.0014			
				Avg. (mstrain)	-140.54667			
13/06/09		before (in)	0.2004	Reading 1	0.5808	0.5963		
(Day 84)		after (in)	0.2005	Reading 2	0.5809	0.5963		
		avg. (in)	0.2005	Reading 3	0.5807	0.5965		v
				Raw average	0.5808	0.5964		
				Real average	0.3804	0.3959		
				Shrinkage	-0.0011	-0.0010		
				Avg.	-0.0011			
				Avg. (mstrain)	-106.6800			
26/06/09		before (in)	0.2004	Reading 1	0.5809	0.5964		
(Day 112)		after (in)	0.2005	Reading 2	0.5809	0.5966		
		avg. (in)	0.2005	Reading 3	0.5811	0.5965		v
				Raw average	0.5810	0.5965		
				Real average	0.3805	0.3961		
				Shrinkage	-0.0009	-0.0009		
				Avg.	-0.0009			
				Avg. (mstrain)	-91.4400			

APPENDIX E - SEAWATER RESISTANCE

Appendix E-1 Chloride Content Potentiometric (NT Build 443)

Concentration of AgNO3 0.0499 M

Lab Sample No	Client Sample ID	Depth (mm)	Weight of sample (g)	Volume of silver nitrate used (ml)	% Chloride by weight concrete
Std 1	P31812		3.5516	3.384	0.169
1	T10-1	0-15	3.044	7.956	0.462
2	T10-1	15-30	3.0192	5.947	0.348
3	T10-1	30-45	3.0055	4.377	0.258
4	T10-2	0-15	3.0305	8.432	0.492
5	T10-2	15-30	3.0702	6.836	0.394
6	T10-2	30-45	3.0486	5.106	0.296
7	T10-3	0-15	2.6423	4.589	0.307
8	T10-3	15-30	3.0792	5.685	0.327
9	T10-3	30-45	3.0102	4.449	0.261
10	T4-1	0-15	2.5616	6.158	0.425
11	T4-1	15-30	2.5223	4.575	0.321
12	T4-1	30-45	2.5224	3.483	0.244
13	T4-2	0-15	2.5428	6.645	0.462
14	T4-2	15-30	2.5348	4.551	0.318
15	T4-2	30-45	2.5369	3.349	0.234
16	T4-3	0-15	2.5143	7.281	0.512
17	T4-3	15-30	2.5698	5.338	0.367
18	T4-3	30-45	2.5562	4.05	0.280
Std 2			3.6526	3.522	0.171
19	T7-1	0-15	2.5223	4.804	0.337
20	T7-1	15-30	2.5694	3.848	0.265
21	T7-1	30-45	2.5313	3.055	0.213
22	T7-2	0-15	2.5028	4.616	0.326
23	T7-2	15-30	2.7782	4.145	0.264
24	T7-2	30-45	2.5797	2.731	0.187
25	T7-3	0-15	2.5387	5.677	0.396
26	T7-3	15-30	2.5636	4.521	0.312
27	T7-3	30-45	2.5528	3.967	0.275
28	OPC-1	0-15	2.2429	5.38	0.424
29	OPC-1	15-30	5.0718	10.46	0.365
30	OPC-1	30-45	1.5918	0.6335	0.070
31	OPC-2	0-15	3.6892	10.35	0.496
32	OPC-2	15-30	5.128	7.547	0.260
33	OPC-2	30-45	7.2679	4.492	0.109
34	OPC-3	0-15	3.5078	10.01	0.505
35	OPC-3	15-30	4.9932	7.112	0.252
36	OPC-3	30-45	7.2575	3.926	0.096
Std 3			3.5048	3.393	0.171
37	T7 Background		3.034	0.182	0.011
38	T4 Background		3.1593	0.179	0.010
39	T10 Background		2.7024	0.180	0.012
40	OPC Background		3.5985	0.189	0.009

APPENDIX E - SEAWATER RESISTANCE

Appendix E-2 Compressive Strength of Specimens Subjected to Continuous Immersion

Mixture	Age (days)	Sample	Diameter (mm)	Height (mm)	Weight (g)	Density (kg/m^3)	Load (kN)	Compressive Strength (MPa)	Average (MPa)	SD	SQRT	ERROR BAR
OPC	7	1	99.97	200.73	3770.60	2408.98	412.10	52.53	51.23	4.94	1.73	2.85
		2	100.18	200.46	3789.90	2428.22	360.60	45.77				
		3	99.29	197.76	3686.60	2289.00	428.70	55.40				
	28	1	99.92	197.00	3692.50	2312.93	459.10	58.58	58.88	0.39	1.73	0.22
		2	100.17	199.85	3768.80	2406.87	462.70	58.74				
		3	99.92	200.34	3751.90	2389.98	464.90	59.32				
	91	1	99.52	199.07	3731.50	2343.04	453.90	58.38	60.87	2.30	1.73	1.33
		2	99.84	197.57	3743.50	2347.89	492.40	62.93				
		3	99.91	200.59	3770.90	2404.60	480.40	61.31				
	365	1	99.80	199.42	3757.50	2376.84	432.40	55.30	64.06	12.38	1.41	8.76
		2	99.72	197.10	3739.40	2334.12	568.40	72.81				
		3				0.00						
T7	7	1	99.60	200.20	3776.70	2388.72	430.90	55.33	54.04	1.83	1.41	1.29
		2	99.75	200.12	3780.20	2397.18	412.00	52.75				
		3	N/A					N/A				
	28	1	100.34	201.35	3802.70	2455.06	376.60	47.65	49.26	4.30	1.73	2.49
		2	100.03	200.89	3723.10	2383.38	361.30	46.00				
		3	100.55	200.83	3761.90	2432.60	429.70	54.14				
	91	1	99.73	201.29	3816.50	2433.38	397.40	50.90	48.43	4.97	1.73	2.87
		2	99.72	202.09	3796.60	2429.82	333.40	42.71				
		3	99.32	201.14	3738.80	2362.51	400.30	51.69				
	365	1	99.52	200.62	3780.00	2391.98	426.00	54.79	56.29	2.12	1.41	1.50
		2	99.82	200.70	3818.40	2431.84	452.00	57.79				
		3				0.00						
T4	7	1	99.66	200.44	3733.30	2366.95	423.10	54.27	55.27	1.42	1.41	1.01
		2	99.83	200.78	3738.20	2382.18	440.30	56.28				
		3	N/A					N/A				
	28	1	100.28	230.27	3797.93	2800.81	381.70	48.35	56.12	6.74	1.73	3.89
		2	99.83	201.07	3747.41	2391.50	466.00	59.57				
		3	100.12	201.16	3808.76	2445.89	475.50	60.43				
	91	1	99.68	200.11	3734.78	2364.94	484.50	62.12	61.68	0.65	1.73	0.37
		2	99.31	201.18	3744.44	2366.07	479.90	61.99				
		3	99.90	200.30	3688.27	2348.04	477.40	60.94				
	365	1	99.71	199.90	3780.40	2392.76	449.30	57.57	59.42	3.87	1.73	2.24
		2	99.78	201.76	3795.80	2428.26	444.10	56.82				
		3	99.42	200.29	3769.80	2376.82	495.60	63.87				
T10	7	1	99.69	199.68	3621.19	2288.54	471.50	60.44	59.08	1.92	1.41	1.36
		2	99.54	200.36	3639.47	2300.99	449.00	57.73				
		3	N/A					N/A				
	28	1	99.88	201.37	3596.20	2300.73	458.90	58.60	60.29	6.49	1.73	3.75
		2	99.63	200.62	3591.69	2277.84	525.60	67.45				
		3	100.15	199.85	3601.88	2299.35	431.50	54.80				
	91	1	99.78	202.00	3640.07	2331.41	490.10	62.71	64.00	2.11	1.73	1.22
		2	97.83	201.00	3675.60	2251.85	499.10	66.43				
		3	98.43	202.00	3676.00	2291.14	478.10	62.86				
	365	1	99.84	202.68	3726.60	2397.75	525.50	67.16	65.78	2.78	1.73	1.61
		2	99.46	202.28	3670.90	2339.34	525.00	67.61				
		3	99.21	200.95	3676.60	2315.88	483.50	62.58				

APPENDIX E - SEAWATER RESISTANCE

Appendix E-3 Compressive Strength of Specimens Subjected to Cyclic Wetting-Drying

Mixture	Age (days)	Sample	Diameter (mm)	Height (mm)	Weight (g)	Density (kg/m^3)	Load (kN)	Compressive Strength (MPa)	Average (MPa)	SD	SQRT	ERROR BAR
OPC	7	1	99.97	200.73	3770.60	2408.98	412.10	52.53	51.23	4.94	1.73	2.85
		2	100.18	200.46	3789.90	2428.22	360.60	45.77				
		3	99.29	197.76	3686.60	2289.00	428.70	55.40				
	28	1	100.08	199.08	3695.90	2347.00	462.90	58.87	59.78	1.72	1.73	1.00
		2	100.03	200.13	3705.00	2362.82	485.20	61.77				
		3	99.56	199.60	3660.90	2306.69	456.80	58.71				
	91	1	99.84	198.8	3672.90	2317.9549	457.50	58.47	57.09	1.83	1.73	1.06
		2	99.77	198.83	3724.00	2347.2637	451.50	57.78				
		3	99.82	198.08	3664.70	2303.4805	430.30	55.01				
	200	1	99.23	201.14	3721.60	2347.39	483.60	62.56	56.55	5.25	1.73	3.03
		2	99.74	201.40	3738.00	2385.11	441.60	56.55				
		3	99.82	201.00	3726.70	2376.98	524.10	67.01				
T4	7	1	99.66	200.44	3733.30	2366.95	423.10	54.27	55.27	1.42	1.41	1.01
		2	99.83	200.78	3738.20	2382.18	440.30	56.28				
		3	N/A					N/A				
	28	1	99.86	201.34	3688.29	2358.35	576.10	73.59	68.95	5.51	1.73	3.18
		2	99.30	201.14	3672.93	2319.96	544.80	70.38				
		3	99.79	202.75	3693.26	2374.73	491.40	62.86				
	91	1	99.56	202.88	3700.02	2369.65	594.70	76.43	72.03	4.76	1.73	2.75
		2	99.83	203.50	3696.54	2387.55	568.70	72.69				
		3	99.64	202.75	3678.23	2357.97	522.00	66.98				
	200	1	99.86	205.91	3725.40	2436.15	475.70	60.77	62.26	3.43	1.73	1.98
		2	99.38	203.88	3655.70	2344.30	513.10	66.18				
		3	99.49	201.03	3629.00	2299.73	464.90	59.83				

APPENDIX E - SEAWATER RESISTANCE

Appendix E-4 Young's Modulus of Elasticity and Poisson's Ratio of Specimens Subjected to Continuous Immersion

Mixture	Age (days)	Sample	YM (GPa)	Average (GPa)	SD	SQRT	ERROR BAR	Poisson's Ratio	Average (GPa)	SD	SQRT	ERROR BAR
OPC	91	1	37.6954	33.96	3.24	1.73	1.87	0.1673	0.18	0.01	1.73	0.01
		2	31.9098					0.1897				
		3	32.2834					0.1893				
	365	1	41.1979	39.50	1.90	1.73	1.10	0.1927	0.18	0.02	1.73	0.01
		2	39.8393					0.1583				
		3	37.4499					0.1815				

Mixture	Age (days)	Sample	YM (GPa)	Average (GPa)	SD	SQRT	ERROR BAR	Poisson's Ratio	Average (GPa)	SD	SQRT	ERROR BAR
T7	91	1	25.1171	27.08	2.78	1.41	1.97	0.1089	0.16	0.07	1.41	0.05
		2	29.0522					0.2131				
		3	N/A					N/A				
	365	1	34.3519	31.47	2.53	1.73	1.46	0.1660	0.19	0.02	1.73	0.01
		2	29.6497					0.1827				
		3	30.4025					0.2147				

Mixture	Age (days)	Sample	YM (GPa)	Average (GPa)	SD	SQRT	ERROR BAR	Poisson's Ratio	Average (GPa)	SD	SQRT	ERROR BAR
T4	91	1	31.1961	32.61	2.07	1.73	1.19	0.1685	0.17	0.03	1.73	0.02
		2	31.6499					0.1859				
		3	34.9846					0.1459				
	365	1	29.8505	28.59	1.60	1.73	0.92	0.1692	0.17	0.05	1.73	0.03
		2	26.7877					0.2207				
		3	29.1318					0.1259				

Mixture	Age (days)	Sample	YM (GPa)	Average (GPa)	SD	SQRT	ERROR BAR	Poisson's Ratio	Average (GPa)	SD	SQRT	ERROR BAR
T10	91	1	26.1732	26.68	0.53	1.73	0.31	0.1482	0.15	0.01	1.73	0.01
		2	27.2391					0.1310				
		3	26.6417					0.1571				
	365	1	28.2714	28.16	0.35	1.73	0.20	0.1767	0.15	0.03	1.73	0.02
		2	27.7691					0.1601				
		3	28.4312					0.1206				

APPENDIX E - SEAWATER RESISTANCE

Appendix E-5 Young's Modulus of Elasticity and Poisson's Ratio of Specimens Subjected to Cyclic Wetting-Drying

Mixture	Cycles	Sample	YM (GPa)	Average (GPa)	SD	SQRT	ERROR BAR	Poisson's Ratio	Average (GPa)	SD	SQRT	ERROR BAR
OPC	45	1	29.6384	28.40	2.69	1.73	1.55	0.1973	0.18	0.01	1.73	0.01
		2	25.3211					0.1741				
		3	30.2509					0.1764				
	100	1	30.8924	32.59	2.10	1.73	1.21	0.1931	0.19	0.02	1.73	0.01
		2	34.9419					0.2019				
		3	31.9303					0.1601				

Mixture	Cycles	Sample	YM (GPa)	Average (GPa)	SD	SQRT	ERROR BAR	Poisson's Ratio	Average (GPa)	SD	SQRT	ERROR BAR
T4	45	1	31.1961	32.61	2.07	1.73	1.19	0.1685	0.17	0.02	1.73	0.01
		2	31.6499					0.1859				
		3	34.9846					0.1459				
	100	1	31.3724	32.09	1.39	1.73	0.80	0.1692	0.17	0.02	1.73	0.01
		2	31.1984					0.1859				
		3	33.6926					0.1462				

APPENDIX E - SEAWATER RESISTANCE

Appendix E-6 Water absorption, AVPV, Effective Porosity of Specimens Subjected to Continuous Immersion

Concrete mix: OPC, T7, T4, T10	Method of compaction: manual stroke
Age of specimen at commencement of test: 91, 365 days	Description of specimen (moulded, cut, cored, broken, irregular, etc): regular cut

Specimen dimension:

Slices	Radius (mm)			Height (mm)			Volume (mm^3)	Volume (cm^3)
	1	2	average	1	2	average		
OPC-91D-1	99.67	99.68	99.68	46.14	46.17	46.16	359812.43	359.81
OPC-91D-2	99.71	99.75	99.73	51.39	51.42	51.41	401075.11	401.08
OPC-365D-1	100.05	100.05	100.05	44.7	44.7	44.70	351245.98	351.25
OPC-365D-2	99.08	99.08	99.08	52.3	52.3	52.30	403035.54	403.04

Slices	Radius (mm)			Height (mm)			Volume (mm^3)	Volume (cm^3)
	1	2	average	1	2	average		
T7-91D-1	99.72	99.74	99.73	51.98	51.90	51.94	405761.16	405.76
T7-91D-2	99.39	99.42	99.41	49.15	52.10	50.63	381134.76	381.13
T7-365D-1	100.04	100.04	100.04	56.90	56.90	56.90	447022.40	447.02
T7-365D-2	99.02	99.02	99.02	52.23	52.23	52.23	402008.77	402.01

Slices	Radius (mm)			Height (mm)			Volume (mm^3)	Volume (cm^3)
	1	2	average	1	2	average		
T4-91D-1	99.75	99.75	99.75	50.43	50.43	50.43	393898.60	393.90
T4-91D-2	99.87	99.87	99.87	49.75	49.75	49.75	389522.76	389.52
T4-365D-1	99.25	99.25	99.25	46.48	46.48	46.48	359415.50	359.42
T4-365D-2	99.53	99.53	99.53	50.94	50.94	50.94	396128.97	396.13

Slices	Radius (mm)			Height (mm)			Volume (mm^3)	Volume (cm^3)
	1	2	average	1	2	average		
T10-91D-1	100.26	100.26	100.26	52.27	52.27	52.27	412455.94	412.46
T10-91D-2	99.86	99.86	99.86	51.27	51.27	51.27	401343.37	401.34
T10-365D-1	99.59	99.59	99.59	53.77	53.77	53.77	418640.42	418.64
T10-365D-2	99.80	99.80	99.80	49.90	49.90	49.90	390149.71	390.15

Slices	M (g)	A (g)	B (g)	Absorption after immersion	C (g)	D (g)	Absorption after boiling (%)	Bulk density, dry (x10^3 g/m^3)	Bulk density after immersion	Bulk density after boiling (Mg/m^3)	Apparent density (Mg/m^3)	Volume of permeable voids (%)	Bulk volume of the sample	Effective porosity (%)
OPC-91D-1	983.99	955.28	999.52	4.63	1000.60	584.71	4.74	2.30	2.40	2.41	2.58	10.90	359.81	12.30
OPC-91D-2	1002.16	938.41	980.98	4.54	982.40	575.88	4.69	2.31	2.41	2.42	2.59	10.82	401.08	10.61
Average				4.58			4.72					10.86		11.45
OPC-365D-1	1056.46	999.08	1047.97	4.89	1049.30	611.57	5.03	2.28	2.39	2.40	2.58	11.47	351.25	13.92
OPC-365D-2	978.82	928.40	971.76	4.67	972.75	568.44	4.78	2.30	2.40	2.41	2.58	10.97	403.04	10.76
Average				4.78								11.00		12.34

T7-91D-1	971.52	937.43	972.92	3.79	975.32	567.24	4.04	2.30	2.38	2.39	2.53	9.28	405.76	8.75
T7-91D-2	916.82	886.50	916.61	3.40	921.48	538.66	3.95	2.32	2.39	2.41	2.55	9.14	381.13	7.90
Average				3.59			3.99					9.21		8.32
T7-365D-1	983.94	941.76	977.82	3.83	979.53	570.53	4.01	2.30	2.39	2.39	2.54	9.23	447.02	8.07
T7-365D-2	821.00	784.38	815.56	3.98	816.76	475.12	4.13	2.30	2.39	2.39	2.54	9.48	402.01	7.76
Average				3.90								9.27		7.91

T4-91D-1	933.68	910.41	943.46	3.63	945.62	549.74	3.87	2.30	2.38	2.39	2.52	8.89	393.90	8.39
T4-91D-2	926.34	904.02	936.03	3.54	937.88	546.37	3.75	2.31	2.39	2.40	2.53	8.65	389.52	8.22
Average				3.59			3.81					8.77		8.30
T4-365D-1	997.76	963.57	996.88	3.46	999.22	580.10	3.70	2.30	2.38	2.38	2.51	8.51	359.42	9.27
T4-365D-2	853.24	842.09	872.09	3.56	874.03	512.75	3.79	2.33	2.41	2.42	2.56	8.84	396.13	7.57
Average				3.51			3.75					8.67		8.42

T10-91D-1	914.88	901.14	938.14	4.11	939.14	583.61	4.22	2.53	2.64	2.64	2.838	10.69	412.46	8.97
T10-91D-2	947.36	933.86	971.25	4.00	970.82	563.44	3.96	2.29	2.38	2.38	2.521	9.07	401.34	9.32
Average				4.05			4.09					9.88		9.14
T10-365D-1	1033.80	1012.45	1057.34	4.43	1060.51	604.08	4.75	2.22	2.32	2.32	2.479	10.53	418.64	10.72
T10-365D-2	905.85	887.83	924.57	4.14	926.16	536.56	4.32	2.28	2.37	2.38	2.527	9.84	390.15	9.42
Average				4.29			4.53					10.18		10.07

APPENDIX E - SEAWATER RESISTANCE

Appendix E-7 Water absorption, AVPV, Effective Porosity Cyclic Immersion

Concrete mix: OPC, T7, T4, T10	Method of compaction: manual stroke
Age of specimen at commencement of test: 91, 365 days	Description of specimen (moulded, cut, cored, broken, irregular, etc): regular cut

Specimen dimension:

Slices	Radius (mm)			Height (mm)			Volume (mm^3)	Volume (cm^3)
	1	2	average	1	2	average		
OPC-91D-1	99.52	99.52	99.52	51.06	51.06	51.06	396982.35	396.98
OPC-91D-2	99.47	99.47	99.47	50.65	50.65	50.65	393399.08	393.40
OPC-365D-1	99.53	99.53	99.53	50.94	50.94	50.94	396128.97	396.13
OPC-365D-2	99.25	99.25	99.25	46.48	46.48	46.48	359415.50	359.42

Slices	Radius (mm)			Height (mm)			Volume (mm^3)	Volume (cm^3)
	1	2	average	1	2	average		
T4-91D-1	99.67	99.67	99.67	49.92	49.92	49.92	389289.91	389.29
T4-91D-2	99.82	99.82	99.82	51.58	51.58	51.58	403446.66	403.45
T4-365D-1	99.62	99.62	99.62	50.85	50.85	50.85	396144.55	396.14
T4-365D-2	99.42	99.42	99.42	52.43	52.43	52.43	406815.07	406.82

Slices	M (g)	A (g)	B (g)	Absorption after immersion	C (g)	D (g)	Absorption after boiling (%)	Bulk density, dry (Mg/m^3)	Bulk density after immersion	Bulk density after boiling (Mg/m^3)	Apparent density (Mg/m^3)	Volume of permeable voids (%)	Bulk volume of the sample	Effective porosity (%)
OPC-91D-1	940.22	907.76	949.20	4.57	950.15	553.23	4.67	2.29	2.39	2.39	2.560	10.680	396.9824	10.4388
OPC-91D-2	945.62	914.07	954.40	4.41	955.11	558.92	4.49	2.31	2.41	2.41	2.574	10.359	393.3991	10.2517
Average				4.49			4.58					10.52		10.3452
OPC-365D-1	897.71	912.99	914.06	0.12	913.41	534.51	0.05	2.41	2.41	2.41	2.41	0.11	403.4467	0.2652
OPC-365D-2	940.01	954.64	956.31	0.17	955.61	559.18	0.10	2.41	2.41	2.41	2.41	0.24	396.1446	0.4216
Average				0.15								6.38		0.3434
T4-91D-1	905.67	888.10	926.56	4.33	920.55	537.22	3.65	2.32	2.42	2.40	2.53	8.47	389.2899	9.8795
T4-91D-2	944.62	926.63	964.13	4.05	963.02	563.70	3.93	2.32	2.41	2.41	2.55	9.11	403.4467	9.2949
Average				4.19			3.79					8.79		9.5872
T4-365D-1	930.60	916.34	948.14	3.47	948.33	555.98	3.49	2.34	2.42	2.42	2.54	8.15	396.1446	8.0274
T4-365D-2	960.60	945.65	978.98	3.52	978.96	573.72	3.52	2.33	2.42	2.42	2.54	8.22	406.8151	8.1929
Average				3.50			3.51					8.19		8.1101

APPENDIX E - SEAWATER RESISTANCE

Appendix E-8 Weight change of Specimens Subjected to Continuous Immersion

Mix T4					
Days	Sample 1	Sample 2	Sample 3	Average	Weight change (%)
0	3726.90	3728.20	3742.90	3732.67	0.000
1	3767.00	3771.50	3785.80	3774.77	1.128
7	3769.90	3774.50	3788.70	3777.70	1.206
14	3764.60	3769.53	3783.55	3772.56	1.069
21	3765.30	3769.53	3784.06	3772.96	1.080
28	3765.72	3770.43	3785.03	3773.73	1.100
42	3765.24	3769.91	3784.48	3773.21	1.086
56	3766.12	3770.88	3785.33	3774.11	1.110
84	3766.59	3771.41	3786.23	3774.74	1.127
91	3766.47	3770.25	3784.94	3773.89	1.104
112	3767.88	3773.03	3787.26	3776.06	1.162
140	3769.50	3774.44	3788.42	3777.45	1.200
168	3769.80	3774.88	3789.16	3777.95	1.213
196	3769.05	3774.01	3789.01	3777.36	1.197
252	3768.80	3774.00	3788.00	3776.93	1.186
280	3769.20	3774.50	3788.50	3777.40	1.198
308	3767.10	3772.50	3786.30	3775.30	1.142
336	3771.30	3776.50	3790.80	3779.53	1.256
364	3768.98	3775.28	3788.28	3777.51	1.201

Mix T10					
Days	Sample 1	Sample 2	Sample 3	Average	Weight change (%)
0	3675.85	3675.75	3660.55	3670.72	0.000
1	3735.70	3730.13	3716.04	3727.29	1.541
7	3739.73	3734.01	3720.38	3731.37	1.652
14	3741.78	3736.23	3722.64	3733.55	1.712
21	3743.40	3737.30	3723.99	3734.90	1.748
28	3744.08	3738.21	3724.18	3735.49	1.765
42	3745.51	3739.37	3724.18	3736.35	1.788
56	3746.93	3740.45	3727.02	3738.13	1.837
84	3749.17	3742.53	3728.86	3740.19	1.893
91	3749.82	3743.45	3729.75	3741.01	1.915
112	3750.35	3744.02	3729.97	3741.45	1.927
168	3750.33	3744.05	3730.16	3741.51	1.929
196	3750.35	3744.26	3730.37	3741.66	1.933
224	3747.08	3741.08	3727.28	3738.48	1.846
252	3749.58	3743.48	3729.18	3740.75	1.908
280	3750.98	3744.88	3731.08	3742.31	1.950
308	3752.28	3746.18	3732.08	3743.51	1.983
364	3751.28	3746.38	3732.88	3743.51	1.983

Mix T7					
Days	Sample 1	Sample 2	Sample 3	Average	Weight change (%)
0	3719.00	3751.60	3685.20	3718.60	0.000
1	3786.10	3811.50	3752.70	3783.43	1.743
7	3788.40	3813.90	3754.70	3785.67	1.804
14	3788.50	3814.10	3755.20	3785.93	1.811
21	3790.30	3815.30	3756.20	3787.27	1.847
28	3788.70	3813.10	3755.00	3785.60	1.802
42	3790.10	3815.20	3756.00	3787.10	1.842
56	3787.40	3812.90	3754.90	3785.07	1.787
84	3791.20	3816.30	3758.10	3788.53	1.881
91	3791.40	3816.90	3758.30	3788.87	1.890
112	3790.20	3815.60	3757.30	3787.70	1.858
140	3793.00	3818.6	3760.5	3790.70	1.939
168	3794.40	3820.10	3761.30	3791.93	1.972
196	3794.50	3819.70	3761.90	3792.03	1.975
252	3794.30	3820.10	3762.60	3792.33	1.983
280	3794.50	3820.00	3762.00	3792.17	1.978
308	3794.80	3819.40	3762.00	3792.07	1.976
336	3794.30	3819.40	3762.00	3791.90	1.971
364	3794.70	3820.50	3762.30	3792.50	1.987

Mix OPC					
Days	Sample 1	Sample 2	Sample 3	Average	Weight change (%)
0	3717.10	3673.00	3750.30	3713.47	0.000
1	3725.70	3684.90	3764.30	3724.97	0.310
7	3728.00	3687.10	3766.50	3727.20	0.370
14	3731.20	3689.60	3769.60	3730.13	0.449
21	3731.70	3689.80	3769.30	3730.27	0.452
28	3734.80	3692.50	3772.20	3733.17	0.531
42	3737.90	3695.60	3776.00	3736.50	0.620
56	3740.70	3697.10	3777.90	3738.57	0.676
84	3740.00	3696.10	3778.20	3738.10	0.663
91	3740.20	3696.10	3778.40	3738.23	0.667
112	3738.90	3694.70	3776.30	3736.63	0.624
140	3743.90	3700.20	3780.80	3741.63	0.759
168	3751.50	3708.10	3788.90	3749.50	0.970
196	3753.30	3708.80	3790.00	3750.70	1.003
252	3753.80	3709.10	3790.60	3751.17	1.015
280	3752.60	3707.00	3788.60	3749.40	0.968
308	3755.20	3710.40	3791.60	3752.40	1.048
336	3757.50	3714.40	3794.50	3755.47	1.131
364	3758.60	3716.30	3795.50	3756.80	1.167

APPENDIX E - SEAWATER RESISTANCE

Appendix E-9 Weight change of Specimens Subjected to Cyclic Wetting-Drying

Cycles	Mix T4									
	Sample 1		Sample 2		Sample 3		Average	Average	dn (%)	W (%)
	Wet	Dry	Wet	Dry	Wet	Dry	Wet	Dry		
0	3748.90		3698.50		3756.10		3723.70		0	0
3	3791.50	3704.50	3744.80	3755.50	3801.00	3714.70	3779.10	3724.90	1.46	101.49
10	3781.29	3695.29	3736.08	3647.22	3791.39	3706.12	3769.59	3682.88	2.35	101.23
20	3782.14	3695.82	3737.01	3647.84	3791.74	3706.64	3770.30	3683.43	2.36	101.25
30	3782.05	3695.78	3736.45	3646.26	3791.71	3705.76	3770.07	3682.60	2.38	101.25
40	3780.85	3694.09	3735.35	3644.77	3790.02	3704.53	3768.74	3681.13	2.38	101.21
45	3778.44	3691.05	3733.07	3641.36	3787.43	3701.36	3766.31	3677.92	2.40	101.14
50	3776.72	3690.64	3730.40	3642.32	3785.89	3700.73	3764.34	3677.90	2.35	101.09
60	3773.12	3687.98	3728.02	3639.96	3782.40	3696.94	3761.18	3674.96	2.35	101.01
70	3765.53	3683.00	3722.44	3637.52	3766.40	3693.90	3751.46	3671.47	2.18	100.75
80	3769.02	3675.31	3716.71	3629.88	3759.39	3686.85	3748.37	3664.01	2.30	100.66
90	3764.82	3670.49	3712.21	3625.48	3754.39	3681.67	3743.81	3659.21	2.31	100.54
100	3764.18	3665.88	3711.98	3622.08	3753.88	3677.28	3743.35	3655.08	2.41	100.53

Cycles	Mix OPC									
	Sample 1		Sample 2		Sample 3		Average	Average	dn (%)	W (%)
	Wet	Dry	Wet	Dry	Wet	Dry	Wet	Dry		
0	3700.40		3745.40		3732.90		3722.90		0	
3	3703.70	3640.50	3748.10	3684.90	3738.60	3673.80	3730.13	3666.40	1.74	100.19
10	3708.00	3651.60	3752.30	3699.10	3743.10	3682.80	3734.47	3677.83	1.54	100.31
20	3711.40	3658.50	3756.30	3706.00	3746.00	3693.50	3737.90	3686.00	1.41	100.40
30	3710.10	3667.10	3754.80	3712.10	3745.70	3700.80	3736.87	3693.33	1.18	100.38
40	3713.60	3670.00	3758.20	3716.00	3749.10	3704.68	3740.30	3696.89	1.17	100.47
45	3715.23	3672.56	3759.31	3718.62	3751.21	3705.22	3741.92	3698.80	1.17	100.51
50	3716.20	3674.58	3760.80	3719.56	3752.10	3706.82	3743.03	3700.32	1.15	100.54
60	3716.10	3676.80	3760.40	3721.60	3751.90	3709.50	3742.80	3702.63	1.08	100.53
70	3716.70	3674.10	3761.00	3719.90	3752.40	3708.30	3743.37	3700.77	1.15	100.55
80	3718.30	3683.20	3763.20	3729.70	3754.50	3717.20	3745.33	3710.03	0.95	100.60
90	3719.60	3684.31	3764.80	3730.33	3755.60	3718.4	3746.67	3711.01	0.96	100.64
100	3721.30	3687.60	3765.40	3731.90	3756.70	3720.30	3747.80	3713.27	0.93	100.67

APPENDIX E - SEAWATER RESISTANCE

Appendix E-10 Shrinkage/Expansion of OPC

Date	Temp.	Ref. Bar			Sample 1	Sample 2	Sample 3	
2/06/09	21.5deg C	before (in)	0.2004	Reading 1	0.806	0.7988	0.7795	
(DAY 0)		after (in)	0.2005	Reading 2	0.8059	0.7989	0.7795	
		avg. (in)	0.2005	Reading 3	0.806	0.7988	0.7798	
				Raw average	0.8060	0.7988	0.7796	
				Real average	0.6055	0.5984	0.5792	
28/12/09		before (in)	0.2003	Reading 1	0.8209	0.82	0.8244	
(DAY 4)		after (in)	0.2003	Reading 2	0.8209	0.82	0.8244	
		avg. (in)	0.2003	Reading 3	0.8209	0.82	0.8245	v
				Raw average	0.8209	0.8200	0.8244	
				Real average	0.6206	0.6197	0.6241	
				Shrinkage	0.0151	0.0213	0.0450	
				Avg.	0.0271			
				Avg. (mstrain)	2756.18222			
14/07/09		before (in)	0.2004	Reading 1	0.8209	0.8201	0.8243	
(DAY 28)		after (in)	0.2003	Reading 2	0.8209	0.8203	0.8242	
		avg. (in)	0.20035	Reading 3	0.8209	0.8202	0.8243	v
				Raw average	0.8209	0.8202	0.8243	
				Real average	0.6206	0.6199	0.6239	
				Shrinkage	0.0150	0.0215	0.0448	
				Avg.	0.0271			
				Avg. (mstrain)	2752.23111			
20/07/09		before (in)	0.2004	Reading 1	0.82	0.821	0.8233	
(DAY 56)		after (in)	0.2005	Reading 2	0.8119	0.821	0.8233	
		avg. (in)	0.2005	Reading 3	0.82	0.821	0.8233	v
				Raw average	0.8173	0.8210	0.8233	
				Real average	0.6169	0.6206	0.6229	
				Shrinkage	0.0113	0.0222	0.0437	
				Avg.	0.0257			
				Avg. (mstrain)	2614.50667			
8/11/09		before (in)	0.2005	Reading 1	0.823	0.8209	0.8236	
(DAY 91)		after (in)	0.2006	Reading 2	0.823	0.8209	0.8236	
		avg. (in)	0.2006	Reading 3	0.823	0.8209	0.8236	v
				Raw average	0.8230	0.8209	0.8236	
				Real average	0.6225	0.6204	0.6231	
				Shrinkage	0.0169	0.0220	0.0439	
				Avg.	0.0276			
				Avg. (mstrain)	2804.16			
8/01/10		before (in)	0.2001	Reading 1	0.8218	0.8219	0.8244	
(DAY 112)		after (in)	0.2001	Reading 2	0.8128	0.8218	0.8244	
		avg. (in)	0.2001	Reading 3	0.8128	0.8218	0.8243	v
				Raw average	0.8158	0.8218	0.8244	
				Real average	0.6157	0.6217	0.6243	
				Shrinkage	0.0102	0.0233	0.0451	
				Avg.	0.0262			
				Avg. (mstrain)	2663.61333			

APPENDIX E - SEAWATER RESISTANCE

Appendix E-11 Shrinkage/Expansion of T4

Date	Temp.	Ref. Bar			Sample 1	Sample 2	Sample 3	
12/04/09	21.5deg C	before (in)	0.2004	Reading 1	0.6464	0.6493	0.6225	
(DAY 0)		after (in)	0.2003	Reading 2	0.6462	0.6497	0.6226	
		avg. (in)	0.2004	Reading 3	0.6464	0.6497	0.6225	v
				Raw average	0.6463	0.6496	0.6225	
				Real average	0.4460	0.4492	0.4222	
8/05/09		before (in)	0.2003	Reading 1	0.6474	0.6254	0.6243	
(DAY 4)		after (in)	0.2004	Reading 2	0.6472	0.6253	0.6236	
		avg. (in)	0.2004	Reading 3	0.6475	0.6253	0.6237	v
				Raw average	0.6474	0.6253	0.6239	
				Real average	0.4470	0.4250	0.4235	
				Shrinkage	0.0010	-0.0242	0.0013	
				Avg.	-0.0073			
				Avg. (mstrain)	-740.55111			
15/05/09		before (in)	0.2001	Reading 1	0.6475	0.6255	0.6235	
(DAY 28)		after (in)	0.2001	Reading 2	0.6474	0.6253	0.6240	
		avg. (in)	0.2001	Reading 3	0.6476	0.6255	0.6240	v
				Raw average	0.6475	0.6254	0.6238	
				Real average	0.4474	0.4253	0.4237	
				Shrinkage	0.0014	-0.0239	0.0016	
				Avg.	-0.0070			
				Avg. (mstrain)	-708.37778			
5/06/09		before (in)	0.2004	Reading 1	0.6477	0.6254	0.6248	
(DAY 56)		after (in)	0.2001	Reading 2	0.6475	0.6252	0.6248	
		avg. (in)	0.2003	Reading 3	0.6476	0.6254	0.6245	
				Raw average	0.6476	0.6253	0.6247	
				Real average	0.4474	0.4251	0.4245	
				Shrinkage	0.0014	-0.0241	0.0023	
				Avg.	-0.0068			
				Avg. (mstrain)	-694.26667			
17/07/09		before (in)	0.2006	Reading 1	0.6474	0.6255	0.6241	
(DAY 91)		after (in)	0.2006	Reading 2	0.6477	0.6255	0.6241	
		avg. (in)	0.2006	Reading 3	0.6475	0.6254	0.624	v
				Raw average	0.6475	0.6255	0.6241	
				Real average	0.4469	0.4249	0.4235	
				Shrinkage	0.0010	-0.0244	0.0013	
				Avg.	-0.0074			
				Avg. (mstrain)	-749.01778			
24/07/09		before (in)	0.2004	Reading 1	0.6476	0.6255	0.6238	
(DAY 112)		after (in)	0.2003	Reading 2	0.6477	0.6257	0.6239	
		avg. (in)	0.2004	Reading 3	0.6473	0.6256	0.6242	v
				Raw average	0.6475	0.6256	0.6240	
				Real average	0.4472	0.4253	0.4236	
				Shrinkage	0.0012	-0.0240	0.0014	
				Avg.	-0.0071			
				Avg. (mstrain)	-722.48889			

APPENDIX E - SEAWATER RESISTANCE

Appendix E-12 Shrinkage/Expansion of T7

Date	Temp.	Ref. Bar			Sample 1	Sample 2	Sample 3	
12/04/09	21.5deg C	before (in)	0.2004	Reading 1	0.8759	0.854	0.8441	
(DAY 0)		after (in)	0.2003	Reading 2	0.876	0.854	0.8439	
		avg. (in)	0.2004	Reading 3	0.8759	0.854	0.844	v
				Raw average	0.8759	0.8540	0.8440	
				Real average	0.6756	0.6537	0.6437	
8/05/09		before (in)	0.2003	Reading 1	0.8758	0.8548	0.8439	
(DAY 4)		after (in)	0.2005	Reading 2	0.8759	0.8548	0.8439	
		avg. (in)	0.2004	Reading 3	0.8759	0.8549	0.8435	v
				Raw average	0.8759	0.8548	0.8438	
				Real average	0.6755	0.6544	0.6434	
				Shrinkage	-0.0001	0.0008	-0.0003	
				Avg.	0.0001			
				Avg. (mstrain)	12.982222			
15/05/09		before (in)	0.2004	Reading 1	0.876	0.8559	0.8449	
(DAY 28)		after (in)	0.2003	Reading 2	0.8759	0.8559	0.8448	
		avg. (in)	0.20035	Reading 3	0.8760	0.8557	0.8449	v
				Raw average	0.8760	0.8558	0.8449	
				Real average	0.6756	0.6555	0.6445	
				Shrinkage	0.0000	0.0018	0.0009	
				Avg.	0.0009			
				Avg. (mstrain)	92.568889			
5/06/09		before (in)	0.2003	Reading 1	0.8759	0.8559	0.8451	
(DAY 56)		after (in)	0.2005	Reading 2	0.876	0.8556	0.8452	
		avg. (in)	0.2004	Reading 3	0.8759	0.8559	0.8451	
				Raw average	0.8759	0.8558	0.8451	
				Real average	0.6755	0.6554	0.6447	
				Shrinkage	0.0000	0.0018	0.0011	
				Avg.	0.0009			
				Avg. (mstrain)	94.262222			
17/07/09		before (in)	0.2001	Reading 1	0.8768	0.8558	0.854	
(DAY 91)		after (in)	0.2004	Reading 2	0.877	0.8559	0.854	
		avg. (in)	0.2003	Reading 3	0.877	0.8561	0.854	v
				Raw average	0.8769	0.8559	0.8540	
				Real average	0.6767	0.6557	0.6538	
				Shrinkage	0.0011	0.0020	0.0101	
				Avg.	0.0044			
				Avg. (mstrain)	448.16889			
24/07/09		before (in)	0.2001	Reading 1	0.8769	0.8558	0.854	
(DAY 112)		after (in)	0.2001	Reading 2	0.8769	0.8559	0.854	
		avg. (in)	0.2001	Reading 3	0.8769	0.856	0.8540	v
				Raw average	0.8769	0.8559	0.8540	
				Real average	0.6768	0.6558	0.6539	
				Shrinkage	0.0012	0.0021	0.0103	
				Avg.	0.0045			
				Avg. (mstrain)	461.15111			

APPENDIX E - SEAWATER RESISTANCE

Appendix E-13 Shrinkage/Expansion of T10

Date	Temp.	Ref. Bar			Sample 1	Sample 2	Sample 3	
12/04/09	21.5deg C	before (in)	0.2004	Reading 1	0.806	0.7988	0.7795	
(DAY 0)		after (in)	0.2005	Reading 2	0.8059	0.7989	0.7795	
		avg. (in)	0.2005	Reading 3	0.806	0.7988	0.7798	v
				Raw average	0.8060	0.7988	0.7796	
				Real average	0.6055	0.5984	0.5792	
8/05/09		before (in)	0.2001	Reading 1	0.8076	0.7999	0.7928	
(DAY 4)		after (in)	0.2001	Reading 2	0.8076	0.8001	0.7927	
		avg. (in)	0.2001	Reading 3	0.7975	0.8001	0.7929	v
				Raw average	0.8042	0.8000	0.7928	
				Real average	0.6041	0.5999	0.5927	
				Shrinkage	-0.0014	0.0016	0.0136	
				Avg.	0.0046			
				Avg. (mstrain)	464.53778			
15/05/09		before (in)	0.2004	Reading 1	0.8071	0.7998	0.7920	
(DAY 28)		after (in)	0.2003	Reading 2	0.807	0.8	0.7921	
		avg. (in)	0.20035	Reading 3	0.8070	0.7998	0.7922	v
				Raw average	0.8070	0.7999	0.7921	
				Real average	0.6067	0.5995	0.5918	
				Shrinkage	0.0012	0.0011	0.0126	
				Avg.	0.0050			
				Avg. (mstrain)	504.61333			
5/06/09		before (in)	0.2005	Reading 1	0.8071	0.7997	0.7921	
(DAY 56)		after (in)	0.2005	Reading 2	0.8069	0.8	0.7916	
		avg. (in)	0.2005	Reading 3	0.8071	0.7998	0.7922	
				Raw average	0.8070	0.7998	0.7920	
				Real average	0.6065	0.5993	0.5915	
				Shrinkage	0.0010	0.0009	0.0123	
				Avg.	0.0048			
				Avg. (mstrain)	483.72889			
17/07/09		before (in)	0.2001	Reading 1	0.806	0.7998	0.792	
(DAY 91)		after (in)	0.2004	Reading 2	0.8061	0.7997	0.7921	
		avg. (in)	0.2003	Reading 3	0.8059	0.7997	0.7921	v
				Raw average	0.8060	0.7997	0.7921	
				Real average	0.6058	0.5995	0.5918	
				Shrinkage	0.0002	0.0011	0.0127	
				Avg.	0.0047			
				Avg. (mstrain)	474.13333			
24/07/09		before (in)	0.2004	Reading 1	0.807	0.8001	0.7929	
(DAY 112)		after (in)	0.2005	Reading 2	0.8069	0.8001	0.7928	
		avg. (in)	0.2005	Reading 3	0.807	0.8002	0.7929	v
				Raw average	0.8070	0.8001	0.7929	
				Real average	0.6065	0.5997	0.5924	
				Shrinkage	0.0010	0.0013	0.0133	
				Avg.	0.0052			
				Avg. (mstrain)	527.19111			

APPENDIX E - SEAWATER RESISTANCE

Appendix E-14 Shrinkage/Expansion of OPC (wet)

Date	Temp.	Ref. Bar			Sample 1	Sample 2	Sample 3	
2/06/09	21.5deg C	before (in)	0.2004	Reading 1	0.8197	0.8196	0.8224	
(DAY 0)		after (in)	0.2003	Reading 2	0.8197	0.8198	0.8225	
		avg. (in)	0.2004	Reading 3	0.8199	0.8198	0.8266	
				Raw average	0.8198	0.8197	0.8238	
				Real average	0.6194	0.6194	0.6235	
28/12/09		before (in)	0.2006	Reading 1	0.7965	0.7781	0.8	
(DAY 4)		after (in)	0.2003	Reading 2	0.7965	0.7781	0.8002	
		avg. (in)	0.2005	Reading 3	0.7965	0.7781	0.8002	v
				Raw average	0.7965	0.7781	0.8001	
				Real average	0.5961	0.5777	0.5997	
				Shrinkage	-0.0234	-0.0417	-0.0238	
				Avg.	-0.0296			
				Avg. (mstrain)	-3010.7467			

Date	Temp.	Ref. Bar			Sample 1	Sample 2	Sample 3	
14/07/09		before (in)	0.2004	Reading 1	0.7975	0.7799	0.8015	
(DAY 28)		after (in)	0.2003	Reading 2	0.7977	0.78	0.8015	
		avg. (in)	0.20035	Reading 3	0.7976	0.78	0.8016	v
				Raw average	0.7976	0.7800	0.8015	
				Real average	0.5973	0.5796	0.6012	
				Shrinkage	-0.0222	-0.0398	-0.0223	
				Avg.	-0.0281			
				Avg. (mstrain)	-2852.7022			
20/07/09		before (in)	0.2001	Reading 1	0.7984	0.7799	0.8023	
(DAY 56)		after (in)	0.2005	Reading 2	0.7985	0.7798	0.8024	
		avg. (in)	0.2003	Reading 3	0.7984	0.7799	0.8022	v
				Raw average	0.7984	0.7799	0.8023	
				Real average	0.5981	0.5796	0.6020	
				Shrinkage	-0.0213	-0.0398	-0.0215	
				Avg.	-0.0275			
				Avg. (mstrain)	-2796.8222			
8/11/09		before (in)	0.2	Reading 1	0.7868	0.7899	0.7808	
(DAY 91)		after (in)	0.2001	Reading 2	0.7869	0.7899	0.7808	
		avg. (in)	0.2001	Reading 3	0.787	0.7898	0.7808	v
				Raw average	0.7869	0.7899	0.7808	
				Real average	0.5869	0.5898	0.5808	
				Shrinkage	-0.0326	-0.0296	-0.0427	
				Avg.	-0.0350			
				Avg. (mstrain)	-3551.4844			
8/01/10		before (in)	0.2001	Reading 1	0.7896	0.7962	0.767	
(DAY 112)		after (in)	0.2001	Reading 2	0.7898	0.7962	0.767	
		avg. (in)	0.2001	Reading 3	0.7898	0.7962	0.7669	v
				Raw average	0.7897	0.7962	0.7670	
				Real average	0.5896	0.5961	0.5669	
				Shrinkage	-0.0298	-0.0233	-0.0566	
				Avg.	-0.0366			
				Avg. (mstrain)	-3714.6089			

APPENDIX E - SEAWATER RESISTANCE

Appendix E-15 Shrinkage/Expansion of OPC (dry)

Date	Temp.	Ref. Bar			Sample 1	Sample 2	Sample 3	
2/06/09	21.5deg C	before (in)	0.2004	Reading 1	0.8197	0.8196	0.8224	
(DAY 0)		after (in)	0.2003	Reading 2	0.8197	0.8198	0.8225	
		avg. (in)	0.2004	Reading 3	0.8199	0.8198	0.8266	
				Raw average	0.8198	0.8197	0.8238	
				Real average	0.6194	0.6194	0.6235	
28/12/09		before (in)	0.2003	Reading 1	0.8020	0.8022	0.8272	
(DAY 4)		after (in)	0.2003	Reading 2	0.8020	0.8023	0.8273	
		avg. (in)	0.2003	Reading 3	0.802	0.8021	0.8270	v
				Raw average	0.8020	0.8022	0.8272	
				Real average	0.6017	0.6019	0.6269	
				Shrinkage	-0.0177	-0.0175	0.0034	
				Avg.	-0.0106			
				Avg. (mstrain)	-1077.5244			
Date	**Temp.**	**Ref. Bar**			**Sample 1**	**Sample 2**	**Sample 3**	
14/07/09		before (in)	0.2004	Reading 1	0.7902	0.7904	0.8178	
(DAY 28)		after (in)	0.2003	Reading 2	0.79	0.7903	0.8177	
		avg. (in)	0.20035	Reading 3	0.7900	0.7905	0.8179	v
				Raw average	0.7901	0.7904	0.8178	
				Real average	0.5897	0.5901	0.6175	
				Shrinkage	-0.0297	-0.0293	-0.0060	
				Avg.	-0.0217			
				Avg. (mstrain)	-2203.5911			
20/07/09		before (in)	0.2004	Reading 1	0.7784	0.7708	0.7983	
(DAY 56)		after (in)	0.2005	Reading 2	0.7784	0.7709	0.7984	
		avg. (in)	0.2005	Reading 3	0.7787	0.7708	0.7984	v
				Raw average	0.7785	0.7708	0.7984	
				Real average	0.5781	0.5704	0.5979	
				Shrinkage	-0.0414	-0.0490	-0.0256	
				Avg.	-0.0386			
				Avg. (mstrain)	-3926.2756			
8/11/09		before (in)	0.2002	Reading 1	0.7803	0.8108	0.7708	
(DAY 91)		after (in)	0.2002	Reading 2	0.7804	0.8109	0.7709	
		avg. (in)	0.2002	Reading 3	0.7802	0.8109	0.7709	v
				Raw average	0.7803	0.8109	0.7709	
				Real average	0.5801	0.6107	0.5707	
				Shrinkage	-0.0393	-0.0087	-0.0528	
				Avg.	-0.0336			
				Avg. (mstrain)	-3415.4533			
8/01/10		before (in)	0.2004	Reading 1	0.7896	0.7962	0.767	
(DAY 112)		after (in)	0.2004	Reading 2	0.7898	0.7962	0.767	
		avg. (in)	0.2004	Reading 3	0.7898	0.7962	0.7669	v
				Raw average	0.7897	0.7962	0.7670	
				Real average	0.5893	0.5958	0.5666	
				Shrinkage	-0.0301	-0.0236	-0.0569	
				Avg.	-0.0369			
				Avg. (mstrain)	-3745.0889			

APPENDIX E - SEAWATER RESISTANCE

Appendix E-16 Shrinkage/Expansion of T4 (wet)

Date	Temp.	Ref. Bar			Sample 1	Sample 2	Sample 3	
21/04/2009	21.5deg C	before (in)	0.2001	Reading 1	0.7756	0.8002	0.772	
(DAY 0)		after (in)	0.2003	Reading 2	0.7757	0.7998	0.7717	
		avg. (in)	0.2002	Reading 3	0.7756	0.7999	0.7717	v
				Raw average	0.7756	0.8000	0.7718	
				Real average	0.5754	0.5998	0.5716	
29/04/09		before (in)	0.2002	Reading 1	0.7756	0.7997	0.7716	
(DAY 4)		after (in)	0.2003	Reading 2	0.7756	0.7997	0.7717	
		avg. (in)	0.2003	Reading 3	0.7756	0.7997	0.7717	v
				Raw average	0.7756	0.7997	0.7717	
				Real average	0.5754	0.5995	0.5714	
				Shrinkage	-0.0001	-0.0003	-0.0002	
				Avg.	-0.0002			
				Avg. (mstrain)	-19.755556			

Date	Temp.	Ref. Bar			Sample 1	Sample 2	Sample 3	
15/05/09		before (in)	0.2001	Reading 1	0.7751	0.7991	0.7711	
(DAY 28)		after (in)	0.2001	Reading 2	0.7751	0.7991	0.7710	
		avg. (in)	0.2001	Reading 3	0.7750	0.7989	0.7711	v
				Raw average	0.7751	0.7990	0.7711	
				Real average	0.5750	0.5989	0.5710	
				Shrinkage	-0.0005	-0.0008	-0.0006	
				Avg.	-0.0006			
				Avg. (mstrain)	-65.475556			
5/06/09		before (in)	0.2003	Reading 1	0.7748	0.799	0.7708	
(DAY 56)		after (in)	0.2003	Reading 2	0.775	0.7989	0.7711	
		avg. (in)	0.2003	Reading 3	0.775	0.7989	0.771	
				Raw average	0.7749	0.7989	0.7710	
				Real average	0.5746	0.5986	0.5707	
				Shrinkage	-0.0008	-0.0011	-0.0009	
				Avg.	-0.0010			
				Avg. (mstrain)	-97.084444			
17/07/09		before (in)	0.2004	Reading 1	0.7739	0.798	0.7707	
(DAY 91)		after (in)	0.2001	Reading 2	0.774	0.7981	0.7707	
		avg. (in)	0.2003	Reading 3	0.7741	0.7981	0.7708	v
				Raw average	0.7740	0.7981	0.7707	
				Real average	0.5738	0.5978	0.5705	
				Shrinkage	-0.0017	-0.0020	-0.0011	
				Avg.	-0.0016			
				Avg. (mstrain)	-160.86667			
12/03/09		before (in)	0.2005	Reading 1	0.774	0.798	0.771	
(DAY 112)		after (in)	0.2003	Reading 2	0.7739	0.798	0.7709	
		avg. (in)	0.2004	Reading 3	0.7741	0.7979	0.7710	v
				Raw average	0.7740	0.7980	0.7710	
				Real average	0.5736	0.5976	0.5706	
				Shrinkage	-0.0018	-0.0022	-0.0010	
				Avg.	-0.0017			
				Avg. (mstrain)	-171.59111			

APPENDIX E - SEAWATER RESISTANCE

Appendix E-17 Shrinkage/Expansion of T4 (dry)

Date	Temp.	Ref. Bar			Sample 1	Sample 2	Sample 3	
21/04/2009	21.5deg C	before (in)	0.2001	Reading 1	0.7756	0.8002	0.772	
(DAY 0)		after (in)	0.2003	Reading 2	0.7757	0.7998	0.7717	
		avg. (in)	0.2002	Reading 3	0.7756	0.7999	0.7717	v
				Raw average	0.7756	0.8000	0.7718	
				Real average	0.5754	0.5998	0.5716	
28/04/09		before (in)	0.2004	Reading 1	0.7795	0.8038	0.7759	
(DAY 4)		after (in)	0.2002	Reading 2	0.7795	0.8038	0.7757	
		avg. (in)	0.2003	Reading 3	0.7796	0.8036	0.7761	v
				Raw average	0.7795	0.8037	0.7759	
				Real average	0.5792	0.6034	0.5756	
				Shrinkage	0.0038	0.0037	0.0040	
				Avg.	0.0038			
				Avg. (mstrain)	388.33778			
15/05/09		before (in)	0.2004	Reading 1	0.7798	0.8036	0.7759	
(DAY 28)		after (in)	0.2000	Reading 2	0.7796	0.8038	0.7758	
		avg. (in)	0.2002	Reading 3	0.7796	0.8035	0.7758	v
				Raw average	0.7797	0.8036	0.7758	
				Real average	0.5795	0.6034	0.5756	
				Shrinkage	0.0040	0.0037	0.0040	
				Avg.	0.0039			
				Avg. (mstrain)	397.36889			
5/06/09		before (in)	0.2004	Reading 1	0.7799	0.8039	0.7759	
(DAY 56)		after (in)	0.2001	Reading 2	0.7799	0.804	0.7759	
		avg. (in)	0.2003	Reading 3	0.7799	0.8038	0.7759	
				Raw average	0.7799	0.8039	0.7759	
				Real average	0.5797	0.6037	0.5757	
				Shrinkage	0.0042	0.0039	0.0040	
				Avg.	0.0040			
				Avg. (mstrain)	411.48			
12/02/09		before (in)	0.2006	Reading 1	0.7789	0.803	0.7749	
(DAY 91)		after (in)	0.2005	Reading 2	0.779	0.803	0.775	
		avg. (in)	0.2006	Reading 3	0.7787	0.803	0.7751	v
				Raw average	0.7789	0.8030	0.7750	
				Real average	0.5783	0.6025	0.5745	
				Shrinkage	0.0029	0.0027	0.0028	
				Avg.	0.0028			
				Avg. (mstrain)	285.04444			
24/07/09		before (in)	0.2004	Reading 1	0.7787	0.8028	0.7747	
(DAY 112)		after (in)	0.2003	Reading 2	0.7789	0.8028	0.7748	
		avg. (in)	0.2004	Reading 3	0.7788	0.8028	0.7748	v
				Raw average	0.7788	0.8028	0.7748	
				Real average	0.5785	0.6025	0.5744	
				Shrinkage	0.0030	0.0027	0.0028	
				Avg.	0.0028			
				Avg. (mstrain)	288.43111			

APPENDIX F - CORROSION OF STEEL REINFORCEMENT BAR

Appendix F-1 Half-Cell Potential Measurement

Mix	Age (days)	Sample 1 Potential (mV)				Sample 2 Potential (mV)				Sample 3 Potential (mV)				Average	SD	COV
		Reading 1 (mV)	Reading 2 (mV)	Reading 3 (mV)	Average Reading (mV)	Reading 1 (mV)	Reading 2 (mV)	Reading 3 (mV)	Average Reading (mV)	Reading 1 (mV)	Reading 2 (mV)	Reading 3 (mV)	Average Reading (mV)			
OPC	0	-38.20	-38.80	-39.40	-38.80	-25.00	-25.20	-25.10	-25.10	-45.80	-45.90	-45.90	-45.87	-36.59	9.15	3.05
	1	-58.90	-58.90	-59.00	-58.93	-57.10	-57.20	-57.10	-57.13	-55.40	-55.40	-55.40	-55.40	-57.16	1.53	0.51
	3	-56.30	-56.40	-56.30	-56.33	-54.40	-54.50	-54.60	-54.50	-53.40	-53.50	-53.50	-53.47	-54.77	1.26	0.42
	7	-301.00	-301.00	-301.00	-301.00	-69.70	-69.70	-69.70	-69.70	-66.20	-66.30	-66.20	-66.23	-145.64	116.53	38.84
	14	-431.00	-431.00	-431.00	-431.00	-66.00	-66.00	-66.00	-66.00	-395.00	-395.00	-395.00	-395.00	-297.33	174.20	58.07
	21	-441.00	-441.00	-441.00	-441.00	-57.20	-57.20	-57.20	-57.20	-590.00	-590.00	-590.00	-590.00	-362.73	238.06	79.35
	28	-545.00	-545.00	-545.00	-545.00	-57.40	-57.40	-57.40	-57.40	-618.00	-618.00	-618.00	-618.00	-406.80	263.95	87.98
	56	-585.00	-585.00	-585.00	-585.00	-93.30	-93.30	-93.30	-93.30	-555.00	-555.00	-555.00	-555.00	-411.10	238.70	79.57
	91	-543.00	-544.00	-543.00	-543.33	-233.00	-234.00	-233.00	-233.33	-524.00	-524.00	-524.00	-524.00	-433.56	150.40	50.13
T7	0	-143.90	-146.10	-146.10	-145.37	-146.30	-146.10	-146.10	-146.17	-350.00	-350.00	-350.00	-350.00	-213.84	102.12	34.04
	1	-163.90	-163.90	-163.90	-163.90	-155.10	-155.20	-155.20	-155.17	-386.00	-386.00	-386.00	-386.00	-235.02	113.30	37.77
	3	-171.80	-171.90	-171.80	-171.83	-199.10	-199.20	-199.10	-199.13	-196.20	-196.20	-196.20	-196.20	-189.06	12.98	4.33
	7	-205.40	-205.30	-205.40	-205.37	-284.00	-285.00	-284.00	-284.33	-408.00	-408.00	-408.00	-408.00	-299.23	88.45	29.48
	14	-239.20	-239.20	-239.20	-239.20	-471.00	-471.00	-471.00	-471.00	-352.00	-352.00	-352.00	-352.00	-354.07	100.38	33.46
	21	-227.40	-227.50	-277.50	-244.13	-437.00	-438.00	-438.00	-437.67	-373.00	-373.00	-373.00	-373.00	-351.60	86.54	28.85
	28	-482.00	-482.00	-482.00	-482.00	-482.00	-482.00	-482.00	-482.00	-327.00	-327.00	-327.00	-327.00	-430.33	77.50	25.83
	56	-530.00	-530.00	-530.00	-530.00	-533.00	-533.00	-533.00	-533.00	-553.00	-553.00	-553.00	-553.00	-538.67	10.83	3.61
	91	-536.00	-536.00	-536.00	-536.00	-536.00	-536.00	-536.00	-536.00	-537.00	-537.00	-537.00	-537.00	-536.33	0.50	0.17
T4	0	-204.30	-204.20	-204.20	-204.23	-145.40	-145.30	-145.20	-145.30	-166.30	-166.20	-166.10	-166.20	-171.91	25.88	8.63
	1	-207.70	-207.80	-207.70	-207.73	-199.00	-199.10	-199.20	-199.10	-171.90	-171.90	-172.00	-171.93	-192.92	16.18	5.39
	3	-268.00	-269.00	-268.00	-268.33	-250.00	-249.00	-250.00	-249.67	-212.70	-212.80	-212.80	-212.77	-243.59	24.49	8.16
	7	-317.00	-317.00	-317.00	-317.00	-286.00	-287.00	-287.00	-286.67	-385.00	-385.00	-385.00	-385.00	-329.56	43.61	14.54
	14	-414.00	-414.00	-414.00	-414.00	-393.00	-393.00	-393.00	-393.00	-404.00	-404.00	-404.00	-404.00	-403.67	9.10	3.03
	21	-409.00	-409.00	-409.00	-409.00	-367.00	-367.00	-367.00	-367.00	-442.00	-442.00	-442.00	-442.00	-406.00	32.55	10.85
	28	-476.00	-477.00	-476.00	-476.33	-493.00	-493.00	-493.00	-493.00	-500.00	-500.00	-500.00	-500.00	-489.78	10.53	3.51
	56	-564.00	-564.00	-564.00	-564.00	-539.00	-539.00	-539.00	-539.00	-522.00	-522.00	-522.00	-522.00	-541.67	18.30	6.10
	91	-554.00	-554.00	-553.00	-553.67	-503.00	-503.00	-503.00	-503.00	-550.00	-550.00	-550.00	-550.00	-535.56	24.47	8.16
T10	0	-189.20	-189.60	-189.70	-189.50	-181.20	-181.20	-181.30	-181.23	-195.80	-195.80	-195.80	-195.80	-188.84	6.33	2.11
	1	-225.80	-225.90	-225.90	-225.87	-218.90	-219.00	-219.10	-219.00	-193.30	-193.30	-193.30	-193.30	-212.72	14.87	4.96
	3	-248.00	-249.00	-249.00	-248.67	-259.00	-259.00	-259.00	-259.00	-147.20	-147.20	-147.20	-147.20	-218.29	53.50	17.83
	7	-270.00	-270.00	-271.00	-270.33	-215.30	-215.40	-215.40	-215.37	-413.00	-413.00	-413.00	-413.00	-299.57	88.34	29.45
	14	-400.00	-400.00	-400.00	-400.00	-399.00	-398.00	-399.00	-398.67	-395.00	-395.00	-395.00	-395.00	-397.89	2.26	0.75
	21	-343.00	-343.00	-343.00	-343.00	-327.00	-328.00	-328.00	-327.67	-444.00	-444.00	-444.00	-444.00	-371.56	54.74	18.25
	28	-423.00	-423.00	-423.00	-423.00	-479.00	-479.00	-479.00	-479.00	-386.00	-386.00	-386.00	-386.00	-429.33	40.55	13.52
	56	-565.00	-565.00	-565.00	-565.00	-536.00	-536.00	-536.00	-536.00	-450.00	-450.00	-450.00	-450.00	-517.00	51.80	17.27
	91	-545.00	-545.00	-545.00	-545.00	-523.00	-523.00	-523.00	-523.00	-524.00	-524.00	-524.00	-524.00	-530.67	10.76	3.59

APPENDIX F - CORROSION OF STEEL REINFORCEMENT BAR

Appendix F-2 pH aquous medium at Half-Cell Potential Measurement

Mix	Age (days)	Ph				
		Sample 1	Sample 2	Sample 3	AVG	SD
OPC	0	6.95	7.32	7.05	7.11	0.19
	1	9.80	10.15	9.88	9.94	0.18
	3	10.47	10.43	10.47	10.46	0.02
	7	10.40	10.27	10.51	10.39	0.12
	14	9.15	9.87	9.65	9.56	0.37
	21	9.59	9.50	9.42	9.50	0.09
	28	9.39	9.34	9.43	9.39	0.05
	56	9.56	9.63	9.50	9.56	0.07
	91	9.57	9.24	9.52	9.44	0.18
T7	0	7.34	7.23	7.59	7.39	0.18
	1	9.31	9.27	9.33	9.30	0.03
	3	9.32	9.22	9.58	9.37	0.19
	7	9.39	9.47	9.49	9.45	0.05
	14	9.22	9.41	9.39	9.34	0.10
	21	9.14	9.38	9.16	9.23	0.13
	28	9.12	9.28	9.19	9.20	0.08
	56	9.11	9.20	8.33	8.88	0.48
	91	9.17	9.10	8.67	8.98	0.27
T4	0	6.98	7.07	6.99	7.01	0.05
	1	9.44	9.45	9.44	9.44	0.01
	3	9.31	9.25	9.55	9.37	0.16
	7	9.43	9.38	9.33	9.38	0.05
	14	9.21	9.30	9.16	9.22	0.07
	21	9.17	9.25	9.10	9.17	0.08
	28	9.16	9.21	9.06	9.14	0.08
	56	9.18	9.19	9.11	9.16	0.04
	91	9.18	9.23	9.15	9.19	0.04
T10	0	7.06	7.23	7.43	7.24	0.19
	1	9.41	9.32	9.21	9.31	0.10
	3	9.36	9.34	9.55	9.42	0.12
	7	9.41	9.45	9.53	9.46	0.06
	14	9.15	9.23	9.38	9.25	0.12
	21	9.09	9.17	9.23	9.16	0.07
	28	9.06	9.12	9.12	9.10	0.03
	56	9.11	9.17	8.50	8.93	0.37
	91	9.18	9.18	8.78	9.05	0.23

APPENDIX F - CORROSION OF STEEL REINFORCEMENT BAR

Appendix F-3 Average Daily Resistance (ADR)

Days	AVERAGE DAILY RESISTANCE 30V (Ohm)			
	T7	T4	T10	OPC
1	1499.264	1036.552	1147.938	183.647
2	4302.430	2761.448	3607.775	216.054
3	4239.966	3109.095	4833.034	199.482
4	4787.242	3548.043	5948.279	164.136
5	4364.620	4020.290	5882.749	144.621
6	4479.376	4103.038	5118.235	136.156
7	5327.214	3712.301	4714.688	121.216
8	6317.189	3682.763	4050.808	100.352
9	7258.894	3514.169	4147.724	89.667
10	4444.522	3311.599	4477.436	82.199
11	4416.828	3806.223	2988.681	79.911
12	6646.307	4007.199	3154.513	77.917
13	5686.508	3425.578	2827.713	72.867
14	3408.596	2755.235	2266.516	66.057
15	2016.209	1917.123	2006.331	56.162
16	1961.976	1878.837	1918.581	52.699
17	1249.469	1696.105	1533.474	
18	747.711	2193.930	965.039	
19	632.232	2150.446	845.411	
20	592.496	1497.621	779.839	
21	392.276	1536.686	746.258	
22	306.970	1580.942	636.508	
23	305.256	1508.329	559.520	
24	170.461	1596.128	545.564	
25	30.197	1729.193	506.454	
26		1698.618	318.072	
27		1537.255	131.855	
28		940.537	64.477	

Days	AVERAGE DAILY RESISTANCE 5V (Ohm)			
	T7	T4	T10	OPC
1	745.234	317.254	401.161	240.726
2	767.732	778.405	1107.327	245.994
3	1103.852	1084.318	1355.842	241.187
4	1605.833	1437.001	1425.795	234.642
5	1763.003	1722.737	1634.052	229.769
6	2117.186	1852.257	1861.191	227.885
7	2509.209	2168.348	1947.378	227.986
8	2651.231	2285.177	2130.272	228.656
9	2651.070	2645.391	2414.264	234.020
10	2780.073	2797.235	2864.839	237.545
11	2879.159	3094.365	3203.096	242.351
12	2629.753	3131.585	3511.356	248.354
13	3062.527	3411.732	4032.032	254.113
14	3148.208	3481.313	4442.963	257.376
15	3089.598	3725.840	4592.569	257.402
16	3159.807	3901.308	4649.346	251.351
17	3004.532	4132.587	5145.779	247.947
18	2843.944	4267.982	5535.736	241.633
19	3372.057	4257.483	5970.075	224.980
20	4071.005	3646.705	6085.681	204.078
21	4148.290	3657.877	6066.019	188.892
22	4355.783	3519.827	6113.040	180.236
23	4715.545	3638.578	6015.515	178.178
24	5049.496	3850.782	6244.119	171.190
25	5189.488	4021.403	6646.358	169.520
26	4717.877	3974.343	6795.658	171.141
27	4790.547	3825.433	7230.005	164.692
28	4785.420	3826.205	7232.111	164.598

APPENDIX F - CORROSION OF STEEL REINFORCEMENT BAR

Appendix F-4 Steel Residual Mass Data

Mixtures	Weight						
	Before (g)	0 (g)	1 (g)	2 (g)	3 (g)	4 (g)	5 (g)
Accelerated Corrosion Test							
T7-1 5V	534.52	533.66	533.44	533.33	533.33	533.31	532.88
T7-2 5V	535.81	535.58	535.42	535.28	535.23	535.13	534.98
T4-1 5V	540.86	539.87	539.44	539.44	539.36	539.36	539.36
T4-2 5V	535.21	532.73	532.75	532.22	532.22	532.22	532.22
T10-1 5V	492.71	491.87	491.73	491.68	491.58	491.52	491.52
T10-2 5V	490.35	487.96	487.94	487.8	487.77	487.77	487.77
OPC-1 5V	534.56	539.07	535.23	533.72	533.40	533.24	533.04
OPC-2 5V	536.36	535.42	534.89	534.15	533.67	532.60	532.60
T7-1 30V	534.33	527.35	527.10	526.97	526.82	526.70	526.70
T7-2 30V	534.36	532.27	531.92	531.88	531.78	531.75	531.65
T7-3 30V	535.01	532.78	532.59	532.26	532.18	532.13	532.11
T4-1 30V	538.22	524.47	523.78	523.66	523.50	523.42	523.40
T4-2 30V	539.37	535.29	533.96	533.60	533.30	533.20	533.05
T4-3 30V	492.30	475.42	475.05	474.73	474.64	474.60	474.42
T10-1 30V	537.02	489.18	487.92	487.74	487.37	487.29	487.26
T10-2 30V	552.68	533.79	532.96	532.86	532.56	532.48	532.48
T10-3 30V	539.57	483.69	483.38	483.22	483.10	483.04	483.00
OPC-1 30V	535.67	434.74	431.54	430.00	429.01	428.70	428.52
OPC-2 30V	534.9	422.85	420.28	419.44	418.86	418.47	418.30
OPC-3 30V	535.37	436.60	432.58	430.64	429.90	429.58	429.36
Half-cell potential measurement							
T7-1	532.19	535.21	532.36	532.15	531.93	531.91	531.85
T7-2	534.27	534.94	534.9	534.11	533.99	533.91	533.84
T7-3	539.45	550.47	539.71	539.13	539.02	538.99	538.95
T4-1	537.56	541.39	538.47	537.56	537.51	537.41	537.39
T4-2	542.42	543.2	542.82	542.6	542.45	542.4	542.38
T4-3	541.5	548.2	541.91	541.65	541.49	541.35	541.33
T10-1	540.92	546.72	542.5	541.5	541.08	540.96	540.88
T10-2	537.77	562.28	538.66	538.11	537.92	537.9	537.74
T10-3	539.24	540.76	539.89	539.44	539.32	539.23	539.19
OPC-1	539.56	536.41	536.08	535.99	535.99	535.91	535.91
OPC-2	541.08	537.24	537.06	536.97	536.87	536.82	536.82
OPC-3	537.38	534.36	533.86	533.79	533.71	533.69	533.69